of Engineers

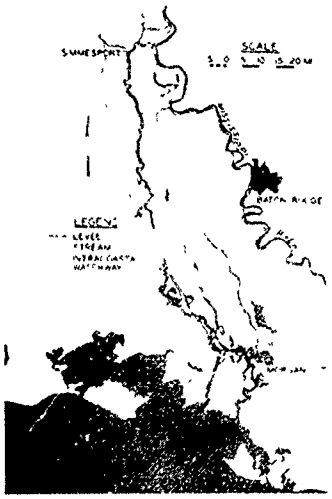

HYDRAULICS LABORATORY

TECHNICAL REPORT HL-82-15

THE ATCHAFALAYA RIVER DELTA

Report 11
TWO-DIMENSIONAL MODELING

by

Barbara Park Donnell, Joseph V. Letter, Jr.,
Allen M. Teeter

Hydraulics Laboratory

DEPARTMENT OF THE ARMY
Waterways Experiment Station, Corps of Engineers
3909 Halls Ferry Road, Vicksburg, Mississippi 39180-6199

May 1991
Report 11 of a Series

Approved For Public Release; Distribution Unlimited

Prepared for US Army Engineer District, New Orleans
New Orleans, Louisiana 70160-0267

When this report is no longer needed return it to the originator.

The findings in this report are not to be construed as an official Department of the Army position unless so designated by other authorized documents.

The contents of this report are not to be used for advertising, publication, or promotional purposes. Citation of trade names does not constitute an official endorsement or approval of the use of such commercial products.

REPORT DOCUMENTATION PAGE

Form Approved
OMB No. 0704-0188

1. AGENCY USE ONLY *(Leave blank)*	2. REPORT DATE	3. REPORT TYPE AND DATES COVERED
	May 1991	Report 11 of a series

4. TITLE AND SUBTITLE

The Atchafalaya River Delta;
Report 11, Two-Dimensional Modeling

5. FUNDING NUMBERS

6. AUTHOR(S)

Barbara Park Donnell
Joseph V. Letter, Jr.
Allen M. Teeter

7. PERFORMING ORGANIZATION NAME(S) AND ADDRESS(ES)

USAE Waterways Experiment Station, Hydraulics Laboratory, 3909 Halls Ferry Road, Vicksburg, MS 39180-6199

8. PERFORMING ORGANIZATION REPORT NUMBER

Technical Report
HL-82-15

9. SPONSORING/MONITORING AGENCY NAME(S) AND ADDRESS(ES)

USAE District, New Orleans, PO Box 60267,
New Orleans, LA 70160-0267

10. SPONSORING/MONITORING AGENCY REPORT NUMBER

11. SUPPLEMENTARY NOTES

Available from National Technical Information Service, 5285 Port Royal Road, Springfield, VA 22161.

12a. DISTRIBUTION/AVAILABILITY STATEMENT

Approved for public release; distribution unlimited.

12b. DISTRIBUTION CODE

13. ABSTRACT *(Maximum 200 words)*

The Wax Lake Outlet and Atchafalaya River deltas in Louisiana have grown dramatically, and concern over the impact of this growth has led the US Army Corps of Engineers to conduct an investigation to predict how the deltas will evolve over the next 50 years. The goal was to design a series of modeling tools capable of predicting delta evolution and the impacts of that growth on navigation, flood control, salinity, and sedimentation. The technical appraoch for this investigation was built upon the TABS-2 finite element modeling system. The fully two-dimensional models for hydrodynamics, salinity, and sediment transport were first verified to extensive prototype data, then employed to predict delta evolution for existing conditions at years 1980, 1995, 2010, and 2030 within the project area. Subsidence estimates for the system were made by regression of historical water-surface elevation gaging stations.

14. SUBJECT TERMS

Delta evolution predictions
Lower Atchafalaya River
Numerical hydrodynamic modeling
Numerical salinity transport modeling
(Continued)

15. NUMBER OF PAGES
200

16. PRICE CODE

17. SECURITY CLASSIFICATION OF REPORT	18. SECURITY CLASSIFICATION OF THIS PAGE	19. SECURITY CLASSIFICATION OF ABSTRACT	20. LIMITATION OF ABSTRACT
UNCLASSIFIED	UNCLASSIFIED		

14. (Concluded).

Numerical sediment transport modeling
TABS-2 numerical modeling system
Subsidence
Terrebonne Marshes
Verification process
Wax Lake Outlet

PREFACE

The work reported herein was performed in the Hydraulics Laboratory of the US Army Engineer Waterways Experiment Station (WES) as a part of the overall investigation to predict the evolution of the Atchafalaya Bay delta for the US Army Engineer District, New Orleans (LMN). This report presents the results of the two-dimensional numerical modeling work.

The investigation was conducted from 1980 to 1989 under the direction of the following personnel: Messrs. F. A. Herrmann, Jr., Chief of the Hydraulics Laboratory; R A. Sager, Assistant Chief of the Hydraulics Laboratory; W. H. McAnally, Chief of the Estuaries Division, Hydraulics Laboratory; J. V. Letter, Chief of the Estuarine Simulation Branch, Estuaries Division, and Technical Advisor; and Project Managers S. A. Adamec and Ms. B. P. Donnell, Estuarine Simulation Branch.

The following individuals contributed to the preparation of this report: Ms. Donnell, Mr. Letter, and Mr. A. M. Teeter, Estuaries Division, authors, and Messrs. Adamec; McAnally; D. P. Bach; and J. P. Stewart, Estuaries Division Messrs. Letter and Stewart prepared Appendix A. Ms. Melinda Wooley, contract student for the Estuarine Simulation Branch, served as preliminary editor and drafting assistant throughout the report preparation. Mrs. M. C. Gay, Information Technology Laboratory, was the editor during the preparation of this report.

Consultants to the project were Mr. H. B. Simmons, Mr. L. R. Beard, Dr. R. B. Krone, Dr. C. R. Kolb, and Mr. F. B. Toffaleti. Mr. B. J. Garrett, LMN, served as the District's project coordinator. This effort was coordinated with the US Fish and Wildlife Service and the Center for Wetland Resources, Louisiana State University, Baton Rouge, LA, through LMN.

The numerical modeling effort was initiated on the CRAY-1 computer at Boeing Computer Services, and completed on the Cyber-205 computer at Power Computing Company (formerly Scientific Information System, which was formerly Control Data Corporation), headquartered in Minneapolis, MN.

Commander and Director of WES during prepaation of this report was COL Larry B. Fulton, EN. Technical Director was Dr. Robert W. Whalin.

CONTENTS

LIST OF TABLES

LIST OF FIGURES

CONVERSION FACTORS, NON-SI TO SI (METRIC) UNITS OF MEASUREMENT

Non-SI units of measurement used in this report can be converted to SI (metric) units as follows:

Multiply	By	To Obtain
acres	4.046873	square kilometres
cubic feet	0.02831685	cubic metres
cubic yards	0.07645549	cubic metres
feet	0.3048	metres
knots (international)	0.514444	metres per second
microns	0.000001	metres
miles (US statute)	1.609344	kilometres
pounds (force) - second per square foot	47.88026	pascals-second
square feet	0.09290304	square metres
square miles	2.589998	square kilometres
tons (2,000 pounds, mass)	907.1847	kilograms

THE ATCHAFALAYA RIVER DELTA

TWO-DIMENSIONAL MODELING

PART I: INTRODUCTION

Objective

1. The objectives of the Atchafalaya River Delta investigation are to answer these questions:

   a. For existing conditions and no actions other than those already practiced (i.e., maintenance of navigation channels), how will the deltas evolve over the short-to-medium term (10-15 years) and the long term (50 years)?

   b. How will the deltas' evolution affect:

      (1) Flood stages?

      (2) Maintenance dredging of the navigation channel?

      (3) Salinity, sedimentation, and circulation in the Atchafalaya Bay system?

   c. What would be the impact of various alternatives on all of the above?

2. This report describes the technical approach and verification of the two-dimensional (2D)* numerical modeling effort, which is the most sophisticated of the predictive delta evolution methods employed in this overall investigation. The first objective of the report is to establish credibility of each of the principal models employed by demonstrating that the results of the models are verified by field observations. Secondly, it provides a detailed description of the long-term modeling approach, its strengths, limitations, and sensitivity, using the base (present) condition as an example.

Background

3. The primary driving force for the system is the supply of water and sediment from the Atchafalaya River. The river captures about 30 percent of

---

* For convenience, unusual abbreviations are listed and defined in the Notation (Appendix B).

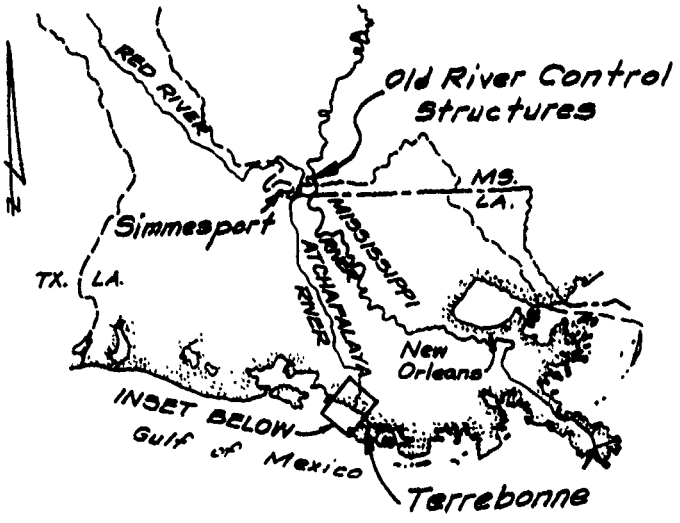

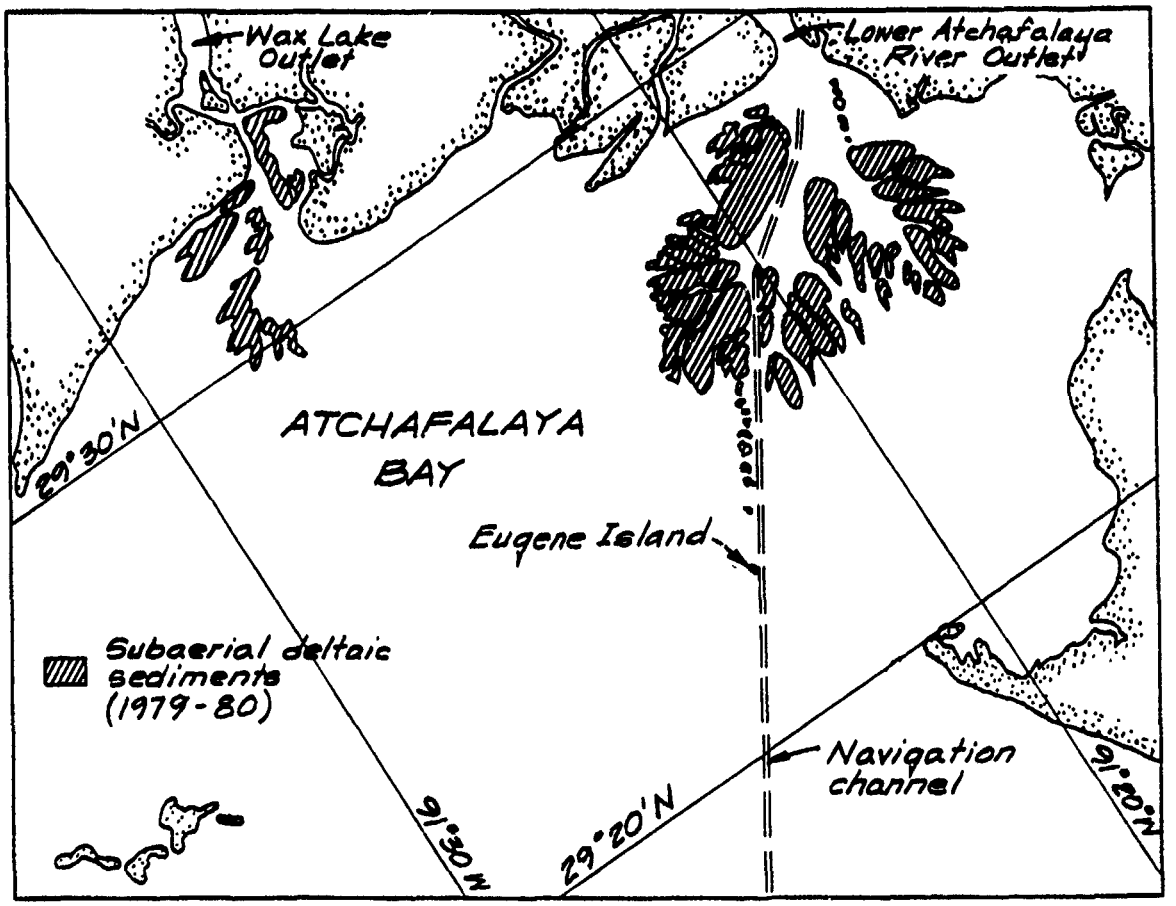

Figure 1. Vicinity sketch showing the Atchafalaya River and Wax Lake Outlet deltas

the latitude flow (combined flow of the Mississippi River and Red River at the latitude of 31 deg north) at the Old River Control Structures (Figure 1), and carries with it an average of 94 million tons* of sediment (Keown, Dardeau, and Causey 1981) in suspension each year. Progressively, the sediment load has filled in the Atchafalaya basin floodway between its natural levee systems over the past several decades and is now depositing rapidly in Atchafalaya Bay (Figure 1 enlargement). As shown, there are two deltas forming in Atchafalaya Bay: at the mouths of Lower Atchafalaya River (LAR) and Wax Lake Outlet (WLO). The evolving deltas became subaerial in 1973 and soon after vegetated. They have since become one of the most dynamic currently active delta systems in the world. The evolving deltas have converted shallow bays into marshes and continue to generate a great deal of interest in deltaic processes. The primary benefit from these two deltas has been the addition of new land to the coast of Louisiana in areas that are otherwise experiencing land loss. The primary concerns with the evolving deltas have been sedimentation in the navigation channels and backwater flooding in the surrounding low-lying coastal parishes of southern Louisiana.

4. Phenomenal growth of the subaerial Atchafalaya River delta and the emerging WLO delta led the US Army Engineer District (USAED), New Orleans, to request that the US Army Engineer Waterways Experiment Station (WES) conduct a thorough investigation to predict future growth of the deltas and effects of that growth.

Approach

5. The plan of investigation includes the following multiple techniques to predict delta growth:

a. Extrapolation of observed bathymetric changes into the future.

b. A generic analysis that predicts future delta growth by constructing an analogy between behavior of the Atchafalaya delta and other deltas in similar environments.

c. Analytical treatment of a jet discharging into a quiescent bay.

d. Quasi-2D numerical modeling of hydrodynamics and sedimentation processes.

---

* A table of factors for converting non-SI units of measurement to SI (metric) units is presented on page 6.

e. Two-dimensional numerical modeling of hydrodynamics and sedimentation processes considering riverflow, tides, Gulf levels, storm surges, wind-induced currents, wind waves, salinity currents, and subsidence.

Each of these builds upon prior work and employs progressively greater degrees of sophistication. A basic description of the overall plan is given by McAnally and Heltzel (Report 1 of this series, in preparation). Although separate reports have been published, a summary of approaches a, b, and d is given in Report 6 (McAnally et al. 1984). A list of all reports of this series is found in Table 1.

6. The 2D modeling approach used to predict the short-term (10-15 years) and long-term (50 years) evolution of the Atchafalaya River delta is the result of years of modeling development, field investigations, and model application. The models used for this study are components of the TABS-2 Numerical Modeling System.

Scope

7. This report presents the verification of the 2D modeling application to the Atchafalaya Bay and Terrebonne Marshes. Model results are compared to actual field data for several sets of discharges, tide ranges and Gulf levels. Verification includes the separate real-time simulations of the principal numerical models employed: the hydrodynamic model (RMA-2), the sediment transport model (STUDH), and the salinity model (RMA-4). In addition, the long-term evolution simulation, based on a statistical ensemble of real-time sediment transport modeling, was verified to historical delta evolution (1967-1977), and to historical LAR channel dredging volumes (1973-1985).

8. The technique used for the long-term (50-year) delta evolution is presented in detail. The Base (i.e., existing conditions) test for the long-term simulation and results of the delta evolution is examined in detail.

9. The discussion section address trends, sensitivity, and limitations of the long-term modeling approach.

Table 1

Reports in this Series*

Report No.	Reference	Subtitle	Contents
1	McAnally and Heltzel in preparation	A Plan for Predicting Delta Evolution	Methods and approach
2, Section 1	Coleman et al. 1988	Field Data: Atchafalaya Bay Program Description and Data [2 volumes]	Field data collection methods and presentation of data (4 sections)
2, Section 2	Teeter and Pankow 1989	Field Data; Settling Characteristics of Bay Sediments	
2, Section 3	Pankow, Teeter, Donnell, and Adamec 1990	Field Data: Grain Size Analysis of Selected Bay Sediments	
2, Section 4	Bensen and Donnell 1990	Field Data: Terrebonne Marshes Program Description and Data	
3	Letter 1982	Extrapolation of Delta Growth	Analytical extrapolation of historical behavior
4	Wells, Chinburg, Coleman 1984	Generic Analysis of Delta Growth	Comparison with similar deltas to identify stage of development and predict future trends
5	Thomas, Heath, Stewart, and Clark 1988	Quasi-Two-Dimensional modeling of Delta Growth and Impacts on River Stages	Quasi-Two Dimensional hydrodynamic and sedimentation river flow modeling

(Continued)

* All Atchafalaya reports are published under the main title, "The Atchafalaya River Delta," Technical Report HL-82-15, US Army Engineer Waterways Experiment Station, Vicksburg, MS.

Table 1 (Concluded)

Report No.	Reference	Subtitle	Contents
6	McAnally, Thomas, Letter, and Stewart 1984	Interim Summary Report Growth Predictions	Summary and analysis of Reports 3, 4, and 5
7	Wang 1985	Analytical Analysis of the Development of the Atchafalaya River Delta	Analytical treatment of a simple jet discharging into a quiet bay
8	Ebersole 1985	Numerical Modeling of Hurricane-Induced Storm Surge	Two-dimensional modeling of hurricane-induced storm surge
9	Ebersole 1985	Wind Climatology	Predictions of wind conditions over the bay
10	Jensen 1985	Wave Hindcasts (3 Appendices)	Modeling of locally-generated wind waves
11	Donnell, Letter and Teeter, in preparation	Two-Dimensional Modeling (1 Appendix)	Two-dimensional finite element modeling of hydrodynamics, salinity, and sedimentation
12	Donnell and Letter, in preparation	2D Modeling of Alternative Plans and Impacts on the Atchafalaya Bay and Terrebonne Marshes	Employs the tools described in Report 11, and shows the effects of plans
13	Donnell and Letter, in preparation	Summary Report of Delta Growth Predictions	Summary and analysis of all delta growth predictions conducted during this investigation

PART II: MODELS USED

Study Options*

10. Solutions to coastal and estuarine hydraulics and sedimentation problems are basically obtained by utilizing one or more of four methods: field investigations, analytical solutions, numerical models, and physical models. Choosing the method or methods which is best suited to a particular problem requires a knowledge of the physical processes causing the problem and an understanding of the strengths and weaknesses of the solution methods.

Field investigations method

11. Prototype data collection and analysis serve both as the foundation for other solution methods and as an independent solution method. Alone, field data show the estuary as it has behaved under certain conditions at the time of data measurement. By skillful data collection scheduling and careful analysis, one can obtain estimates of the separate effects of tides, river discharge, wind, and other factors. Field data can reveal problem areas, define the magnitude of those problems, and to a limited extent, estimate the estuary's response to different conditions of tide and river discharge. Field data are an indispensable element in verification of numerical and physical models.

12. Obtaining sufficient temporal and spatial data coverage in the field is a formidable and expensive task. Available field data are often too sparse to define the estuarine processes in anything but the most general terms. Field data are often looked upon as being totally accurate and reliable, when in truth, field data must be evaluated using good engineering judgment as to its reasonableness and the potential of measurement errors. Special care must be taken with field data to identify the meteorological impacts on the data. Furthermore, analysis of field data cannot provide reliable estimates of the estuary's response to proposed modifications to the estuary.

13. For a complete description of the field data collection program for the Atchafalaya Bay system, see Report 2, Section 1, in two volumes of this series Coleman et al. (1988).

---

* Paragraphs 10-12 and 14-20 have been adapted from McAnally et al. (1983).

Analytical solution methods

14. Analytical solutions use mathematical expressions to describe physical phenomena. The solutions themselves are either exact analytical solutions to some simplified differential equation or are expressions that are developed based on empiricism. Substitutions for each independent variable will determine the dependent variable. For example, Manning's equation is a simple analytical model of the complex process of energy losses in open channel flows. Analytical solution methods have the advantage of speed and simplicity, but cannot provide many details or needed accuracy for difficult problems.

15. In estuaries, analytical solutions can be used only for gross representations of tidal propagation and average cross-sectional velocities in simple geometries. Details of flow cannot be predicted. The usefulness of analytical solutions declines with increasing complexity of geometry or increasing detail of desired results.

Numerical modeling

16. Numerical modeling has evolved with the advancement in computer speed and efficiency. It includes techniques of approximation and iteration. A numerical model obtains approximate solutions to mathematical models. If a mathematical model becomes so complex that it must be solved by numerical methods, it becomes a numerical model.

17. Numerical models are grouped by the numerical method by which the equations are solved. The finite difference method (FD) approximates derivatives with differences in the value of the variable over finite intervals of space and time. This requires discretization of space and time into regular (usually) grids of computational points. FD obtains an exact solution to an approximate equation. The finite element method (FE) approximates variables with piecewise continuous mathematical expressions in space (and sometimes time) and then substitutes these expressions into the differential equations to be solved. The assemblage of all the piecewise approximations is solved as a set of simultaneous equations to provide results at specified computational points (nodes). FE obtains an approximate solution to an exact equation. The FE technique allows for a more lifelike representation of the geometry and the ability to obtain answers at any point within the computational mesh.

18. Numerical models are further classified by the number of spatial dimensions over which the variables are permitted to change. For instance, in

a one-dimensional model, currents are averaged over two dimensions (usually width and depth) and vary only in one direction (usually longitudinally). Two-dimensional models average variables over one spatial dimension. For instance, the TABS-2 models are "horizontal" models, meaning that variables are averaged over depth.

19. Numerical models provide much more detailed results than analytical methods, but do so at the expense of time and money. If a numerical model has been well formulated and verified for a given area, it can be easily modified to provide results for different conditions.

Physical models

20. Scaled-down replicas of estuaries have been cast in concrete and used for many years to solve coastal and estuarine hydraulic problems. Distorted physical models have successfully been used to model tides and three-dimensional variations in current. However, physical models fail to model certain aspects of sedimentation, particularly for silts and clays. The primary disadvantage of physical models is that they can be costly and inflexible in addressing a shifting study emphasis.

21. The Mississippi Basin physical model (MBM), which contains the Atchafalaya Bay estuary, was used to provide verification data for the Multiple Channel Model (MCM) discussed in Report 5 of this series (Thomas et al. 1988), and additional corroboration in checking the boundary conditions and water-surface profiles for the TABS-2 models (described in the following section).

TABS-2 Finite Element Numerical Modeling System

22. Accurate prediction of delta growth required that sedimentation processes of transport, erosion, deposition, and consolidation were properly represented for the two major classes of sediments: cohesive and noncohesive. Both classes appear in the bay area in sufficient quantities to require inclusion in the analysis. Predicting sedimentation processes also required prediction of sediment supply, water-surface elevations, circulation patterns, and wind-wave mixing. These processes can be addressed appropriately in Atchafalaya Bay by a 2D treatment that integrates over depth. One possible exception is sediment and salinity transport in the relatively deep navigation channel where multiple layers would be required to model stratification which

may occur at high riverflows. The overall 2D approach was appropriate because field observations showed stratification to be mild and limited in duration.

23. Because of the unusually long time frame of the investigation, it was desirable to have the flexibility to modify the approach as new and innovative technology became available without beginning anew. The FE method provided that flexibility by allowing arbitrarily shaped triangles or quadrilaterals (elements) to discretize the modeling domain and permitting addition of new elements and subdivision of existing elements at any time. These elements are composed of corner and midside nodes (Figure 2) at which model results are output. The FE solution, however, is a continuous solution in space and time over each element.

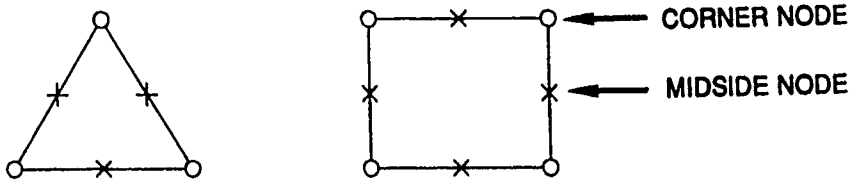

a. Triangular element: three corner and three midside computational points

b. Quadrilateral element: four corner and four midside computational points

Figure 2. Triangle and quadrilateral 2D elements

24. The 2D FE numerical modeling system used for this project, TABS-2, was developed by the Estuaries Division and the Waterways Division of the WES Hydraulics Laboratory and Resource Management Associates, Lafayette, CA. It is a generalized numerical modeling system used for hydraulic engineering studies in rivers, reservoirs, estuaries, and bays. TABS-2 consists of three generalized computer programs used to model 2D hydrodynamics (RMA-2), transport (RMA-4), and sedimentation (STUDH), plus numerous utility programs to form a complete numerical modeling system. TABS-2 has the capability of wetting and drying areas of the computational mesh to simulate the water level. This feature was of particular importance for the Terrebonne Marshes area. For a detailed description of TABS-2, see Thomas and McAnally (1985).

RMA-2 hydrodynamic model

25. RMA-2 (version 3.3B) is a time-dependent, nonlinear, 2D, horizontal model for open-channel hydrodynamics. The model solves the depth-integrated

x- and y-momentum equations along with the continuity equation (Reynolds form of Navier-Stokes equations). An eddy-viscosity formulation is used for turbulent exchanges of momentum. Other terms in the momentum equation include gravity bottom friction, Coriolis effects, and surface wind stress. Bed friction is calculated with Manning's equation. The program allows for the turbulent exchange coefficients to be specified in a local coordinate system for each element. This permits an exchange coefficient for directions parallel to and perpendicular to the predominant direction of flow.

26. This version of the hydrodynamic model permits simulating wetting and drying by adding or deleting elements from the computational solution. For instance, if one or more nodes of an element are determined to be less than the critical depth (typically 0.275 ft), then all elements involving that node are removed from the solution and the area is designated "dry." "Rewetting" occurs when all nodes within an element are projected to be satisfactorily deep (typically 0.60 ft).

27. Another feature developed in the hydrodynamic model was a non-reflecting boundary module. The method of characteristics in conjunction with the linearized long wave equation is used to define the reflected wave as a combination of the tide and velocity fluctuations. The estimate of the reflected wave is then set to zero. The module requires a steady-state initialization using the velocity specification and stores the computed steady-state depth from the inflow. In dynamic mode, the module uses the water-surface elevation computed at the downstream end of the inflow element and a quadratic extrapolation to find an effective depth at the inflow. The inflow velocity is adjusted using a shallow-water wave speed based on the difference between the steady state and dynamic effective depth at the inflow. The quadratic extrapolation was found to be more stable than using RMA-2's computed inflow depth.

28. Results from RMA-2 consist of water depths and current velocities at each computational point. However, water levels, velocities, and discharge results can be displayed at any location within the area modeled based on the solution being continuous in space. The optimal forms of output consist of printed tables, time-history plots, contour plots, factor maps, and velocity vector plots.

STUDH sediment transport model

29. STUDH is a 2D, vertically integrated, horizontal, sediment

transport, FE model. The model has the capability of addressing either cohesive (silt and clay) or noncohesive (silt and sand) sedimentation processes. The model solves the 2D convection diffusion equation with bed source/sink terms. A structured bed layering with consolidation can be specified. It requires water level and velocity results from RMA-2 as input.

30. MUXTRAP. Although STUDH is capable of relatively long-term simulations by a run-extrapolate-run sequence, "long-term" is typically days or weeks. For the Atchafalaya Bay numerical modeling, long-term meant decades to half a century. To address these truly long-term issues, a tool (or program) called MUXTRAP (multiple event extrapolation) was developed. MUXTRAP statistically combines multiple short-term STUDH simulations (called events) of bed elevation change at each node in the computational mesh. MUXTRAP then extrapolates this short-term bed change into long-term predictions of bed change while including the effects of subsidence, bay channel navigation dredging/disposal, and inhibited deposition of sediments caused by waves. Output from this program includes minimum and maximum subsidence values over space, total sediment volume above an arbitrary datum, average deposit thickness by defined zone, channel dredging and disposal information, and an updated geometry input file to be used for analysis or additional circulation modeling with RMA-2.

31. MUXTRAP can operate on as many as 10 STUDH concentration-bed change results files (i.e., 10 events) normally produced from short-term real-time simulations. For the purposes of this study, an event implies a tidal cycle simulation of a given discharge, Gulf level, and sediment characteristic. The program extrapolates to user-selectable units of time: seconds, hours, days, weeks, months, or years. The option of selecting a rectangular region (i.e., window) within which to extrapolate was employed. The long-term extrapolation window selected for this investigation is shown in Figure 3 and is defined by Louisiana state grid coordinates XMIN = 1,859,885.0 ft; XMAX = 2,044,730.0 ft; YMIN = 170,495.0 ft; YMAX = 336,640.0 ft. The inset window is called the verification window and was used to compare results with previous work accomplished within this series of reports. In addition, the user may request special treatment within the window. The following special treatments were used for the Atchafalaya-Terrebonne Marshes numerical modeling study: omit

---

* All elevations (el) cited herein are in feet referred to the National Geodetic Vertical Datum (NGVD).

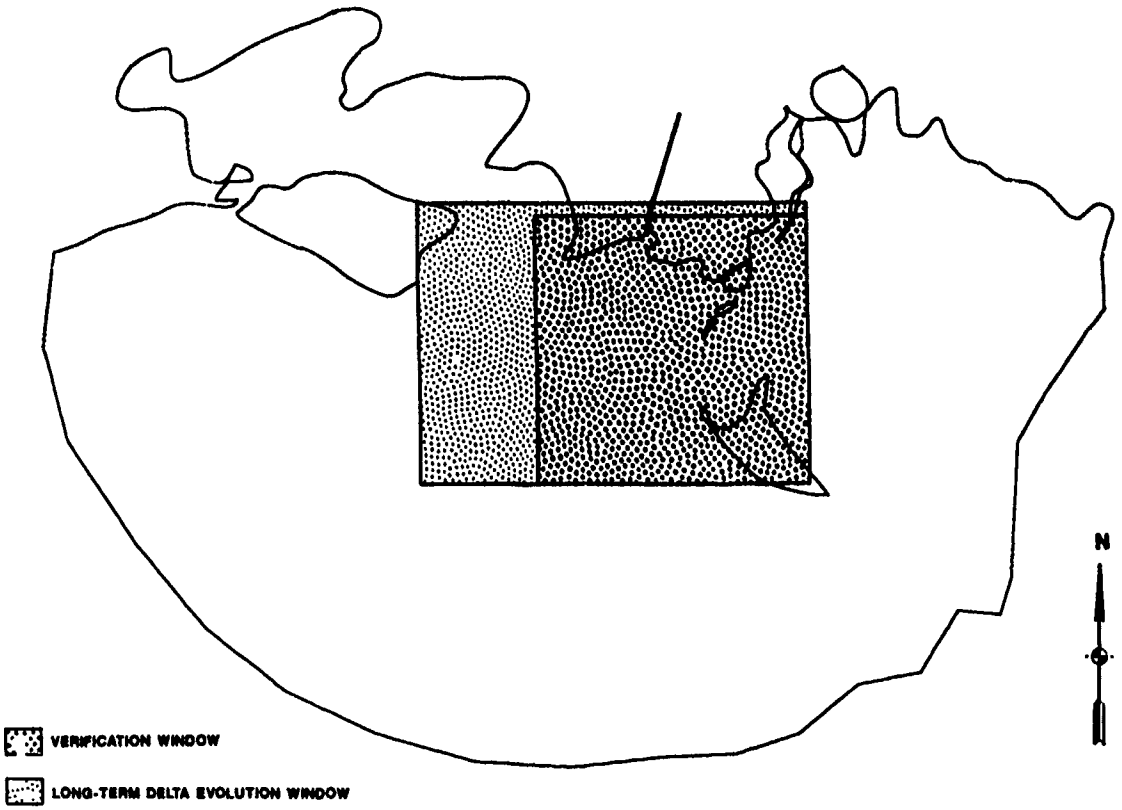

Figure 3. Numerical model extrapolation windows

special locations from extrapolation (such as the marshes east of LAR); do not allow deposition resulting in subaerial growth to exceed +2.5 ft (delta and dredge disposal zones); limit erosion to 50 ft; select locations for dredging (LAR bay channel); select locations for dredged material placement (3,000-6,000 ft either side of LAR channel), select locations exposed to wave redistribution of deposits (outer Gulf); and apply spatially varying apparent subsidence to the area (see Appendix A of this report for subsidence analysis).

32. SEDDIST. For purposes of analysis of the distribution of sediment supply in the Terrebonne Marshes, a tool (or program) called SEDDIST was designed. It examines the concentration-bed change final results file of one STUDH event simulation and calculates the sedimentation distribution for given zones defining the areas of interest. The sedimentation distribution is defined in percent as the ratio of sediment accumulating in a zone by the total amount of sediment entering the entire system over a tidal cycle. Input data consist of a listing of the elements defining the zones as well as the associated frequencies (days/year) for each event. Output from this program is printed in tabular form and gives the following statistics for each zone: wet areas, dry areas, mean and standard deviation of deposition, volume of

sediment entering the zone per unit of time, rate of deposition or erosion, rate of subsidence, and the sedimentation distribution.

RMA-4 water quality model

33. RMA-4 is a 2D, horizontal, depth-integrated, FE model used in modeling salinity, pollutant spread, and residence time calculations. The model solves the conservative form of the convection diffusion equation, with first-order decay of constituents. It requires as input the FE mesh and velocity field results from RMA-2. Results consist of concentrations at computational points. The forms of output consist of printed tables, a time-history plot for a location, contour plots, and factor maps.

Mesh Description

34. The Atchafalaya-Terrebonne Marshes study was an effort which evolved with time, experience, and requirements for the study of alternative plans. As the study evolved, so did the computational meshes on which the 2D modeling was performed.

MESH1

35. The 2D numerical modeling effort began in 1981 with a basic coarse-resolution FE mesh of the Atchafalaya Bay with 1977 bathymetry, MESH1 (Figure 4). MESH1 geographically spanned from Morgan City, LA, to the Gulf of Mexico, and from Vermilion Bay to Fourleague Bay. MESH1 contained 1,084 nodes and 304 elements and was used primarily as an economical steppingstone toward hydrodynamic verification. MESH1 was the common building block of all of the numerical modeling work.

MESH2

36. MESH2 was a finer resolution mesh of the Atchafalaya Bay. It had a total of 2,017 nodes and 589 elements with the majority of additional resolution in the vicinity of subaerial delta growth. The geographical boundaries and bathymetry of MESH2 were the same as MESH1. Figure 5 shows MESH2 overlaid upon a map of the area. MESH2 was used for extensive hydrodynamic verification to 1981 and 1982 prototype data for several discharges and tide ranges. In addition it was used for sedimentation verification of subaerial delta growth patterns over a 10-year period (1967-1977). To accomplish the 10-year delta growth verification, MESH2 was temporarily modified and named MESH2-67 because it contained 1967 bathymetry.

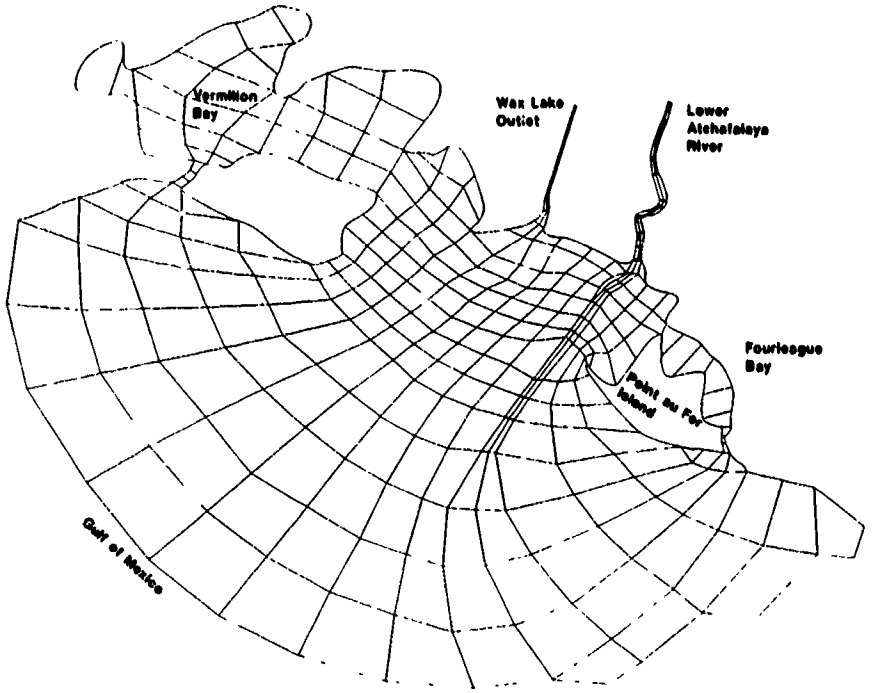

Figure 4. Numerical computational MESH1 for the Atchafalaya Bay, 1,084 nodes, 304 elements

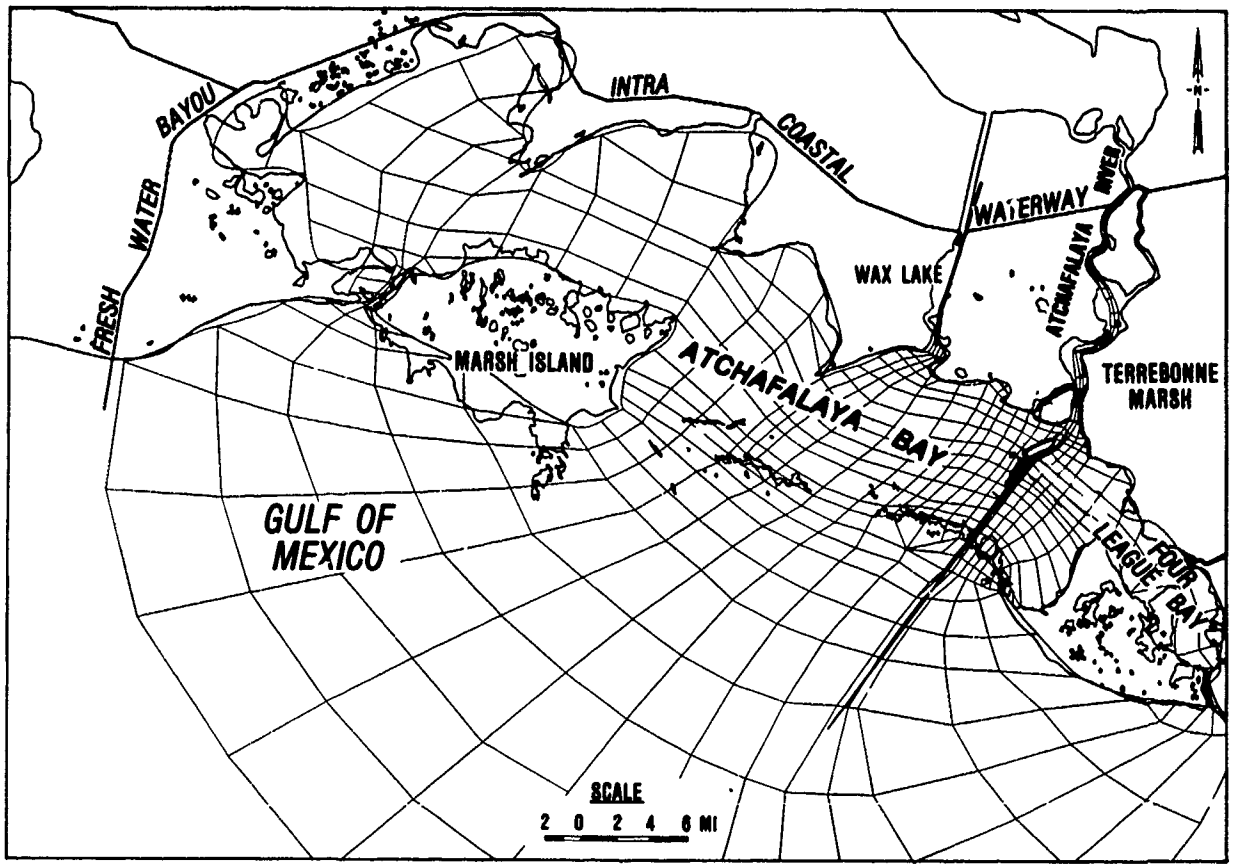

Figure 5. Numerical computational MESH2 (2,017 nodes and 589 elements) for the Atchafalaya Bay

MESH3

37. MESH3 was an expansion of MESH2 with additional resolution to define th marshes between the LAR and WLO. It was not used beyond the initial testing phase due to the state of the art of wetting and drying capability at the time.

MESH4

38. In 1983, when the Terrebonne Marshes modeling effort was proposed by the New Orleans District, MESH1 had been verified to hydrodynamics. Because a numerical model is capable of providing results only within the confines of the computational mesh, it was again necessary to make modifications. To form the western boundary of MESH4 (Terrebonne Marshes computation mesh), MESH1 was divided between LAR and WLO and tapered to the Gulf 20-ft contour. A schematization of existing bathymetry from 1983 surveys of the major bayous, lakes, canals, and marshes east of the LAR was added. The Terrebonne Marshes mesh contained 2,361 nodes and 777 elements. MESH4 geographically spanned from Lake Palourde to the Gulf of Mexico, and from East Bay to Bayou du Large. Figure 6 shows MESH4 with appropriate shading depicting areas of land, marsh, and open water for the low-discharge verification event. MESH4 received its open-water boundary conditions from like runs of MESH1 using a technique called JOBSTREAM. This mesh was used primarily to economically verify and test the wetting and drying feature of the hydrodynamic model, RMA-2, and the sediment transport model, STUDH, for the Terrebonne Marshes.

MESH6

39. In 1986 much of the modeling groundwork had been completed: sufficient field data were available, hydrodynamic verification for water levels and velocity was complete for both Atchafalaya Bay (MESH2) and for Terrebonne Marshes (MESH4), sedimentation verification for 10-year delta growth predictions was performed for Atchafalaya Bay (MESH2), the wetting and drying capability was demonstrated to be effective, knowledge of the study area was established, and a technically sound plan for long-term delta growth simulation was determined. At this time it became clear that the most efficient way to model both the Atchafalaya Bay and the Terrebonne Marshes was to combine the two areas into one computational network. MESH6 (Figure 7) is so named because it was initially a combination of MESH2 and MESH4. The external boundaries of MESH6 spanned from Lake Palourde to the Gulf of Mexico, and from Vermilion Bay to Bayou du Large near Houma, LA. It contained 3,999 nodes and

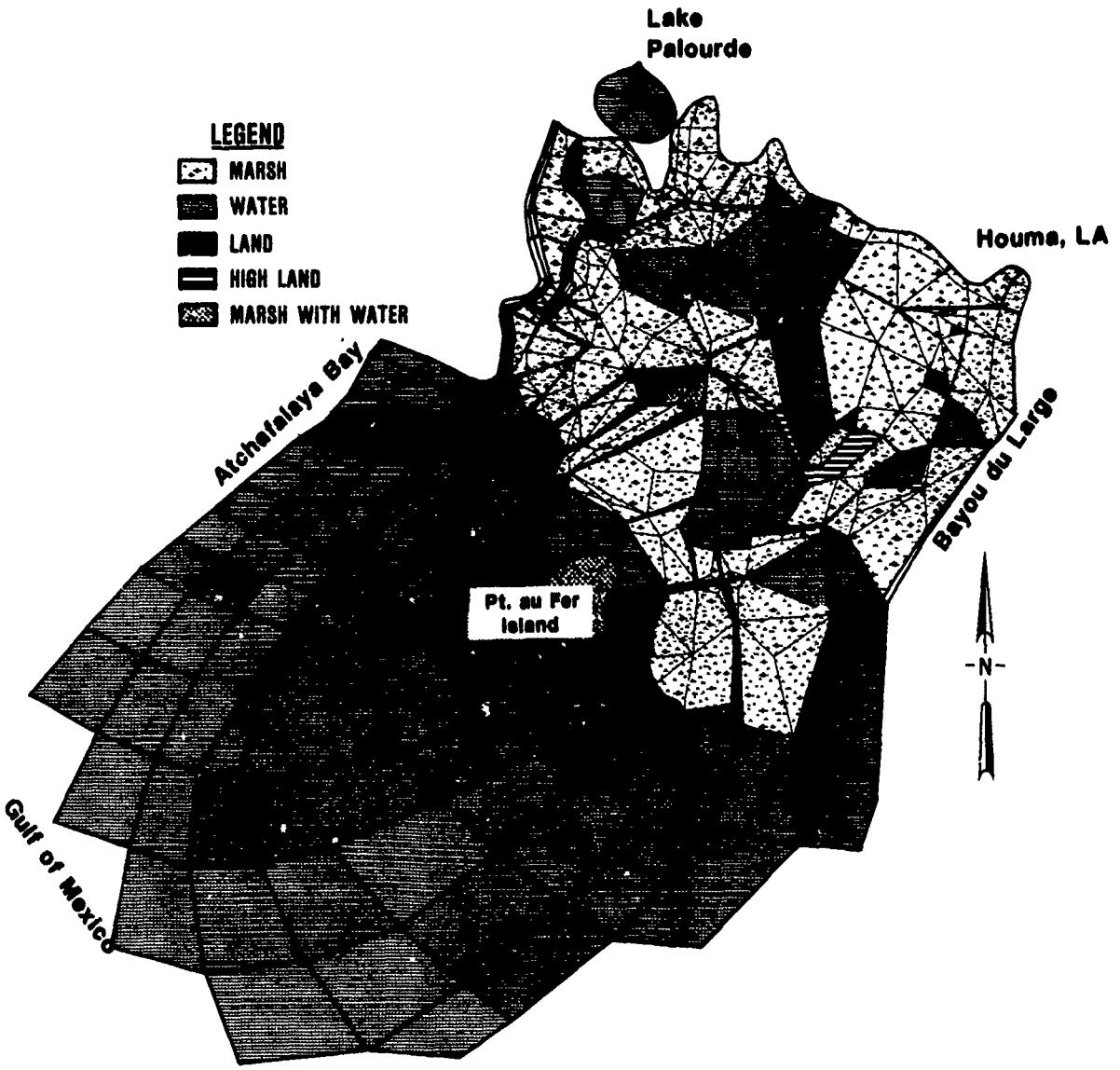

Figure 6. Numerical computational MESH4 for the Terrebonne Marshes of the Atchafalaya Bay system, 2,361 nodes and 777 elements

1,278 elements. MESH6 underwent one verification check to ensure that the combined computation mesh still performed up to verification standards. MESH6 was used extensively for testing alternatives without dredged material disposal.

MESH7

40. For testing alternatives involving dredged material placement, it was necessary to add sufficient resolution along both sides of the LAR navigation channel within the bay proper. This additional resolution allowed for

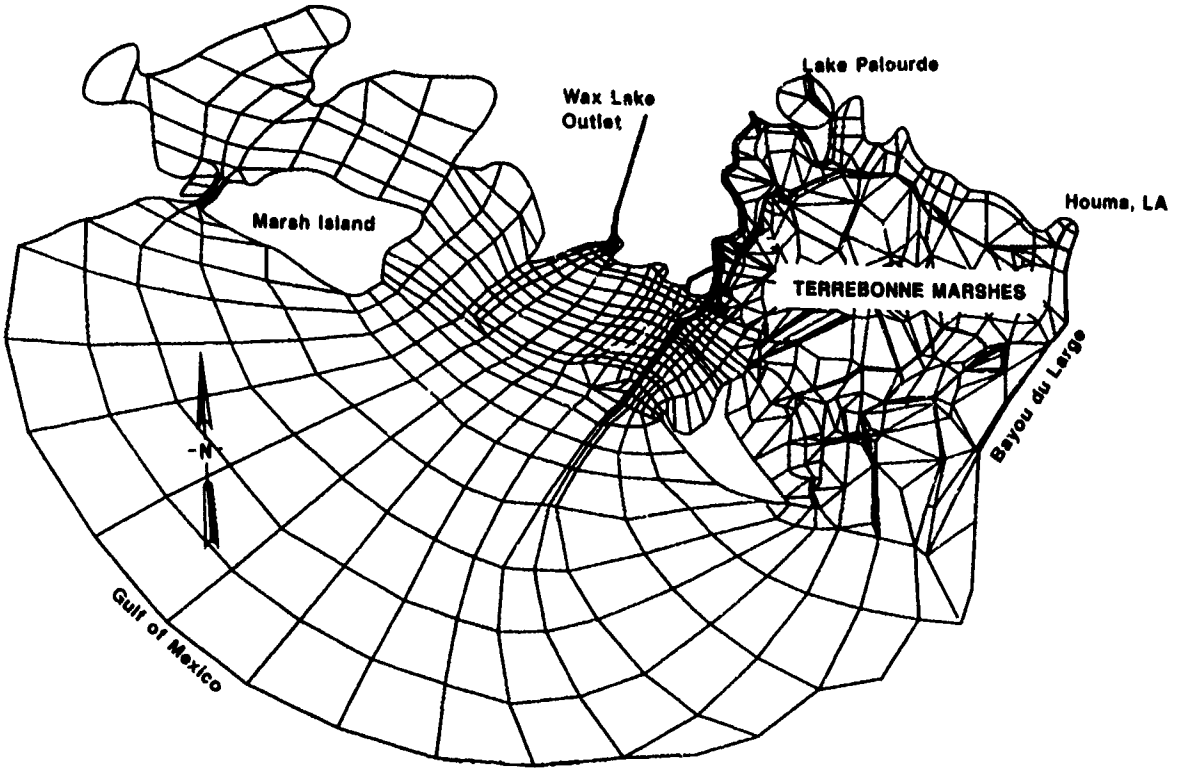

Figure 7. Numerical computational MESH6 for the Atchafalaya Bay and Terrebonne Marshes, 3,999 nodes and 1,278 elements

dredged material placement 3,000 ft along either side of the channel from the coastline to Eugene Island. The Atchafalaya Bay also received additional resolution in areas where previous simulations had stability problems due to "semisubaerial" delta wetting and drying. Figure 8 shows MESH7 to have 4,694 nodes and 1,539 elements. This mesh was also used to verify the sediment transport model to individual events associated with field observations of suspended sediment concentrations for the period 1980-1981.

41. Midway into the long-term predictions of the delta growth the disposal areas filled to capacity. A modification was necessary to allow for additional disposal area.

MESH8

42. After consultation with the New Orleans District concerning the infilling of the 3,000-ft disposal areas, MESH7 was modified to widen the disposal areas to 6,000-ft and to extend those areas to Bar Reach 2. Figure 9 shows the revision, MESH8, with a detailed view of the Atchafalaya Bay channel. The refined MESH8 schematization of the Atchafalaya Bay-Terrebonne Marsh

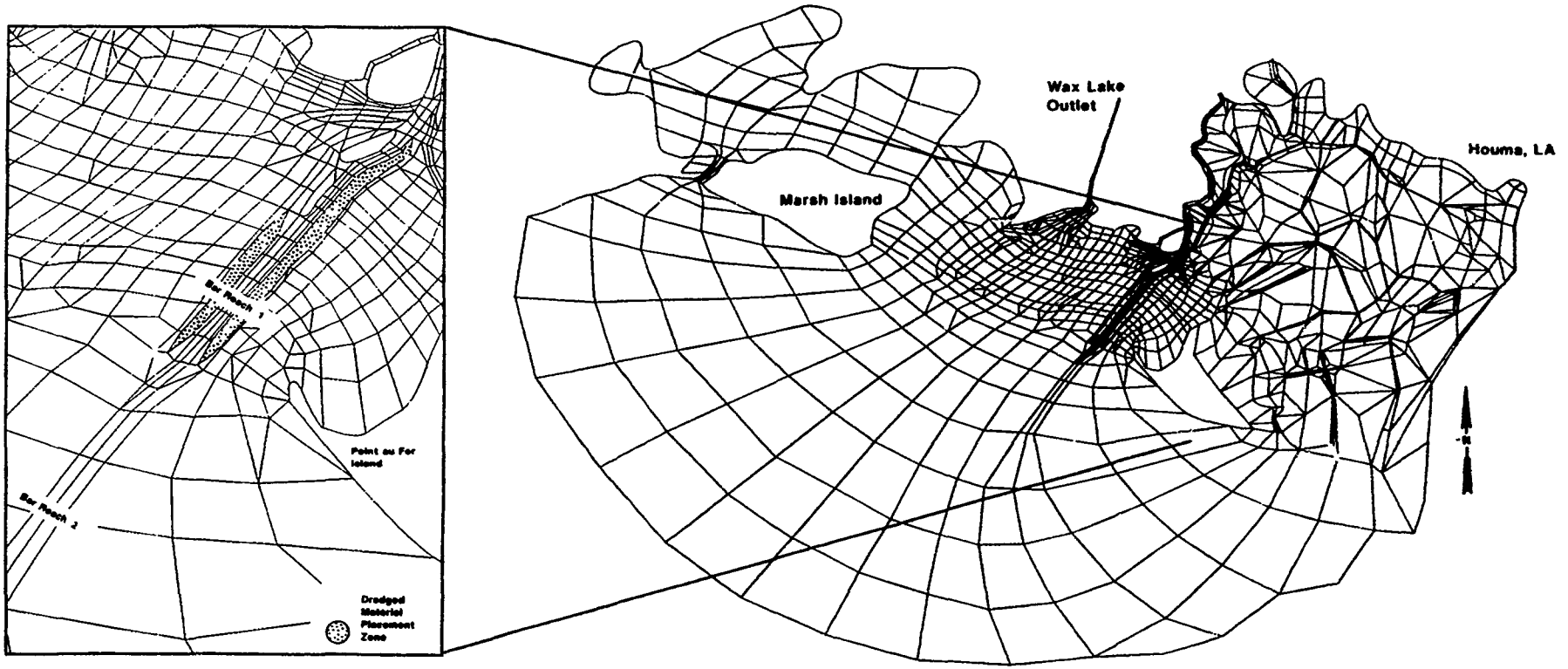

Figure 8. Numerical computational MESH7 for the Atchafalaya Bay and Terrebonne Marshes with a 3,000-ft -wide dredged material disposal zone (inset) 4,694 nodes and 1,539 elements

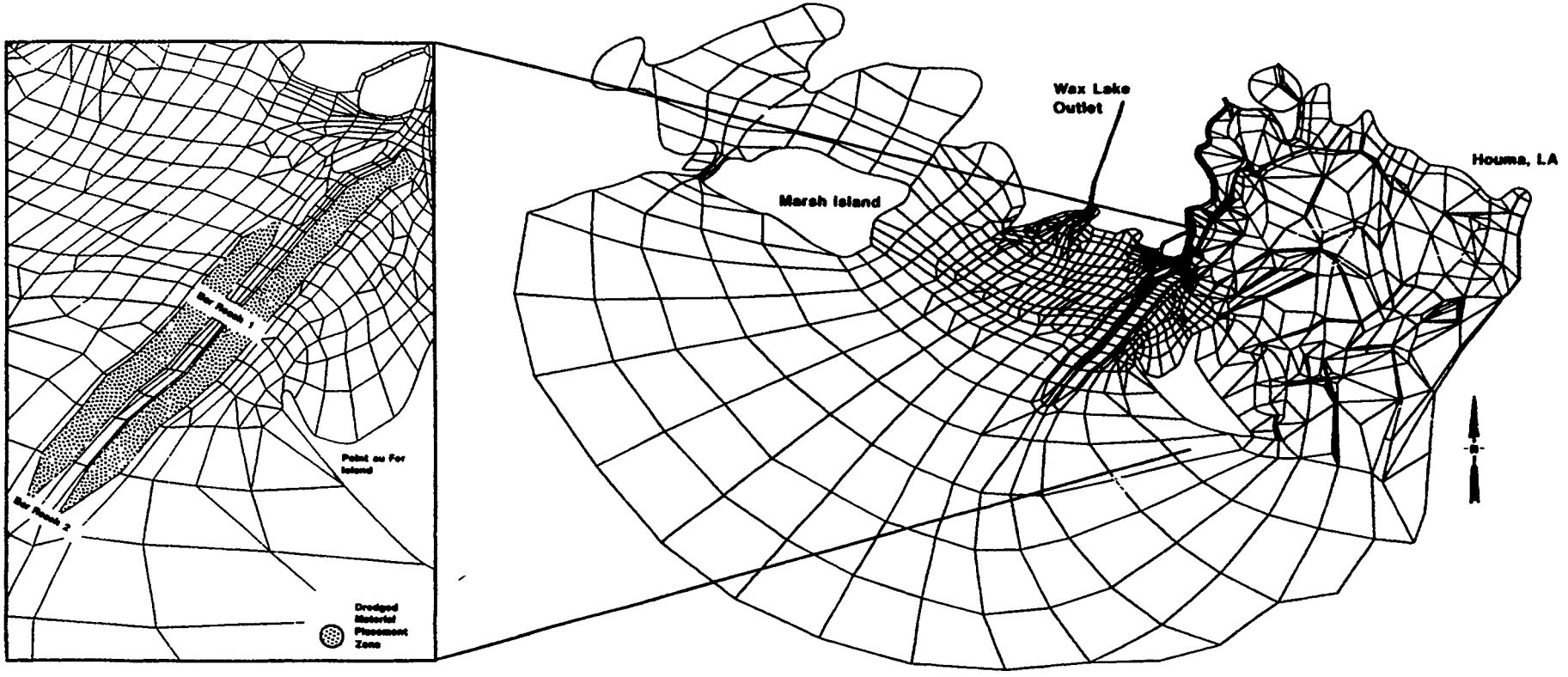

Figure 9. Numerical computational MESH8 for the Atchafalaya Bay and Terrebonne Marshes with a 6,000-ft-wide dredged material disposal zone to Bar Reach 2 (inset), 4,806 nodes and 1,583 element

computational network, with 4,806 nodes and 1,583 elements, was used for delta growth predictions in years 30 and 50.

MESH9

43. In 1988, MESH9 was developed to test the project flood flow in the Atchafalaya Basin. MESH9 (Figure 10) consisted of the same basic resolution of MESH8 except with an additional western overbank area along the LAR. MESH9 consisted of 1,735 elements and 5,217 nodes.

44. These meshes provided an expanding capability to simulate the long-term evolution of the delta and subsequently provided a basis for isolating and identifying the impacts of various individual aspects of man's control efforts on the system.

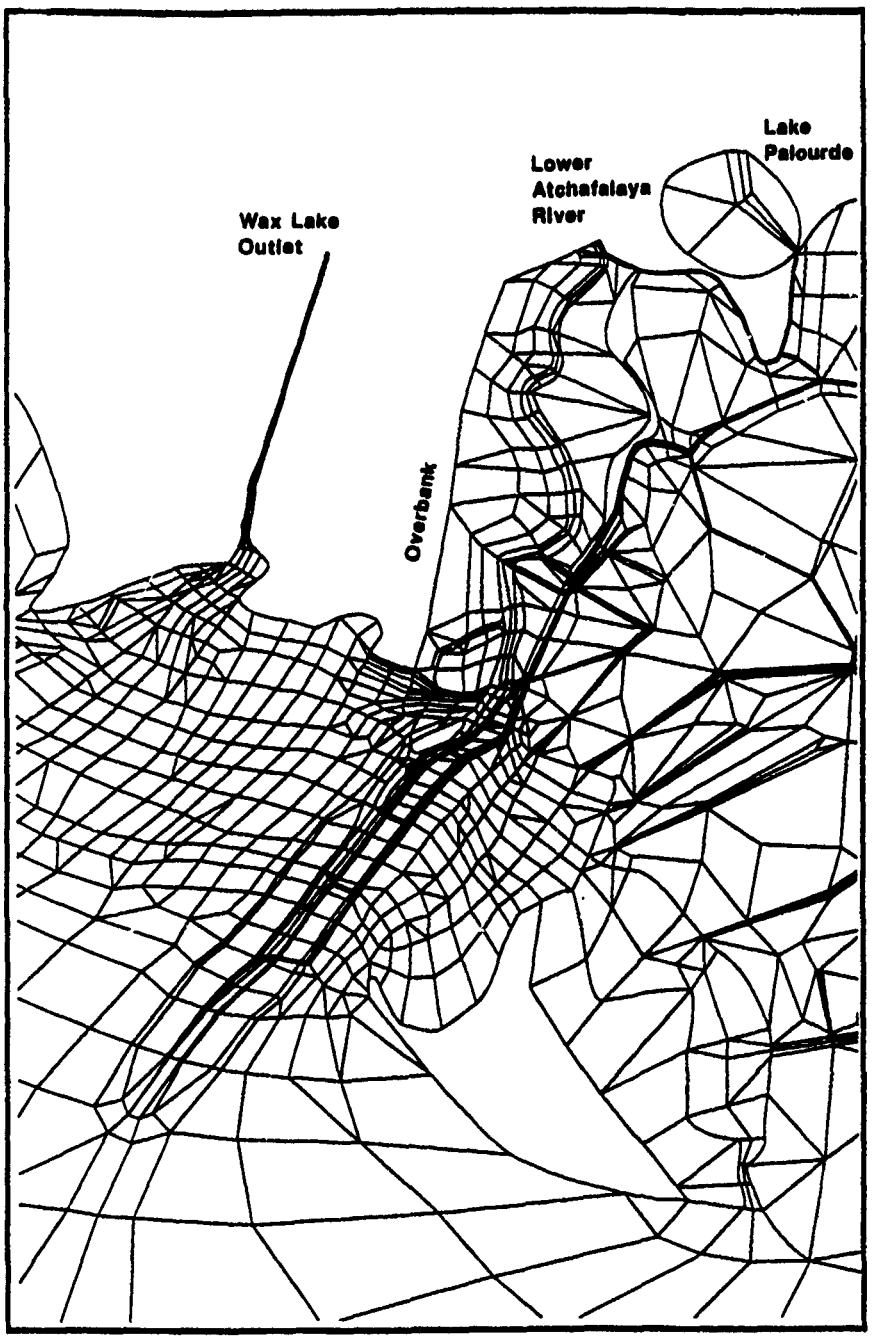

Figure 10. Numerical computational MESH9, used to investigate project floods, 1,735 elements and 5,217 nodes

PART III: HYDRODYNAMIC VERIFICATION

Purposes

45. Hydrodynamic verification will be presented in sections. The first verification concerned the Atchafalaya Bay MESH1 and MESH2, described earlier, in conjunction with the 1980-1983 field data collection efforts within the surrounding open estuarine waters. The second section describes the union of the Atchafalaya Bay with the Terrebonne Marshes and its verification to additional field data collected from 1983 to 1986 within the marshes east of the LAR and associated bays. The objective of hydrodynamic verification is to reproduce observed water levels and current patterns.

Atchafalaya Bay Hydrodynamic Verification

46. The first section of the hydrodynamic verification was concerned with the geographical areas described earlier by MESH1 and MESH2 (Figures 4 and 5, respectively). The Atchafalaya Bay is a part of a broad, shallow bay complex which includes an inshore estuarine area of about 1.6 billion square metres (17 billion square feet) and has a mean depth of 1.7 m (5.5 ft). Its average annual inflow has been 5,130 cu m/sec (181,000 cu ft/sec). Average monthly flows reach 9,200 cu m/sec (325,000 cu ft/sec) in April and decrease to 2,070 cu m/sec (73,000 cu ft/sec) in September.

47. All numerical models require field data for purposes of verification, and for this effort very little prior information was readily available. A field data collection program was initiated.

Field data (1980-1983)

48. Report 2, Section 1, of this series (Coleman et al. 1988) describes in detail the data collected for use in development and verification of numerical and physical models employed to predict the evolution of the Atchafalaya Bay deltas. Only the data pertaining to hydrodynamic verification will be discussed here.

49. Tides. Tide stations were located throughout the system as indicated in Figure 11. Data were continuously recorded at 15-min intervals using Fisher-Porter gages.

50. Velocities. Velocity station locations for the verification periods

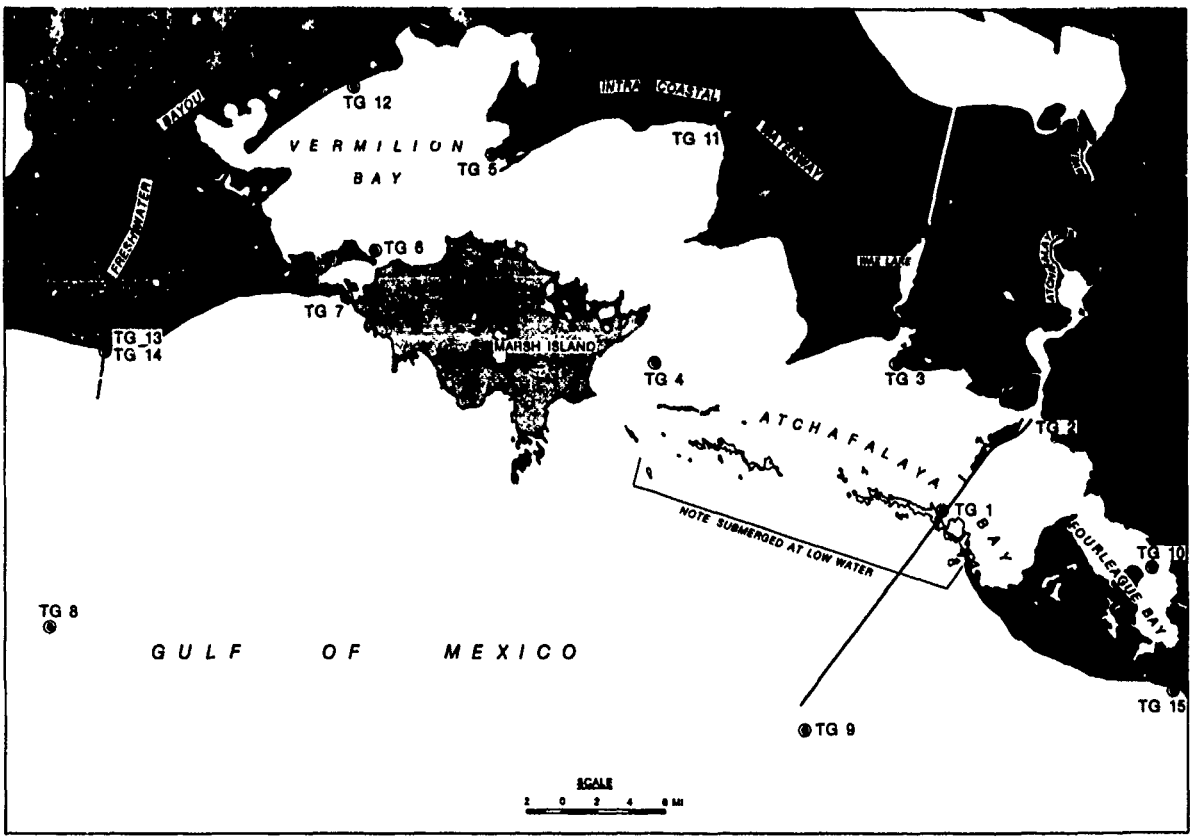

Figure 11. Tide gage locations from 1980 to 1983

listed in Table 2 and discussed in paragraph 56 are shown in Figure 12. Current magnitude and direction were recorded at 2-min intervals using Endeco moored meters.

51. Bathymetric data. Corps of Engineers surveys were used where available to set the bed elevations within the computational mesh. Gaps in the data were filled in by digitizing contours on National Ocean Survey (NOS) navigational charts. Charts 11349 (April 1977), 11351 (February 1977), and 11356 (January 1975) were used.

52. Soundings of the Atchafalaya Bay proper were made by the Corps of Engineers. The surveys were conducted in years 1967 and 1977, and adjusted for tidal variation during the survey by Louisiana State University.

53. Additional data. Data from the MBM and the MCM (each described in Report 5 of this series (Thomas et al. 1988)) were used to adjust the water-surface profiles in the LAR and WLO for each river inflow boundary condition.

Approach

54. Initial steps toward hydrodynamic verification began with the coarse-resolution Atchafalaya Bay computational MESH1, described earlier.

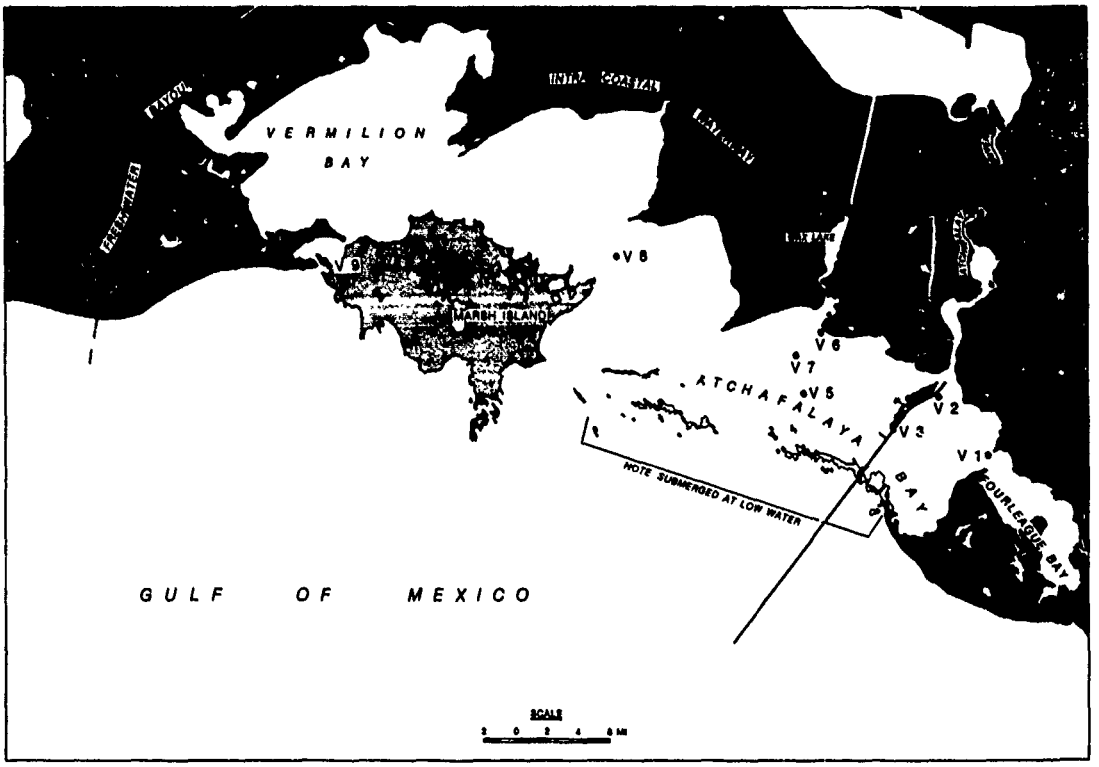

a. Atchafalaya Station Locations, Velocity Survey 1 (July–August 1980)

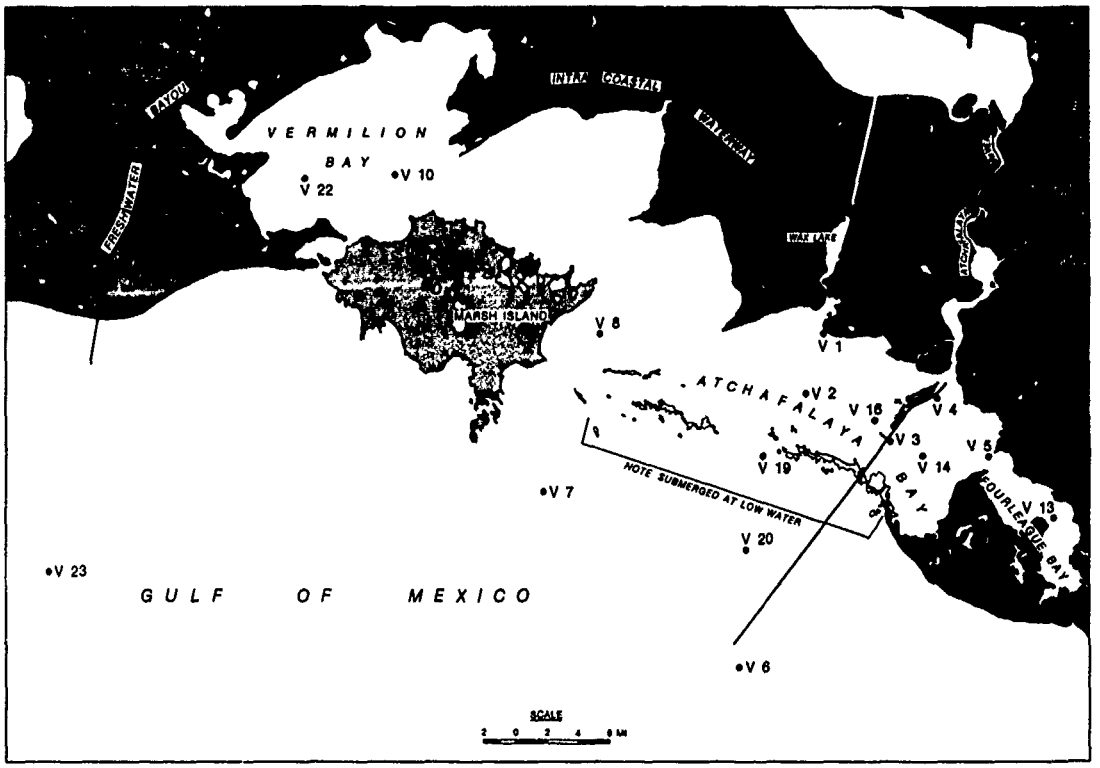

b. Atchafalaya Station Locations, Velocity Surveys 2 through 5 (January–March 1981, June–July 1981, June–August 1982, January–June 1983, respectively)

Figure 12. Velocity station locations from January 1981 to June 1983

With the onset of the 10-year delta evolution sediment verification, it became apparent that additional resolution would be required to describe the new subaerial land. The fine-resolution Atchafalaya Bay computational MESH2, described earlier, satisfied that requirement. Therefore, the complete hydrodynamic verification using MESH2 will be presented in this section.

55. Computational MESH2 developed. The 1977 bed elevations from the NOS charts and Corps surveys were smoothed in MESH1 and MESH2 to avoid numerical instabilities and to better maintain the cross-sectional areas where the meshes had coarser resolution. Additionally, the delta areas within MESH2 were shallowed much more than the 1977 survey indicated because an aerial inspection showed the delta had grown from the time the soundings were taken to the time the hydrodynamic data were collected. Therefore, the bathymetry of MESH2 was more indicative of 1980 conditions.

56. Verification periods selected. Verification runs using RMA-2 were made for periods when the best data were available. Items such as the number of field sampling stations in operation, low wind conditions, combined discharge of the LAR and WLO, and tidal conditions were criterion used in the selection process for verification. Table 2 shows the selected periods and the prototype conditions.

Table 2

RMA-2 Verification Periods for MESH2

Starting		Combined	Tide	
Date	Time	Discharge, cfs	Range, ft	Type
1/13/81	0700	50,000	1.7	Mean
6/27/81	1200	330,000	2.3	Mean
6/29/81	2300	330,000	3.1	Spring
6/18/82	1200	320,000	2.7	Spring

57. Tables 3 and 4 indicate the available tide and velocity data, respectively, available for each verification period.

58. Synthesized Gulf boundary conditions. Water-surface elevations at the model's ocean boundary were computed using the coefficients obtained from harmonic analysis of tidal data. Harmonic analysis was performed on the field data to filter noise and to calculate harmonic constituents used in setting

Table 3

Available Tide Data for Each Verification Period

Station	Starting Date for Period			
	1/13/81	6/27/81	6/29/81	6/18/82
TG 1	*	*	*	*
TG 2	*	*	*	*
TG 3	*	*	*	*
TG 4	*	*	*	*
TG 5	*	*	*	*
TG 6	*	*	*	
TG 7	*	*	*	
TG 8	*	*	*	
TG 9	*	*	*	
TG 10	*		*	
TG 11	*	*	*	*
TG 12	*	*	*	*
TG 13	*			
TG 14		*	*	*
TG 15		*	*	

Table 4

Available Velocity Data for Each Verification Period

Station	Starting Date for Period			
	1/13/81	6/27/81	6/29/81	6/18/82
V 1	*	*	*	*
V 2		*	*	*
V 3	*	*	*	*
V 4	*	*	*	*
V 5				
V 6	*			*
V 7				
V 8	*			*
V 14		*	*	*
V 16		*	*	*

ocean boundary conditions for RMA-2. Six primary constituents were extracted from tidal analysis: M2, S2, N2, K1, O1, and P1. These components are described as follows:*

* For a discussion of tidal constituents, see Neuman and Pierson (1966), page 310.

a. M2 semidiurnal principal lunar with period of 12.42 hr.

b. S2 semidiurnal principal solar with period of 12.00 hr.

c. N2 semidiurnal larger lunar elliptic with period of 12.66 hr.

d. K1 lunisolar diurnal with period of 23.93 hr.

e. O1 principal lunar diurnal with period of 25.82 hr.

f. P1 principal solar diurnal with period of 24.07 hr.

Amplitude and phase of these constituents were interpolated at boundary nodes to create a synthesized ocean boundary condition.

59. Nonreflecting riverine boundary module. During the initial model runs, constant velocity or unit discharge specifications were attempted at Calumet and Morgan City. These constant specifications caused a large amount of reflection during tidal simulations. The velocity specification was found to be much more stable than the unit discharge specification because the RMA-2 model solves discharge as one of its primary variables. To overcome the reflection, the nonreflecting boundary module was used, as described in Paragraph 27.

60. Coefficients. The Manning's n value was generally 0.025. For MESH1 and MESH2, the roughness was raised in the delta area between LAR and WLO. Roughness was individually adjusted in the LAR and WLO to match the water-surface profile calculations to those of MBM and MCM.

61. Eddy viscosities were generally assigned by element size with a value of 400 lb-sec/ft^2 for the smaller elements and 750 lb-sec/ft^2 for the larger elements. Because of the high energy in LAR and WLO, a value of 500 lb-sec/ft^2 was assigned in these reaches even though the element size was small.

62. RMA-2 time-step. Fifteen, thirty, and sixty-minute time-steps were tested using MESH2. The 15- and 30-min time-steps produced identical results, but minor differences were apparent at the hourly time-step. Consequently, MESH2 used the 30-min time-step for verification.

63. RMA-2 spin-up. Model spin-up is a term used to measure the amount of model time required for a model to repeat a tidal cycle and to eliminate effects of initialization. For MESH2 there was an 8-hr model spin-up at Eugene Island (station 1, Figure 11).

Results of MESH2

64. Plates 1-22 compare dynamic numerical model results with actual field data values and synthesized calculations of water surface and velocity.

The synthesized field data were generated at station locations by interpolating phase and amplitude of each harmonic constituent and summing all constituents. For the field stations near the LAR and WLO, too much riverine influence occurs for application of the analysis technique. No synthesized calculations were made for tide station 10, as this station was not in operation during the period that the harmonic analysis was conducted. The model results lie roughly between the curves for actual and synthesized data and show generally good to fair agreement. The only exception appears to be that the model velocities at station 4 (near the delta building edge of LAR) were higher than those measured in the field.

Atchafalaya Bay and Terrebonne Marshes Hydrodynamic Verification

65. The Terrebonne Marshes study was an adjunct to the Atchafalaya Bay investigation. Its purpose was to predict the effects of delta growth on the western Terrebonne marshes, and to study various alternatives, particularly those concerning the Avoca Island Levee. The New Orleans District authorized hydrodynamic verification of the Terrebonne numerical model to be performed to a limited extent to reproduce water levels and flows within the marsh. (Poor knowledge of the water depths and the ability to model wetland did not justify the efforts of a rigorous verification). MESH4 was the economical choice for verification of the marshes. Upon completion of marsh verification, the two areas were combined into a common computation mesh: MESH6, the predecessor of MESH7, MESH8, and MESH9. The combined meshes underwent a check for compliance of verification standards. In support of the numerical modeling effort and expanded study area, an additional field data collection program was required.

Terrebonne Marshes field data, 1983-1986

66. Report 2, Section 4 (Bensen and Donnell 1990), of this series describes the Terrebonne Marshes prototype data acquisition program. The program was initiated in June 1983 and continued through February 1986 by WES. Figure 13 shows the locations of continuously recorded tide (10) and velocity (9) stations within the Terrebonne Marshes. Discharge ranges (7) were collected in conjunction with monthly servicing of equipment, and are shown in Figure 14. The site map shown in these figures, composed by the WES field crew, was the byproduct of firsthand experience, local fishing maps, and

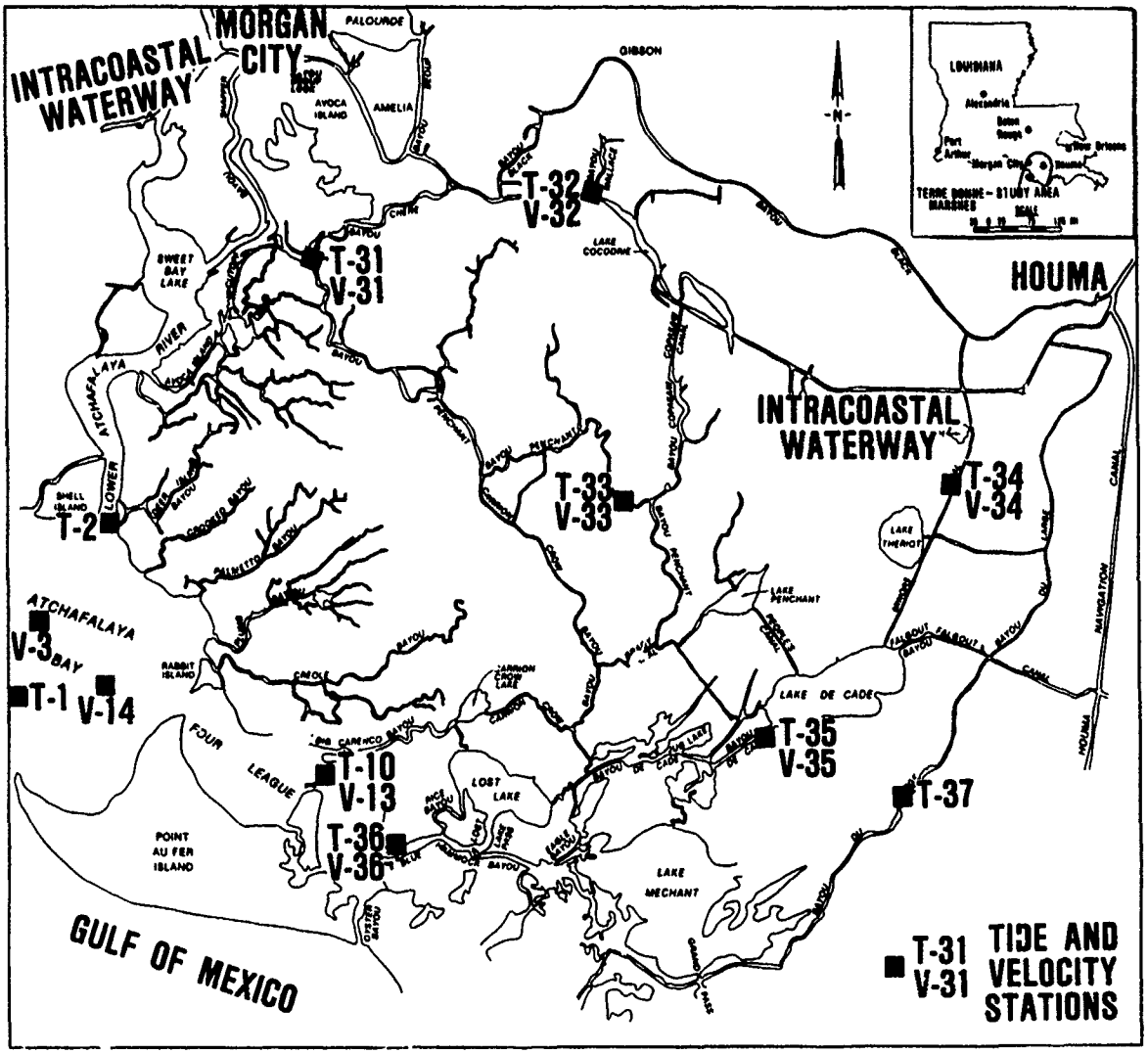

Figure 13. Tide and velocity station locations within Terrebonne Marshes

LANDSAT imagery. It proved to be as valuable to the Terrebonne verification as the data themselves.

67. Tides. Water-surface elevations were recorded on punched tape using a Fischer and Porter Company Type 1550. They were continuously measured at 15-min intervals. A low-pass filter to 34 hr was applied to each station for the low-flow (135,000-cfs combined discharge of the LAR and WLO) verification period, then spectrally analyzed to determine amplitude and phase in hours with respect to Eugene Island. Both the analyzed and the original data were used to verify the hydrodynamic model.

68. Velocities. At each velocity station, temperature, conductivity, speed, and direction were recorded on magnetic cassette tape via an Endeco

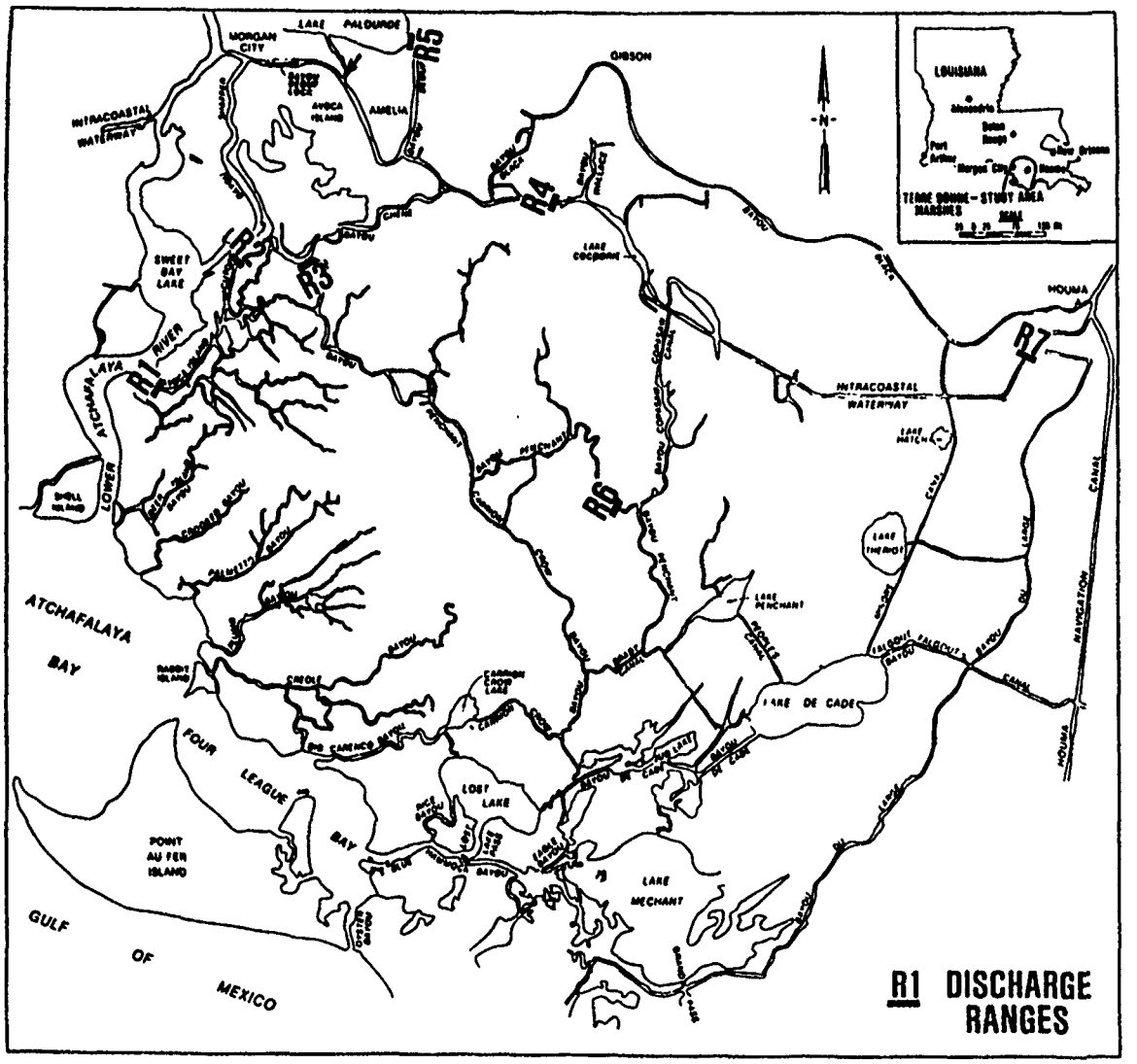

Figure 14. Discharge range locations within Terrebonne Marshes

176 meter at 2-min intervals. The data were used to compute mean flow and diurnal flow components, both in cubic feet per second. This information was used in the verification of the hydrodynamic model.

69. Discharge ranges. The discharge ranges were collected once or twice a month, as weather conditions permitted. The data were reduced to determine total discharge, direction, channel width, and cross-sectional area. This information was used to establish the geometry in MESH4 and to provide velocity boundary conditions for Lake Palourde.

70. Supplemental data. At the onset of the project, accurate maps of the study area were nonexistent. The marsh wet and dry patterns during a tidal cycle for various discharges were unknown. To better understand these

conditions, a mosaic of aerial photography was compiled, under the direction of the New Orleans District, during the high-flow (500,000-475,000 cfs) verification period. In addition, several helicopter overflights and marsh boat tours were taken by key personnel. The District also provided WES with selections of LANDSAT imagery during both the low- and high-flow verification periods (described in the rest of this part). Photo 1 is an example of a National Aeronautics and Space Administration (NASA) LANDSAT (catalog number 040800-132 band M3) taken 6 January 1983 with a Simmesport discharge of approximately 475,000 cfs. Note the sediment plume.

71. To provide bathymetric information in connecting canals, center-line depth soundings were conducted, under the direction of the New Orleans District, and completed the first quarter of 1984. These combined sets of information provided a means of estimating marsh elevations, circulation patterns, channel depths, and wet/dry characteristics within the network. Although the information did not answer every question, it was adequate to provide a limited verification of the Terrebonne Marshes.

MESH4 approach

72. MESH4, the Terrebonne Marshes computational mesh, was an extension of MESH1, the verified coarse Atchafalaya Bay mesh. MESH4 was designed to test the then newly developed wetting and drying technique (described in paragraph 38) and to economically verify the Terrebonne Marshes area model.

73. Verification conditions selected. Availability of reliable data was a key ingredient toward selecting the conditions for hydrodynamic verification. Two periods were selected, as shown in Table 5. The discharge at Lake Palourde (LP) was obtained from mean discharge values obtained from range 5 during the specified period. The high discharge period actually began at 500,000 cfs and dropped 500 cfs per hour throughout the simulation until 475,000 cfs was reached. For each period, the mean tide was centered 0.5 ft

Table 5

RMA-2 Verification Conditions for MESH4

Date	Discharge, cfs		Tide		Bayou Boeuf Lock
	LAP and WLO	LP	Range, ft	Type	
11/03/83	135,000	1,080	1.8	Mean	Open
6/22/83	500,000	5,386	1.8	Mean	Closed

above zero NGVD. The operating procedure for the Bayou Boeuf Lock, located just east of Morgan City, dictates that the gates are closed when the difference between the west gage and east gage exceeds 0.5 ft.

74. Boundary conditions. MESH4 was unusual in that its western bay edge stopped between the two outlets. Since the open water estuary boundary was a subset of MESH1, the JOBSTREAM technique was applicable. First, a synthesized tide with a 25-hr repeating diurnal period was obtained from the prototype harmonic analysis of tide data and applied as Gulf boundary condition for MESH1. Then, the boundary conditions for MESH4 were extracted from MESH1 RMA-2V results using JOBSTREAM.

75. Use of the nonreflecting boundary module was not required in MESH4, because the velocity boundary conditions at LAR and WLO were extracted by JOBSTREAM results which had used the module. Similarly, the flow split down the LAR was dictated by conditions that were applied to create the results from which JOBSTREAM extracted the velocity boundary conditions. For these verification runs, the flow distribution was 70/30 between LAR and WLO.

76. Coefficients. Available "tuning" coefficients for verification of RMA-2 are turbulent exchange and Manning's n values based on element type. MESH4 had nine element types, five of which were in common and identical (i.e., size, shape, and assigned coefficients) to the verified MESH1. Those element types distinct to MESH4 were for the bayous, lakes, marsh, and high-energy channels found within the marsh. The elements representing bayous and marsh received a turbulence exchange coefficient in both the parallel, perpendicular and cross-term directions of 25-90 lb-sec/ft^2 while the lakes received a value of 100 lb-sec/ft^2. Mannings n values ranged from 0.01 to 0.02 for bayous, 0.03 to 0.06 for obstructed canals, 0.037 to 0.05 for the Bayou Boeuf Lock, and 0.2 to 0.5 for marsh areas.

77. Time-step. A series of sensitivity runs were made to determine an appropriate time-step and model spin-up for the hydrodynamic model, RMA-2. The model revealed that the economical 1-hr time-step was satisfactory for MESH4, as will be evident when comparisons of hydrodynamic model versus prototype are presented. The only other time-step tested was a 30-min time-step. A smaller time-step was ruled out due to the associated large computer time requirements without significant improvement in results.

78. Wetting and drying. RMA-2 experienced convergence difficulties primarily because of numerical shocks due to wetting and drying of marsh

areas. Checks for drying or rewetting elements occurred at the end of each time-step. If the water depth at a wet node fell on or below 0.275 ft, the element containing that node would be eliminated from the computation. In other words, if one node within an element dried, then the entire element was eliminated from computation. The depth at which a node would be considered wet after it had dried was 0.6 ft. All nodes within an element had to achieve this criterion in order to be reinstated in the computation.

79. Spin-up. Figure 15 illustrates that for Eugene Island the first hour at which repetition occurs is at hour 15, because the value of hour 15 is identical to that of hour 40, as would be expected with a 25-hr repetitive tide boundary condition. However, as much as 21 hr was required to adequately spinup within the locations experiencing wetting and drying (such as the marshes). Spin-up can be in excess of two times greater for a wetting and drying simulation.

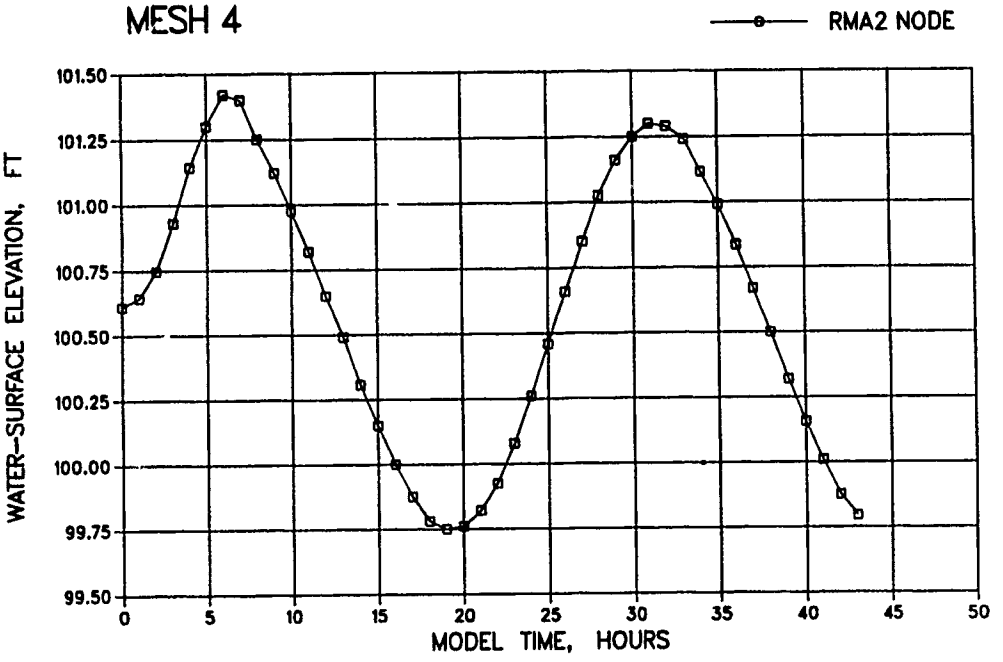

Figure 15. Illustration of RMA-2 model spin-up for MESH4

Results of MESH4

80. Low-discharge condition. Spectral analysis of field data (month of November 1983) was employed to calculate diurnal tide amplitude and phase with respect to Eugene Island. The results from the field analysis were compared with the numerical model results for the low discharge verification, and are shown in Table 6. To study circulation patterns given by RMA-2, velocity

Table 6

MESH4 Low-Discharge (135,000 cfs) Hydrodynamic Verification

Tide Station	November 1983 Field Amplitude Ratio	November 1983 Field Phase hr	RMA-2 Amplitude Ratio	RMA-2 Phase hr
TG1	0.79	0.0	0.77	0.0
TG2	0.74	0.3	0.77	-1.0
TG31	0.31	-2.6	0.34	-3.0
TG32	0.14	-5.1	0.14	-6.0
TG33	0.11	-8.8	0.08	-11.0
TG34	0.13	-2.9*	0.30	-8.0
TG35	0.17	-7.3	0.28	-8.0
TG36	0.75	-2.7*	0.71	-1.0
TG37	0.45	-3.4	0.40	-4.0

Velocity Station	November 1983 Field Mean Flow	November 1983 Field Diurnal Component	November 1983 Field Area sq ft	RMA-2 Mean Flow	RMA-2 Diurnal Component	RMA-2 Area sq ft
V-33	123	441	2,100	183	173	2,182
V-35	261	1,512	2,250	295	810	2,025
V-36	36	7,278	12,150	1,759	7,316	12,112

* The prototype phase is in question.

vector plots are given in Figure 16. The length of the vector shaft indicates the magnitude of the velocity according to the scale at the upper righthand corner, while the arrow points toward the direction of flow. All velocities exceeding 1 fps were truncated in length, as indicated by a solid arrowhead, to enhance readability.

81. High-discharge Condition. The next step toward verification was to test the highest discharge condition available during the field data acquisition period. This provided a second data set for verification that was at the opposite end of the spectrum from the first data set. The highest such discharge occurred in mid-June 1983 (Photo 2). The diurnal mixed tide from the field data was smoothed and used as a Gulf boundary condition for the numerical model.

82. Results from RMA-2, obtained from nodal locations corresponding to prototype water-surface elevation stations, are shown in Figures 17 and 18. The dashed line is raw prototype water-surface data, with appropriate field station identifier. For example, the Eugene Island identifier TT010683 refers to Terrebonne Tide Station 1 for June 1983. The solid line shows the

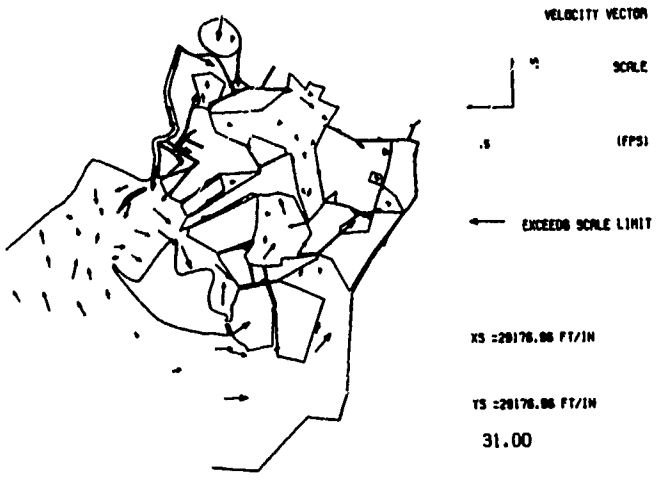

a. High tide at Eugene Island

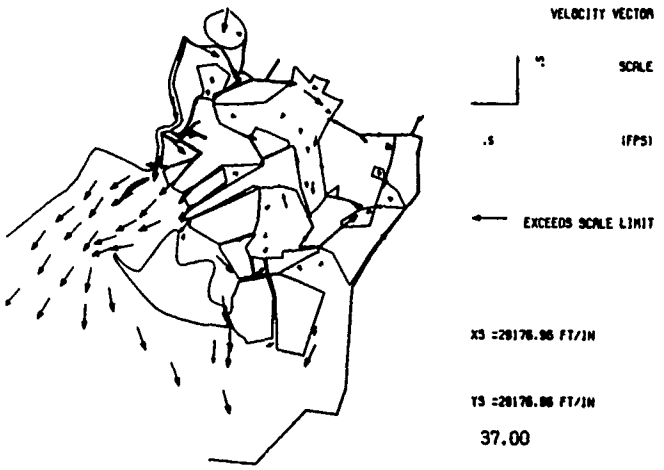

b. Falling tide at Eugene Island

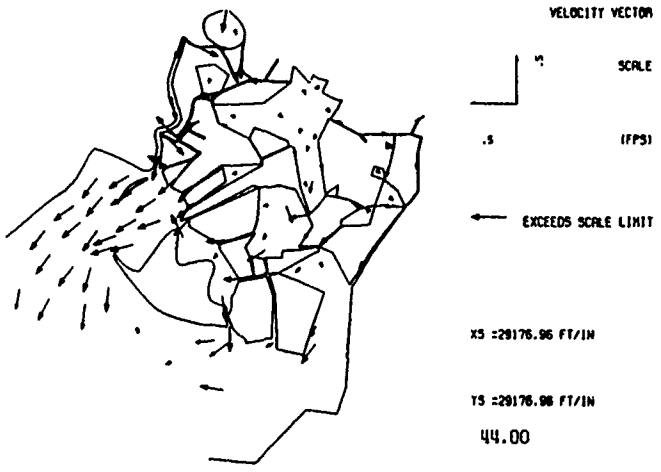

c. Low tide at Eugene Island

Figure 16. Velocity vectors for the low-discharge hydrodynamic verification of Terrebonne Marshes

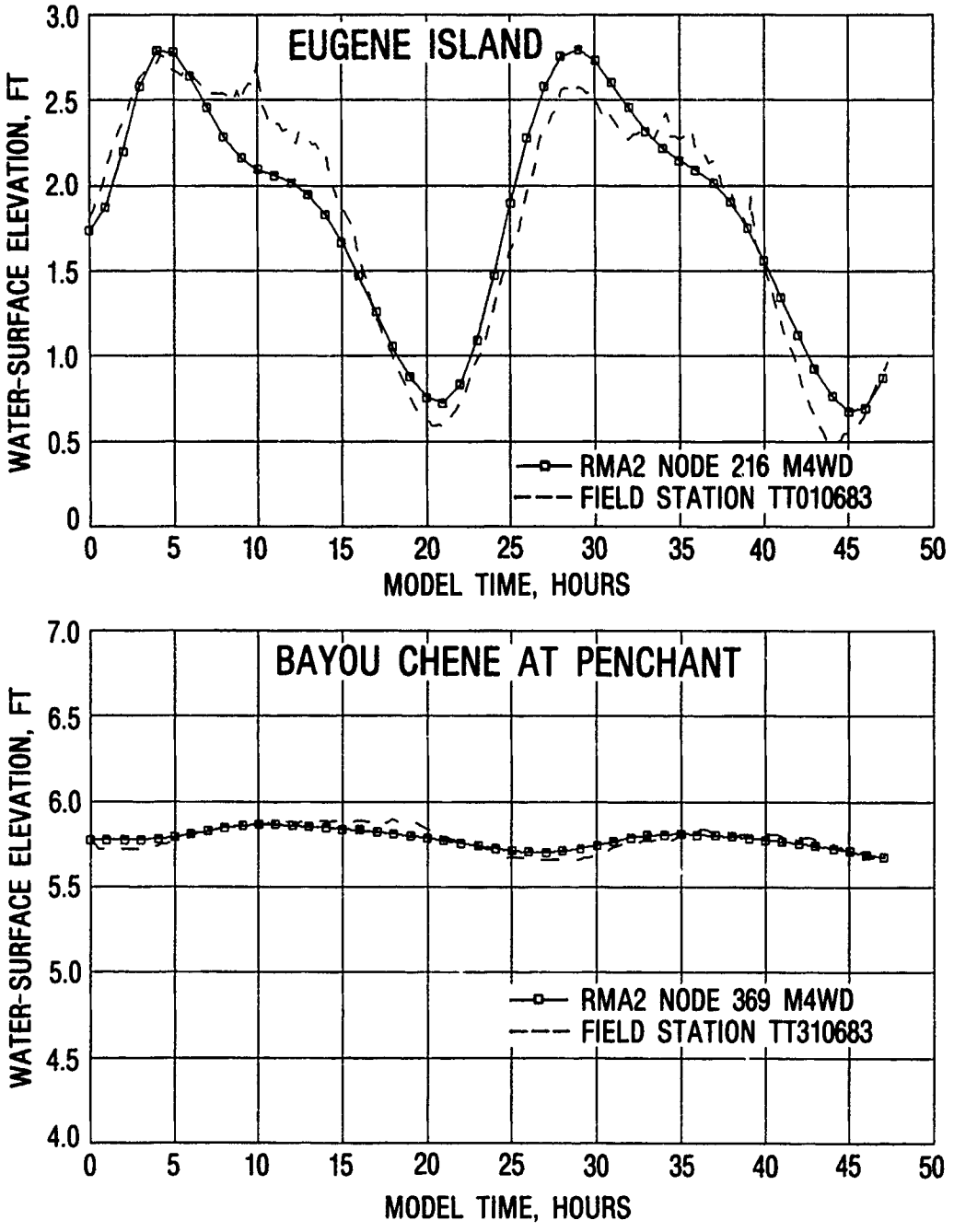

Figure 17. High-discharge hydrodynamic verification of Terrebonne tide stations 1 and 31

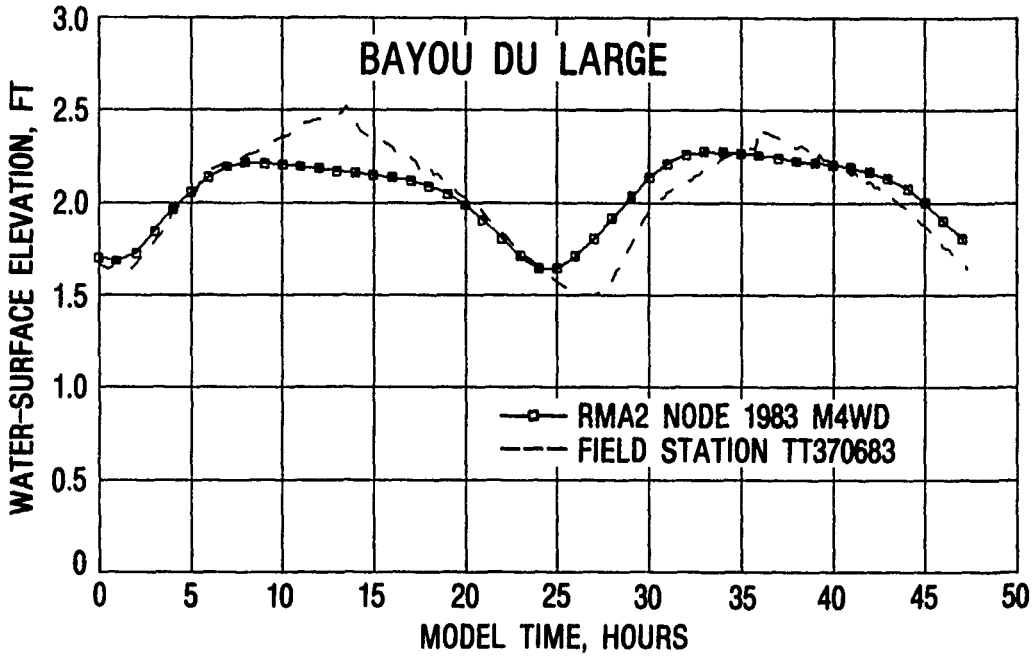

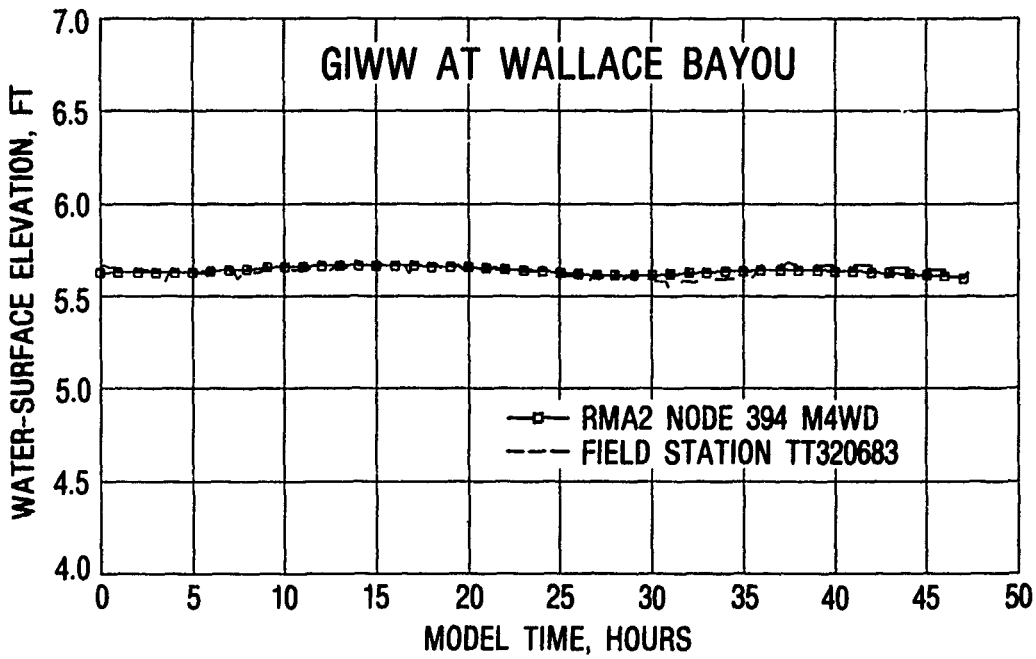

Figure 18. High-discharge hydrodynamic verification of Terrebonne tide stations 32 and 37

numerical model results, with each square symbol denoting values for each 1-hr time-step. Because of the great difficulty in trying to establish a mean datum by which to compare stations in the marshes, the mean of the prototype data was set equal to the mean of the numerical model data at each station.

83. Comparisons of prototype velocity stations to the numerical model results are shown in Figure 19. The dashed line indicates raw prototype data, and the solid line with square symbols shows the corresponding numerical model values. The field station identifiers are similar to those described in the preceding paragraph.

84. Circulation patterns of the high-discharge verification are given in Figure 20. Scaling is identical to that given for the low-discharge verification for ease of comparison. One primary difference between the two discharge events is along the Gulf Intracoastal Waterway (GIWW), in that the high discharge does not allow an east-to-west flow.

Combined mesh checked for
verification performance

85. The verifications for MESH1, MESH2, and MESH4 were utilized in prescribing model coefficients for each of the combined networks, MESH6 and MESH7. Coefficients such as Manning's n value, eddy viscosity, and wetting/drying criterion were set according to reasonableness and adjustments made during verification. The range of values are given in Table 7. As the delta evolved, the coefficients were adjusted to reflect the current bathymetric conditions for each element of the mesh. Both of the combined networks were checked for one verification period to ensure performance of verification standards.

86. For the purposes of low-flow verification the combined meshes used synthesized Gulf boundary conditions, 135,000-cfs combined velocity inflow with a 63 percent - 37 percent flow distribution between LAR and WLO, the nonreflecting boundary module, 1-hr time-step, 19 element types by which to specify input parameters, and the same wetting and drying criteria as used in the Terrebonne Marshes MESH4.

87. Table 8 shows the MESH7 numerical model results compared to field data for the low-discharge hydrodynamic verification period. As expected, the verification for the combined mesh was very similar to the MESH4 verification presented in Table 6. The decreased flow down the LAR, as dictated by the flow split, resulted in less resistance to the tide, thereby causing a slight

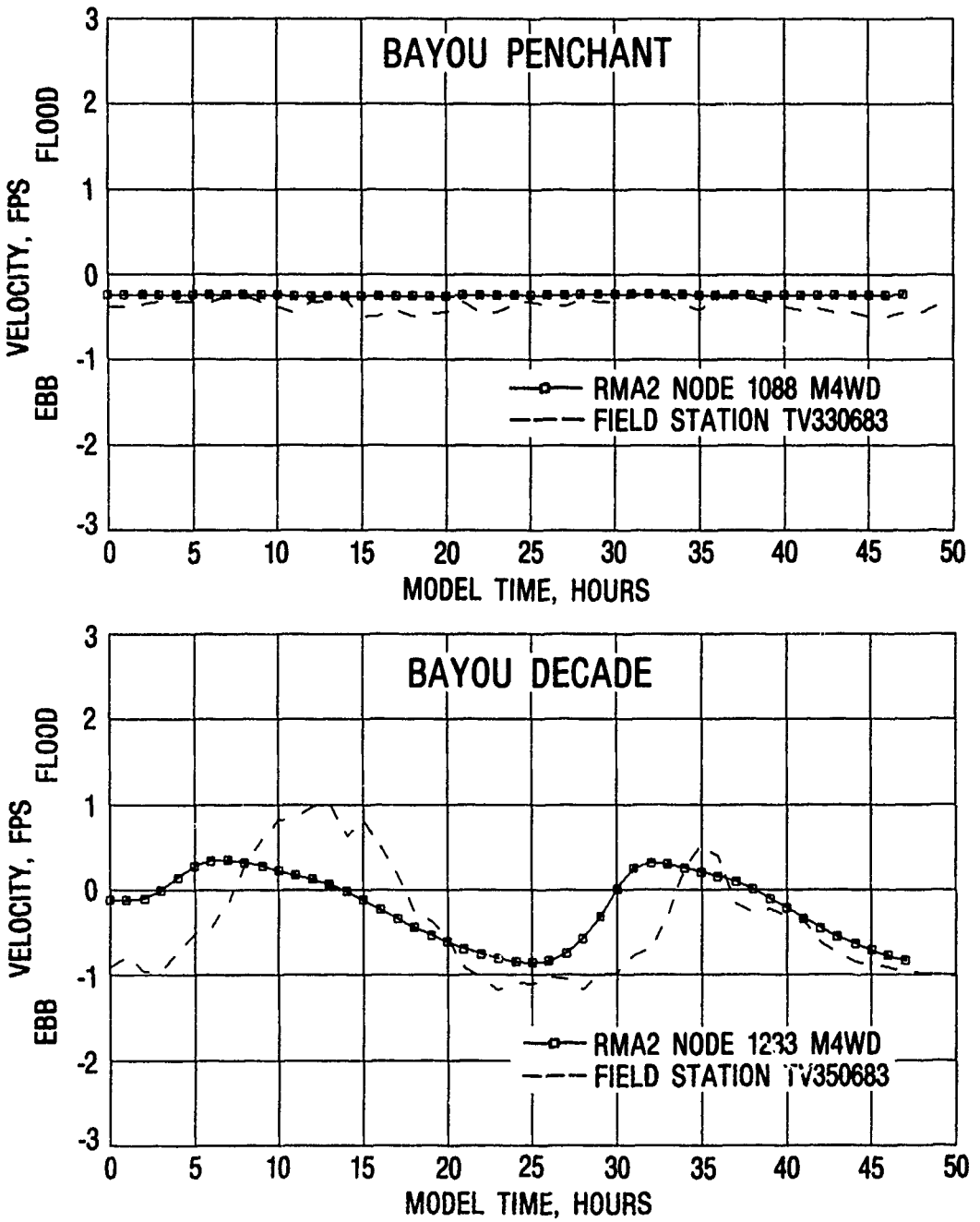

Figure 19. High-discharge hydrodynamic verification of Terrebonne tide stations 33 and 35

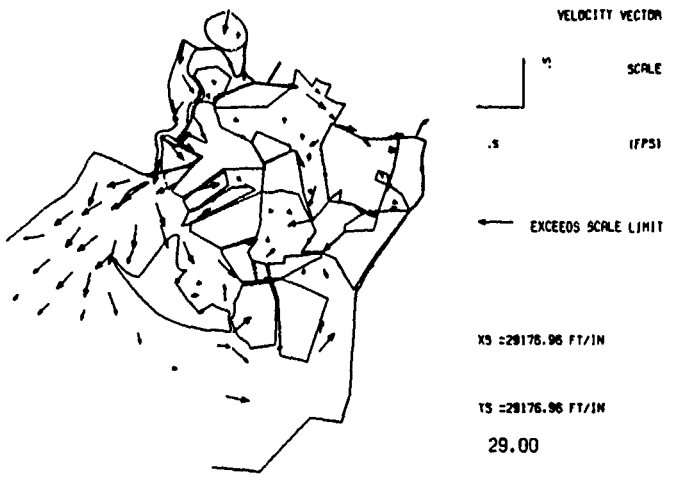

a. High tide at Eugene Island

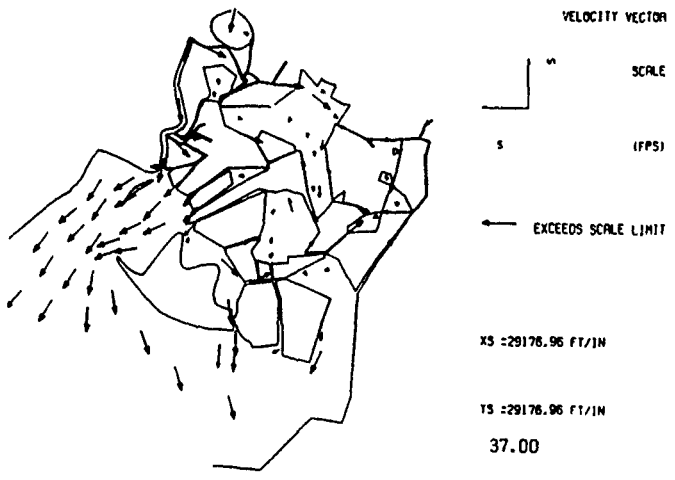

b. Falling tide at Eugene Island

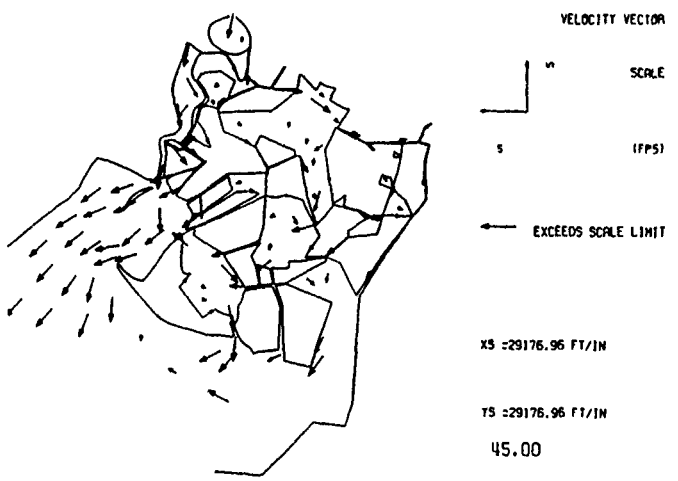

c. Low tide at Eugene Island

Figure 20. Velocity vectors for the high-discharge hydrodynamic verification or Terrebonne Marshes

Table 7

Hydrodynamic Coefficients

Element Type	Eddy Viscosity lb-sec/ft^2	Manning's n ft$^{1/6}$
LAR and WLO	500	0.02
Submerged delta	400	0.02
Fourleague Bay	450	0.02
Inner Gulf	500	0.02
Middle Gulf	550	0.02
Outer Gulf	600-750	0.02
Bayous	25-200	0.01-0.02
< 1 ft subaerial delta	400	0.10
> 1 ft subaerial delta	400	0.20
Lakes	100-300	0.02-0.06
Marsh	25-350	0.20-0.50

Table 8

MESH7 Low-Discharge (135,000 cfs) Hydrodynamic Verification

	November 1983 Field		RMA-2	
Tide Station	Amplitude Ratio	Phase hr	Amplitude Ratio	Phase hr
TG1	0.79	0.0	0.84	0.0
TG2	0.74	0.3	0.80	-1.0
TG31	0.31	-2.6	0.38	-3.0
TG32	0.14	-5.1	0.16	-5.0
TG33	0.11	-8.8	0.10	-10.0
TG34	0.13	-2.9*	0.29	-8.0
TG35	0.17	-7.3	0.29	-7.0
TG36	0.75	-2.7*	0.63	-3.0
TG37	0.45	-3.4	0.47	-3.0

	November 1983 Field			RMA-2		
Velocity Station	Mean Flow	Diurnal Component	Area sq ft	Mean Flow	Diurnal Component	Area sq ft
V-33	123	441	2,100	123	217	2,182
V-35	261	1,512	2,250	238	736	2,025
V-36	36	7,278	12,150	1639	8,945	12,112

* The prototype phase is in question.

increase in amplitude. However, there was an improvement in phase for the combined mesh.

88. The TABS-2 numerical model for hydrodynamics, RMA-2, adequately reproduced observed water levels and current patterns over a tidal cycle for all computational meshes. Each mesh can be credited for its strong and weak points: economy versus resolution. However, the combined meshes of Atchafalaya Bay and Terrebonne Marshes are believed to give the best predictions for interactions between the open-water estuary and the Terrebonne Marshes.

PART IV: SALINITY VERIFICATION

Purpose

89. The purpose of salinity verification for the numerical model, RMA-4, was to reproduce observed salinity patterns. Salinity patterns in the evolving Atchafalaya Bay system are of concern to resource agencies as they affect fisheries resources, general ecological conditions, water quality, and water supply systems. There is also much concern for salinity conditions in marsh areas. Salinity verification was conducted in two parts, the bay and the marsh.

90. The availability of a verified salinity model will allow future testing to gage the effects of natural delta development in the Atchafalaya Bay or structural measures associated with levees, channels, dikes, and sills on general salinity conditions. Salinity verification also acts as another, indirect verification for the hydrodynamic model which drives the salinity transport model.

Site Characteristics

91. Salinity affects many physical processes and biological regimes, and is one of the few nearly conservative constituents within the estuarine environment. Salinity, a measure of the amount of dissolved salts in water, is usually expressed in parts per thousand (ppt) by weight. Instruments are used in the prototype to measure the conductivity of the water and these values are then converted to salinity.

92. Atchafalaya Bay has very low salinities due to the magnitude of the freshwater inflow relative to its volume, and to its mixing characteristics. The northern part of the bay is generally 1 ppt or less all year. Other parts of the bay complex (Fourleague Bay, East and West Cote Blanche Bays, and Vermilion Bay) have salinities which vary with freshwater inflow, tide, and wind conditions. Salinities are generally higher in the western bays from Gulf water intruding through Southwest Pass. Salinities here average 6.1 ppt. Offshore salinities range from 20 to 35 ppt. Figure 21 shows a typical distribution of depth-averaged salinity from a previous study (Juneau 1975).

93. Changes in the Atchafalaya River over the past few decades have

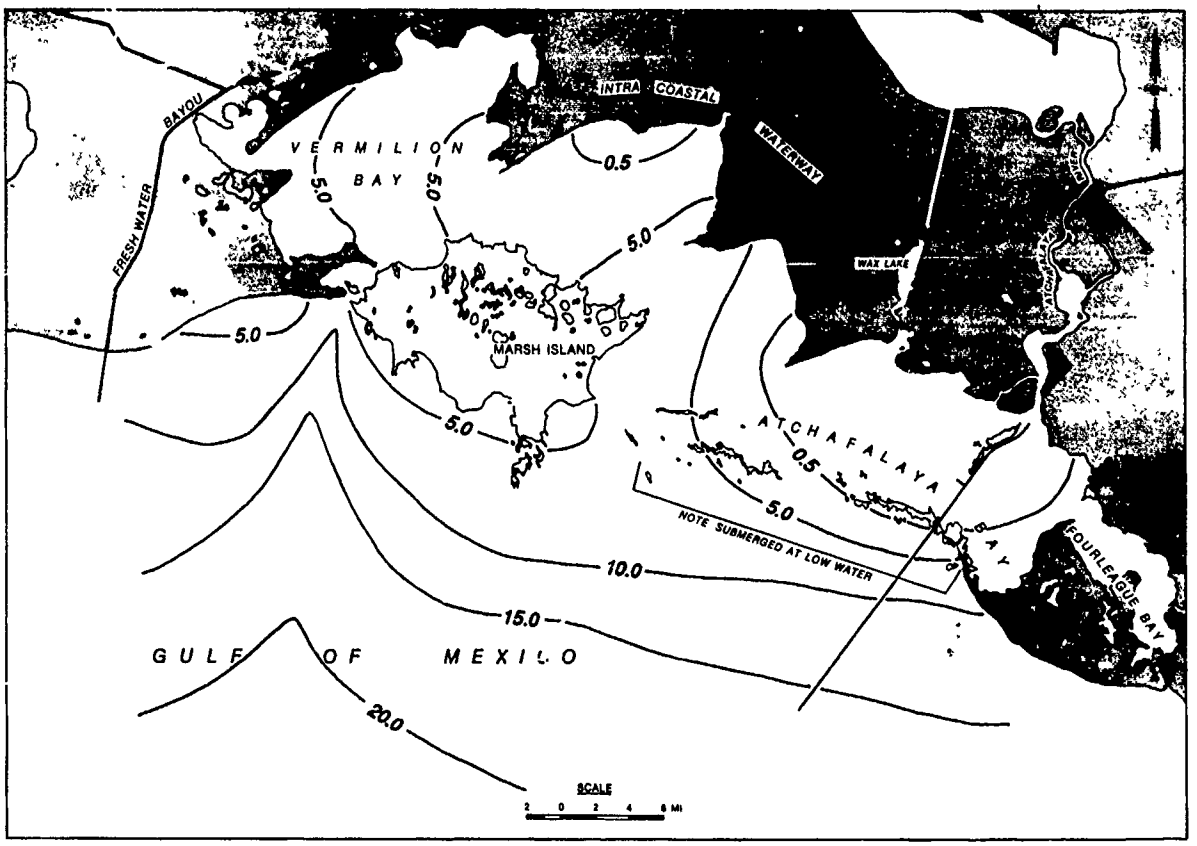

Figure 21. Typical distribution of depth-averaged salinity

produced sharp changes in salinity distribution in the bay system. Marsh grass species composition around the bay system has also changed, reflecting the shift to fresher water. Massive oyster reefs and the bay bottom no longer support oyst. ing, and old reefs have disappeared in most cases. Salinity intrusion into the Terrebonne Marshes occurs only during periods of low discharge.

Model and Process Description

94. Computer codes RMA-2 and RMA-4 of the TABS-2 numerical modeling system were used to model 2D, depth-averaged hydrodynamics and salinity transport, respectively. Salinity modeling first requires hydrodynamic model calculations which in turn provide the water levels and velocity field for the salinity transport calculations.

95. The process modeled was vertically well mixed salinity intrusion and mixing, a condition imposed in part by the modeling approach. The assumption of complete vertical mixing was found to generally agree with field

observations in the bays and offshore areas. Deep channels and passes were found to become stratified during periods of low flow, and deeper offshore areas stratified during moderate to high flow. The intrusion of salinity into deep areas during periods of low flow was not within the resolution of this modeling effort, however.

96. The intrusion of salinity into the bay system results from diffusion, trapping, and tidal pumping of saline and fresh waters, similar to an unsteady, free-surface jet or plume issuing into a coastal ocean. This view of the process is consistent with satellite photos (Photo 1) which frequently display large-scale eddies seaward of Eugene Island, and suggests that prototype salinity spatial and temporal variability in the mixing zone is great.

97. Figure 22 shows the variability of salinities in Atchafalaya Bay and approach channel over three field surveys for the flow range of 275,000 to 330,000 cfs. Water sample station locations from the 1980-1983 field data collection program are alphabetically labeled. The variability near the approach channel is believed to have resulted from the dynamic nature of the

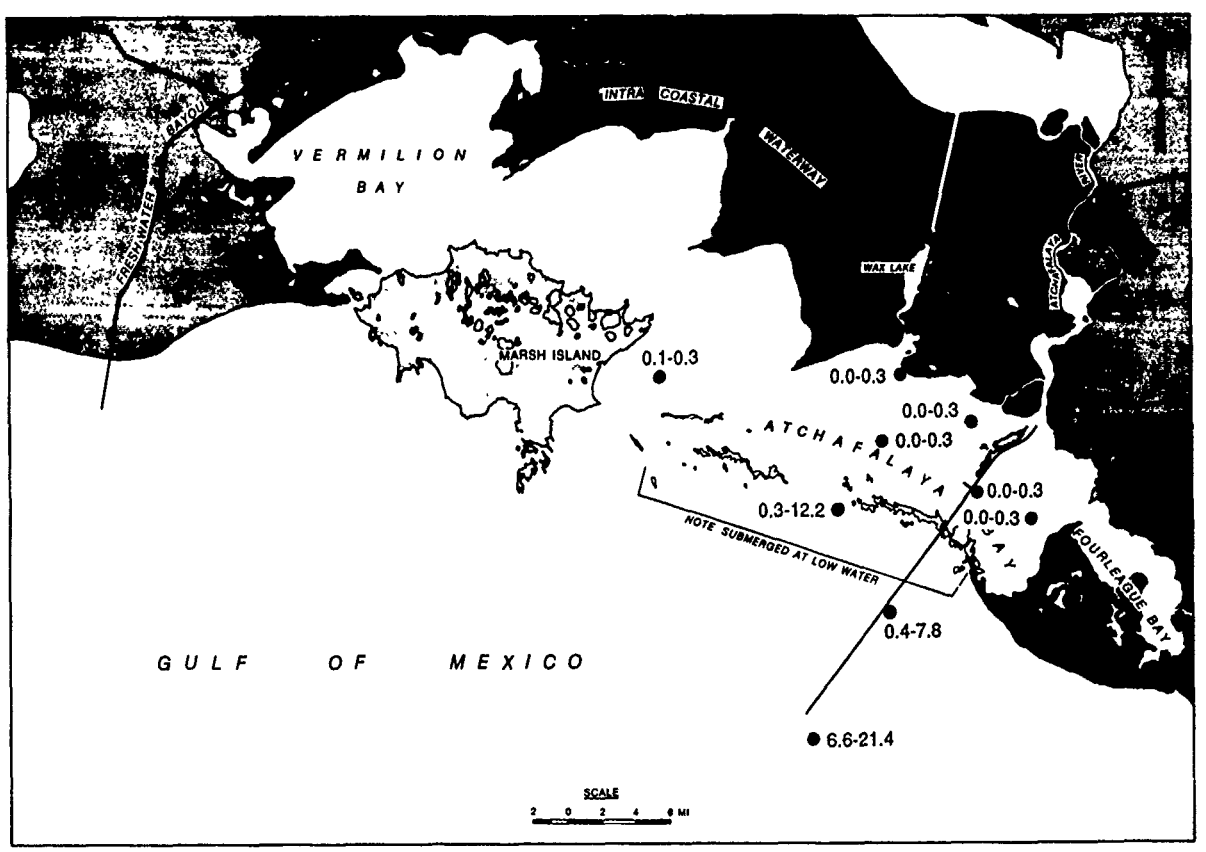

Figure 22. Range of salinities in Atchafalaya Bay and approach channel over three field surveys for a discharge

large-scale mixing process, a fact which should be considered in the evaluation of the salinity verification. Additional variability could have come from the coastal salinity regime.

Atchafalaya Bay Salinity Verification

Selected field conditions

98. WES field sampling is described in detail in Report 2 of this series (Coleman et al. 1988). Quasi-synoptic point samples were collected from throughout the system over usually 2 or 3 days.

99. Prototype conditions of 330,000-cfs combined inflow, a 70/30 split between the LAR and WLO, and a repeating mean tide with a 2.0-ft range were selected for the salinity verification because they represent average conditions, they are close to previous model test conditions, and field data were available. Corresponding field data for these conditions were collected 23-26 June 1981. Figure 23 shows the salinity regime for the selected prototype condition.

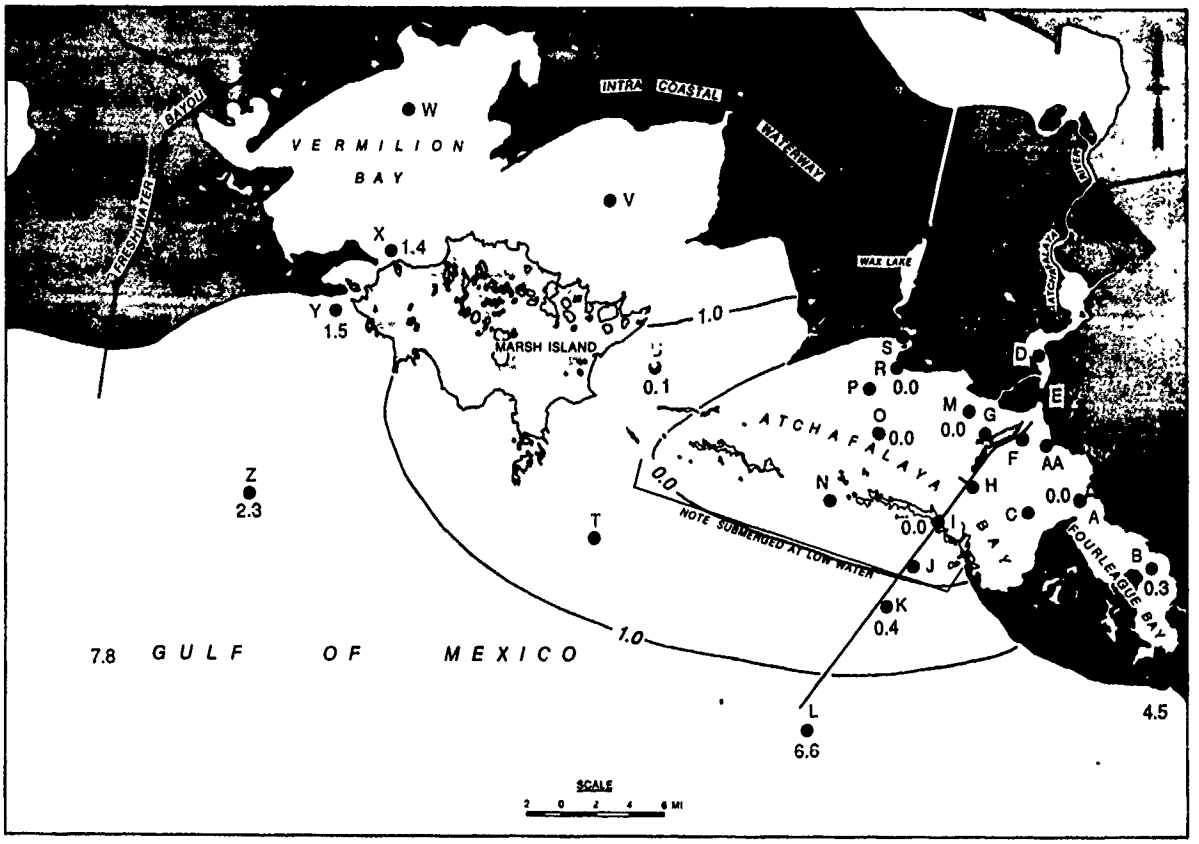

Figure 23. Prototype salinity data taken 23-26 June 1981, combined inflow of 330,000 cfs

100. The New Orleans District collected and consolidated field data taken between 1974 and 1978 for several discharges. Results from this effort for a 320,000-cfs combined discharge and present conditions were taken from the General Design Memorandum of the Atchafalaya Basin Floodway System, Louisiana, and are shown in Figure 24. It should be noted that considerable data were missing within Terrebonne Marshes and that extended "straight" contour lines reflect lack of data.

Modeling procedure

101. The numerical computational meshes have been previously described. Initial salinity modeling was performed using MESH1, but the primary verification was performed using MESH2. Verification checks conducted with MESH6 and subsequent meshes, which contained the combined Atchafalaya Bay and Terrebonne Marshes, will be discussed later.

102. MESH2 was run dynamically (unsteady, tidally driven flow and transport) with half-hour time-steps. Because salinity verification followed hydrodynamic verification, no further adjustments were made to the hydrodynamic model.

103. The major salinity model parameter which required adjustment was the diffusion coefficient used in the convection-diffusion equations. For MESH2, these coefficients were initially specified by nine element types based on element size and average friction velocities. A schematic functional equation guided initial coefficient selection:

$$D_{x,y} = f(HU_*, L^2) \tag{1}$$

where

D_x, D_y = diffusion coefficients

H = depth

U_* = frictional velocity

L = length scale of the elements

The first term in the function represents the contribution of shear dispersion; and the second term, the contribution of length scale resulting from the distinction between convection and diffusion imposed by the mesh.

104. Sensitivity tests were performed on the salinity model with a range of diffusion coefficients. The salinity transport results were found not to

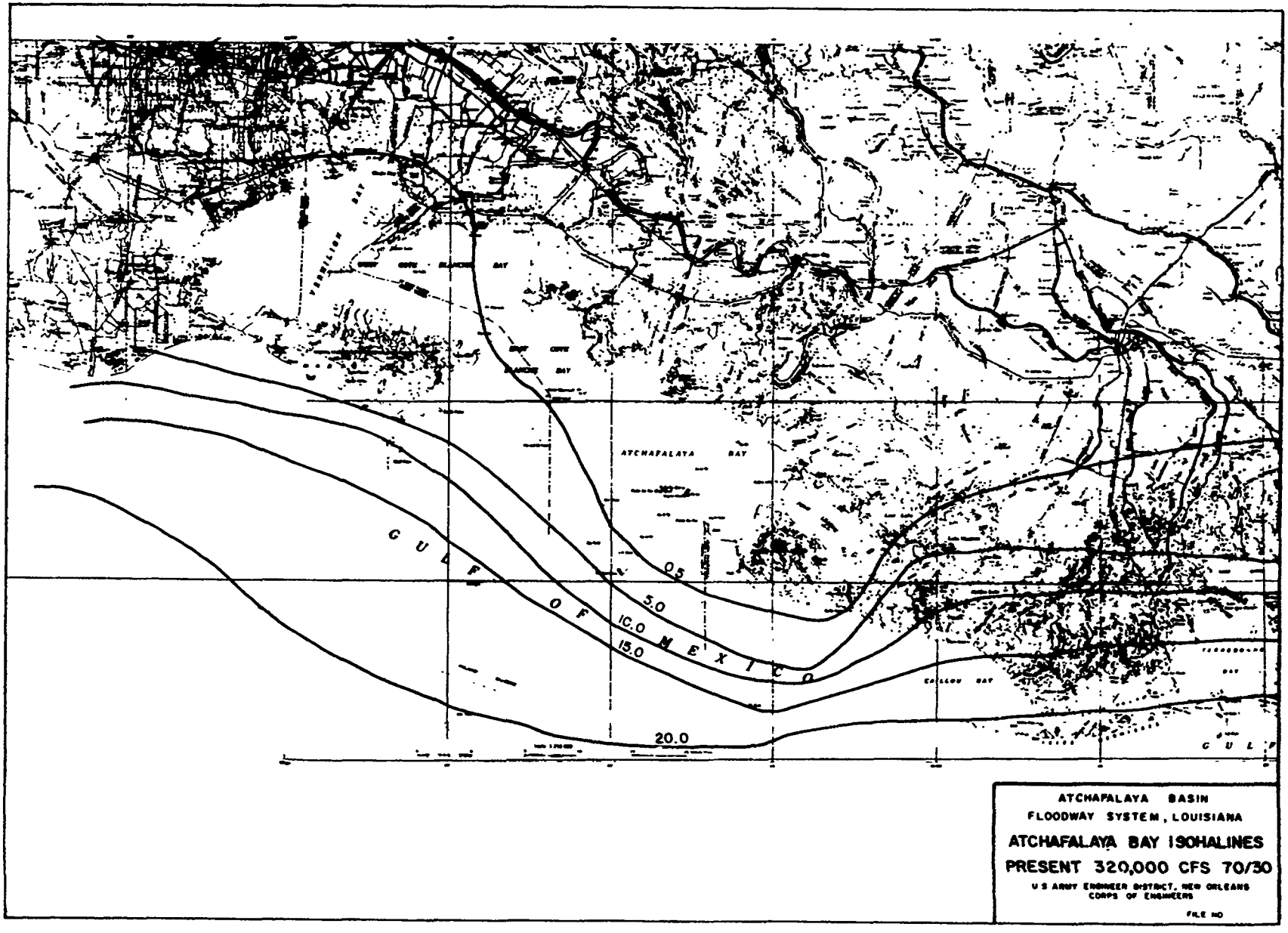

Figure 24. Isohalines compiled from prototype data collected from 1974 to 1978

be very sensitive to the diffusion coefficients. Results showed that the Atchafalaya Bay and channel areas were dominated by th advection of the fresh water and therefore insensitive to the diffusion coefficient, and that diffusion transport occurred only in the coastal area and in the western bays.

105. The process of selecting diffusion coefficients for verification also considered the uncertainty in coefficient specification for test meshes with projected delta growth geometry. Uniform coefficients are a definite advantage for test meshes, since no adjustment of coefficients will be possible. Based on the results of the sensitivity tests, a uniform diffusion coefficient of 100 sq m/sec was selected for use in the salinity verification. The magnitude of this coefficient reflects mainly the model element size in the region of the salinity mixing.

106. MESH2 was initialized to 0.0 ppt in the Atchafalaya Bay, 2.0 ppt in the other bays, and 10.0 ppt in the ocean area. The inflow concentration was set to 0.0 ppt. The offshore boundary was set from the field data at between 10.0 and 20.0 ppt. The model was run 100 hr with steady flow only, then hot-started for a 3-week dynamic tidal simulation until "dynamic equilibrium" was reached. This condition was characterized by salinity conditions which repeated very closely between tidal cycles.

Results

107. Figure 25 shows contours of model salinities for the present condition computed using MESH2 and 1980 bathymetry (year 0). The salinity pattern shows that the freshwater inflow to the system expelled salinity from Atchafalaya Bay and the salinity mixing zone extended well seaward of the bay. Salinities from the end of the 330,000-cfs verification run were interpolated in time and space to the same tidal stage and station locations as the field data were collected and plotted in Figure 26. Figure 26 can also be compared to Figure 23. Table 9 compares prototype and model data only for areas outside Atchafalaya Bay (where salinities in both cases were near 0.0 ppt). Model salinities were about 1.0 ppt higher than the prototype in the western bays. The model results were lower on the eastern edge of the plume (station L) and higher on the western edge of the plume (station Z) than prototype values. These stations were located in the strong gradients of the mixing zone, and the earlier discussion on salinity variability applies. Contour plots of the model and prototype data show a good correspondence.

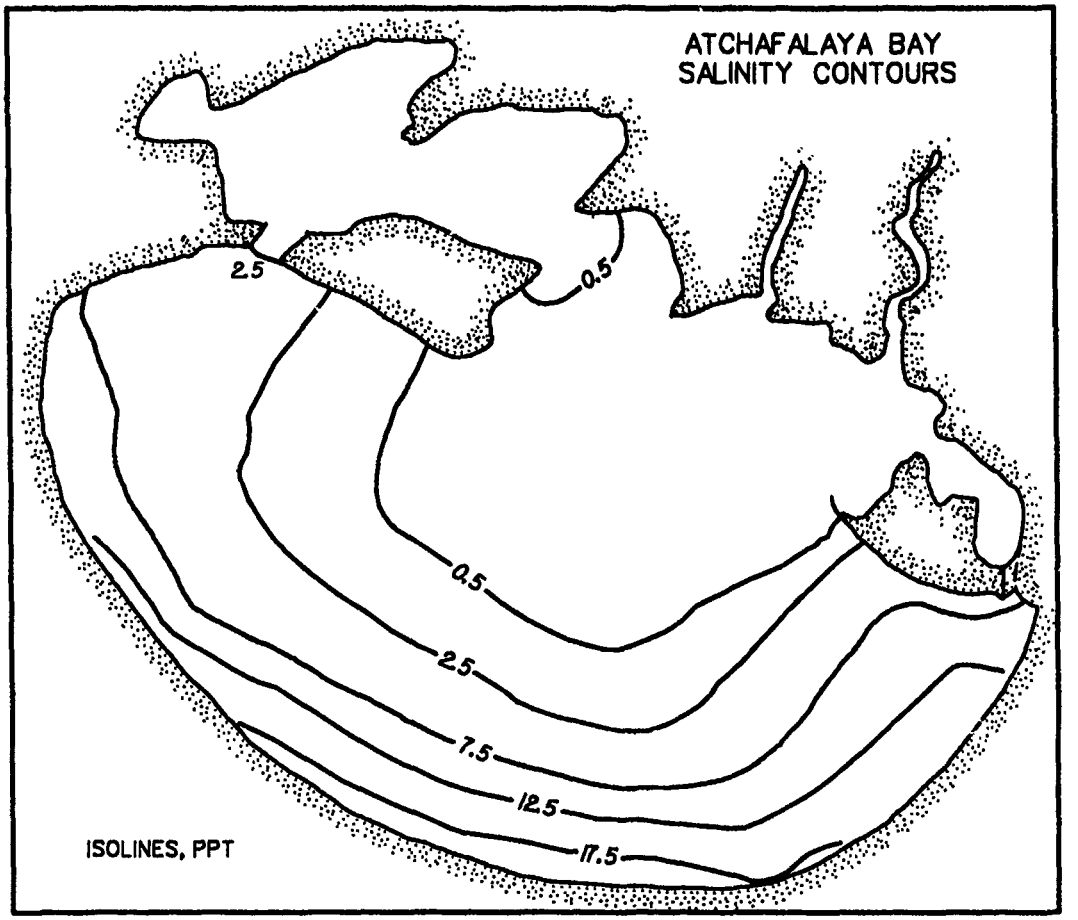

Figure 25. Isohalines, MESH2, 1-ft amplitude, 25-hr repeating diurnal tide, 330,000-cfs total discharge, existing conditions with project, year 0, 3-week simulation, 0.50-hr time-step

Hence, the salinity model using MESH2 can simulate general salinity conditions without detailed adjustment of coefficients.

Atchafalaya Bay-Terrebonne Marshes Salinity Verification

Selected field condition

108. Because salinity intrusion is practically non-existent within the Terrebonne Marshes during periods of high discharge, a low-discharge condition was selected for verification. Figure 27 shows the locations of the surface grab water sample station locations for the 1983-1986 field data program and associated salinities for the low-discharge condition. Two salinity sampling periods had approximately the same conditions: 28-29 September and 2-3 November 1983. The average salinity values for these two periods are also shown in Figure 27. Flows prior to 28 September were fairly steady between 50,000 and 70,000 cfs and the tides were diurnal with a 1.8-ft range.

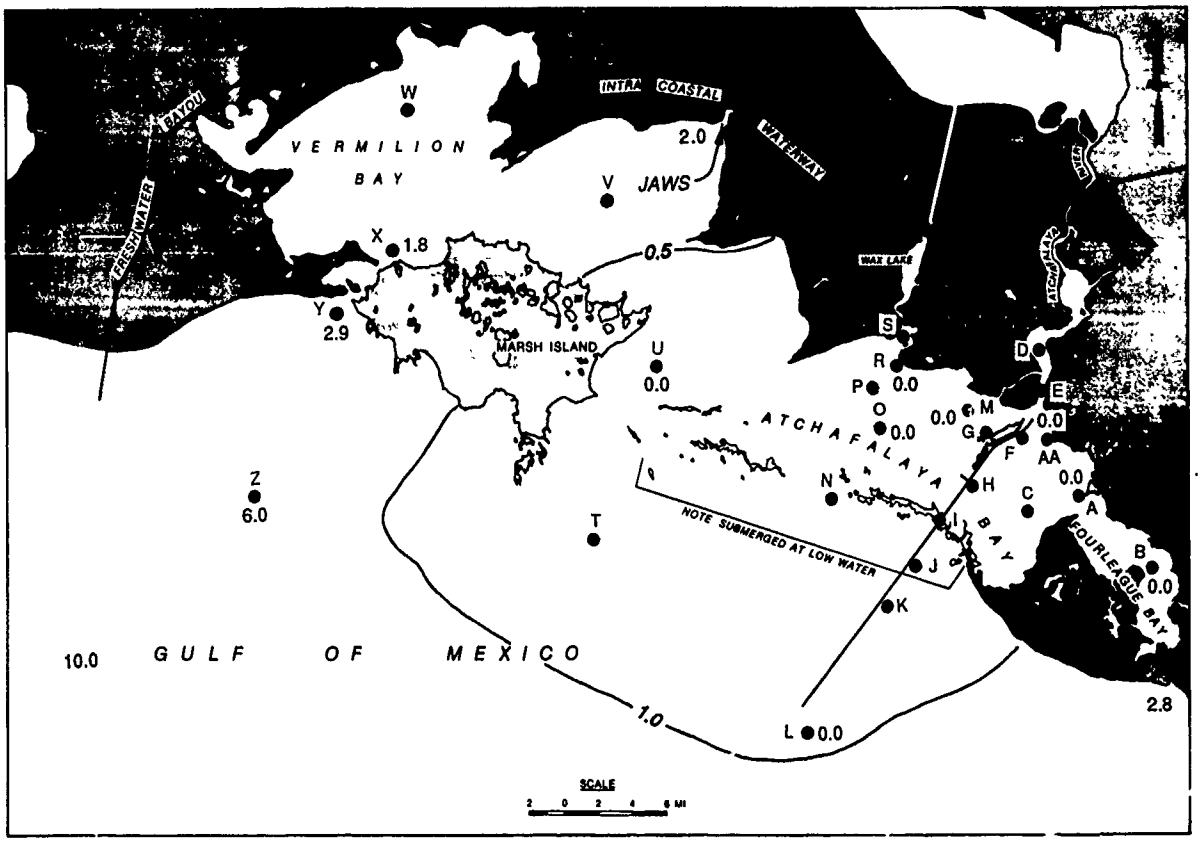

Figure 26. Numerical model MESH2 salinities interpolated to prototype sampling station locations

Table 9

Model to Prototype Salinity Comparison (Outside of Atchafalaya Bay)

Station	Model Values			Prototype
	Low Water	High Water	Interpolated*	
X	2.4	4.1	2.8	1.4
TG-7	2.0	5.0	2.7	1.5
L	0.0	0.0	0.0	6.6
U	0.3	2.0	1.1	0.1
Z	8.0	8.2	8.1	2.3
TG-15	4.2	3.5	3.8	4.5
B	0.0	0.0	0.0	0.3
WS-C	2.0	2.0	2.0	1.3

* Refer to paragraph 107 for explanation.

Freshwater inflows during the 2 November period were on the rise; however, allowing a 6-day lag time between Simmesport and Morgan City (~110 miles), the effective flow was 75,000 cfs and had been steady for several weeks between

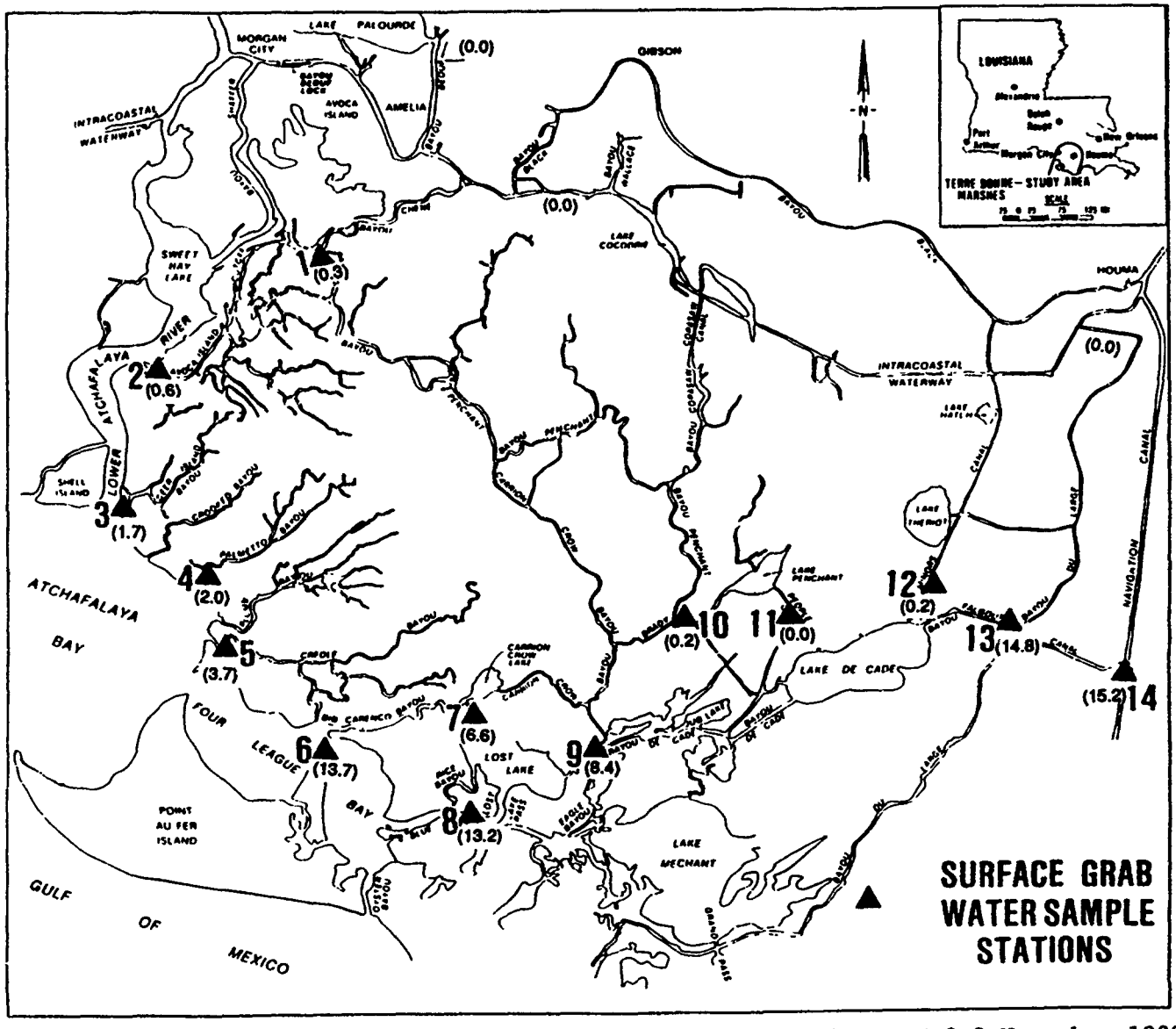

Figure 27. Average prototype salinity values, 28-29 September and 2-3 November 1983, with a total discharge of approximately 70,000 cfs

60,000 and 80,000 cfs. The tides during the 2 November period were semi-diurnal and had a range of about 1.5 ft. No substantial subtidal effects were present for these periods.

Modeling procedures

109. Initial testing with MESH4 revealed that RMA-4 performed well with a 1-hr time-step, but JOBSTREAM boundary locations were too close to the area of interest. MESH4 was abandoned and the combined meshes which incorporated both the Terrebonne Marshes and the Atchafalaya study area were chosen. MESH6 successfully used a 1-hr time-step with uniform diffusion coefficients of 100 m^2/sec. Using these computed isolines as guidelines, an extended time-stepping method utilizing residual currents was employed. The residual currents were calculated from the last 25-hr tidal cycle of the hydrodynamic results from RMA-2 and supplied as the velocity field to RMA-4 with a 25-hr extended time-step. For low discharges, the diffusion coefficients in the Gulf required slightly higher values when employing the extended time-step. For the mean discharge of 330,000 cfs, no alteration of diffusion coefficients were required. To illustrate the success of the technique, Figure 28 shows

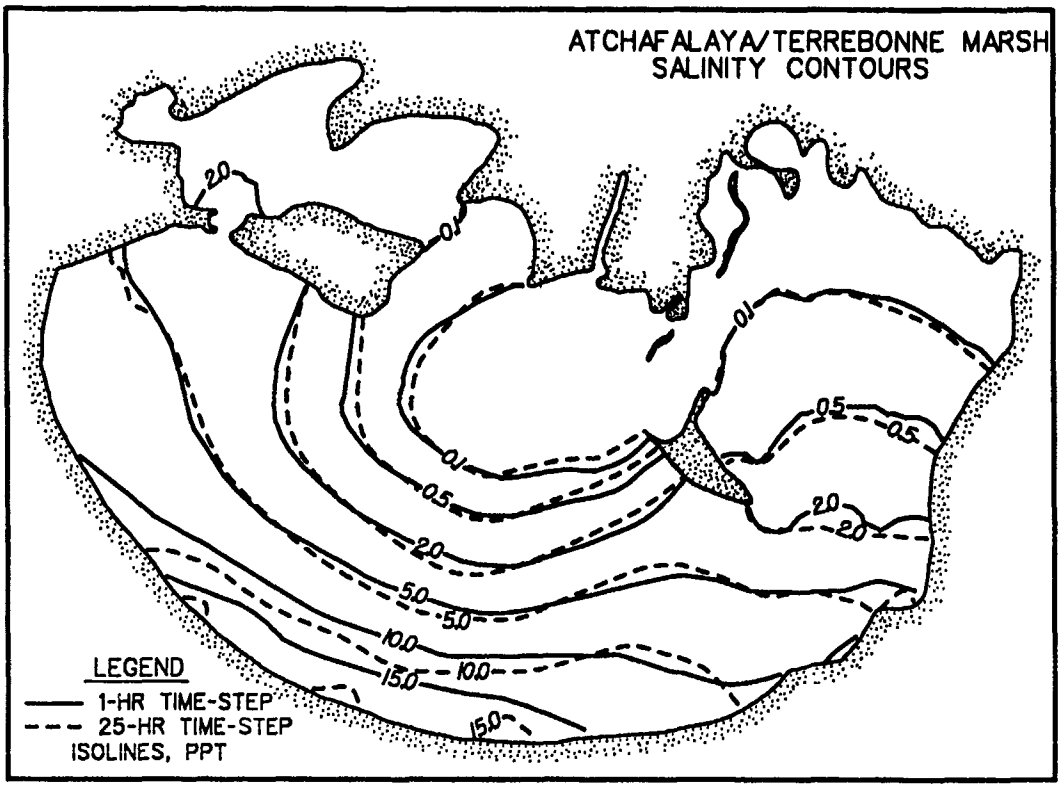

Figure 28. Isohalines, MESH6, 0.9-ft amplitude, 25-hr repeating diurnal tide, 330,000-cfs total discharge, existing conditions with project, year 0, 350-hr simuluation

the end of a 350-hr simulation, comparing contours of a 1-hr time-step (solid line) versus the extended 25-hr time-stepping method (dashed line) with present conditions for a discharge of 330,000 cfs. The model results comply with the overall pattern of prototype data presented earlier. Therefore, the combined network mesh reproduces prototype isolines satisfactorily with an extended time-step for the mean discharge.

110. With success of the extended time-stepping technique, low-flow salinity verification continued. Models were run dynamically for a minimum of 350-hr with a 78,000-cfs combined discharge, 25-hr repeating diurnal tide with a mean Gulf level and a 1.8-ft range.

111. At the beginning of a model computation, the mesh was initialized by zone according to field measurements. The Atchafalaya Bay was set to 0.1 ppt, Vermillion Bay 3.0 ppt, Fourleague Bay 5.0 ppt, Terrebonne Marshes 0.0 to 0.75 ppt, and the ocean area 15 ppt. The inflow salinity concentrations at WLO, LAR, and Lake Palourde each were specified to be 0.0 ppt. The offshore boundary was set between 10.0 and 32.0 ppt during inflowing conditions.

Results

112. Figure 29 shows contours of salinities from RMA-4 for present conditions at the 78,000-cfs discharge with mean tide described in paragraph 110. Comparison of Figure 29 to the September and November 1983 prototype data in Figure 27 shows that the model is generally comparable to the prototype.

113. The salinity model using MESH2 can simulate general salinity conditions without detailed adjustments of coefficients. Furthermore, the RMA-4 model running the combination of the Atchafalaya Bay and Terrebonne Marshes (MESH6 and subsequent meshes) was capable of reproducing demarcations of fresh to saline waters within the marshes.

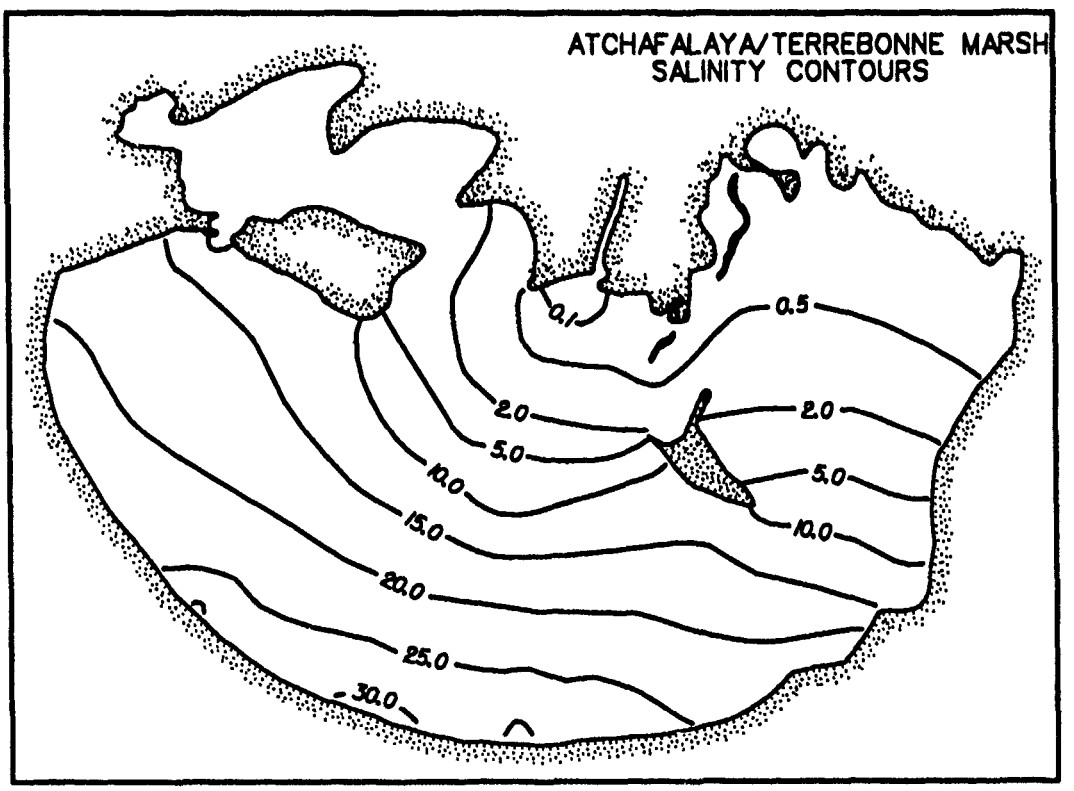

Figure 29. Isohalines, MESH6, 0.9-ft amplitude, 25-hr repeating diurnal tide, 78,000-cfs total discharge, existing conditions with project, year 0, 350-hr simulation, 25-hr time-step

PART V: SEDIMENTATION VERIFICATION OF DELTA GROWTH

Purpose

114. The purpose of the sediment transport model verification was to demonstrate reproduction of concentrations for the real-time simulation on a time scale of tidal cycles and the ability to statistically compose these events to simulate a 10-year trend. The 10-year delta evolution trend was verified for the period of 1967 through 1977, which incompasses significant delta formation.

115. Verification of sediment transport to specific events or for time scales of tidal cycles was performed by comparing computed suspended sediment concentrations with field observations at the appropriate discharge level.

116. Verification for delta evolution was accomplished by comparing the predicted delta configuration with observed deltaic growth for the period of 1967 through 1977. In addition, the sediment model channel dredging predictions were compared to 1973-1985 prototype LAR dredging records.

Site Characteristics

Deltaic sediments

117. Atchafalaya Bay sediments are classic deltaic sediments. The earlier deposits are prodelta clays deposited slowly and uniformly at lower river stages over time. Then sand deposits followed with the passage of high river flows. These sand deposits were either very thin and subsequently covered by more clay deposits, or very thick, eventually becoming subaerial. Once subaerial, sand lobes were vegetated and stabilized. Over the past 20 years, the size distribution of the material entering the bay has shifted from dominantly silts and clays toward fine sands, silts, and clays (McAnally and Heltzel, in preparation). An example of this layering is evident in Core J (Photo 3), collected 2,500 m east of the Atchafalaya Bay navigation channel in the spring of 1980. The radiograph analysis by Wells follows.* At the 36- to 47-cm depth, the core shows fine-grained sediment deposition in a low-energy

---

* John T. Wells, presonal communication, 12 December 1980, Coastal Studies Institute, Louisiana State University, Baton Rouge, LA.

environment, typical of the back-bar algal flats that occur within the delta. Overlying this, at the 26- to 36-cm depth, are cross-laminated fine-grained sands (lighter tones), indicating a relatively high discharge event, such as the 1975 flood. Fine-grained sedimentation is again evident in the 11- to 26-cm depth. The different sediment texture is probably the result of seasonal variations in weather, river discharge, and sediment load. The deformation at the 11-cm depth may have formed from human footsteps. Organic-rich layers at 7 cm occurred when marsh vegetation began to establish. The upper 3 cm of this core sample are deposits that occurred during the 1979 flood. Core J is located where the elevation is now slightly above mean sea level, and a vigorous marsh growth exists, as evidenced by the numerous root burrows at the top.

Grain size distribution

118. Prototype sediment analysis found that sediment inflows to the basin are normally 22 percent sand and 78 percent silt/clay. During high-flow years, the proportion of sand seems to increase to about 25 percent. Grain size analyses indicate that near the river mouths, sediments are also about 20 percent sand but that sand fractions decrease with distance seaward to less than 10 percent sand. Sand is generally not transported beyond the throat of the LAR except for higher discharges. Reports 3 (Letter 1982) and 4 (Wells, Chinburg, and Coleman 1984) of this series suggest that the major increases in the subaerial land in the bay occurred between 1973 and 1975 as a result of high inflows and associated movement of an accumulation of sediment, especially sand, in the basin.

119. The station locations for field bottom grab samples are presented in Figure 30. The results of the grain size analysis (Report 2, Section 3 (Pankow, Teeter, Donnell, and Adamec 1990)) are summarized in Figure 31. Presented are the extremes, the mean, and standard deviations about the mean for the grain size distribution. The mean grain size ranged from 1 micron to 233 microns.

Bed material densities

120. Based on laboratory tests, initial concentrations of newly deposited sediment are expected to be relatively high (0.7 g/cc) near river mouths. Out in the bay where sediments are finer and more cohesive, newly deposited sediments are expected to be on the order of 0.4 g/cc (Report 2, Section 2 (Teeter and Pankow 1989)).

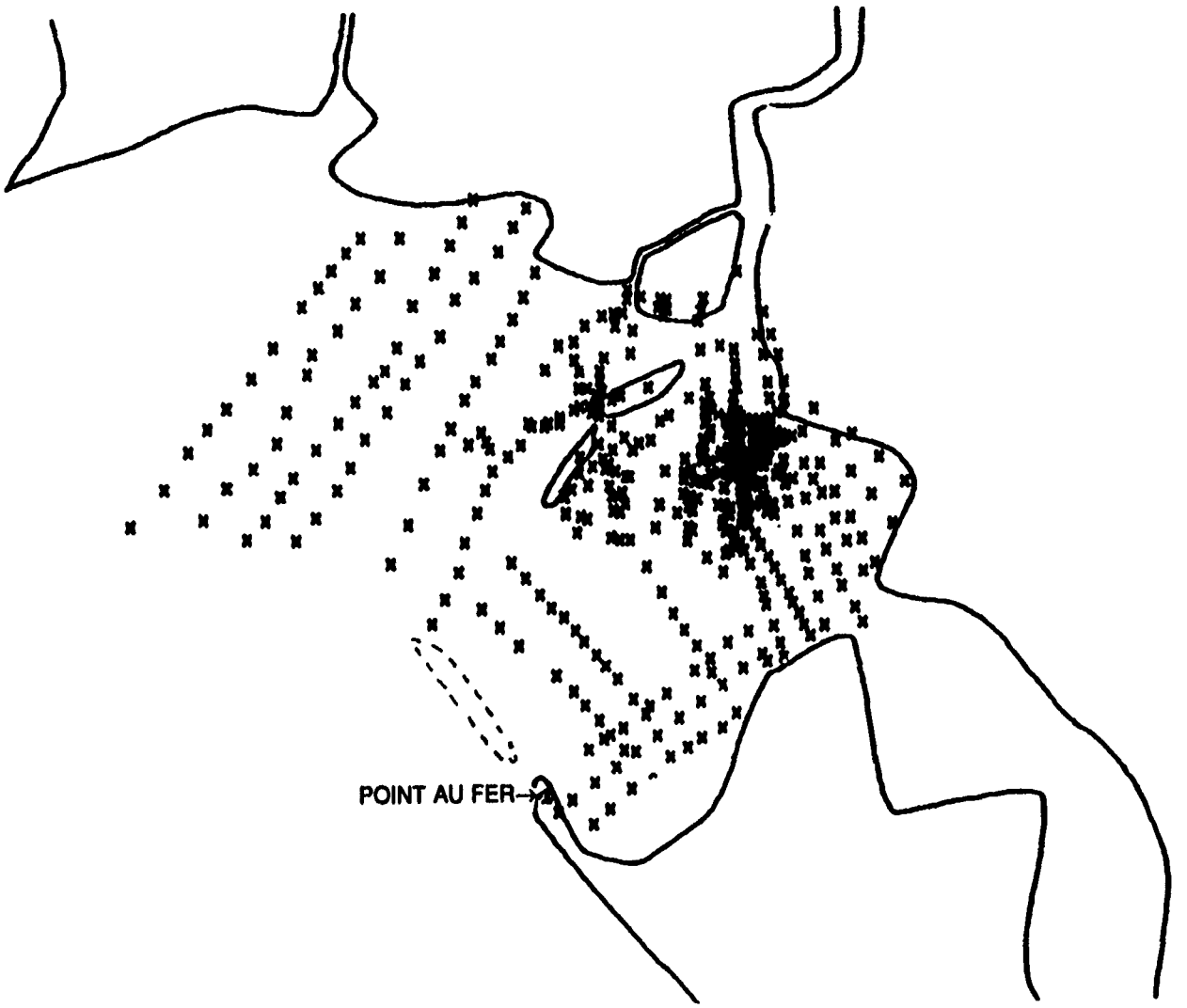

Figure 30. Station locations for field bottom grab samples

Suspended material

121. The average annual suspended sediment load of the LAR for the period 1965-1971 was estimated to be 47 million tons (USAED, New Orleans, 1974). The average annual suspended sediment load during the high-flow year of 1973-1975 was 98 million tons.

122. Suspended material sampling was conducted intermittently from July 1980 through June 1983. Sampling stations for suspended material are shown in Figure 32. The sampling indicated that the concentrations in the bay often exceed those of the river inflow. The tide (range and phase) appeared to be the dominant influence on suspended concentrations, with higher concentrations at spring tide and generally during flood phase. Wind had little influence on the concentrations during the sampling, which had maximum winds of about

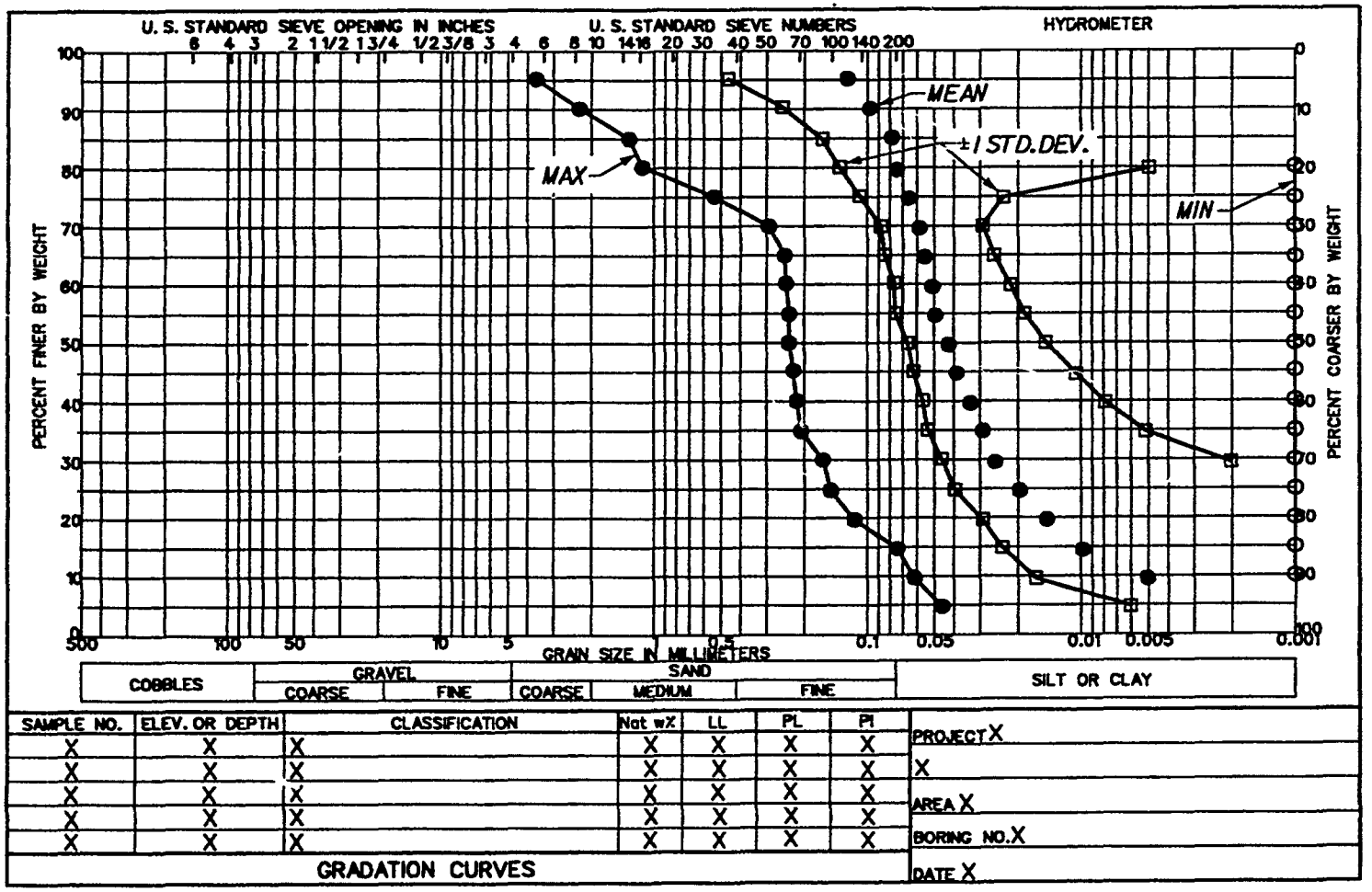

ENG FORM 1 MAY 63 2087

Figure 31. Composite bed gradation curve for all bay samples

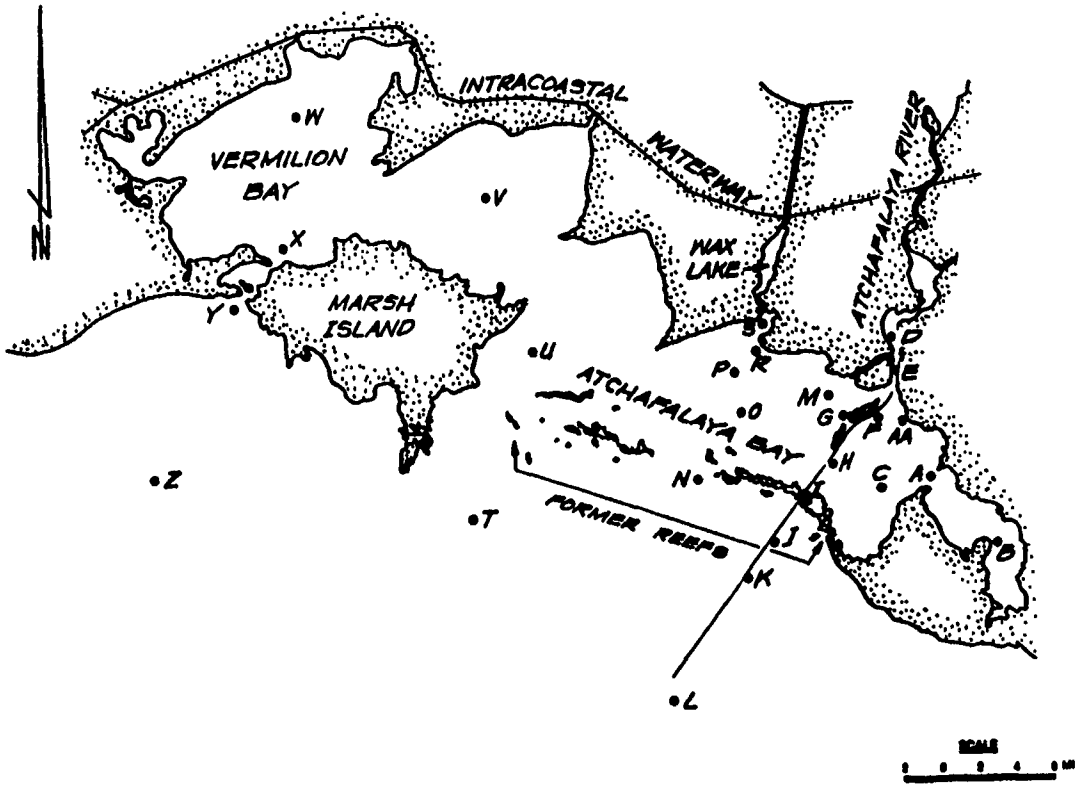

Figure 32. Suspended material sampling stations in the Atchafalaya Bay system, Louisiana

15 knots, with 2-ft waves (Report 2, Section 2 (Teeter and Pankow 1989)).

Settling velocities

123. Field settling velocity tests were conducted, yielding a probability distribution of settling velocity (Figure 33). Settling velocities of suspended material, in general, showed higher rates near river mouths but were also large offshore of Eugene Island where flocculation of cohesive materials may be accelerated (Report 2, Section 2 (Teeter and Pankow 1989)). Field settling velocities showed no correlation to suspended concentration, although laboratory tests showed that, for a given sediment, such a correlation existed. Mean settling velocities of suspended material were found to vary from 0.005 to 0.3 mm/sec, while median values ranged from 0.001 to 0.1 mm/sec.

Critical shear stresses

124. Analyses performed at WES and by Mehta (1984) showed that the critical shear stress for erosion (the bed shear stress above which erosion of sediment occurs) in the Atchafalaya system fell between 0.05 and 0.17 N/sq m, while the critical shear stress for deposition (the bed shear stress below which deposition of suspended sediment occurs) was less than 0.08 N/sq m.

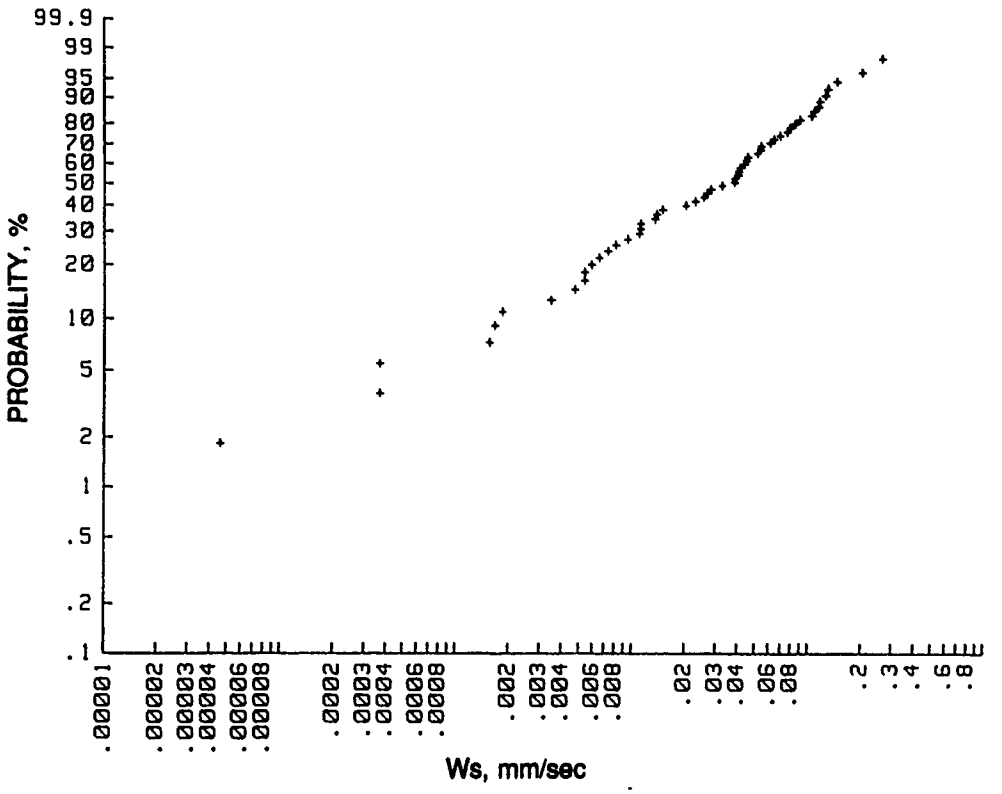

Figure 33. Probability distribution of field settling data

Model and Process Description

125. Computer code STUDH of the TABS-2 numerical modeling system was used to model 2D depth-averaged sediment transport using hydrodynamics previously computed with RMA-2.

126. The sediment transport model, STUDH, solves the depth-averaged equation of conservation of suspended sediment mass, normally referred to as the convection-diffusion equation. The equation has a source-sink term for bed interaction, which is handled differently for cohesive and noncohesive materials. For sand, the term is proportional to the difference between the ambient concentration and the concentration representing transport potential for the specified hydrodynamic conditions. The source-sink term for cohesive material is based on the relationship between the bottom shear stress and the entrainment rate of material for erosion, and the fall velocity for deposition. The equation uses dispersion coefficients for the diffusion terms. The model is described in detail by Thomas and McAnally (1985).

127. The process modeled was depth-integrated sediment transport in a shallow bay with little or no vertical variation. Locally generated wind

waves contribute to the well-mixed conditions within the bay. For flows without significant density stratification, the depth-integrated calculation of sediment transport (average velocity times average concentration) is a reasonable approximation for most sediment sizes, including the clays, silts, and fine to medium sands occurring in Atchafalaya Bay (McAnally 1989).

Modeling Procedure

Delta evolution simulation strategy

128. The modeling procedure for the long-term (50-year) simulation of delta evolution in the bay was subdivided into a series of shorter steps (10-20 years) within which the details of the hydrodynamic and sediment transport processes were defined for the current delta configuration. The total 50-year simulation was made in three steps, described in detail in the next section of the report. The methodology logic is presented in Figure 34. An event will be described in the following paragraphs.

Verification period

129. The period selected for verification of delta evolution was from 1967 through 1977, the historical period of most rapid subaerial delta growth. The New Orleans District provided WES with the starting prototype bathymetric condition in 1967. These depths were incorporated in MESH2-67 as shown in Plate 23. Depths in areas without recent detailed survey coverage were taken from available navigation charts of the area. This approach normally yields depths shallower than actual depths, since navigation charts are typically conservative with regard to navigable depth; however, since those charts were several years old, deltaic sedimentation would have made those depths shallower.

130. This verification can be viewed as a verification of one of the medium-term delta evolution increments of Figure 34 (inside the outermost loop). The verification also addresses the short-term processes of each event on atime scale of tidal cycles. The verification procedure (1967-1977) logic is presented in Figure 35.

Definition of an Event

131. Extrapolating sedimentation rates from real-time tidal cycle simulations to longer periods was performed by application of joint probabilities to the combinations of river discharge, wave conditions, and Gulf water levels

FLOWCHART OF THE LONG-TERM DELTA EVOLUTION SIMULATION

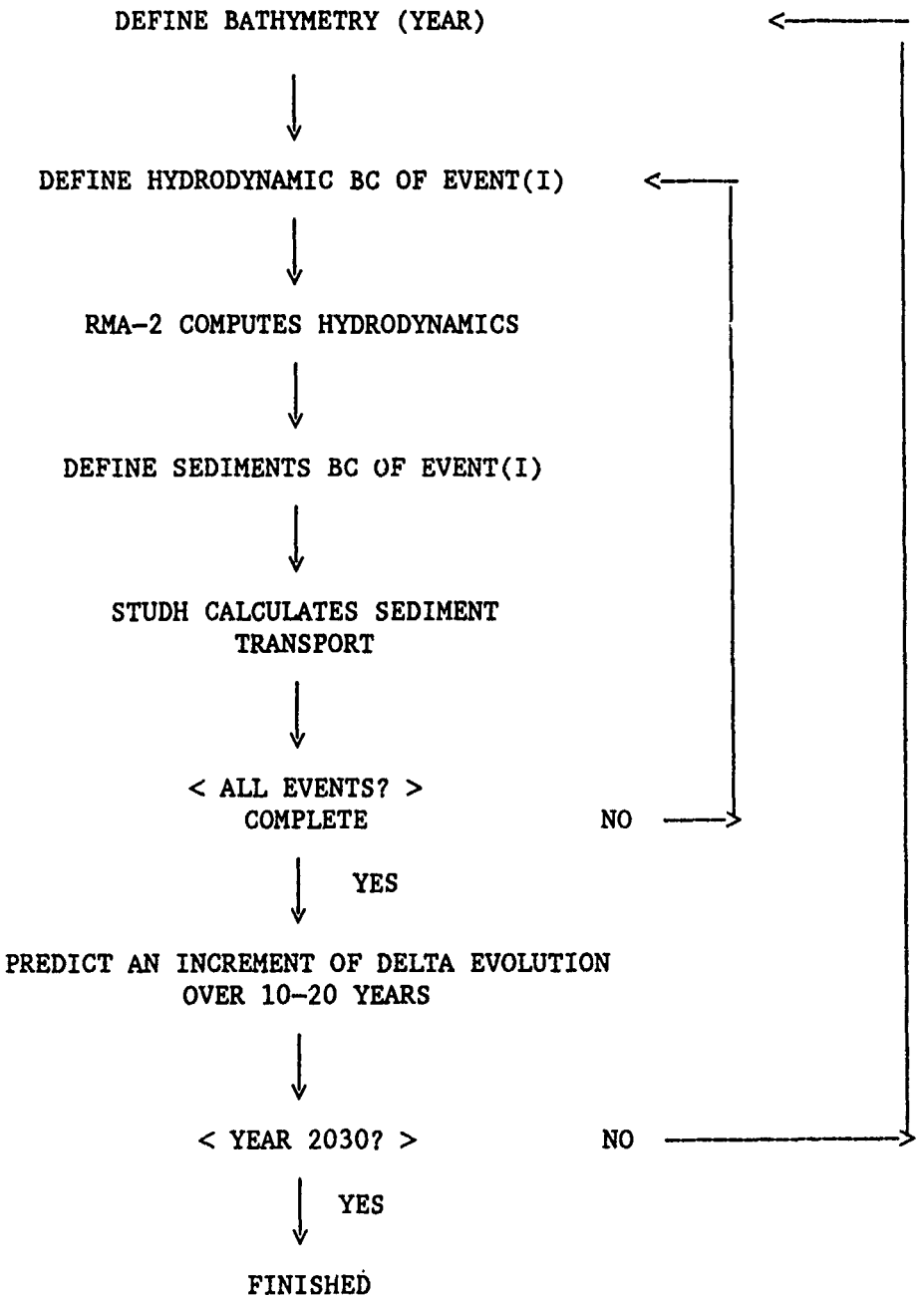

Figure 34. Flowchart of the long-term delta evolution simulation

FLOWCHART OF THE SHORT-TERM DELTA EVOLUTION VERIFICATION

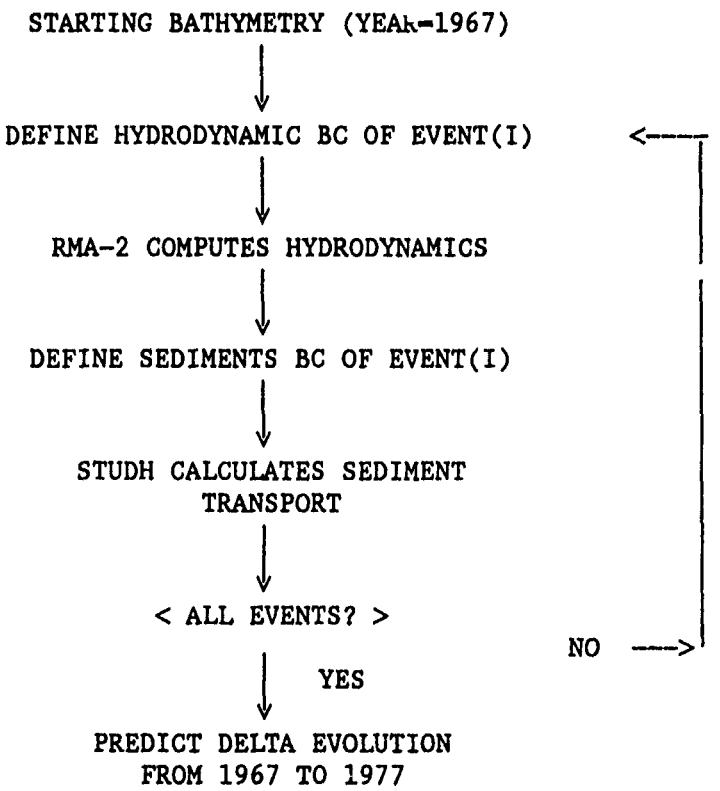

Figure 35. Sedimentation verification procedure

used for real-time simulation "events." These simulation events were used to define sedimentation rates. These event rates were then combined with the corresponding joint probability for each event and extended over the period of the verification and then summed.

132. River discharge schematization. The river discharges at Simmesport, LA, for the period of 1961 through 1977 are presented in Figure 36. These flows were analyzed to develop a probability curve for the period from 1967 through 1977 (Figure 37). The river discharges were schematized as shown graphically in Figure 38. Representative discharges of 150,000, 330,000 and 570,000 cfs were chosen to be consistent with the discharges schematized in the quasi-2D modeling work (Report 5 (Thomas et al. 1988)). The discharge probabilities associated with these flows were 0.54, 0.37 and 0.09, respectively.

133. The discharge at Simmesport was distributed as 30 percent to WLO and 70 percent to the LAR for all discharges used in the sedimentation verification from 1967 to 1977.

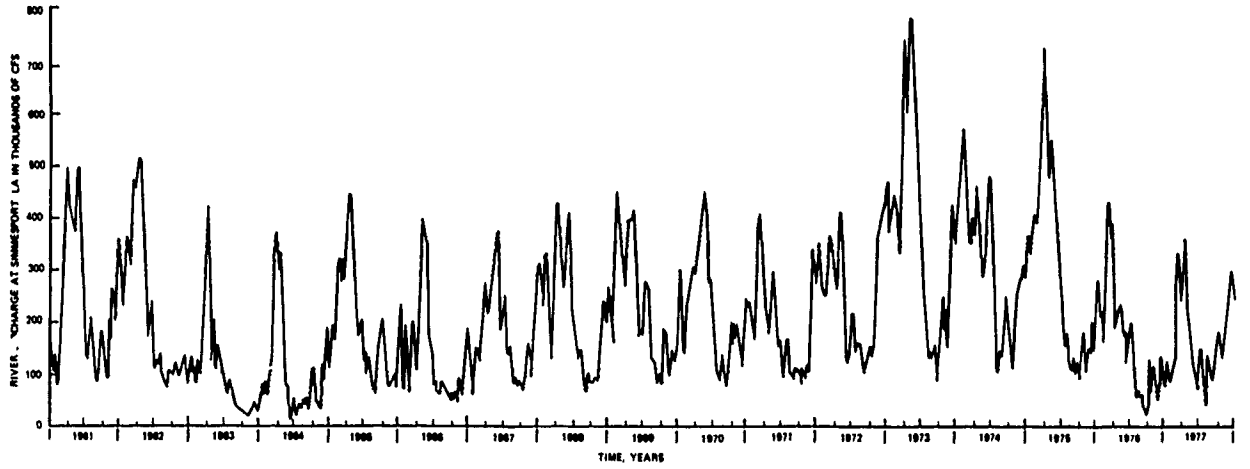

Figure 36. Discharge hydrograph for the Atchafalaya River at Simmesport, LA, 1961-1977 (New Orleans District 1974)

134. Wave conditions schematization. The wave conditions for the Atchafalaya Bay were defined in Report 10 by Jensen (1985) using field data collected from November 1981 to February 1982. The average cumulative probability distribution for the bay (wave stations WG-25 and WG-66, Figure 39) for the bay is presented in Figure 40. The wave conditions were discretized to wave heights of 0.0, 0.25, and 0.50 ft with no consideration given to wave direction. The probabilities associated with these wave heights are presented in Table 10, and the joint probabilities (assuming that waves and riverflow are uncorrelated) between the wave heights and the discretized river discharges are computed:

Table 10

Joint Probabilities of Wave and Discharge

For Delta Growth Verification (1967-1977)

Wave		Discharge, cfs (Probability)		
Wave Height ft	Probability	150,000 (0.54)	330,000 (0.37)	570,000 (0.09)
0.0	(0.08)	0.04	0.03	0.01
0.25	(0.44)	0.24	0.03	0.04
0.75	(0.48)	0.26	0.18	0.04

135. Gulf level. For the verification simulations, the Gulf tide mean water level was chosen to be NGVD (1929 adjustment). A mean Gulf level adequately represents the primary processes being modeled over periods greater than 1 year.

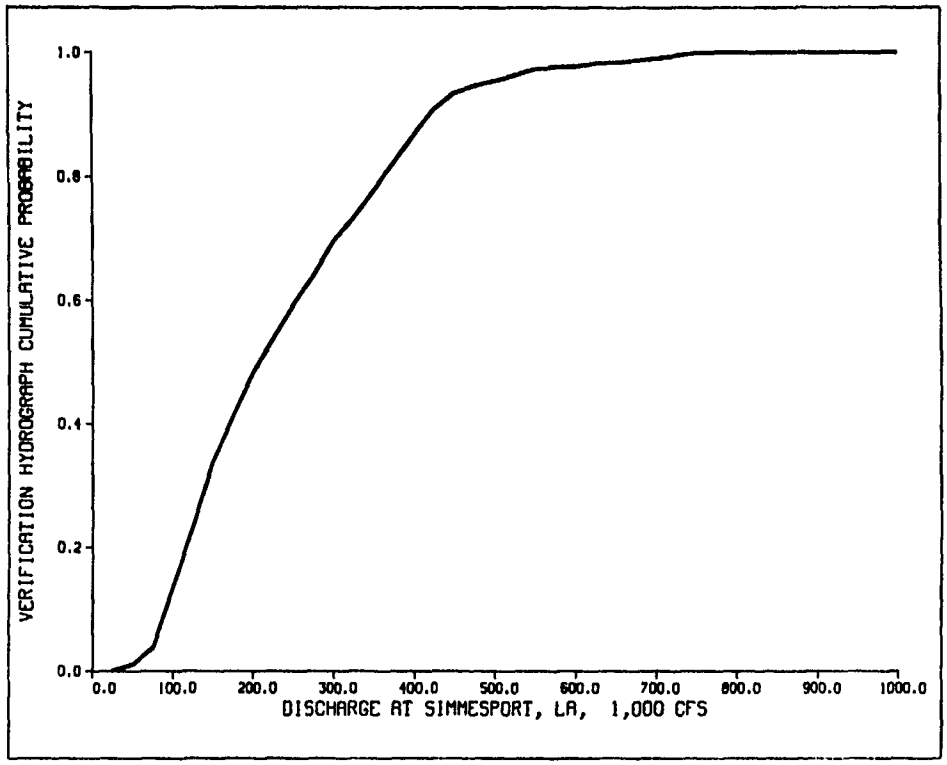

Figure 37. Probability curve for river discharge at Simmesport, LA

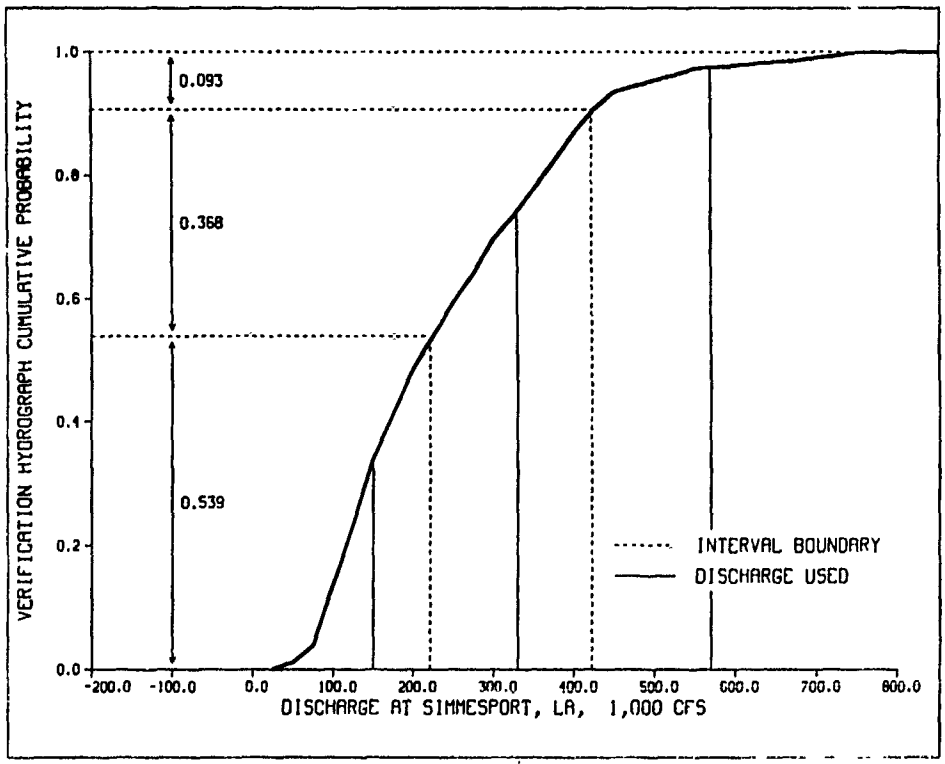

Figure 38. Schematized probability curve for river discharge at Simmesport, LA, for the period 1967-1977

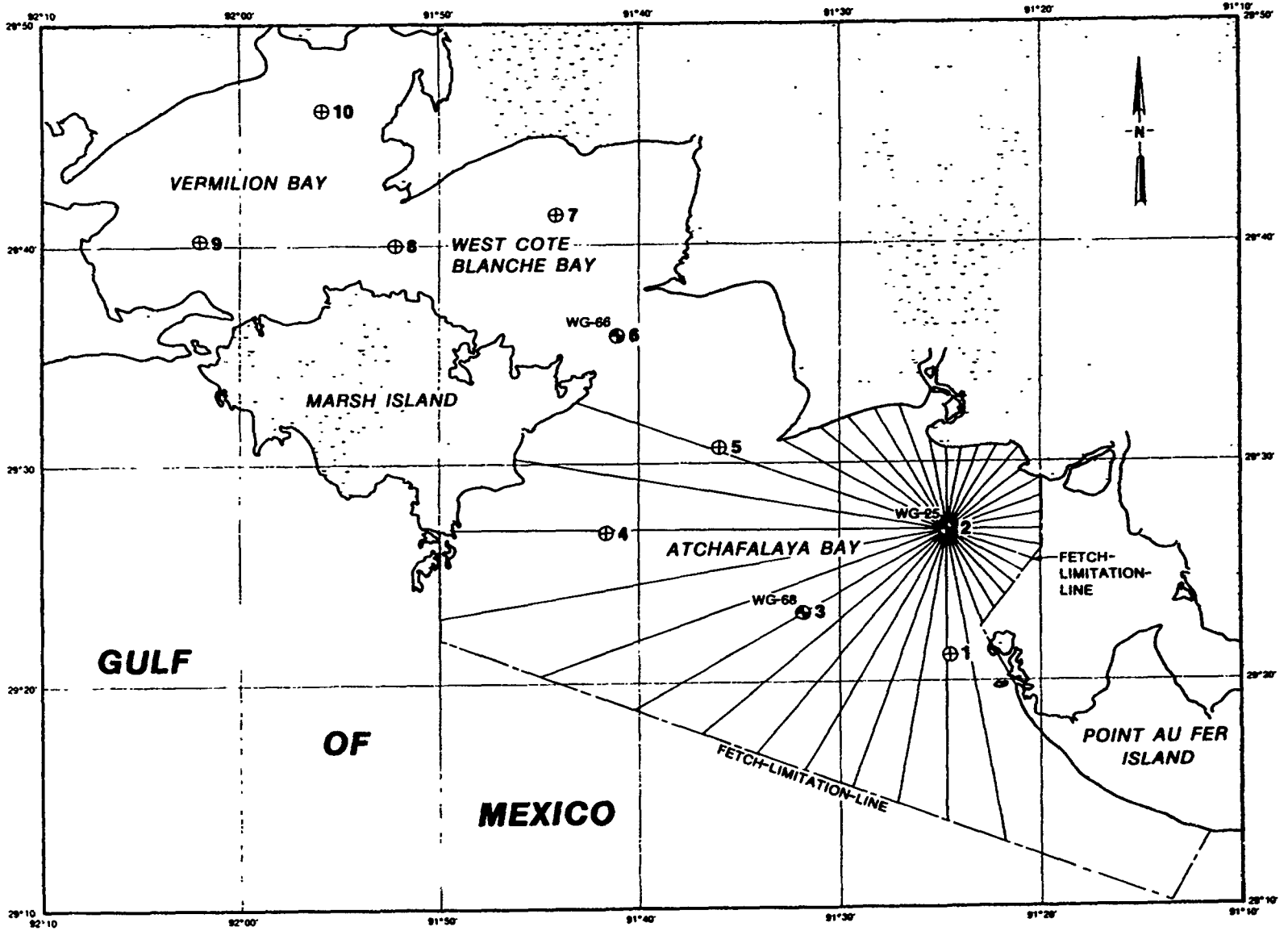

Figure 39. Wave hindcast study area displaying station and wave gage locations

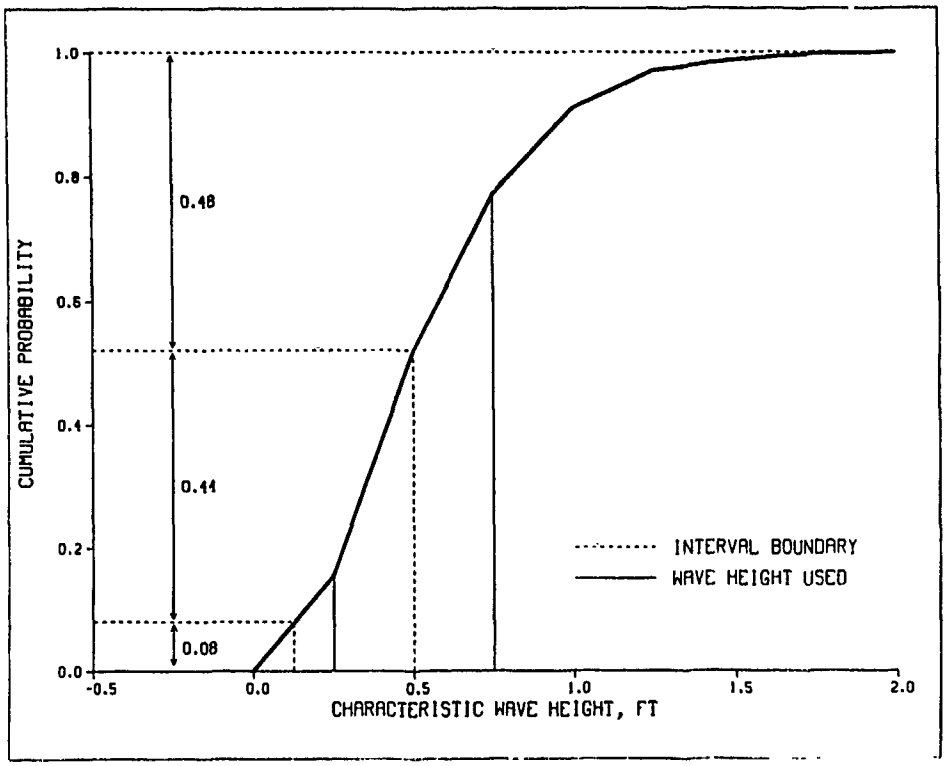

Figure 40. Average cumulative frequency distribution for wave stations WG-25 and WG-66 (November 1981-February 1982)

136. Sediment class. The depositional environment of Atchafalaya Bay results in complex bed structures. It was assumed for the modeling work that the cohesive and noncohesive sediment deposition processes are independent of one another. Therefore, these two classes of sedimentation were treated as independent separate events, with the same probabilities (defined by the hydrodynamics) applied to both the cohesive and noncohesive classes. The spatial sorting of the sediment classes was handled automatically in the modeling by the transport capacities during each event.

137. The processes modeled included both cohesive (COH) and noncohesive (NONCO) sediments at discharges which are significant to their contribution to delta growth. That is, the model showed little transport of noncohesive sediments for discharges below 330,000 cfs; therefore, sand simulations were assumed to be negligible for those discharges. However, the cohesive sediments were modeled at all selected flows.

138. The events tested for the verification are summarized in Table 11. These simulations were run early in the study to assess the sensitivity of the sedimentation to various conditions. It was observed that with any wave

Table 11

Events Tested for Verification of Delta Evolution

Event Number	Simmesport Discharge, cfs	Wave Height, ft	Gulf Level		Sediment Type		Joint Probability
			Mean	High	NONCO	COH	
1.1	570,000	0.00	*		*		0.01
1.2	570,000	0.25	*		*		0.04
1.3	570,000	0.75	*		*		0.04
2.1	570,000	0.00	*			*	0.01
2.2	570,000	0.25	*			*	0.04
2.3	570,000	0.75	*			*	0.04
3.1	330,000	0.00	*		*		0.03
3.2	330,000	0.25	*		*		0.03
3.3	330,000	0.75	*		*		0.18
4.1	330,000	0.00	*			*	0.03
4.2	330,000	0.25	*			*	0.03
4.3	330,000	0.75	*			*	0.18
5.1	150,000	0.00	*			*	0.04
5.2	150,000	0.25	*			*	0.24
5.3	150,000	0.75	*			*	0.26

energy, deposition for cohesive material was inhibited to the point where essentially all suspended material was flushed through the system. The simulations of sand transport were found to be essentially independent of the wave energy, with the majority of the sand depositing near the mouth of WLO and of LAR, primarily dependent on river discharge.

139. In an effort to reduce the number of conditions to be run in a single short-term step, a revised verification scenario was developed which reflected these observations (Table 12). Therefore, only the simulations with no waves were subsequently included in the extrapolation scenario. The cohesive runs had probabilities from Table 12 (0.04, 0.03, and 0.01) applied for the particular discharge, reflecting the impact on cohesive sedimentation when wave energy is present. The sand simulations were also limited to the no-wave condition, but with the total discharge probabilities of 0.37 for the 330,000-cfs, and 0.09 for the 570,000-cfs discharge applied to the sedimentation rates, reflecting the lack of sensitivity of noncohesive sedimentation to the specific wave condition.

140. Tidal boundary condition. Harmonic analysis of prototype field data, using the M2, S2, K1, O1, P1, and N2 tidal components (Part III)

Table 12

Revised Events Used for Verification of Delta Evolution

Event Number	Simmesport Discharge, cfs	Wave Height, ft	Gulf Level		Sediment Type		Joint Probability
			Mean	High	NONCO	COH	
1	570,000	0.00	*		*		0.09
2	570,000	0.00	*			*	0.01
3	330,000	0.00	*		*		0.37
4	330,000	0.00	*			*	0.03
5	150,000	0.00	*			*	0.04

resulted in the use of a diurnal synthesized tide with a 1.8-ft amplitude at the Gulf of Mexico border. A 25-hr repeating diurnal tide at the outermost tide station (TG-8) was chosen as a representative computationally efficient tidal boundary condition for the long-term delta growth prediction.

141. Sediment boundary conditions. The LAR and WLO boundary conditions for the sediment transport model, STUDH, were taken from the quasi-2D study (Report 5 (Thomas et al. 1988) of this series). Both cohesive (silt and clay) and noncohesive (0.11-mm sand and silt) sediment transport model runs were used to simulate the evolving delta for the 10-year verification period, as mentioned earlier. These data are summarized in Table 13. The Gulf boundary condition was specified as a outward flux only, with no return of material to the model.

Table 13

Sediment Concentration Boundary Conditions for Each Event

Sediment Type	Discharge cfs	Concentrations, ppm	
		LAR	WLO
Noncohesive*	570,000	500	500
Cohesive	570,000	500	500
Noncohesive*	330,000	500	500
Cohesive	330,000	230	230
Cohesive	150,000	133	133

* Noncohesive events had a grain size of 0.11 mm.

142. Coefficients. Hydrodynamic coefficients such as Manning's n value and eddy viscosity were set according to the RMA-2 verification as described in Part IV. The following sedimentation coefficients were determined by

analysis of prototype samples and used for the sediment transport model in predicting delta growth rates:

a. Critical shear stress for erosion = 0.05 N/m^2

b. Critical shear stress for deposition = 0.03 N/m^2

c. Dispersion coefficients = 50 to 25 m^2/sec

d. Settling velocity of sand = 0.01 m/sec

e. Particle size of sand = 0.11 mm

f. Settling velocity of clay = 0.5 mm/sec

g. Particle erosion rate constant for clay = 0.002 $kg/m^2/sec$

Results

143. The results of the sediment transport simulations were compared with field data in two ways: to measured total suspended solids at locations over the bay and adjacent waters and to delta growth.

Suspended sediment concentrations

144. The field observations of suspended sediment concentrations were made during 1981. Therefore, the numerical model simulations used for comparison to the field data were made using MESH7 with the current bathymetric conditions (1980) for the bay.

145. The sediment transport model results for noncohesive suspended sediment concentrations at a river discharge of 150,000 cfs are compared with observed field concentrations for a river discharge of 140,000 cfs in Table 14 and Figure 41. The numerical model results are shown as the range from the minimum to the maximum concentrations over the tidal cycle as well as the average concentration over the cycle. The field data presented, though sparse for this discharge, indicate the range of concentrations measured at various phases of the tide and reflect sampling from either near bottom or middepth. The field data for suspended sediment concentrations were not monitored over complete tidal cycles.

146. The spatial distribution of the numerical model suspended concentrations for the 1980 bathymetry is presented in Plate 24 for the 150,000-cfs test case. No attempt was made to develop contours of suspended sediment concentrations for the field data since the data were too sparse and contouring would be too subject to judgment.

147. The suspended concentrations for the 330,000 cfs are presented in

Table 14

Sediment Concentrations Collected 27-29 November 1981 Compared to STUDH 150,000-cfs Cohesive Event MESH7 (Plan D) Existing Conditions, Year 1980

Field Station Identifier	Prototype Min - Max mg/l	STUDH Cohesive Min - Max mg/l	STUDH Avg mg/l
A	N/A	0 - 360	48
B	N/A	0 - 1	0
C	97*	8 - 110	47
DM#3	N/A	124 - 160	138
E	N/A	120 - 161	138
F	N/A	82 - 195	130
G	N/A	1 - 66	23
H	N/A	21 - 169	90
I	N/A	6 - 82	38
J	23*	3 - 102	41
K	21*	2 - 25	10
L	N/A	3 - 11	6
M	472*	4 - 70	27
N	95*	1 - 25	5
O	N/A	34 - 240	124
P	N/A	50 - 277	129
R	560*	126 - 142	131
S	N/A	132 - 133	133
T	N/A	1 - 8	5
U	N/A	2 - 106	50
V	N/A	1 - 5	0
W	N/A	0 - 0	0
X	N/A	46 - 449	196
Y	N/A	1 - 326	162
Z	N/A	3 - 12	7
AA	N/A	62 - 173	97
JAWS	N/A	0 - 1	0
TG15	N/A	4 - 392	69

* Indicates only one reading.

Table 15. The comparisons between model and field concentrations are shown graphically in Figure 41. There is a fairly large scatter in the range of concentrations observed.

148. The spatial distribution of the concentrations of sand and clay from

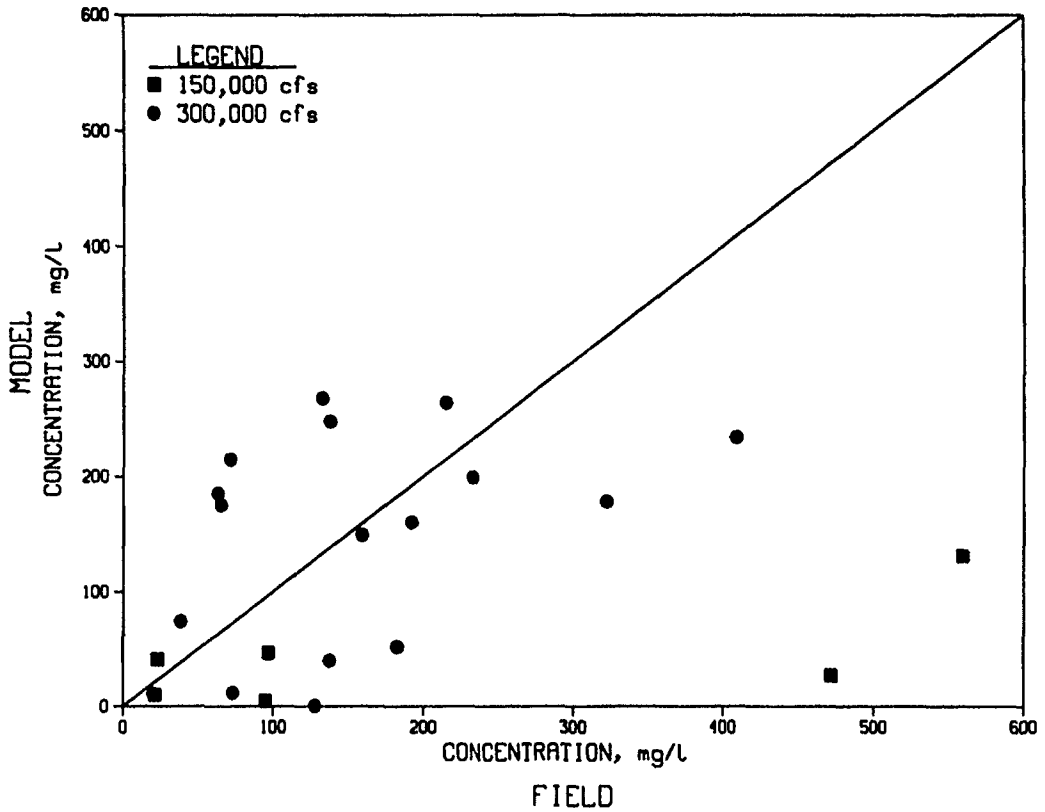

Figure 41. STUDH model versus prototype suspended sediment concentrations, 1980 delta

the 1980 bathymetric condition of the STUDH numerical model for the 330,000-cfs condition are presented in Plates 25 and 26.

149. The spatial distribution of the concentrations of sand and clay from 1980 bathymetric condition of the STUDH numerical model for the 570,000-cfs condition are presented in Plates 27 and 28. No prototype suspended data were collected at a river discharge high enough for comparison with the 570,000-cfs model simulations.

Delta evolution prediction

150. The predicted 1977 delta configuration (with subsidence) based on a starting bathymetry of 1967 using the same extrapolation procedure is presented in Figure 42. This is compared with the actual 1977 bathymetry in Figure 43. Legible LANDSAT images obtained between February and November 1977 indicate that the size of the LAR and WLO prototype deltas fall between the extremes of 4.5 and 15.5 square miles. The majority of the newly developed predicted delta (18.6 square miles subaerial) is located in the northern section of the bay adjacent to the river mouths.

Table 15

Sediment Concentrations Collected 23-26 June 1981, Compared to STUDH 330,000-cfs Cohesive and Noncohesive Events MESH7 (D) Existing Conditions, Year 1980

Field Station	Prototype Min - Max (mg/l)	STUDH, mg/l COH Min - Max	NONCO Min - Max	Combination Min - Max	Avg
A	180 *	30 - 451	0 - 0.3	30 - 451	93
B	67 - 188	0.1 - 1	0 - 0	0.1 - 1	0.5
C	125 - 259	65 - 375	0 - 0	65 - 375	160
DM#3	120 - 698	207 - 215	11 - 36	218 - 251	234
E	95 - 171	207 - 215	27 - 90	234 - 305	268
F	113 - 317	204 - 209	12 - 123	216 - 332	264
G	N/A	40 - 179	0 - 0	40 - 179	116
H	164 - 301	153 - 240	0 - 5	153 - 245	199
I	136 - 507	68 - 251	0 - 0.5	68 - 252	178
J	N/A	31 - 201	0 - 0	31 - 201	112
K	181 - 185	9 - 121	0 - 0	9 - 121	52
L	7 - 33	6 - 19	0 - 0	6 - 19	11
M	85 - 233	62 - 237	0 - 1	62 - 238	149
N	N/A	23 - 117	0 - 0	23 - 117	72
O	63 - 213	206 - 214	5 - 95	211 - 309	248
P	N/A	208 - 214	10 - 110	218 - 324	261
R	189 - 365	229 - 230	323 -1259	552 -1489	989
S	N/A	229 - 230	152 - 284	381 - 514	449
T	N/A	6 - 42	0 - 0	6 - 42	19
U	133 - 143	4 - 96	0 - 0	4 - 96	40
V	N/A	0 - 9	0 - 0	0 - 9	1
W	N/A	0 - 1	0 - 0	0 - 1	0
X	55 - 70	31 - 431	0 - 1	31 - 432	185
Y	59 - 72	0 - 321	0 - 20	0 - 341	175
Z	2 - 143	3 - 21	0 - 0	3 - 21	12
AA	43 - 98	190 - 197	7 - 39	197 - 236	215
JAWS	93 *	0 - 8	0 - 0	0 - 8	0
TG15	13 - 59	1 - 390	0 - 67	1 - 457	74

* Indicates only one reading.

151. The sediment transport model projected that the total volume of sediments deposited within the immediate Atchafalaya Bay area for the 1967-1977 period was 225 million cubic yards (without subsidence). This is 23 percent of the total estimated sediment yield from the upper Atchafalaya River basin (120 million tons/year, or 987 million cubic yards). This agrees

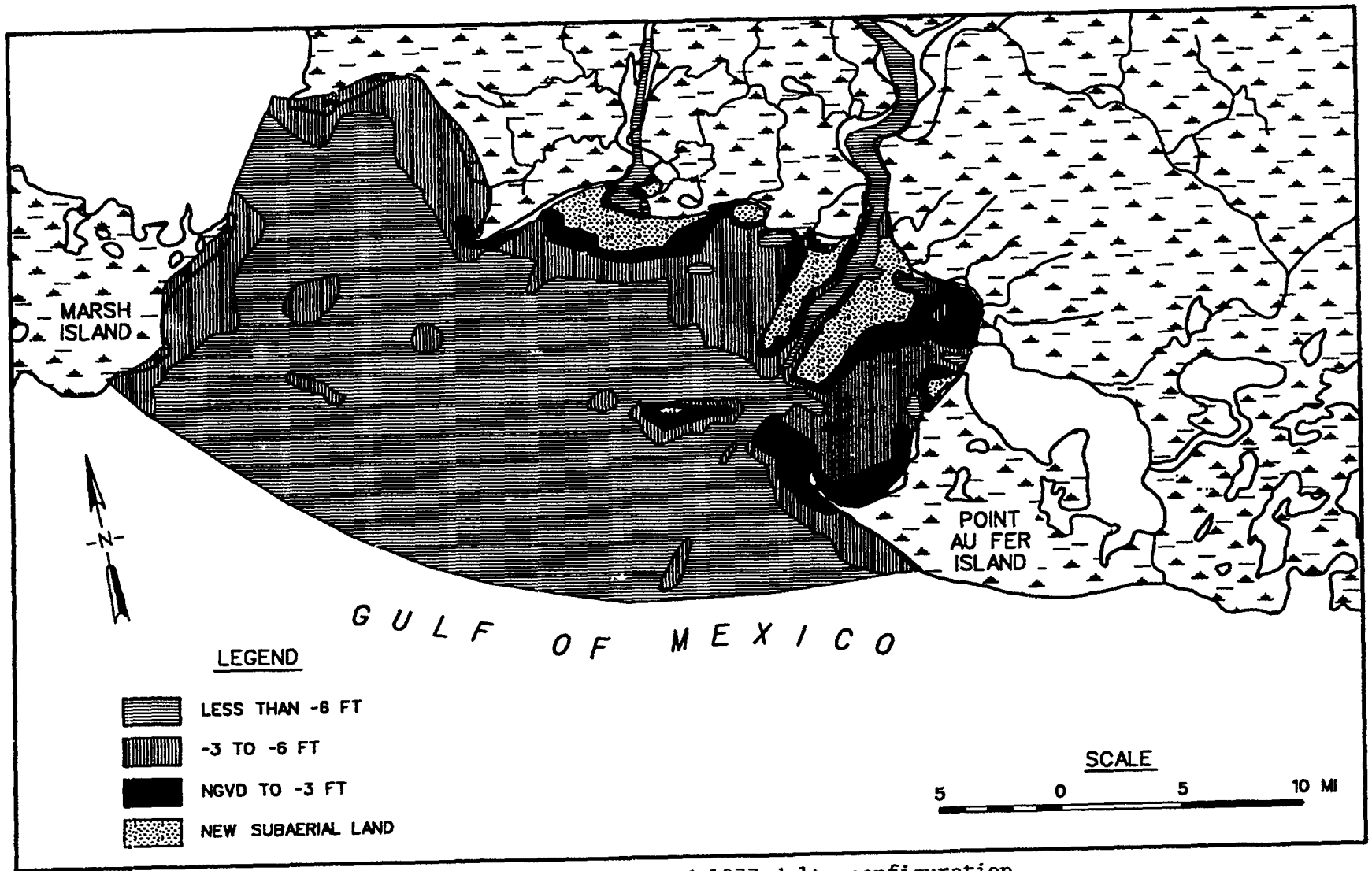

Figure 42. STUDH-predicted 1977 delta configuration

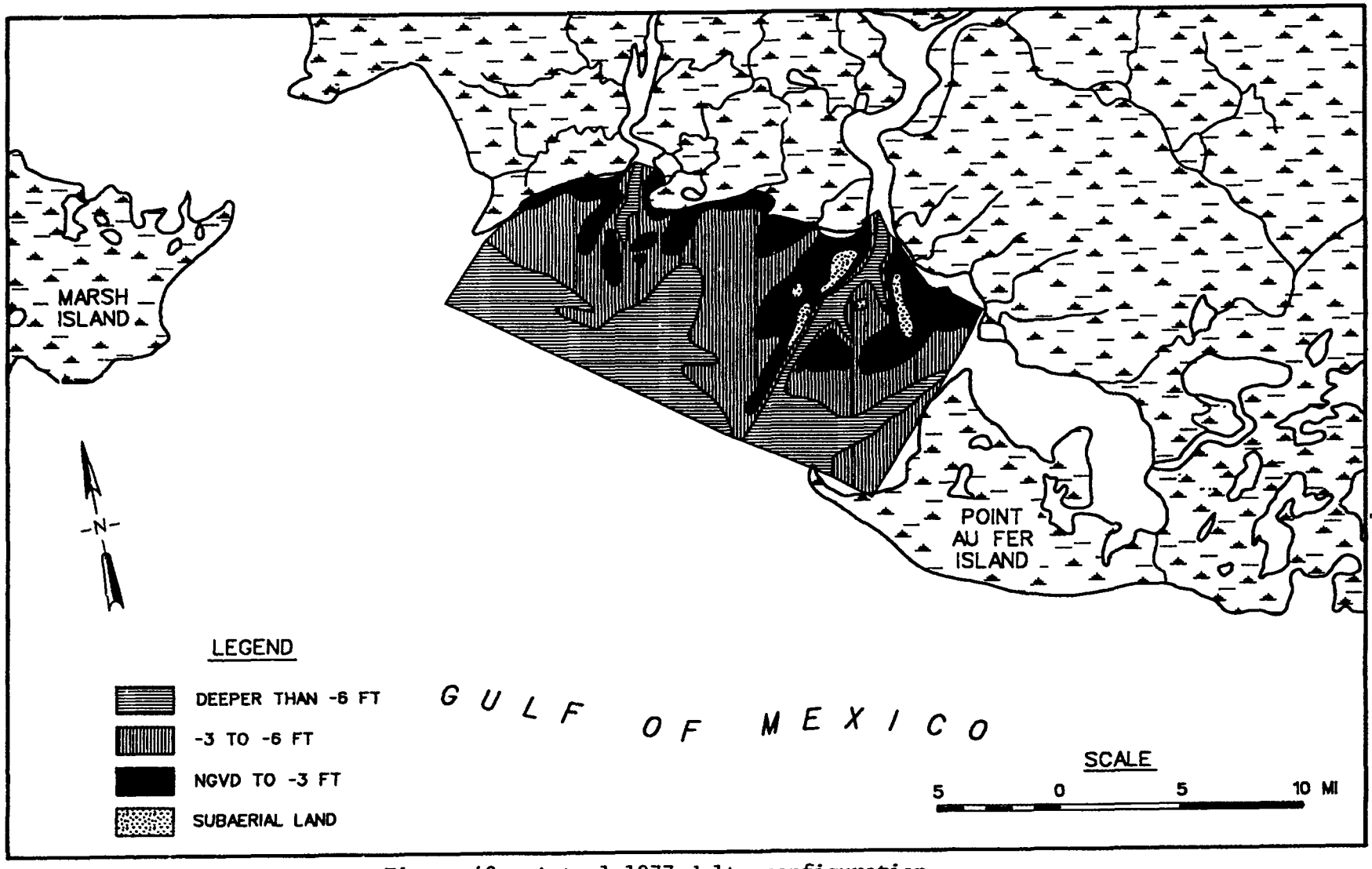

Figure 43. Actual 1977 delta configuration

well with the first 10-year estimates given by the extrapolation technique, (Letter 1982), the quasi-2D approach, (Thomas et al. 1988), and the generic analysis (Wells, Chinberg, and Coleman 1984). Table 16 provides a comparison.

Table 16

Comparison of Projected Total Volume of Sediments Trapped in Atchafalaya Bay Over 10 Years

Tool	Trapped Sediments million cubic yards	Projected Year From - To
STUDH 2D FE	225	1967 - 1977
Quasi-2D	266	1980 - 1990
Extrapolation	218	1980 - 1990
Generic Analysis	181	1980 - 1990

152. The verification process has demonstrated that the numerical model of sediment transport credibly estimates the magnitude and distribution of suspended concentrations for two river discharge conditions. Furthermore, the delta evolution from 1967 to 1977 was reproduced by the model with reasonable accuracy.

Navigation channel dredging

153. The LAR channel was dredged and maintained at its year 0 existing condition (20 ft below NGVD). Table 17 summarizes the prototype LAR dredging

Table 17

New Orleans District Historical Dredging Records

	Atchafalaya River Navigation Channel Dredging cu yd		
Year	Sta 0+00 to 475+00 Coastline to Reach 1	Sta 475+00 to 1325+00 Reach 1 to Reach 2	Total
1973	2,482,792	3,557,062	6,039,854
1974	9,121,456	14,409,109	23,530,565
1976	2,200,668	8,629,199	10,829,867
1977	14,066,493	-	14,066,493
1979	3,021,518	8,007,220	11,028,738
1981	17,754,281	9,236,530	26,990,811
83	2,706,670	10,826,681	13,533,351
84	1,143,273	9,055,868	10,199,141
1985	4,528,630	9,623,339	14,151,969
13-Year Average	4,386,598	5,641,924	10,028,522

records provided by the New Orleans District for the period 1973 to 1985. This 13-year period contained both the 1973 and 1977 flood events, and average yearly prototype dredging was just over 10 million cubic yards. The average annual dredging predicted from the numerical sediment transport model was corrected for the estimated sediment yield (Letter 1982) based upon probabilities associated with the 13-year hydrograph. The numerical model estimate of 7.9 million cubic yards for this period compares reasonably well with the 13-year average annual 10 million cubic yards dredged.

PART VI: LONG-TERM PREDICTIONS FOR EXISTING CONDITIONS

Purpose

154. The purpose of the 50-year growth predictions of the deltas associated with the LAR and WLO was to establish a procedure which would help the New Orleans District to study the effects of present and future alternatives. The procedure assumed that the following "existing practices" will continue for the entire 50-year simulation: the LAR will be fully maintained for navigation purposes, dredged material will be equally distributed on either side of the LAR channel, a proposed project will be built on the WLO to maintain an approximate 70/30 flow split between the LAR and WLO, and no new levees or other structures will be built. Sensitivity of these assumptions will be discussed in Part VII.

Approach

155. The approach for the long-term prediction of the evolution of the deltas with the Atchafalaya Bay was to accumulate knowledge from previous modeling and prototype experiences and combine that knowledge with sound engineering judgment in a numerical simulation of the processes. Real-time tidal simulations of selected events were statistically merged and extrapolated for periods of 15-20 years to yield predicted future bathymetry, which in turn was used to recalculate future hydrodynamic conditions. The flowchart presented earlier in Figure 34 demonstrates this process. By accumulating a series of extrapolations with updated bathymetry between real-time simulations, an overall long-term prediction was achieved.

Definition of an event

156. A 50-year period of delta growth reflects the result of a continuously varying set of climatic, hydrodynamic, sedimentary processes. Continuous simulation of 50 years was impractical for the 2D models with existing computer resources. This led to selection of a finite number of conditions that would be representative of conditions in the 50 years. Combinations of the finite number of conditions (tide, discharge, wave, etc) are defined as events. These event probabilities are combined in a joint probability approach.

157. Tide condition. Tides in the bay complex are basically a diurnal type with enough of a semidiurnal component to sometimes appear to be semidiurnal. The spring-tide ranges at Eugene Island (station TG 1, Figure 11) are about 3 ft. Mean tide ranges are about 1.9 ft. All events for the long-term delta evolution used a 25-hr repeating diurnal mean tide with a mean range amplitude. Further discussion of the tidal condition is presented when hydrodynamic boundary conditions are described.

158. Discharge. The extrapolation hydrograph was based on the Atchafalaya River hydrograph at Simmesport which was developed by the New Orleans District for use in HEC-2 models of the Atchafalaya River basin and bay. The hydrograph is shown in Figure 44 and is from Report 3 of this series (Letter 1982). It has a duration of 50 years, beginning with a portion of the 1974 prototype hydrograph and running through part of 1978, where it falls back to the 1949 hydrograph. The hydrograph continues sequentially each year through the same fraction of the 1978 hydrograph as before, whence it returns to the 1949 hydrograph and cycles up through a portion of the 1966 hydrograph. Figure 45 compares the verification and extrapolation hydrographs.

159. The accumulated probabilities associated with this hydrograph are presented in Figure 46. The four river discharges were bracketed on the cumulative frequency curve, as shown, to determine the following associated frequencies:

Combined Discharge cfs	Probability
570,000	0.04
330,000	0.33
150,000	0.44
78,000	0.19

For the long-term delta growth predictions, inflow was also included for the Lake Palourde basin. This flow was determined from field discharge data collected between 1983-1986.

160. Gulf level. A mean Gulf level was chosen for all events except for one low discharge event. In the interest of investigating the Terrebonne Marsh, a 78,000-cfs combined discharge event with a 0.9-ft amplitude tide and a mean tide level 0.5 ft above mean Gulf level was added. No event lower than

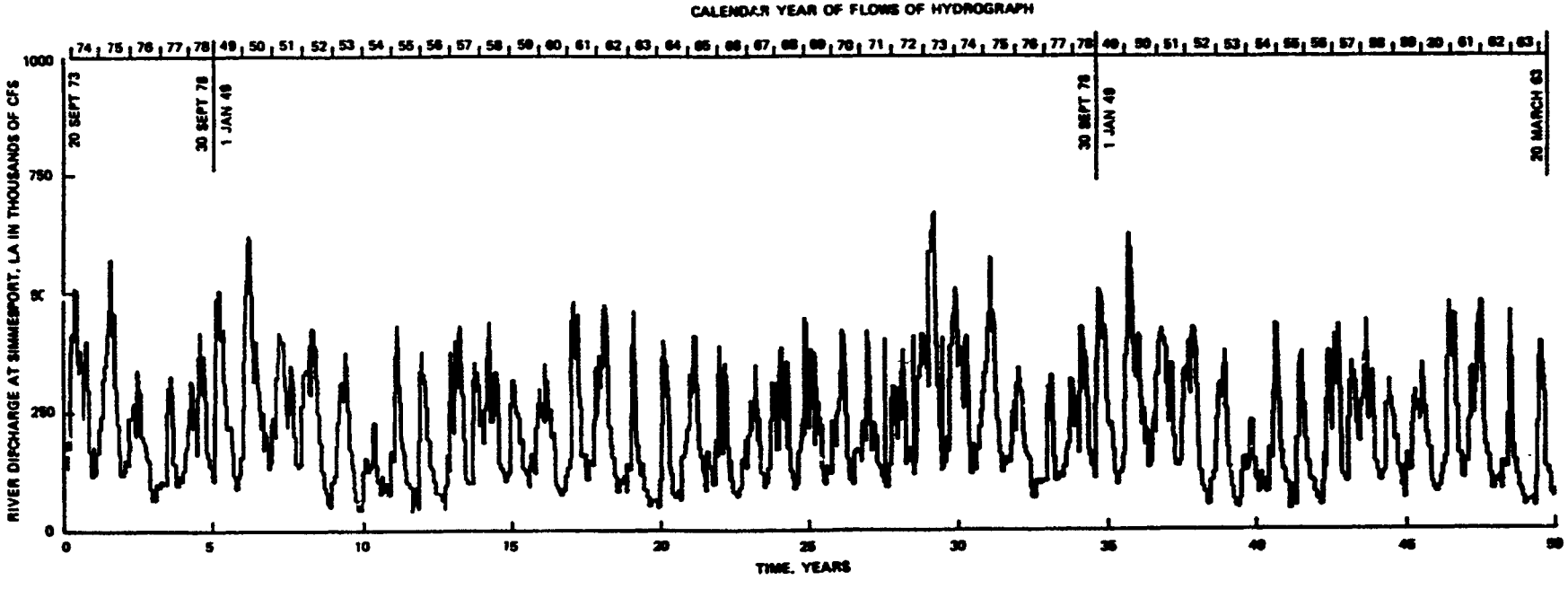

Figure 44. Fifty-year extrapolation hydrograph for Simmesport, LA

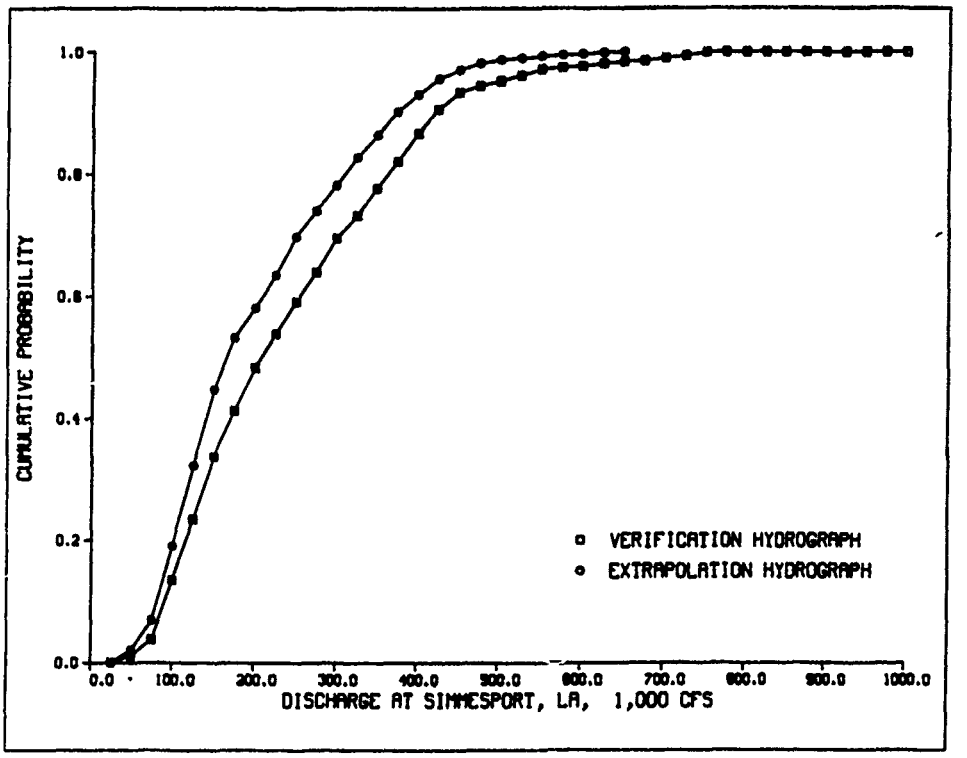

Figure 45. Simmesport, LA, discharge hydrograph comparisons

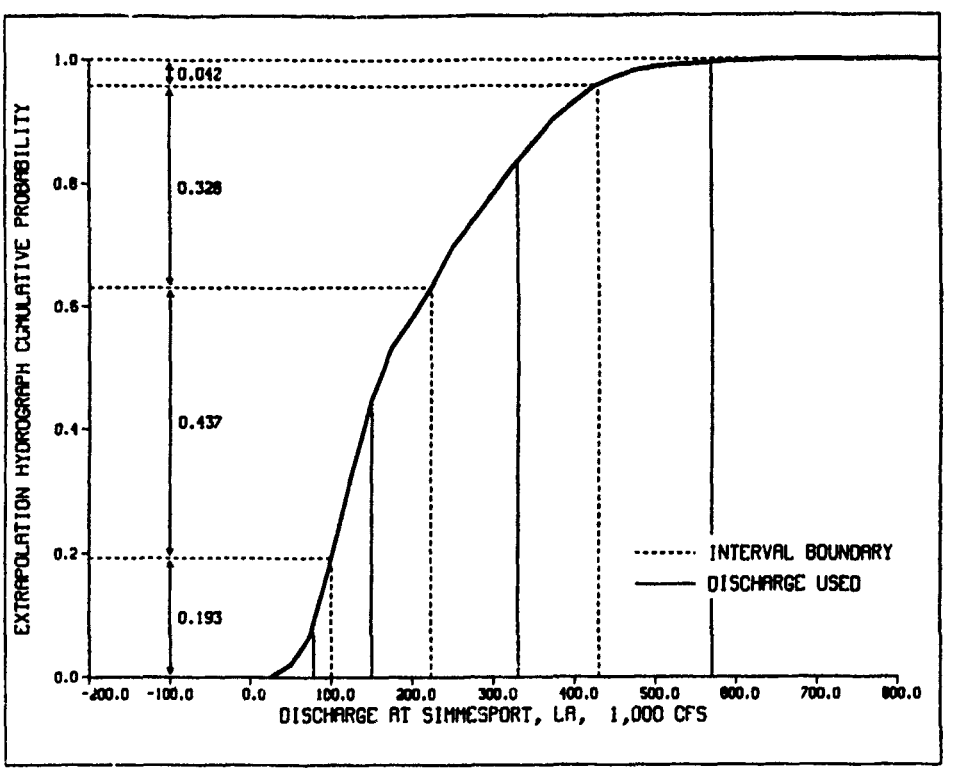

Figure 46. Cumulative probability curve for extrapolation hydrograph

mean Gulf level was tested because sensitivity runs suggested very little impact to subaerial growth.

161. Sediment characteristics. For the purposes of this study the separate independent sediment model runs for cohesive and noncohesive are considered separate events and are referenced accordingly for convenience.

162. Wave conditions. The wave conditions for the Atchafalaya Bay were defined by Jensen (1985) in Report 10 of this series. The average cumulative probability distribution for the bay was previously presented in Figure 40. The sediment transport model was run with wave heights of 0.0, 0.25, and 0.75 ft, with the probabilities presented:

Wave Height ft	Probability
0.0	0.08
0.25	0.44
0.75	0.48

Event selection

163. Table 18 lists all of the events which were considered and tested early in the study. As mentioned, the 25-hr repeating diurnal mean tide was used for all events. In an effort to reduce the number of events to be run in a single short-term step (innermost loop of Figure 34), the sensitivity to each condition of delta building was tested at year 0. It was observed that the sediment transport model essentially flushed all suspended material beyond the delta area whenever wave energy was applied. Therefore only the "no wave in the bay" simulations needed to be included in the long term extrapolation scenario. (Refer to paragraph 176 for an explanation of offshore wave activity.) Event 7, the low-discharge high-Gulf condition, was not included in the extrapolation process, but was run for purposes of salinity effects as the delta evolved. Table 19 shows the final list of events with their joint probabilities which were assembled to predict delta evolutions.

Boundary Conditions for Each Event

Hydrodynamic conditions

164. The data required to satisfy the boundary conditions for the hydrodynamic model were velocity components for all river inflow points and water-surface elevations for all Gulf boundary points for each dynamic time-step of

Table 18

Events Tested for Long-Term Delta Evolution Predictions

Event Number	Simmesport Discharge, cfs	Wave Height, ft	Gulf Level		Sediment Type		Joint Probability
			Mean	High	NONCO	COH	
1.1	570,000	0.00	*		*		0.003
1.2	570,000	0.25	*		*		0.018
1.3	570,000	0.75	*		*		0.019
2.1	570,000	0.00	*			*	0.003
2.2	570,000	0.25	*			*	0.018
2.3	570,000	0.75	*			*	0.019
3.1	330,000	0.00	*		*		0.026
3.2	330,000	0.25	*		*		0.145
3.3	330,000	0.75	*		*		0.158
4.1	330,000	0.00	*			*	0.026
4.2	330,000	0.25	*			*	0.145
4.3	330,000	0.75	*			*	0.158
5.1	150,000	0.00	*			*	0.035
5.2	150,000	0.25	*			*	0.193
5.3	150,000	0.75	*			*	0.211
6.1	78,000	0.00	*			*	0.012
6.2	78,000	0.25	*			*	0.066
6.3	78,000	0.75	*			*	0.072
7.1	78,000	0.00	*	*		*	0.003
7.2	78,000	0.25	*	*		*	0.018
7.3	78,000	0.75	*	*		*	0.019

Table 19

Revised Events Used for Long-Term Delta Evolution Prediction

Event Number	Simmesport Discharge, cfs	Wave Height, ft	Gulf Level		Sediment Type		Joint Probability
			Mean	High	NONCO	COH	
1	570,000	0.00	*		*		0.003
2	570,000	0.00	*			*	0.003
3	330,000	0.00	*		*		0.026
4	330,000	0.00	*			*	0.026
5	150,000	0.00	*			*	0.035
6	78,000	0.00	*			*	0.015

the simulation. Table 20 provides the inflow velocity values for each event throughout the 50-year simulation. These values required an iteration of the steady-state solution so that the backwater effects of the emerging delta could be incorporated into velocity adjustments such that the discharge remained constant. However, the Lake Palourde boundary conditions were derived directly from field velocity measurements over a period of time.

Table 20

Freshwater Inflow Boundary Specifications

Event Number	Flow Split LAR/WLO	Velocity Magnitude, fps LAR	WLO	LP
1 & 2	70/30	4.979	6.413	1.549
3 & 4	65/35	2.855	4.619	0.754
5	63/37	1.323	2.336	0.306
6 & 7	60/40	0.448	1.342	0.163

165. Sediment concentrations. The LAR and WLO boundary conditions for the sediment transport model, STUDH, were taken from the quasi-2D study, Report 5 of this series (Thomas et al. 1988). These boundary conditions are summarized in Table 21. The concentrations at the Lake Palourde (LP) boundary were determined based upon an assumption of full transport capacity (using Akers-White total transport formulation) for noncohesive sediment.

Table 21

Sediment Concentration Boundary Conditions for Each Event

Sediment Type	Discharge cfs	Concentrations, ppm LAR	WLO	LP
Cohesive	570,000	500	500	250
Noncohesive*	570,000	500	500	0
Cohesive	330,000	230	230	115
Noncohesive*	330,000	500	500	0
Cohesive	150,000	133	133	67
Cohesive	78,000	75	75	30

* Noncohesive events had a grain size of 0.11 mm.

166. The coefficients used for the sediment transport model in predicting long-term delta growth are the same as those used during the verification (see paragraph 142).

167. Salinity. The same procedure described for the Atchafalaya

Bay-Terrebonne Marshes salinity verification was used to determine the concentration boundary conditions. A summary of the boundary concentrations is given in Table 22.

Table 22

Salinity Concentration Boundary Conditions

Discharge	Boundary Concentrations, ppt			
cfs	LAR	WLO	LP	Gulf
78,000	0.0	0.0	0.0	15-32
150,000	0.0	0.0	0.0	5-30
330,000	0.0	0.0	0.0	5-20

Long-term simulation process

168. As noted in the sedimentation verification, the 1967-1977 delta growth period was accomplished with one 10-year extrapolation of five events. The 50-year evolution of the delta required a redefinition of the hydrodynamics as the delta progressed through time. The multiple leap approach allowed a more realistic delta lobing formation because of potential erosion and path cutting resulting from increased velocities and head differences as the delta evolved. Hydrodynamics were defined with updated bathymetry at years 0 (1980), 15 (1995), 30 (2010), and 50 (2030).

169. Table 23 illustrates the long-term predictive process and the bed structure and concentration initialization procedures required to complete each step for each of the seven events described in Table 20. As shown, the hydrodynamics for the present conditions (HYDRO-0) were calculated using RMA-2 with the mesh bathymetry set to prototype year 1980. The sediment model, STUDH was cold-started for year 0 (i.e., STAB-0) of the simulation. In a cold start, the model run begins with a uniform initial concentration. The STUDH hot start for year 0 (i.e., SED-0) used the last time-step of the concentration field saved from STAB-0. Changes in bed elevations from year 0 for all seven events were supplied to the MUXTRAP program (described in Part II) and extrapolated 15 years into the future to predict the delta evolution for year 1995. The revised bathymetry (i.e., year 1995) was used to recalculate the hydrodynamics using RMA-2. The newly defined 1995 hydrodynamics along with the bed structure and bed concentrations from the previous real-time simulation were used to initialize the sediment transport model for the run labeled STAB-15. The purpose of the second hot start, labeled SED-15, was to ensure

Table 23

Long-Term Extrapolation Simulation Bed Structure/Concentration Initialization Procedures

		Initial Conditions			
Year	Run	Bed Elevation	Bed Change	Concentration	Bed Structure
* 0	HYDRO-0	1980	N/A	N/A	N/A
* 0	STAB-0	1980	0	constant†	default
0	SED-0	1980	0	STAB-0	default
0-15	MUXTRAP-15		SED-0		
* 15	HYDRO-15	1995	N/A	N/A	N/A
* 15	STAB-15	1995	0	SED-0	SED-0
15	SED-15	1995	0	STAB-15	SED-0
15-30	MUXTRAP-30		SED-15		
* 30	HYDRO-30	2010	N/A	N/A	N/A
* 30	STAB-30	2010	0	SED-15	SED-15
30	SED-30	2010	0	STAB-30	SED-15
30-50	MUXTRAP-50		SED-30		
* 50	HYDRO-50	2030	N/A	N/A	N/A
* 50	STAB-50	2030	0	SED-30	SED-30
50	SED-50	2030	0	STAB-50	SED-30

where HYDRO - RMA-2 hydrodynamic simulation.
STAB - STUDH stabilization run of concentration.
SED - STUDH final run with all sedimentation characteristics for that year activated.
MUXTRAP - Multiple Events Combined and Extrapolated.
* Indicates to repeat the procedure for all events.
† Constant initial concentration that varied with event.

the elimination of any concentration (and subsequent bed change) transient results from the previous hot start before calculating the sedimentation rates which would be used to extrapolate bed change to year 30. The procedure continued until the projected 50-year deltas (year 2030) and their impacts on circulation and sediment supply were determined.

Extrapolation process

170. Extrapolation was performed by the MUXTRAP program, described earlier. It statistically merges multiple STUDH results files and extends the calculated bed change at each computational point into the future. The following paragraphs describe the controlling factors of extrapolating results into the future.

171. Statistical combination of events. The frequencies introduced in Table 24 were applied within program MUXTRAP. Each of the bed change calculations from these six events (78,000-cfs high Gulf level omitted) was weighted by these probabilities and combined as shown.

Table 24

Multiple Event Statistical Extrapolation

Combined Discharge, cfs	Cohesive Probability	Noncohesive Probability
570,000	0.04	0.04
330,000	0.33	0.33
150,000	0.44	n/a
78,000	0.19	n/a
Total	1.00	0.37

MUXTRAP = {[Rate of Bed Change for Event (i) - Rate of Subsidence] × Probability) × Δ Time

172. Subsidence. Appendix A of this report provides the background data and resulting regression equation used to address the subsidence issue within the Atchafalaya Bay. The same window used by program MUXTRAP was susceptible to subsidence.

173. Terrebonne Marshes elevations held constant. The Terrebonne Marshes geometry was fixed so that the study could isolate the impacts of the levee extension and delta evolution on conditions within the marshes. The bottom elevations of the marshes and bayous east of the LAR remained equivalent to their year 0 existing conditions. They were not subjected to either extrapolation or subsidence, and were not altered in any form unless for purposes of numerical stability. In cases where elevations along the entrance of the bayou became subaerial and resulted in allowing the wetting/drying technique to dry the bayou, adjustments were required.

174. Maximum subaerial height. The constraint of a maximum delta or disposal mound height of 2.5 ft (subaerial) was applied to the extrapolated elevations based on field observations. The vertical growth of the delta ceased at that elevation.

175. Channel dredging and material placement. The two-element-wide representation of the Atchafalaya Bay channel was dredged from the mouth of the LAR near Deer Island to outer bar Reach 2 (see Figure 9). The depth of the

channel was maintained at 20 ft below NGVD (as authorized by the River and Harbor Act of 13 Aug 1968). Dredged material was placed along a 3,000-ft zone on either side of the bay channel down to the tip of Point Au Fer Island (Figure 47a). When the 3,000-ft-wide disposal zone elevation exceeded the maximum 2.5-ft height above NGVD at year 30, the disposal zone was widened to 6,000 ft (Figure 47b) and extended gulfward to outer bar Reach 2.

176. Lateral diffusion of extrapolation results. The long-term extrapolation results tend to amplify minor spatial gradients in sedimentation rates into large relative depth variations after multiple years of extrapolation. These variations are somewhat artificial in that wave and tidal energy tend to smooth out those differences in nature. Therefore, the final extrapolation bathymetries were exposed to an elemental averaging process based on the degree of wave energy in that zone. The equation for this process is as follows:

$$\Delta D = \Delta D_N(1-A) + \Delta D_E A \qquad (2)$$

where

ΔD = applied depth change at a node

ΔD_N = raw nodal depth change computed by MUXTRAP

ΔD_E = elemental average of ΔD_N depth change computed by MUXTRAP and the coefficient A varied between 0.0 for the bay and 1.0 for the offshore Gulf (based on the degree of wave-induced smoothing).

Results

Delta evolution for Years 0, 15, 30, and 50

177. The starting bathymetry for the base (Plan D), or existing condition is presented in Plate 29. Plates 30 through 32 show the contours of -6 ft, -3 ft, and subaerial delta growth within the bay at the end of each extrapolation period for the base simulation. Specific quantities of sediment above these elevation planes are summarized in Table 25. Figure 48 shows the subaerial growth curve with an upper and lower bound. These bounds were developed by applying the sensitivity results from the extrapolation technique

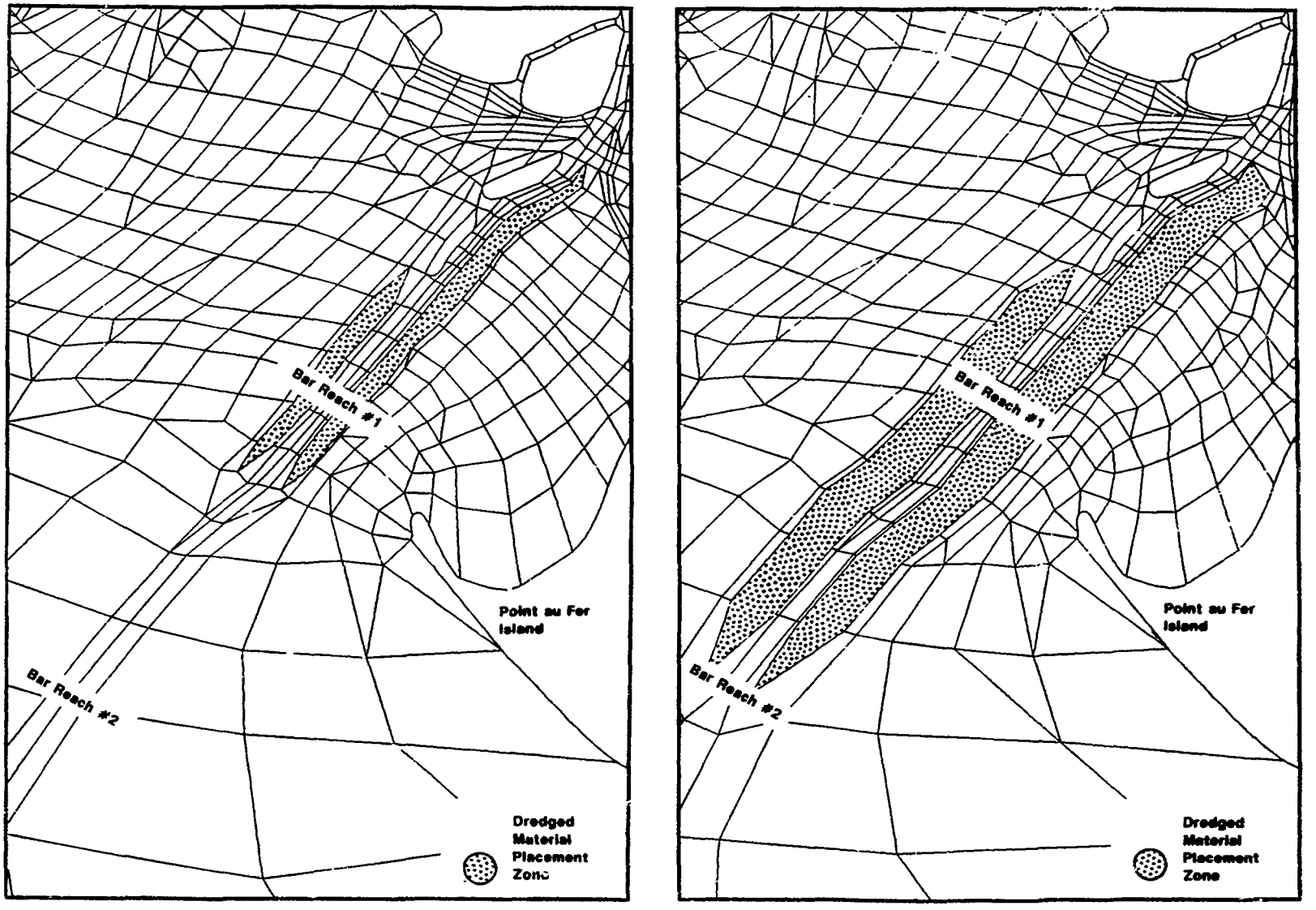

a. MESH7 with 3000-ft-wide disposal zone

b. MESH8 with 6000-ft-wide disposal zone

Figure 47. Designated dredged material disposal placement locations

Table 25

Sediment Above Elevation Plane For the Base Simulation*

Year	Volume of Sediment, cubic km			Subaerial Area	
	-6 ft	-3 ft	0 ft	sq km	sq miles
0	0.363	0.083	0.007	21.5	8.3
15	0.522	0.138	0.016	47.5	18.3
30	0.847	0.299	0.059	141.3	54.6
50	1.464	0.634	0.158	346.3	133.7

* Within the long-term delta evolution window.

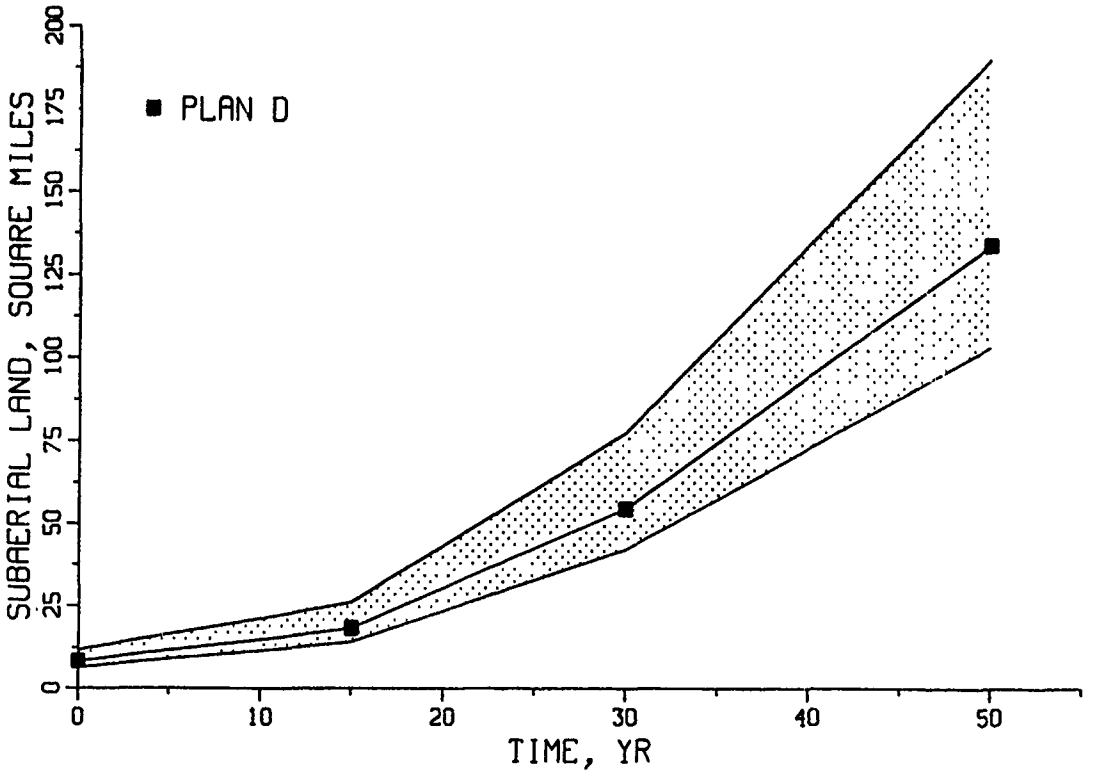

Figure 48. Subaerial land growth curve for the base simulation

(Letter 1982), which showed bounds from 77 to 142 percent of the year 50 delta area. After 15 years there is considerable expansion of the zone of depths less than 6 ft, with some new subaerial land forming both within the bay and gulfward of Point Au Fer adjacent the navigation channel. After 30 years there is extensive land forming within the bay, but with loss of most subaerial land in the offshore that formed at year 15. By year 50 dramatic subaerial development has occurred within the bay, gulfward to the west. The subaerial area of new land has reached 133 square miles by year 50. The upper

and lower bounds at year 50 are 102 to 189 square miles.

Water-surface elevation changes

178. Table 26 presents the change of water-surface elevation for the highest discharge event (570,000 cfs) at various locations through the computational network from year 0 to each extrapolated year. Each value was determined by interpolating tidally averaged values from a cluster of computational points centered around the area of interest in order to avoid any potential numerical oscillations.

Table 26

Change in Water-Surface Elevation Relative to Year 0 For the Base (Existing Practices and Projects) at 570,000-cfs Discharge

Location	Year 15 ft	Year 30 ft	Year 50 ft
Atchafalaya Bay (west)	-0.03	0.15	2.86
Atchafalaya Bay (central)	-0.16	0.12	4.05
Atchafalaya Bay (east)	1.91	3.34	5.29
LAR at coastline	3.13	4.00	5.14
WLO at coastline	4.28	1.82	2.60
Fourleague Bay (north)	1.73	2.42	4.62
Fourleague Bay (South)	1.60	1.46	4.08
Tip of existing Avoca Levee	2.10	2.68	3.10
Bayou Beouf at Amelia	2.35	2.93	5.06
GIWW near Houma	2.29	2.86	4.10
Lake Decade	2.40	2.55	3.69
Bayou Penchant at Chene	1.54	1.84	2.05

Maintenance dredging of the navigation channel

179. Table 27 provides the bay channel dredging volumes (from the LAR coastline to Point Au Fer) predicted at the end of each extrapolation year. As shown previously in Table 17, the average annual prototype dredging from 1973-1985 was 10,028,522 cu yd.

Circulation patterns for years 0, 15, 30, and 50

180. Plates 33 through 37 are velocity vector plots for each base event at year 0 (1980 bathymetry). The velocity was averaged over the 25-hr tidal cycle for open water within the bay. The vectors are interpolated and plotted at regular spatial intervals for sake of readability. A solid arrowhead

Table 27

Predicted Atchafalaya Bay Total Channel Dredging Volumes

Period	Annual Dredging Volume cu m	cu yd
1980-1995	2,600,000	3,400,000
1995-2010	8,600,000	11,200,000
2010-2030	5,100,000	7,900,000

indicates that the velocity magnitude exceeded 1 fps. If a computational point temporarily became wet during the tidal cycle, an average vector was calculated and plotted at that location. If a computational point remained subaerial throughout the tidal cycle, then no vector was plotted.

181. Plates 38 through 40 are the velocity vector plots for the base 330,000-cfs event at each year of hydrodynamic update. These plates are representative of the other discharge events. Although magnitudes varied with each discharge, the general pattern of wetting more marsh as the delta evolved with time is evident, due to backwater effects. By year 15 a large portion of the flow to the west from the LAR delta has been cutoff and more flow diverted through Fourleague Bay. By year 30 a breakout to the west from the LAR delta has developed and the WLO delta has formed bifurcating channels. After 50 years significant diversion of flow through Fourleague Bay has occurred and the WLO has channelized through the bay. Flow through the LAR delta has greatly diminished.

Salinity contours for years 0 and 50

182. Plates 41 through 46 present the salinity contours for years 0 and 50 for three discharge events: 330,000, 150,000, and 78,000 cfs. All three discharges exhibit a freshening of the Terrebonne Marshes after 50 years of delta evolution compared to the salinity conditions for year 0.

Sedimentation changes from years 0 to 50

183. Figure 49 indicates the area included in the SEDDIST computation previously described in paragraph 32. The net gain or loss of sediment over the 50-year simulation within a designated zone for the base is provided in Table 28. The net deposition rate is the predicted rate of SEDDIST with subsidence. Note that the subsidence rate listed is computed as the average over the given zone and from results described in Appendix A. The effect of the

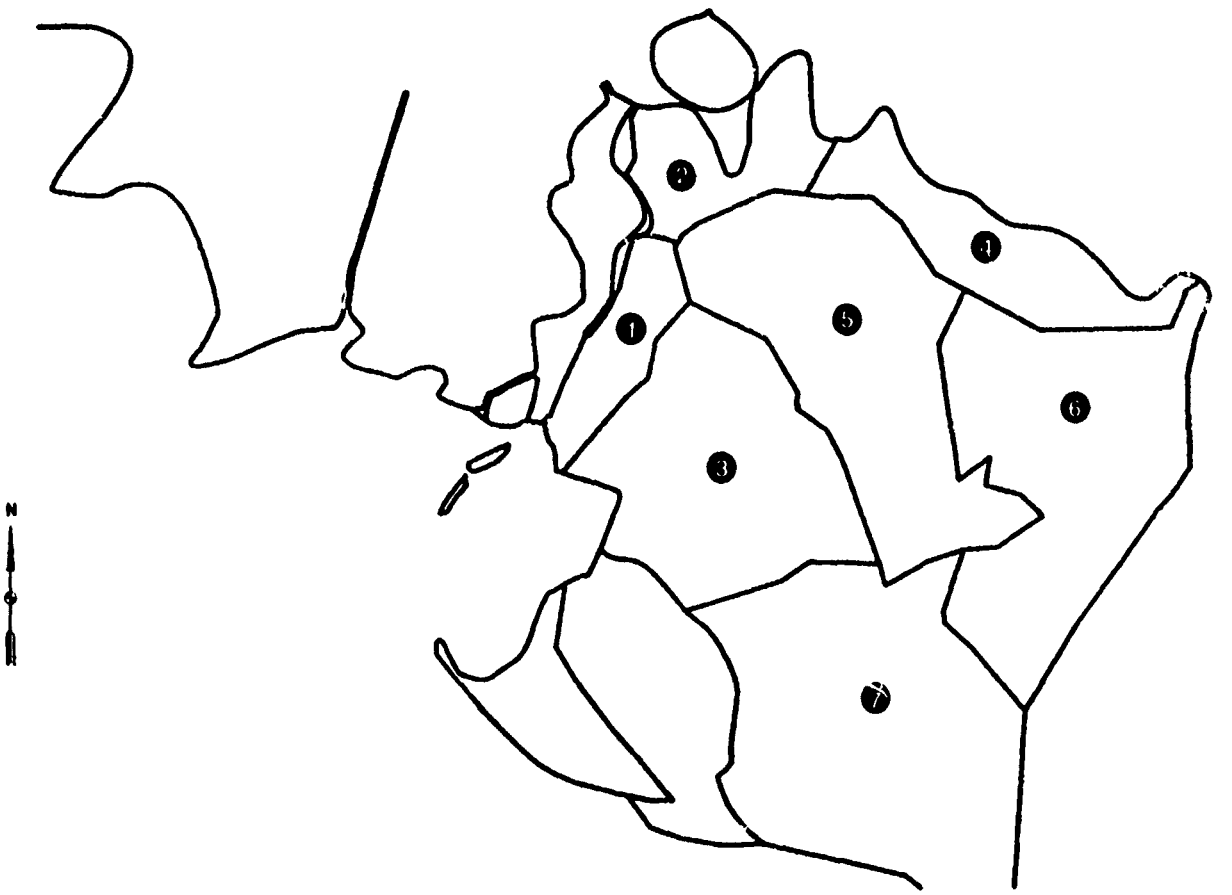

Figure 49. Sedimentation distribution zones for Terrebonne Marshes

Table 28

Rate of Net Gain or Loss of Sediment by Zone for the Base Plan D

Zone	Average Subsidence cm/year	Year 0 Net Deposition Rate, cm/year	Year 50 Net Deposition Rate, cm/year
1	1.55	0.71	5.64
2	1.46	2.23	2.91
3	1.42	-1.26	0.02
4	0.87	0.05	0.03
5	1.19	-0.94	-0.95
6	0.74	-0.57	4.19
7	1.13	0.07	5.15

delta building is evident for several zones. The majority of the zones experienced a relative increase in net deposition. The only zones with a net decrease (zones 4 and 5) are in the northeast portion of the system.

PART VII: DISCUSSION

Sensitivity

Geometric sensitivity

184. Each of the models used here is sensitive to geometry, grid resolution, and the wetting and drying strategy. A clear example of geometric effects on hydrodynamics can be seen in the circulation patterns of year 0 versus those of the 50-year delta (Plate 33 versus Plates 37 through 39). As seen, the water is being diverted more toward Fourleague Bay as the delta builds.

185. Grid resolution is typically determined by the criterion of using the minimal number of elements to adequately resolve geometry and velocity gradients. For this study, all channels were represented by at least a two-element-wide schematization (i.e., a V-shaped bottom profile). To assure proper comparison between plans while using the wet/dry technique, comparable resolution in the mesh should be maintained, in the face of differences in ultimate delta configuration. Therefore, judgment was required in revising the grid to facilitate emerging delta and the associated interaction with hydrodynamics.

186. The elemental wet/dry strategy is highly dependent on the geometric schematization of the study area and the model's initial steady-state water slope which controls the initial wet/dry pattern. Tidal fluctuations had minimal effect on the wet/dry patterns after the spin-up period, a remnant of fairly coarse grid resolution for elements with bottom elevations in the area of midtide level.

Hydrodynamic sensitivity

187. The success of the transport models, STUDH and RMA-4, was dependent on the driving hydrodynamics supplied by RMA-2. Subtle changes in hydrodynamics can create fairly dramatic local changes in sedimentation and salinity. However, when addressing the large-scale delta evolution issues of Atchafalaya Bay, based on sensitivity runs, the subtle changes in hydrodynamics create little change in the overall sedimentation delta building process.

188. Additional sensitivities of the hydrodynamic model, RMA-2, are to boundary conditions, Manning's n , eddy viscosity coefficients, and wind.

189. Hydrodynamic boundary conditions consist of river discharge

(magnitude and flow split), and the tide (range and mean Gulf level). For this model, river discharge was achieved by assigning velocity magnitude and Manning's n coefficients to adjust the water slope in the LAR and the WLO, which in turn affected backwater elevation. Hence, the discharge is the result of water depth plus assigned velocities at the boundaries. The velocity specification was used at the flow boundary because it is more stable than the discharge specification.

190. The nonreflecting boundary condition applied to the LAR and WLO is dependent on the mean water level. The condition absorbs 100 percent of tidal energy that reaches the boundary. Zero reflection may not be exactly correct, but it is much better than 100 percent reflection which would occur otherwise, unless a tidal variation were specified at the boundary. The problem, however, arises in determining the impact of the delta evolution on that boundary fluctuation. The condition automatically handles those effects.

191. The future distribution of flow between the LAR and WLO was estimated, based on historical observations (Figure 17 of Report 5 (Thomas et al. 1988) in this series) and New Orleans District guidance. The model does respond to flow split variations. Other configurations of flow split which had a higher percentage of flow down the WLO were run (described in Report 12 (Donnell and Letter, in preparation)), and results indicated less subaerial delta at year 50 because more sediment was transported out of the bay. Results presented herein are sensitive to deviations from the current flow split.

192. Both the range and mean water level of the tidal boundary condition impact wetting and drying and in turn the circulation patterns. The resulting current velocity magnitudes are altered in a nonlinear fashion based on wetting and drying patterns. Given the same tide range, a higher Gulf level will yield lower velocities because of increased cross-sectional area at all tidal stages. However, a higher tide range for a given Gulf level will yield higher velocities due to both tidal energy and wet/dry patterns.

193. Manning's n values were used to adjust the water-surface slope for both the LAR and WLO. As the n value is increased the water-surface slope increases and there are effects on backwater elevations. Manning's n values were also adjusted to simulate vegetation and increased as the delta formed. For instance, as the delta formation approached mean Gulf level, the n value of the elements representing that formation was increased to 0.10. When the

delta became subaerial and "vegetated," the n value was increased to a maximum of 0.20. Such increases in Manning's n values encourage the water to channelize. However, excessive levels of Manning's n in the tidal marshes can cause overly dissipative and hence smeared results.

194. The eddy viscosity coefficients are typically assigned as low as possible while allowing the numerical model to remain computationally stable. As the eddy viscosity values are increased, the flow appears more viscous. If the eddy viscosity is lowered, then the model will show more lateral velocity variation in the channel areas and the model responds with greater sensitivity to Manning's n . The sensitivity of the eddy viscosity in the hydrodynamic model and in turn the effects on the sediment model results are very complicated.

195. Wind can affect mean water levels in the bay and the overall setup in the marsh with attendant effects on the velocity field. These effects have been, however, omitted from explicit consideration in the long-term delta evolution simulation.

Sediment transport sensitivity

196. Sediment transport, as determined by the numerical model STUDH, is sensitive to the boundary conditions (river inflow and Gulf sediment concentrations), the driving hydrodynamics provided by the RMA-2 model, mesh resolution, and various coefficients.

197. The LAR and WLO were the two primary upstream boundary condition specification locations, along with Lake Palourde. For noncohesive transport, the upstream boundaries of the LAR and WLO were far enough removed from the bay that the sediment flux into the bay was insensitive to minor inconsistencies at the boundary.

198. The unsteady tidal Gulf sediment concentration boundary condition is more complicated than that of a constant inflow boundary. There is a switch of the boundary condition concentration specification keyed to the current velocity normal to the boundary. When the flow is leaving the model, the gradient in concentration at the boundary is set to zero. When the flow on the boundary is entering the model, the user-specified boundary concentration is enforced. The model self-determines the appropriate concentration for an exit boundary where the current velocity leaves the model. The problem is in determining the appropriate boundary concentration level for specifying when the tide turns and water then enters the model at a point where historically

(over the last several hours) the water was exiting the model. For instance, Figure 50 shows that at slack water the calculated concentrations at the boundary are C_b . As the tide turns, and water begins to flood and return to the model, the previously assigned boundary condition specification C_a will

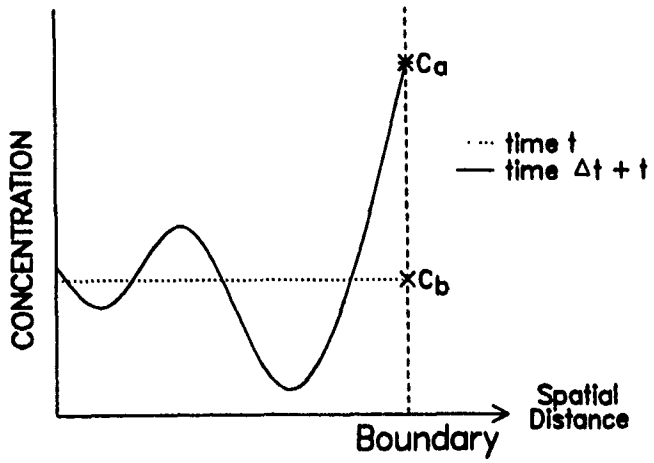

Figure 50. Potential boundary concentration oscillations

immediately replace the computed concentration at the boundary C_b . This leads to numerical oscillations near the boundary. The model verification was performed to minimize the oscillation, but as the delta grows and the hydrodynamics change, the oscillations may return. However, there were no indications of oscillations by year 50. This problem should be localized to the boundary when it occurs and have little influence on bay sedimentation.

199. Although the impact of various coefficient changes within STUDH can be evaluated in an idealized case, when combined in a complex tidal environment, the overall impacts are difficult to generalize. Generally, a high fall velocity would yield deposition closer to the river mouth, and a low fall velocity would lower the percentage retention of sediment yield within the delta. If the grain size is too small, then the general effect would be higher transport rates and then greater loss of sediment from the delta. Similarly, if the grain size is too large, then there would be greater retention and more delta building. A higher critical shear stress for deposition would result in more deposition, while a lower value would result in less deposition. A higher critical shear stress for erosion would allow less resuspension and greater delta building assuming resuspension is currently a factor. The erosion rate constant is a controlling parameter only when

erosion begins. This can be important relative to the percentage of time within the tidal cycle where shear stresses are greater than critical for erosion. The dispersion coefficient contributes to the spatial distribution of concentration and, therefore, to potential sediment supply to low energy zones.

200. The verification is the process wherein the boundary conditions, hydrodynamic interations, and coefficients are adjusted to match observed behavior. The coefficients (fall velocity, grain size, critical shear stresses) were based on field/laboratory experiments using Atchafalaya Bay sediments.

Extrapolation sensitivity

201. The extrapolation technique is sensitive to the probabilities applied to each event, the extrapolation window, subsidence, and dredged material disposal strategies. However, the extrapolation event probabilities were derived from the full 50-year extrapolation hydrograph (Figure 44). Therefore, the sequencing of the flows during the 50-year period were not considered.

202. The frequencies applied to each event within MUXTRAP are input parameters determined as the joint probabilities between the wave heights and the discretized river discharges, as summarized in Table 10. The frequencies have a strong effect on the future bed configuration in that there is a linear dependence between the frequencies and the extrapolated (i.e., predicted) bed change.

203. The extrapolation window, as described in paragraph 31, defines the zone within which sedimentation predictions can be made with confidence. Sedimentation predictions were not made beyond the boundaries of the bay verification. Hence, the bathymetries for areas outside of the extrapolation window remained constant throughout the 50-year prediction. For comparison, it is important to report delta growth area/volumes only for the same extrapolation window.

204. As described in Appendix A, the value of apparent subsidence applied to the results varied in space from 0.4 to 1.4 cm/year. Subsidence was not applied outside of the extrapolation window, so that the net effect is the assumption that subsidence balances any deposition that occurs outside of the extrapolation window.

205. The length of the extrapolation period for the short-term intervals has a direct impact on the number of intermediate adjustments within the

overall long-term projection. At the time of configuration of the process, the total number of real-time simulations had a significant impact on computational requirements and therefore study cost. It is recognized that the mesh adjustments required to achieve successful extrapolated hydrodynamic simulations were a function of the length of the extrapolation. However, these subjective decisions do have an impact on the overall delta configuration. It is felt that the three steps used allowed for reasonable adjustments to be made without those adjustments becoming a dominant part of the process.

Salinity sensitivity

206. The salinity model, RMA-4, is sensitive to initial conditions, boundary conditions, and diffusion coefficients as well as hydrodynamics.

207. The process of initializing concentrations for the study area is one means of reducing the amount of run time to achieve a quasi-equilibrium. If the simulation is started from an arbitrary state, as would be required if there were no supporting field data to assign initial concentrations, the length of time required to achieve a condition independent of the initial condition is approximately twice as long as it takes a particle of water to move across the area being simulated. When RMA-4 is allowed to run for weeks, or until there is no change in the salinity contours from tidal cycle to tidal cycle, the final answer is largely independent of the initial conditions. There is an exponential relationship between the initial condition and the time required to achieve equilibrium. For this modeling effort, the same initial salinity condition was used for both present and future salinity predictions, and the simulation was run for 350 hr to overcome initialization sensitivity.

208. The following boundary conditions were supplied to the model: the zero concentration for the three freshwater inflows (LAR, WLO, LP) and the offshore boundary concentration specifications. Like STUDH, RMA-4 self-solves for boundary concentrations for exit flow, but uses the specified boundary condition for flow entering the model. The salinity model results are much more sensitive to boundary condition than the sediment model. The sediment model solution is strongly influenced by the bed interaction, while the salinity model results are strongly dictated by the boundary condition salinities.

209. If the diffusion coefficients are set too low, there is a tendency for the numerical solution to have oscillations near sharp gradients where there may be inadequate resolution. Raising the diffusion coefficients will

control the oscillations but may cause excessive diffusive flux; hence the salinity gradients will be smeared.

Limitations

210. Limitations of this modeling effort were associated with the discretization of time and space, the unsteady influence of physical processes that were not explicitly simulated, and the degree to which certain assumptions remained valid over the study period.

Time discretization

211. Limitations associated with time discretization can be further broken down into effects at time scales beyond those being simulated (either shorter or longer). The time scale of the real-time simulations made with this model was several days with time-stepping at 1-hr. River discharges and average Gulf level were held constant over the tidal simulations, so the time scale of variations in the modeling scenario could be viewed as seasonal.

212. The processes of significance at time scales shorter than the modeling time-step are essentially wave and wind energy. There is also loss of dynamic influence at time scales shorter than the modeling scenario, associated with the unsteady nature of the river discharge and with dynamic variations in the average Gulf level over the tidal cycle, perhaps in response to meteorological forcings. The short-term processes are blurred into 1-hr time-steps of the hydrodynamic model by means of the dispersion coefficients and frequency assignments.

213. With regard to effects at longer intervals, the modeling approach discretized a typical year into a maximum of four river discharges and two Gulf levels. The limited number of events results in the loss of long-term extreme fluctuations (weekly/monthly) such as river discharge, and seasonal wave and wind conditions. There are also limitations associated with the joint probability method's assumption of independent events. The "memory" of the system to antecedent conditions is ignored. For instance, any hysteresis effect between river discharge and sediment discharge is overlooked.

214. The forward-stepping extrapolation is a linear projection in time of the sedimentation rates at the beginning of the extrapolation period. If the delta evolution is nonlinear over the extrapolation interval, the forward-stepping can introduce significant under- or overestimation of the extent of

delta at the end of the period (Figure 51). The linearly extrapolated area A_{i+1} is calculated by

$$A_{i+1} = A_i + \left(\frac{dA}{dT}\right)_i (T_{i+1} - T_i) \quad (3)$$

where

A = subaerial area

i = interval

T = time, years

In order to assess the possibility of serious deviation due to this effect, a fairly simple analytical evaluation was performed. This analysis assumes that the delta growth and decay cycle (Wells, Chinberg, and Coleman 1984) can be represented as a Gaussian function:

$$A = A_m \; e^{-k(T-T_m)^2} \quad (4)$$

where

A_m = maximum subaerial area

k = growth/decay coefficient (per year^2)

T_m = time of maximum delta area

The time rate of change of delta area R will therefore be

$$R = \frac{dA}{dT} = -A_m \, 2k(T - T_m) \; e^{-k(T-T_m)^2} \quad (5)$$

or

$$R = -2k(T - T_m)A \quad (6)$$

The underlying assumption of this analysis is that it can be said with confidence only that when the subaerial extent of the delta is at some arbitrary size, A_i (as developed during the modeling work), that the rate of change

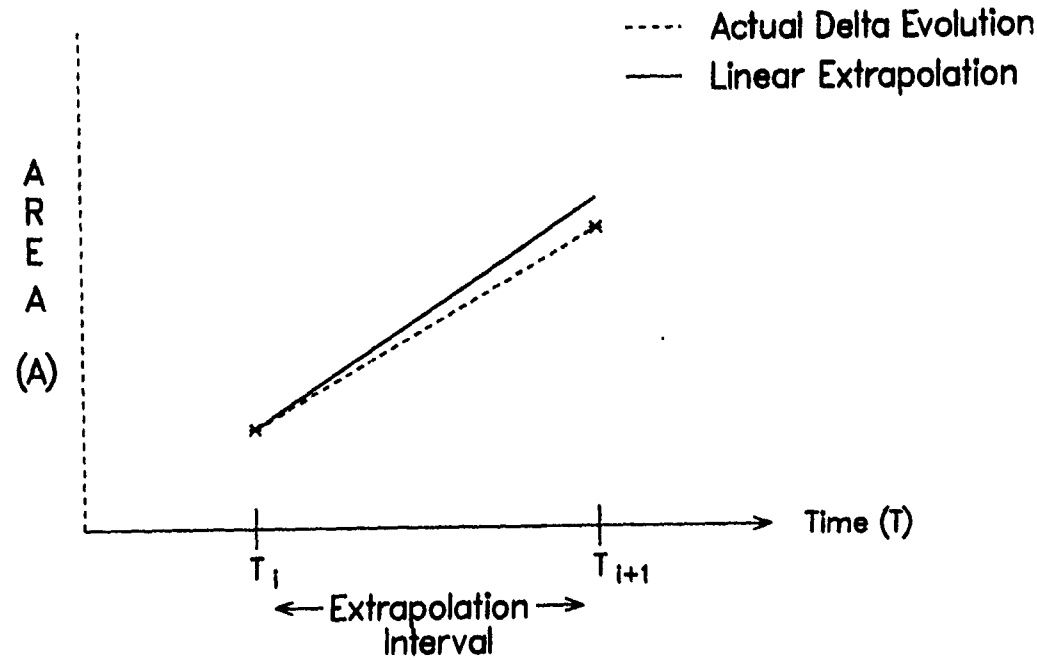

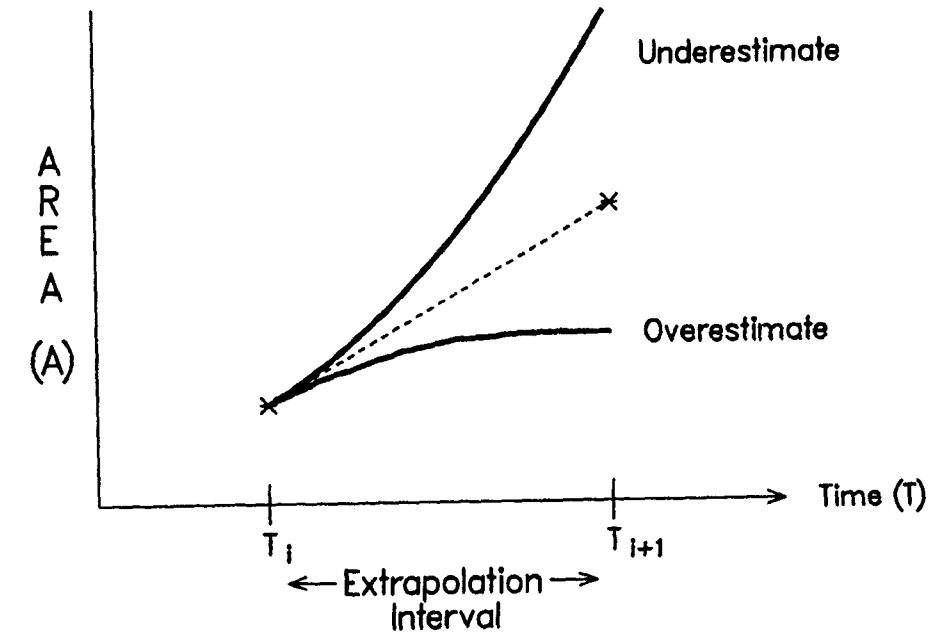

b. Nonlinear

Figure 51. Examples of (a) nearly linear and (b) nonlinear delta growth compared with forward-stepping linear extrapolation

R_i has been defined from the sediment model. It is assumed that the time of occurrence of that delta size is unknown, but can be estimated from the Gaussian sensitivity analysis (equation 4). The impact of the forward-stepping extrapolation can be gauged by how closely the times of occurrence of the specific delta sizes agree with the model prediction years (15, 30 and 50).

Table 29

Forward Time-Stepping Sensitivity Analysis

i	Extrapolation Year	Area square miles	Rate of change square miles/year	Gaussian T_i
0	0	8.3	0.67	0
1	15	18.3	2.42	11.0
2	30	54.6	3.96	28.8
3	50	133.7	4.10	49.9

215. In order to solve for the unknown coefficients in Equation 4 (A_m, k, and T_m) three equations are required:

$$A = A_o = 8.3 \text{ square miles at } T = 0 \tag{7}$$

$$R = R_o = 0.67 \text{ square miles/year at } T = 0 \tag{8}$$

and

$$A = A_{50} = 133.7 \text{ square miles when } R = R_{50} = 4.1 \text{ square miles/year} \tag{9}$$

After considerable algebraic manipulation, equation 4 can be solved:

$$A = 214\, e^{-0.000502(T-81)^2} \tag{10}$$

This solution indicates a maximum delta size of 214 square miles at year 81.

216. The time of occurrence T_{50} of a given delta size, rate of growth data pair A_{50}, R_{50} can be calculated as

$$T_{50} = \frac{2\,\ell n \left[\frac{A_{50}}{A_o}\right]}{\left[\frac{R_o}{A_o} + \frac{R_{50}}{A_{50}}\right]} \qquad (11)$$

Note that the TABS time scale (T=50) does not enter into this estimate and the Gaussian time T_{50} is dependent only on A_i and R_i. The estimated time of A_{15} and A_{30} are then determined by solving Equation 4 for T_i

$$T_i = T_m - \sqrt{-\frac{1}{k}\,\ell n \left[\frac{A_i}{A_o}\right]} \qquad (12)$$

217. The Gaussian analysis estimated T_i for the year 15, 30, and 50 deltas of the modeling are presented in Table 29. The Gaussian analysis for year 50 conditions indicates excellent agreement (year 49.9 versus 50.0). The agreement at year 15 conditions is not as good (year 11.0) and year 30 conditions agree fairly well (year 28.8). This analysis suggests that the short-term delta evolution projections may be influenced by nonlinear contributions, but that in the longer term (50 years) the influences are not significant. This observation is supported by the large changes in the rate of delta growth between year 0 and 15 (0.67 to 2.42 sq. mi/year) but less dramatic changes for the following delta extrapolation steps: 2.42 to 3.96 and 3.96 to 4.10.

Spatial discretization

218. The predictions are limited by the spatial resolution of the numerical computational mesh. Consequently, the nodal changes must be viewed as the average changes over a zone approximately the size of an element. Strict association of predicted changes at a point in space would not be appropriate.

219. An additional spatial issue pertains to the fact that the prediction has been limited to the vicinity near the area over which the modeling approach was verified. Furthermore, the area being modeled had to be truncated at some point, leaving a boundary zone over which results must be viewed with skepticism. Therefore, delta growth beyond the verification area should

be viewed only in terms of tendencies and not in terms of absolutes. For the hydrodynamic/salinity results, the crude schematization of the Bayou DuLarge at the east boundary of the Terrebonne Marshes is one example of the effect of the boundary zone's geometry on modeling. The numerical model salinity contours typically reflect a straight east-to-west contour for southeast Bayou DuLarge, while in actuality there are open-water bays beyond the mesh limits which are not being modeled.

220. The smallest spatial scale used in the model study was still not sufficiently small to resolve the development of small secondary channels within the evolving delta lobes. Therefore, no ability existed to simulate the shifting of flow from primary to secondary channels as the primary channels became hydraulically inefficient.

221. The large-scale spatial limitation also concerns the mesh limits and the confidence in the model's results with time. As the delta evolves close to the limits of the extrapolation window, the confidence breaks down. Therefore the confidence level for the 15-year predictions of delta evolution are higher than for the 50-year delta predictions.

Unsteady influences

222. During the course of 50 years all of the forcing influences on the bay will exhibit extreme variation. At the time of the study execution, direct simulation of 50 years of combined forcings at a subtidal time-step was beyond the existing computational capability if sufficient spatial resolution to define deltaic evolution were used. The unsteady influences, even with respect to sequencing of annual statistics, were not incorporated into the extrapolation procedures. These influences are reserved for future research.

Assumptions

223. The primary assumption made at the outset of the study was that the limits of the domain of the model were assumed to be far enough removed so that the evolving delta would not affect the boundary conditions applied to the model. All model results supported this assumption by comparing the behavior near the boundary at year 50 versus year 0.

Trends Identified

224. Of further interest is the predicted time to and area of maximum delta growth from the Gaussian analysis. Based on the model prediction of

delta size at year 50, equation 10 predicts a maximum delta of 214 square miles after 81 years. This projection generally agrees with the generic analysis projection (Wells, Chinburg, and Coleman 1984) of 66 years. The Gaussian projection of the 2D model results indicates a substantially larger subaerial extent. This difference can be explained in part by the fact that the 2D modeling approach identified extensive zones as completely subaerial over mesh elements, while the generic analysis strictly addressed subaerial land, not including the areas of feeder/secondary channels within a more fragmented delta. The 2D modeling is not capable of addressing the fine details within delta lobes due to relatively coarse mesh resolution.

PART VIII: CONCLUSIONS

225. A series of modeling tools has been developed that are capable of predicting Atchafalaya Bay delta evolution over both short and long terms and the impact of that delta evolution.

226. The delta that will evolve over 50 years under existing conditions of the project was predicted have the following characteristics and impacts:

a. The subaerial extent of the delta will dramatically increase to potentially over 100 square miles.

b. This delta will result in significantly higher stages within the entire system.

c. Circulation will be altered to divert more flow through Four-league Bay.

d. As a result of circulation alteration, salinities will be reduced in Terrebonne Marshes.

e. Dredging requirements may be reduced in the short term, but will increase to exceed the current experience for the long term.

227. The sensitivity analysis suggests that these results are at least qualitatively accurate, and may have quantitative accuracy for general trends.

228. These tools may now be used to assess the impact of changing the project conditions on the delta evolution and associated changes in the processes.

REFERENCES

Benson, H. A., and Donnell, B. P. 1990 (Aug). "The Atchafalaya River Delta; Report 2, Field Data; Section 4: Terrebonne Marshes Program Description and Data," Technical Report HL-82-15, US Army Engineer Waterways Experiment Station, Vicksburg, MS.

Coleman, C. J., Teeter, A. M., Donnell, B. P., Fisackerly, G. M., Crouse, D. A., and Parman, J. W. 1988 (Jun). "The Atchafalaya River Delta; Report 2, Field Data; Section 1: Atchafalaya Bay Program Description and Data," Technical Report HL-82-15, US Army Engineer Waterways Experiment Station, Vicksburg, MS.

Donnell, B. P., and Letter, J. V., Jr. "The Atchafalaya River Delta; Report 12, Two-dimensional Modeling of Alternative Plans and Impacts on the Atchafalaya Bay and Terrebonne Marshes" (in preparation), Technical Report HL-82-15, US Army Engineer Waterways Experiment Station, Vicksburg, MS.

Ebersole, B. A. 1985 (Jan). "The Atchafalaya River Delta; Report 8, Numerical Modeling of Hurricane-Induced Storm Surge," Technical Report HL-82-15, US Army Engineer Waterways Experiment Station, Vicksburg, MS.

Ebersole, B. A. 1985 (Jan). "The Atchafalaya River Delta; Report 9, Wind Climatology," Technical Report HL-82-15, US Army Engineer Waterways Experiment Station, Vicksburg, MS.

Jensen, R. E. 1985 (Mar). "The Atchafalaya River Delta; Report 10, Wave Hindcasts," Technical Report HL-82-15, US Army Engineer Waterways Experiment Station, Vicksburg, MS.

Juneau, C. L., Jr. 1975. "An Inventory and Study of the Vermilion Bay-Atchafalaya Bay Complex," Technical Bulletin No. 13, Louisiana Wildlife and Fisheries Commission, New Orleans, LA.

Keown, M. P., Dardeau, E. A., Jr., and Causey, E. M. 1981 (Aug). "Characterization of the Suspended-Sediment Regime and Bed-Material Gradation of the Mississippi River Basin," Potomology Investigation Report 22-1, US Army Engineer Waterways Experiment Station, Vicksburg, MS.

Letter, J. V., Jr. 1982 (Jul). "The Atchafalaya River Delta; Report 3, Extrapolation of Delta Growth," Technical Report HL-82-15, US Army Engineer Waterways Experiment Station, Vicksburg, MS.

McAnally, W. H., Jr. 1989. "Lessons from 10 years Experience in 2D Sediment Modeling," Sediment Transport Modeling, Proceedings of the International Symposium, American Society of Civil Engineers, S. Y. Wnag, ed., New York, pp 350-355.

McAnally, W. H., Jr., and Heltzel, S. B. "The Atchafalaya River Delta; Report 1, A Plan for Predicting Delta Evolution" (in preparation), Technical Report HL-82-15, US Army Engineer Waterways Experiment Station, Vicksburg, MS.

McAnally, W. H., Jr., Brogdon, N. J., Jr., Letter, J. V., Jr., Stewart, J. P., and Thomas, W. A. 1983 (Sep). "Columbia River Estuary Hybrid Model Studies; Report 1, Verification of Hybrid Modeling of the Columbia River Mouth," Technical Report HL-83-16, U.S. Army Engineer Waterways Experiment Stations, Vicksburg, MS.

McAnally, W. H., Jr., Thomas, W. A., Letter, J. V., Jr., and Stewart, J. P. 1984 (Jul). "The Atchafalaya River Delta; Report 6, Interim Summary Report of Growth Predictions," Technical Report HL-82-15, US Army Engineer Waterways Experiment Station, Vicksburg, MS.

Mehta, A. J. "Characterization of Cohesive Sediment Properties and Transport Processes in Estuaries," Lecture Notes on Coastal and Estuarine Studies: Estuarine Cohesive Sediment Dynamics, Tampa, FL.

Neuman, G. and Pierson, W. J., Jr. 1966. Principles of Physical Oceanography, Prentice-Hall, Englewood Cliffs, NJ.

Pankow, W., Teeter, A. M., Donnell, B. P., and Adamec, S. A. 1990 (Aug). "The Atchafalaya River Delta; Report 2, Feild Data; Section 3: Grain Size Analysis of Selected Bay Sediments," Technical Report HL-82-15, US Army Engineer Waterways Experiment Station, Vicksburg, MS.

Teeter, A. M. and Pankow, W. 1989 (Sep). "The Atchafalaya River Delta; Report 2, Field Data, Section 2: Settling Characteristics of Bay Sediments", Technical Report HL-82-15, US Army Engineer Waterways Experiment Station, Vicksburg, MS.

Thomas, W. A., Heath, R. E., Stewart, J. P., and Clark, D. G. 1988 (Dec). "The Atchafalaya River Delta; Report 5, The Atchafalaya River Delta Quasi-Two-Dimensional Model of Delta Growth and Impacts on River Stages," Technical Report HL-82-15, US Army Engineer Waterways Experiment Station, Vicksburg, MS.

Thomas, W. A., and McAnally, W. H., Jr. 1985 (Jul). "User's Manual for the Generalized Computer Program System: Open-Channel Flow and Sedimentation, TABS-2," Instruction Report HL-85-1, US Army Engineer Waterways Experiment Station, Vicksburg, MS.

US Army Engineer District, New Orleans. 1982 (Jan). "Atchafalaya Basin Floodway System, Louisiana, Feasibility Study," Volume 2 with Technical Appendixes A, B, C, and D, New Orleans, LA.

US Army Army Engineer District, New Orleans, 1974, "Preliminary Drafy Environmental Impact Statement, Atchafalaya Basin Floodway," New Orleans, LA.

Wang, F. C., 1985 (Sep). "The Atchafalaya River Delta; Report 7, Analytical Analysis of the Development of the Atchafalaya River Delta," Technical Report HL-82-15, US Army Engineer Waterways Experiment Station, Vicksburg, MS.

Wells, J. T., Chinburg, S. J., and Coleman, J. M. 1984 (Jan). "The Atchafalaya River Delta; Report 4, Generic Analysis of Delta Development," Technical Report HL-82-15, US Army Engineer Waterways Experiment Station, Vicksburg, MS.

Photo 1. NASA LANDSAT illustrating sediment plume recorded 6 January 1983 at a 475,000-cfs discharge

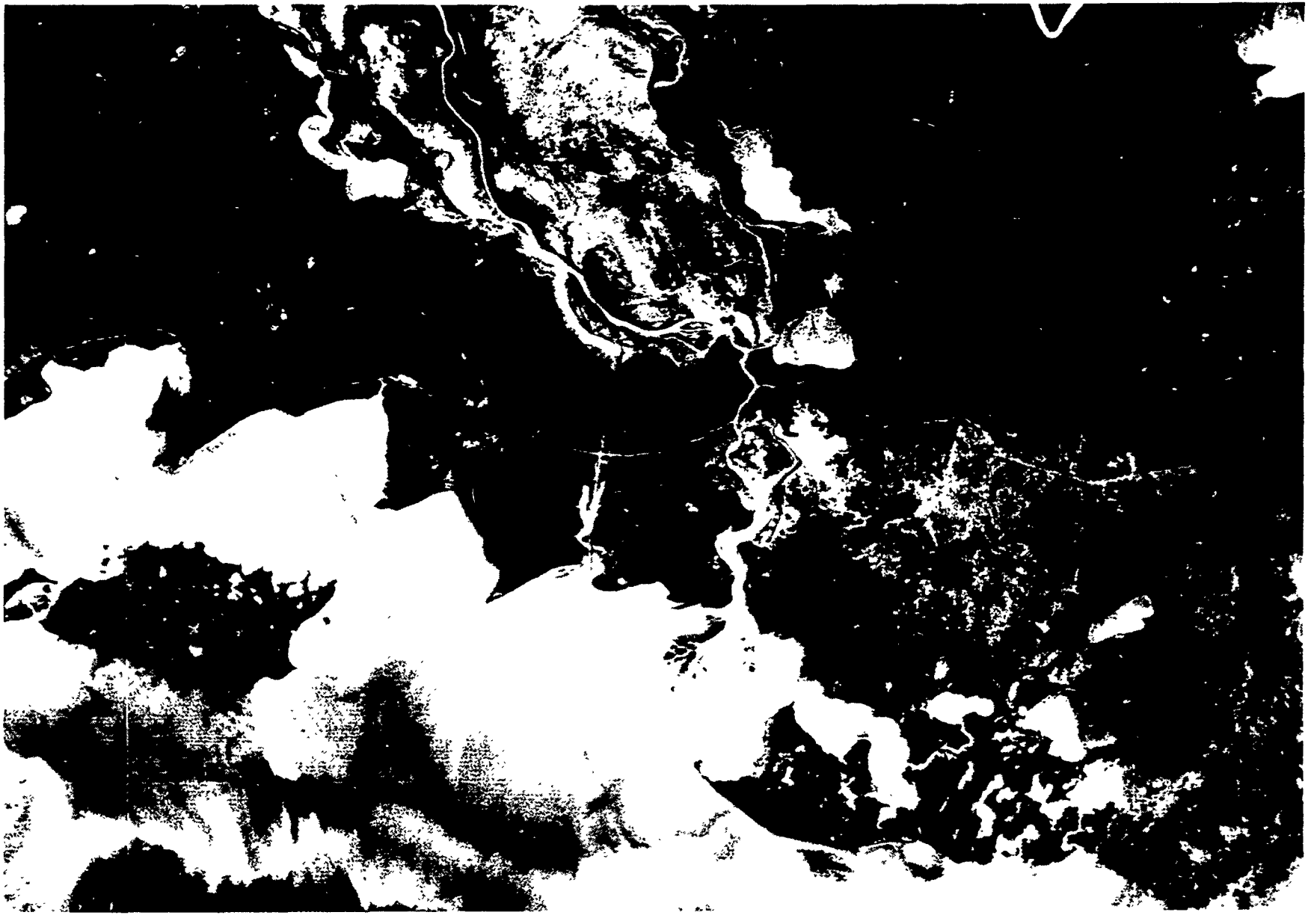

Photo 2. NASA LANDSAT image of the Atchafalaya Bay and Terrebonne Marshes at approximately 475,000 cfs

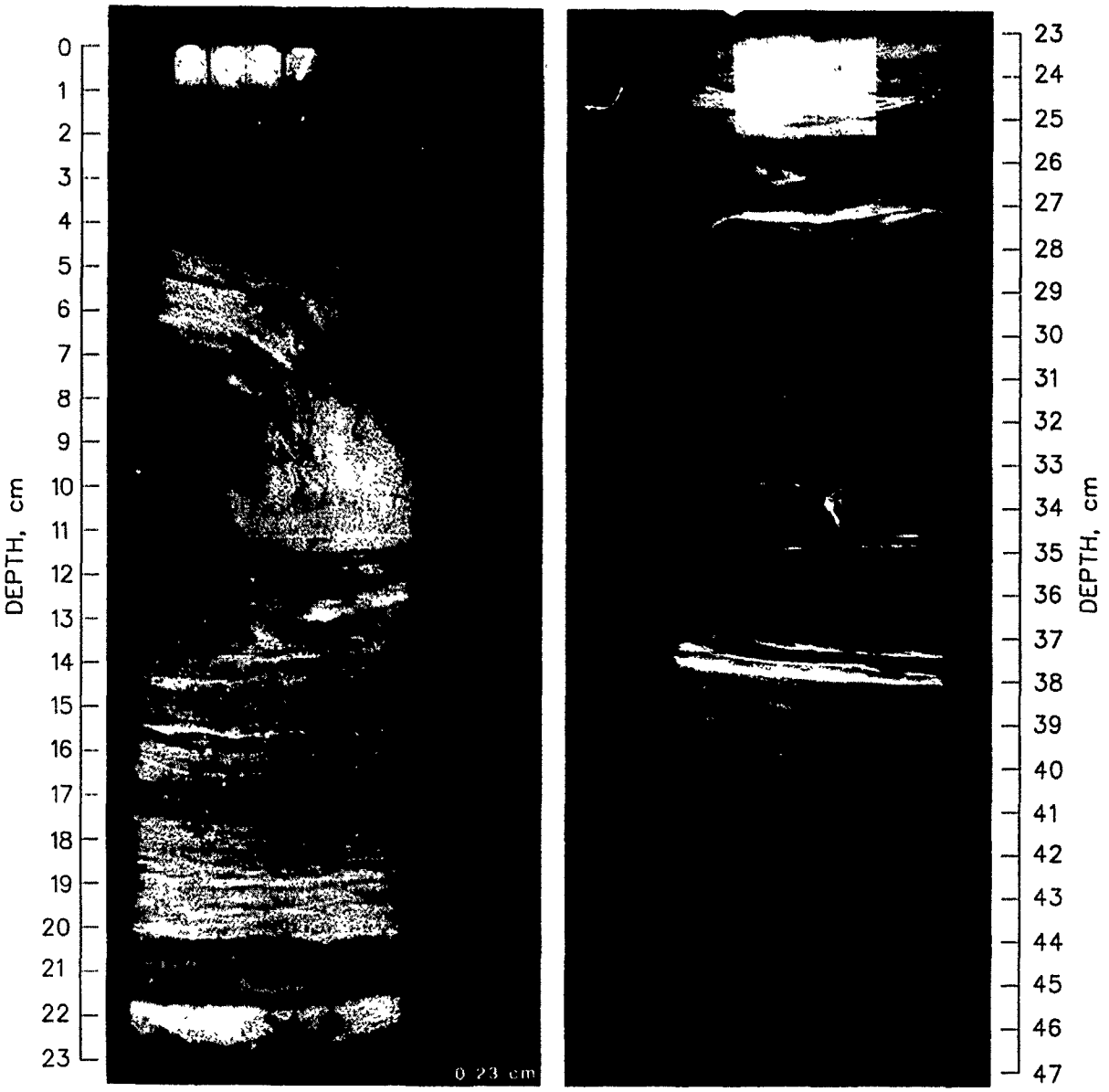

Photo 3. Core sample J collected 2,500 m east of Atchafalaya Bay navigation channel in the spring of 1980

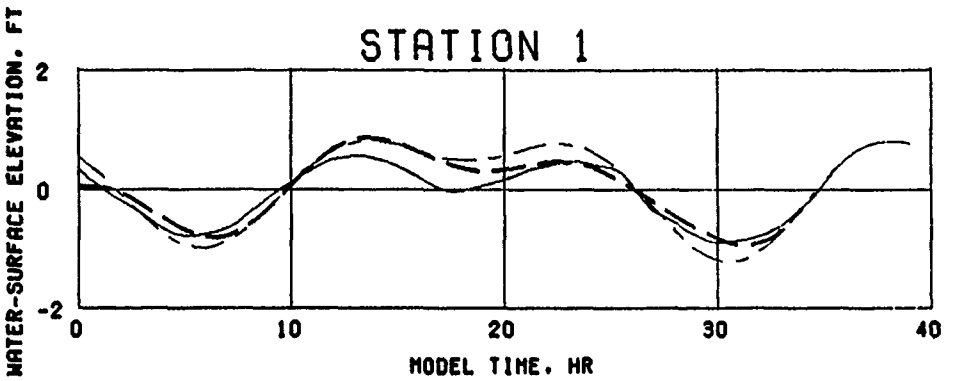

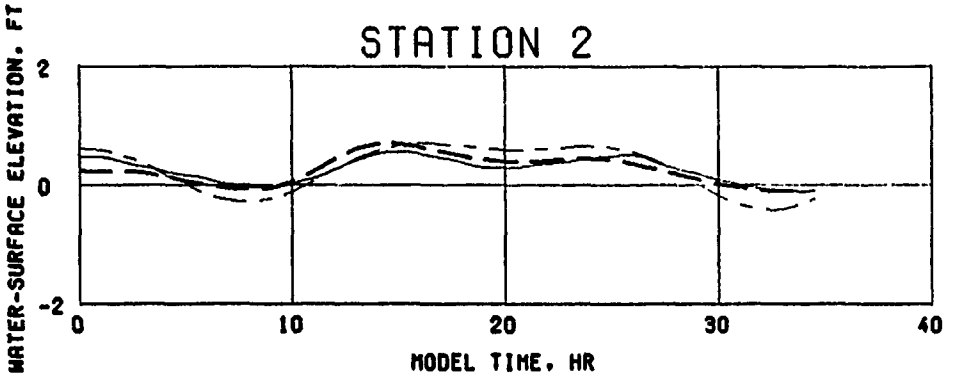

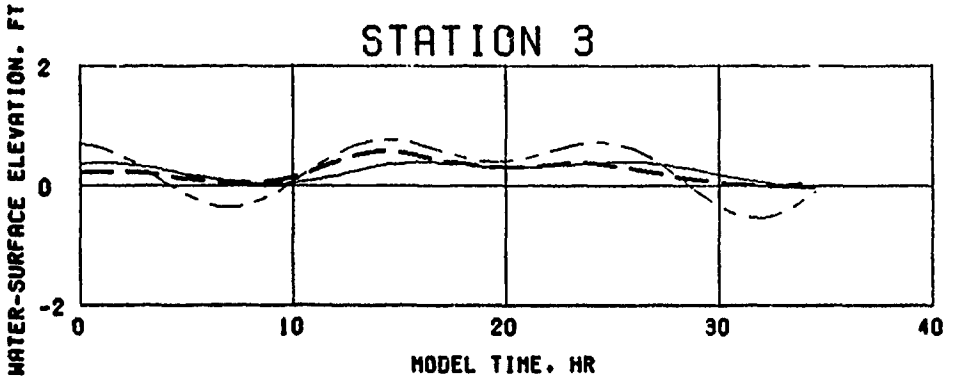

LEGEND

— — MODEL

——— PROTOTYPE

— - — SYNTHESIZED

VERIFICATION OF TIDAL HEIGHTS

MESH 2
Q = 330,000 CFS
MEAN TIDE
STATIONS 1-3

PLATE 1

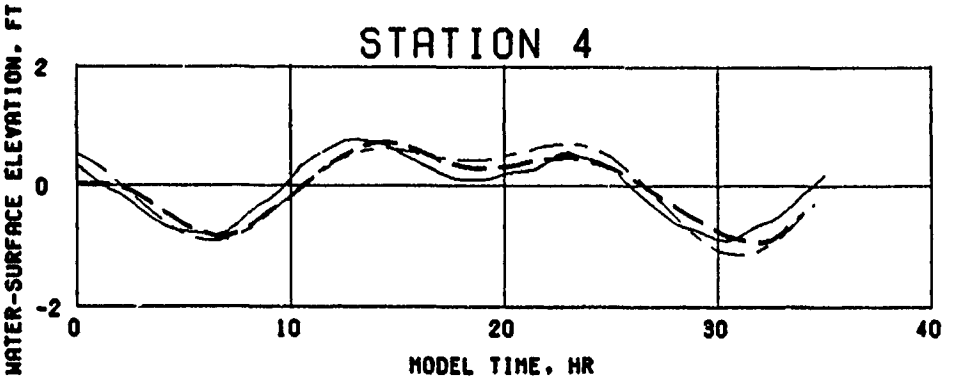

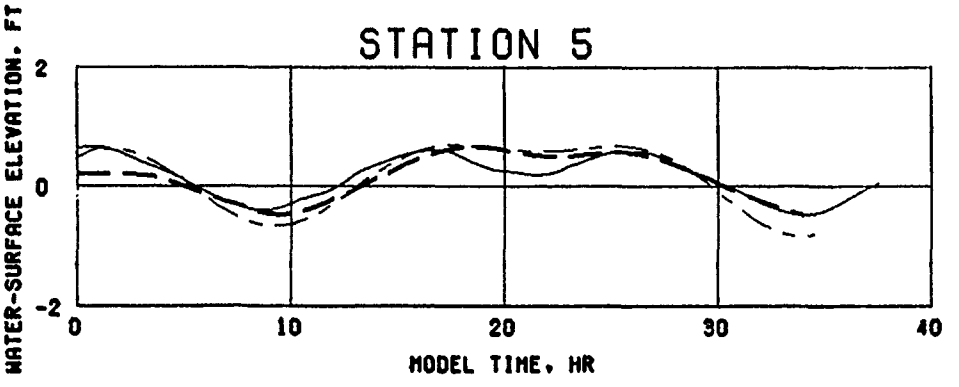

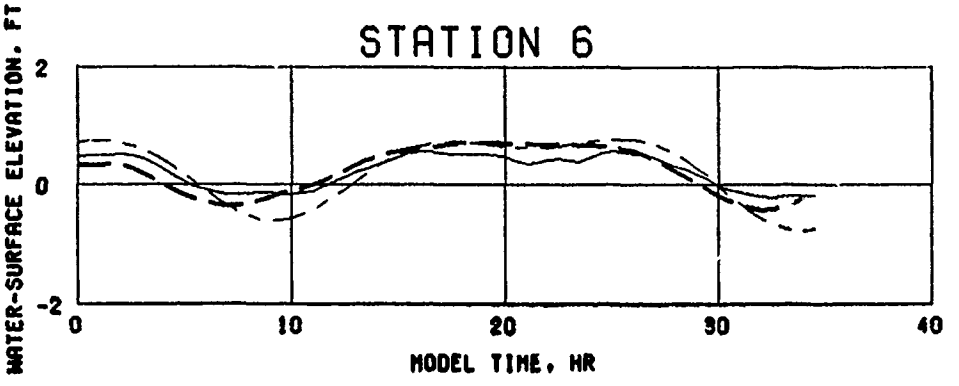

LEGEND

— — MODEL

——— PROTOTYPE

— — — SYNTHESIZED

VERIFICATION OF TIDAL HEIGHTS

MESH 2
Q = 330,000 CFS
MEAN TIDE
STATIONS 4-6

PLATE 2

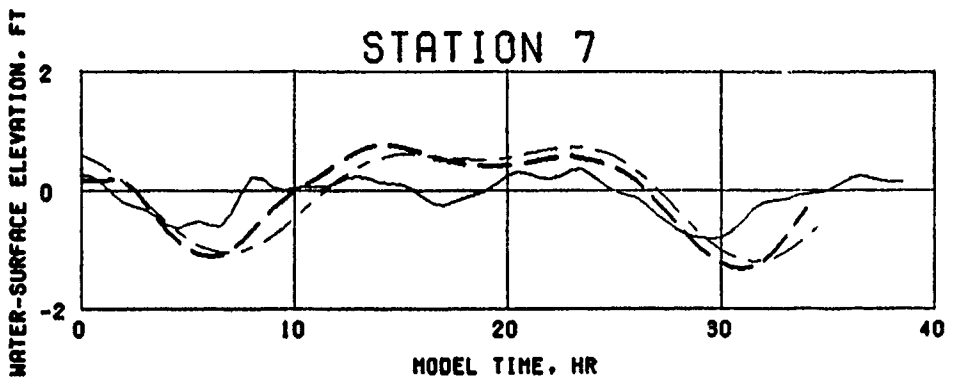

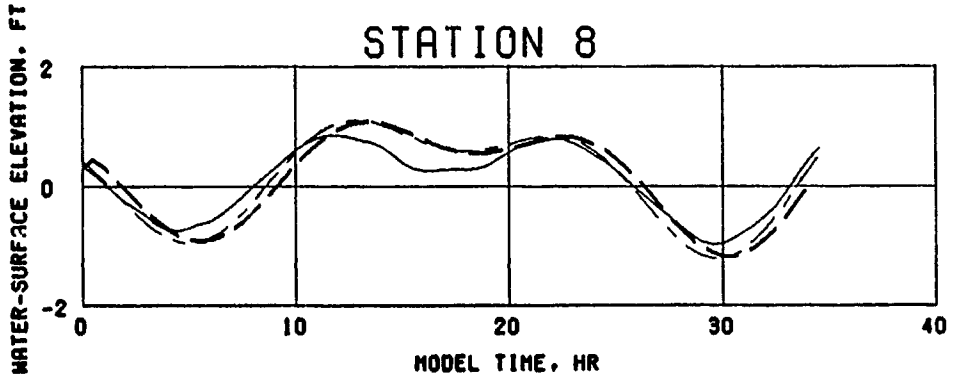

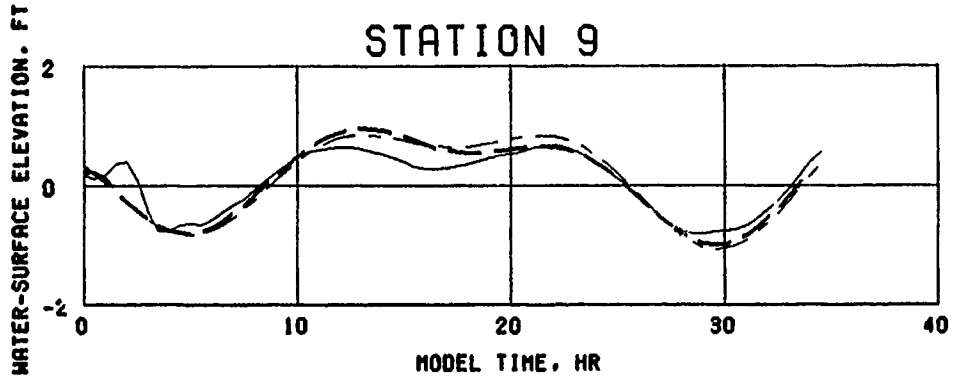

LEGEND

— — MODEL

——— PROTOTYPE

— - — SYNTHESIZED

VERIFICATION OF TIDAL HEIGHTS

MESH 2
Q = 330,000 CFS
MEAN TIDE
STATIONS 7-9

PLATE 3

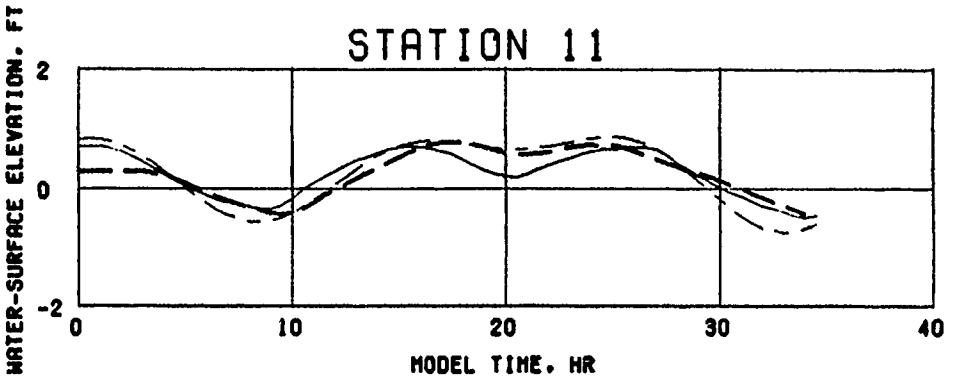

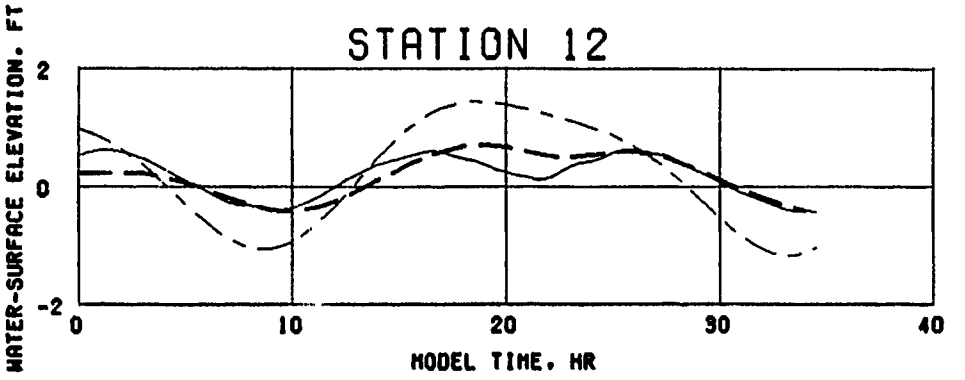

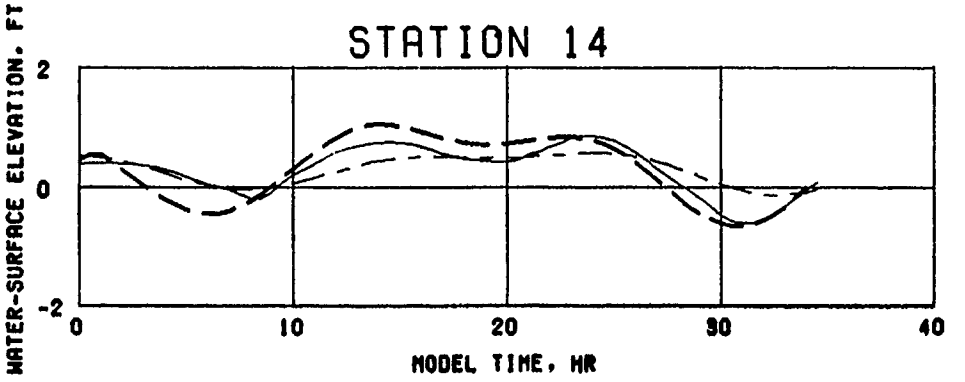

LEGEND

— — MODEL

——— PROTOTYPE

— - — SYNTHESIZED

VERIFICATION OF TIDAL HEIGHTS

MESH 2
Q = 330,000 CFS
MEAN TIDE
STATIONS 11, 12, AND 14

PLATE 4

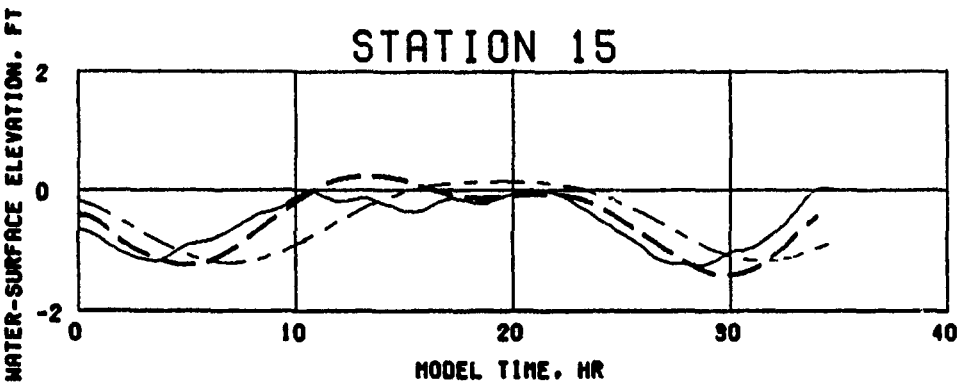

LEGEND
— — MODEL
——— PROTOTYPE
— - — SYNTHESIZED

VERIFICATION OF TIDAL HEIGHTS

MESH 2
Q = 330,000 CFS
MEAN TIDE
STATION 15

PLATE 5

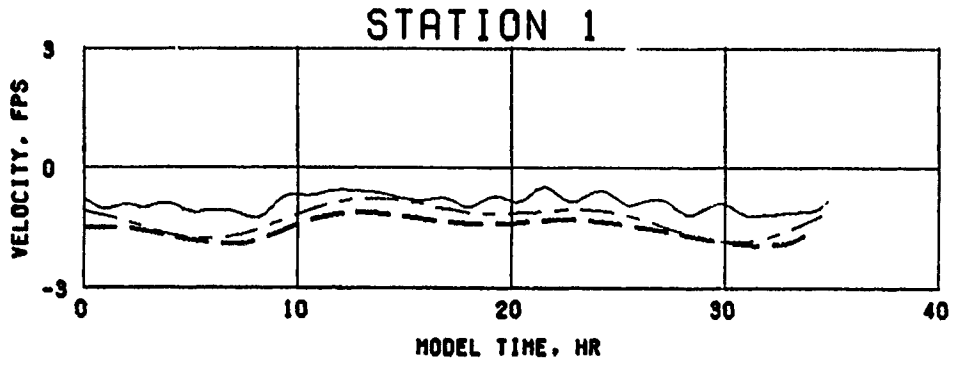

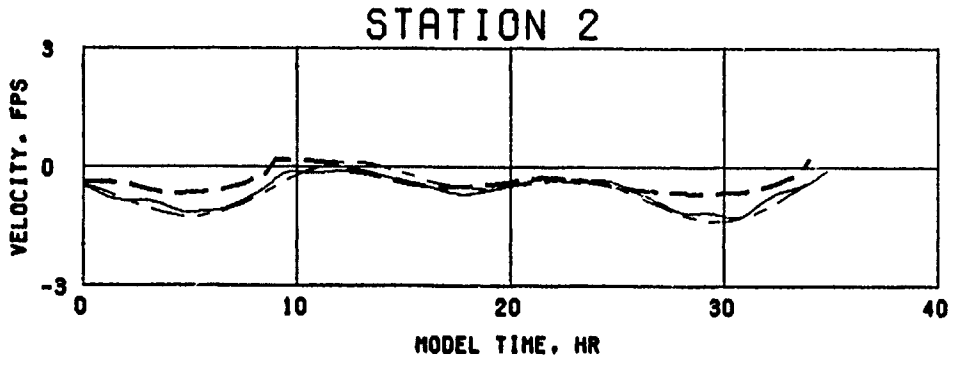

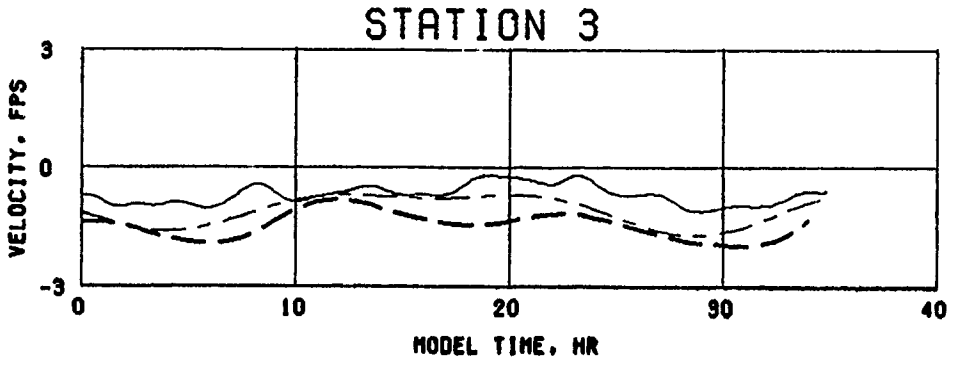

LEGEND

— — MODEL

——— PROTOTYPE

— — — SYNTHESIZED

VERIFICATION OF CURRENT VELOCITIES

MESH 2
Q = 330,000 CFS
MEAN TIDE
STATIONS 1-3

PLATE 6

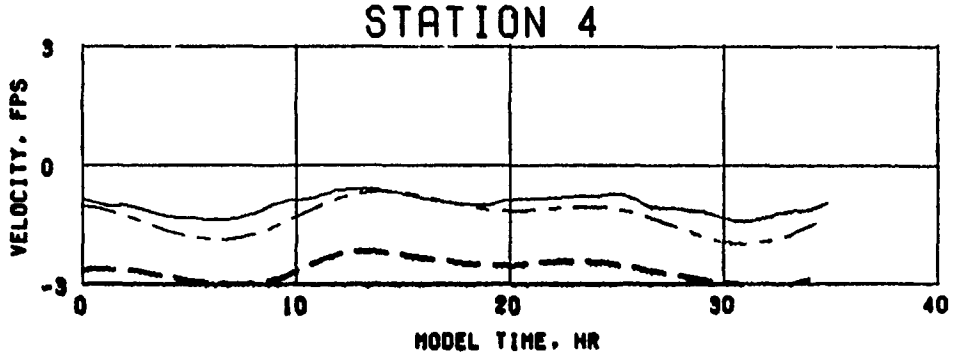

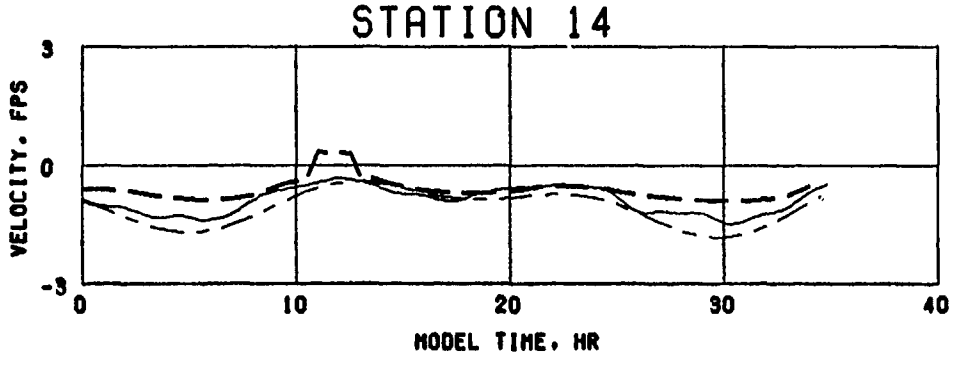

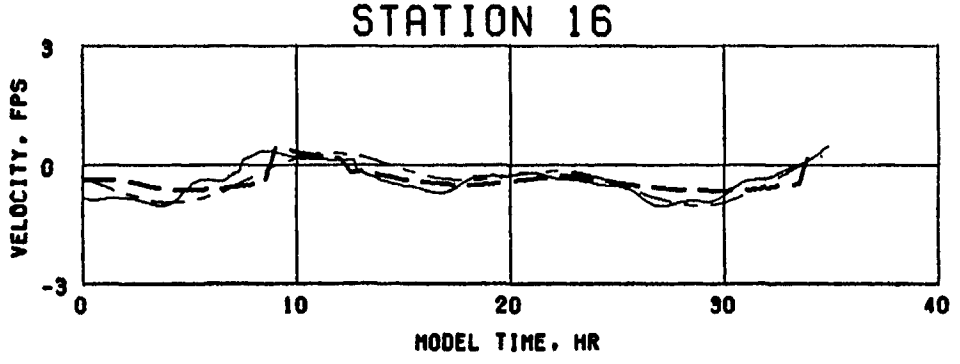

LEGEND

— — MODEL

——— PROTOTYPE

— - — SYNTHESIZED

VERIFICATION OF CURRENT VELOCITIES

MESH 2
Q = 330,000 CFS
MEAN TIDE
STATIONS 4, 14, AND 16

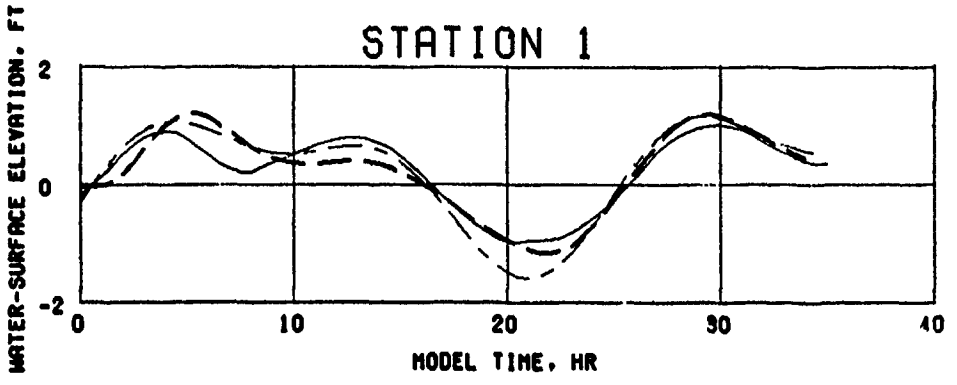

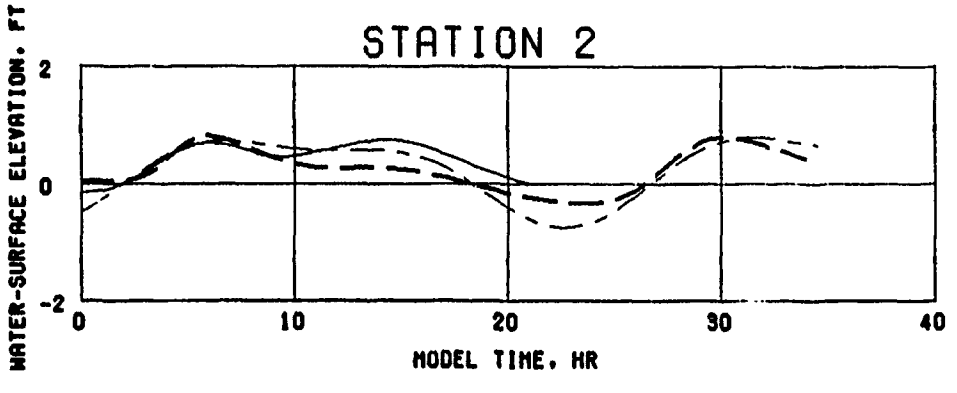

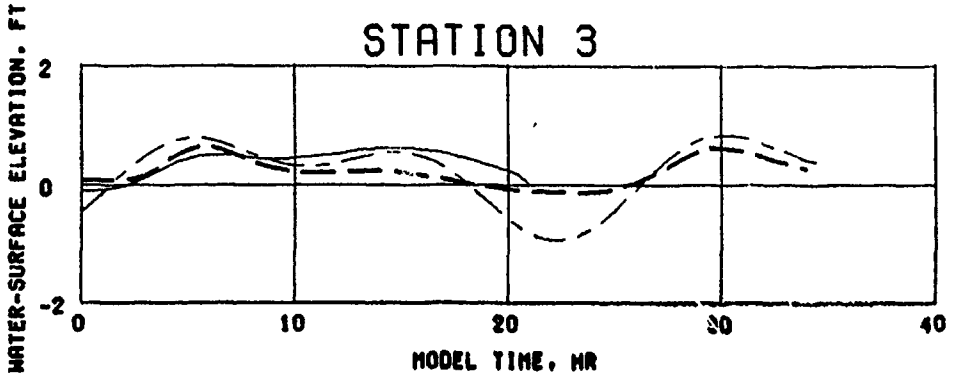

LEGEND

— — MODEL

——— PROTOTYPE

— — — SYNTHESIZED

VERIFICATION OF TIDAL HEIGHTS

MESH 2
Q = 330,000 CFS
SPRING TIDE
STATIONS 1-3

PLATE 8

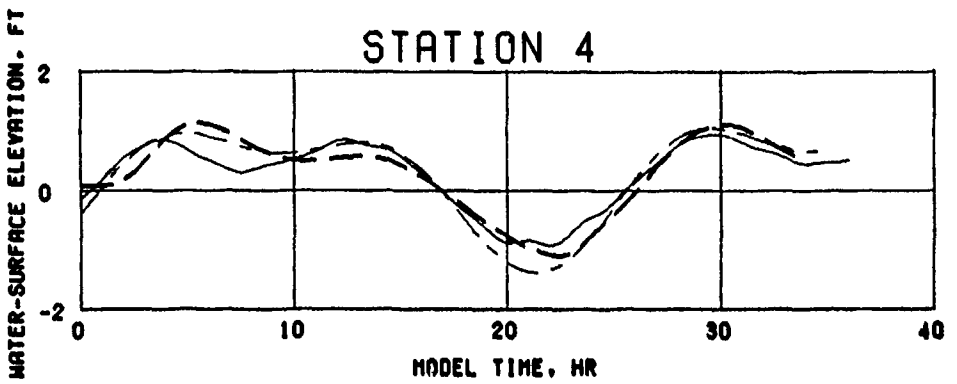

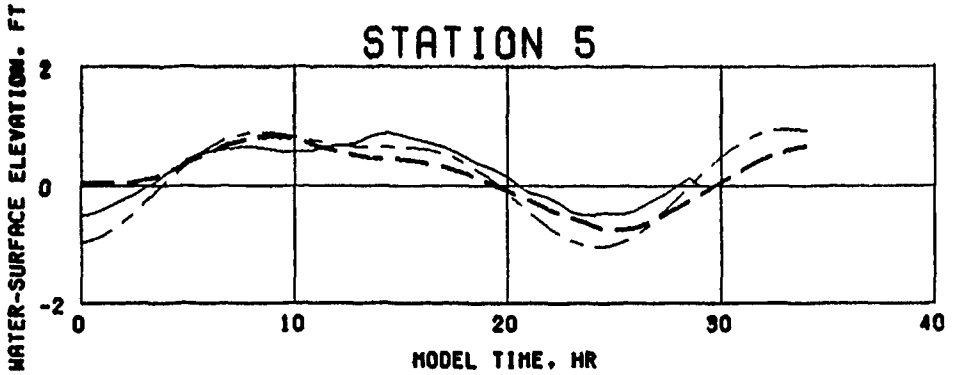

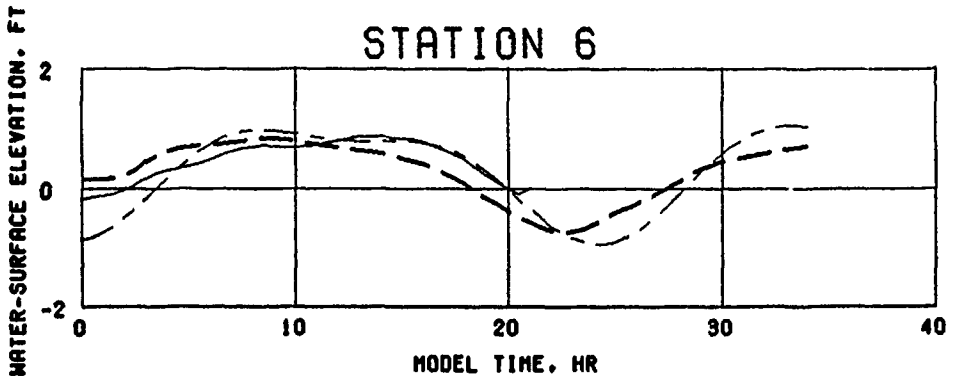

LEGEND

— — MODEL

——— PROTOTYPE

— — — SYNTHESIZED

VERIFICATION OF TIDAL HEIGHTS

MESH 2
Q = 330,000 CFS
SPRING TIDE
STATIONS 4-6

PLATE 9

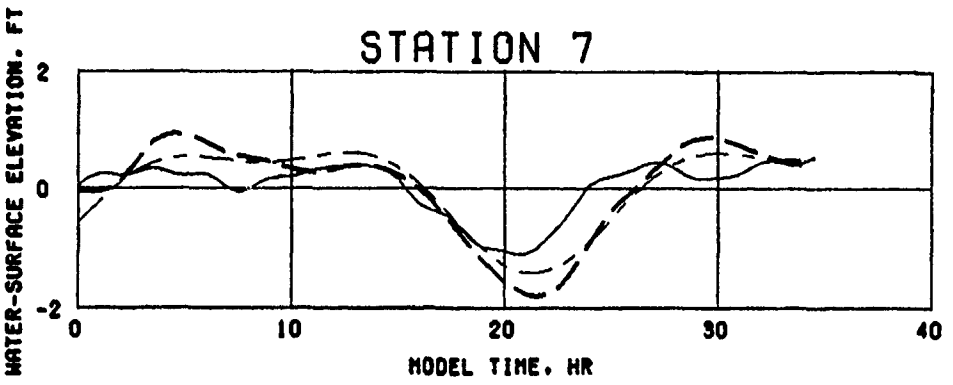

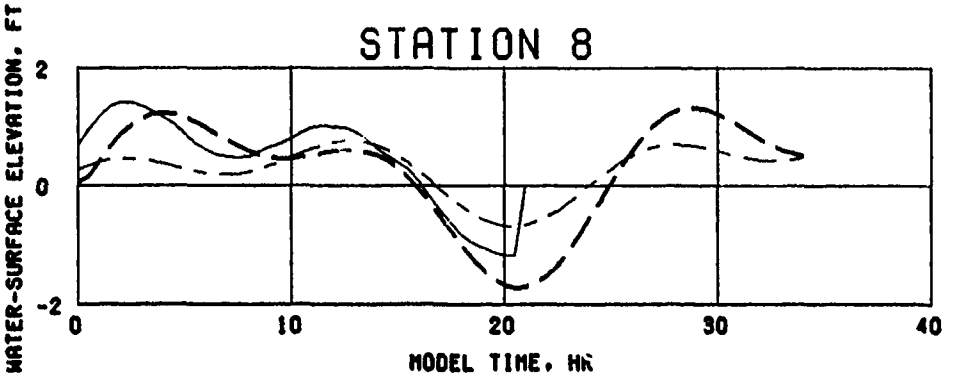

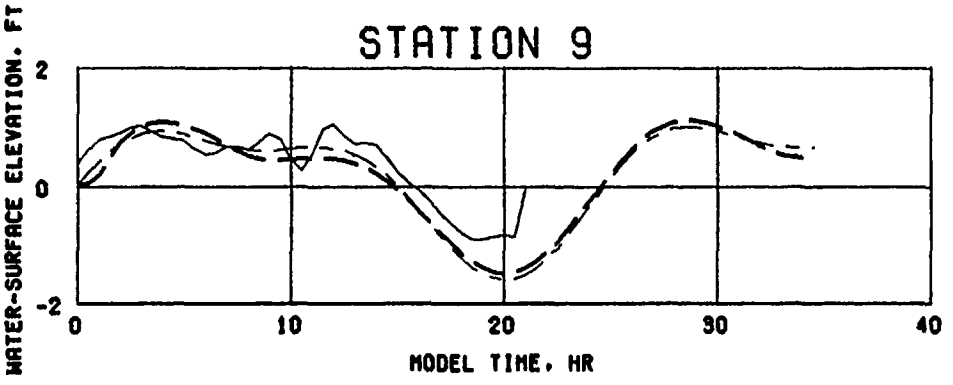

LEGEND

— — MODEL

——— PROTOTYPE

— - — SYNTHESIZED

VERIFICATION OF TIDAL HEIGHTS

MESH 2
Q = 330,000 CFS
SPRING TIDE
STATIONS 7-9

PLATE 10

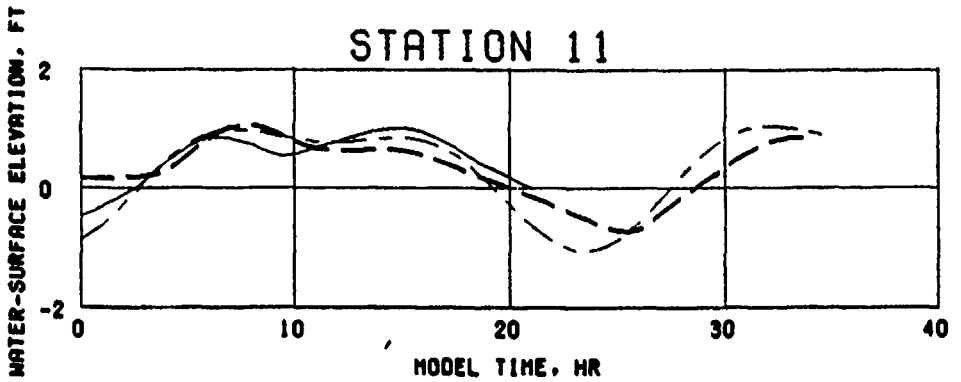

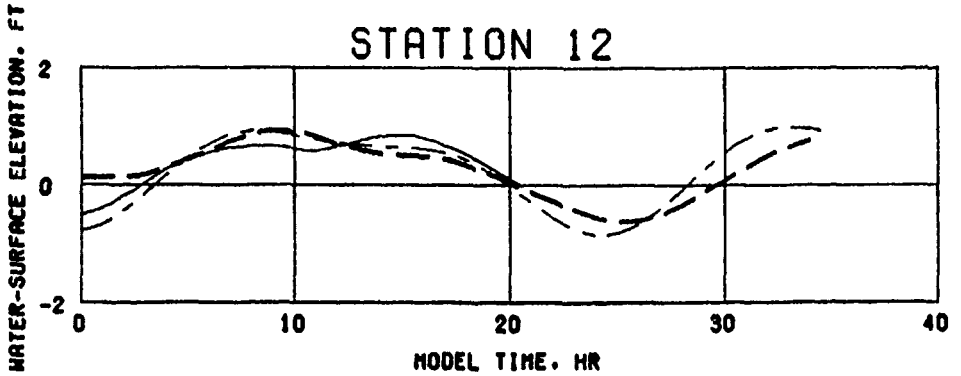

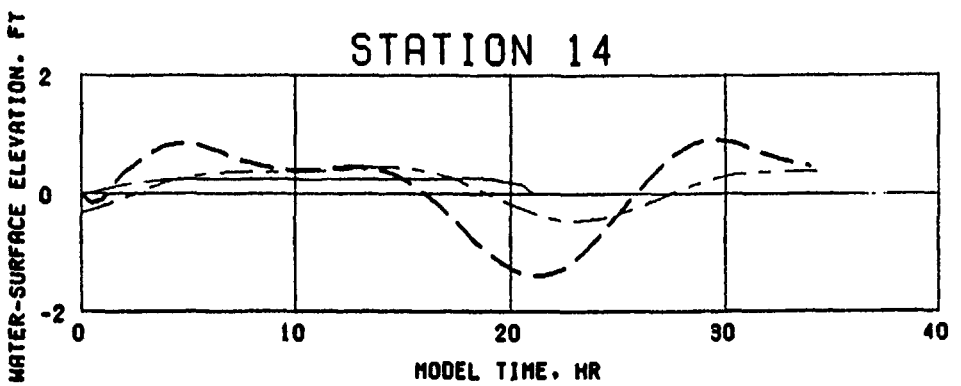

LEGEND

— — MODEL

——— PROTOTYPE

— - — SYNTHESIZED

VERIFICATION OF TIDAL HEIGHTS

MESH 2
Q = 330,000 CFS
SPRING TIDE
STATIONS 11, 12, AND 14

PLATE 11

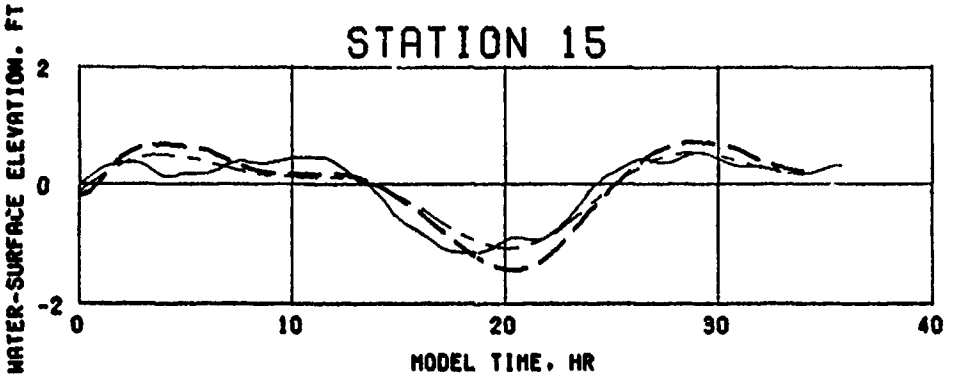

LEGEND
MODEL
PROTOTYPE
SYNTHESIZED

VERIFICATION OF TIDAL HEIGHTS

MESH 2
Q = 330,000 CFS
SPRING TIDE
STATION 15

PLATE 12

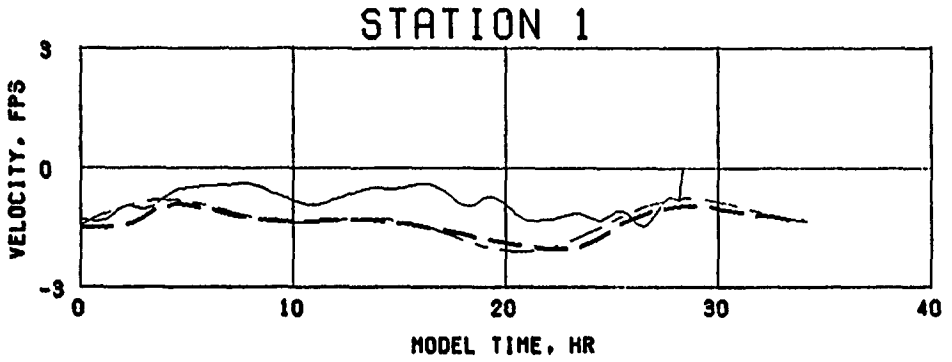

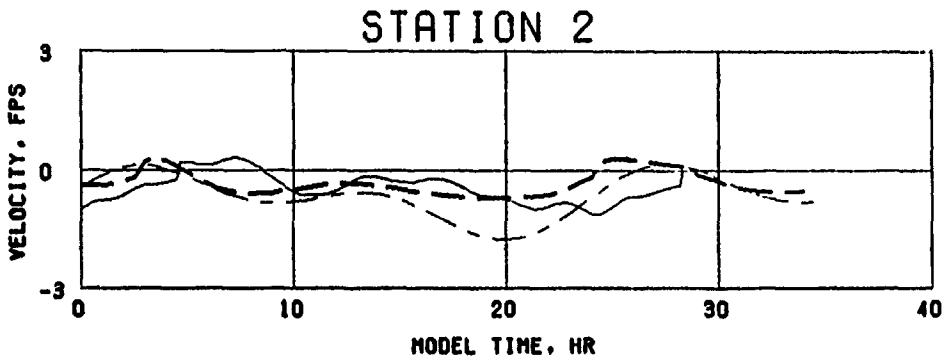

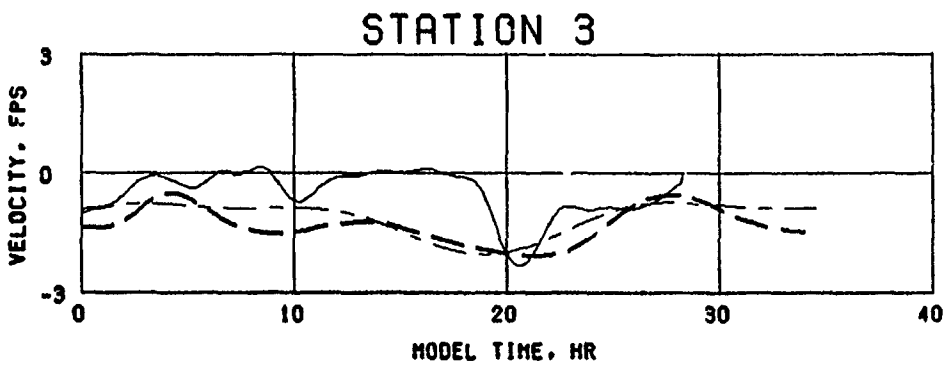

LEGEND

— — MODEL

——— PROTOTYPE

— - — SYNTHESIZED

VERIFICATION OF CURRENT VELOCITIES

MESH 2
Q = 330,000 CFS
SPRING TIDE
STATIONS 1-3

PLATE 13

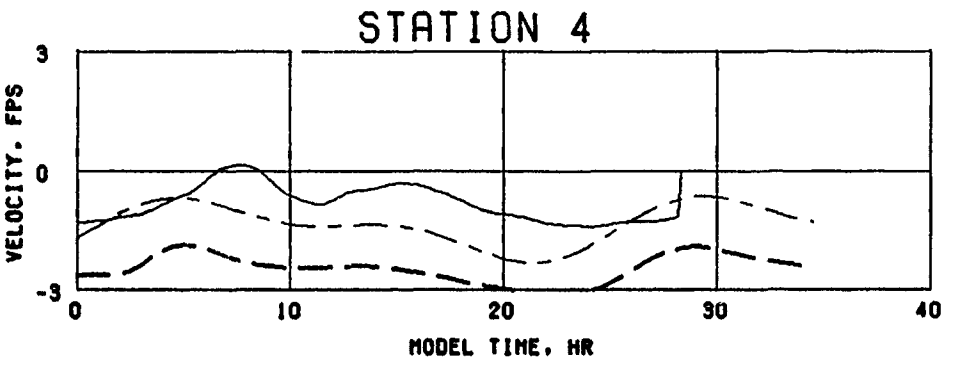

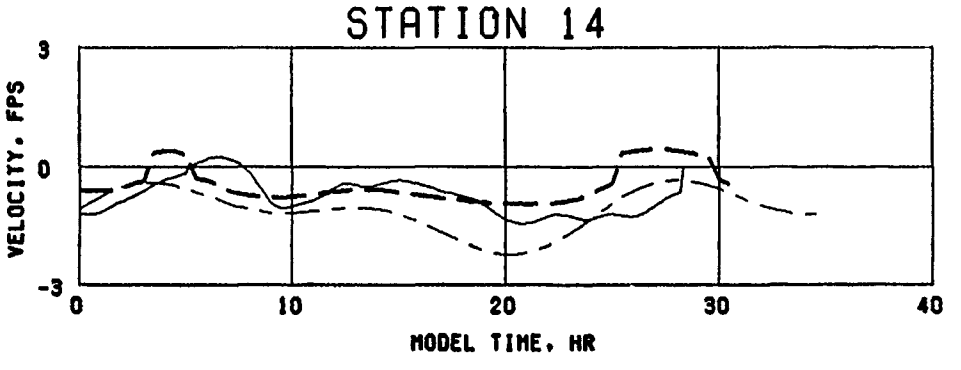

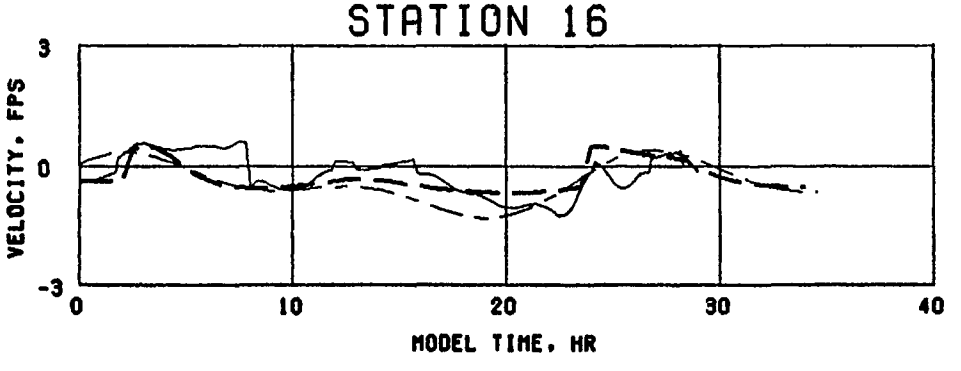

LEGEND

— — MODEL

——— PROTOTYPE

— — — SYNTHESIZED

VERIFICATION OF CURRENT VELOCITIES

MESH 2
Q = 330,000 CFS
SPRING TIDE
STATIONS 4, 14, AND 16

PLATE 14

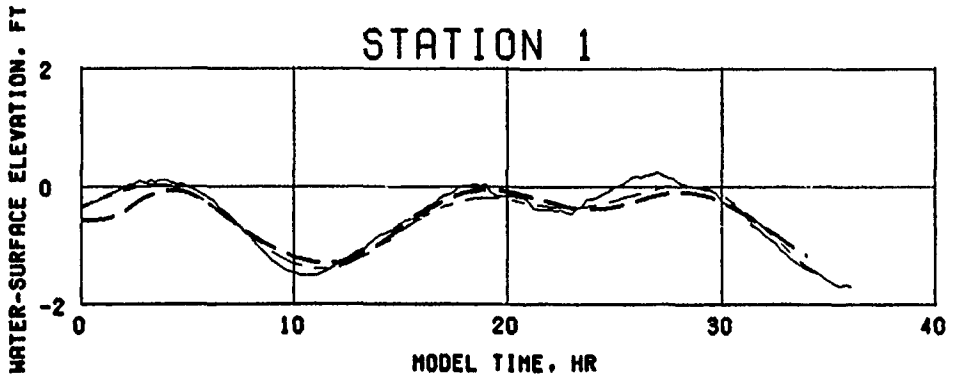

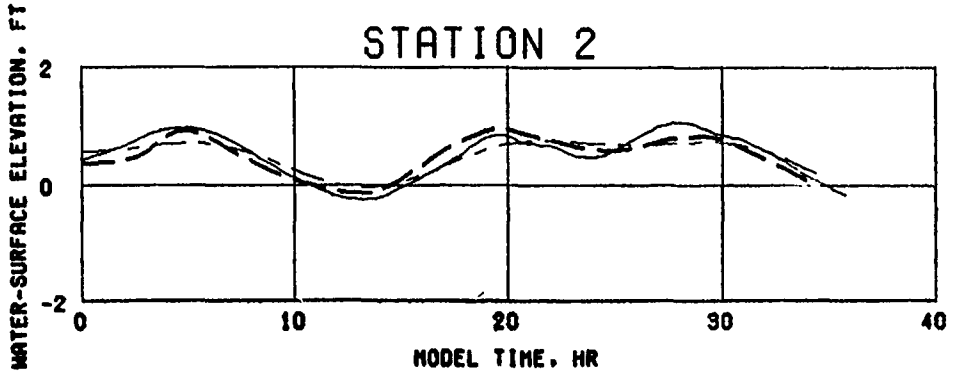

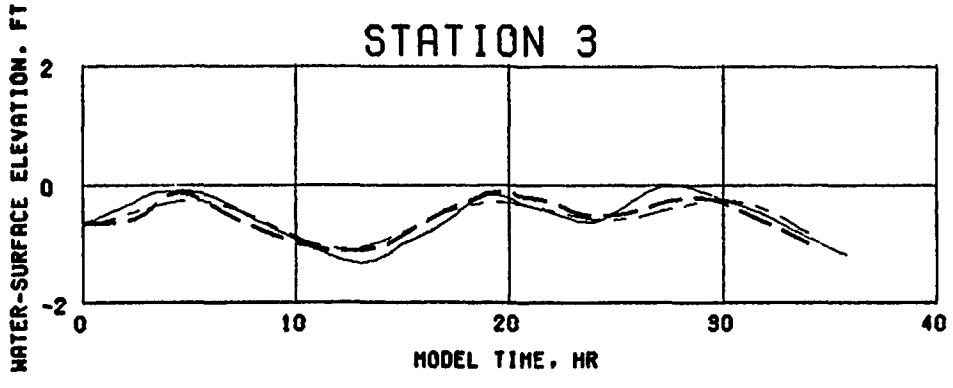

LEGEND

— — MODEL

——— PROTOTYPE

— - — SYNTHESIZED

VERIFICATION OF TIDAL HEIGHTS

MESH 2
Q = 50,000 CFS
MEAN TIDE
STATIONS 1-3

PLATE 15

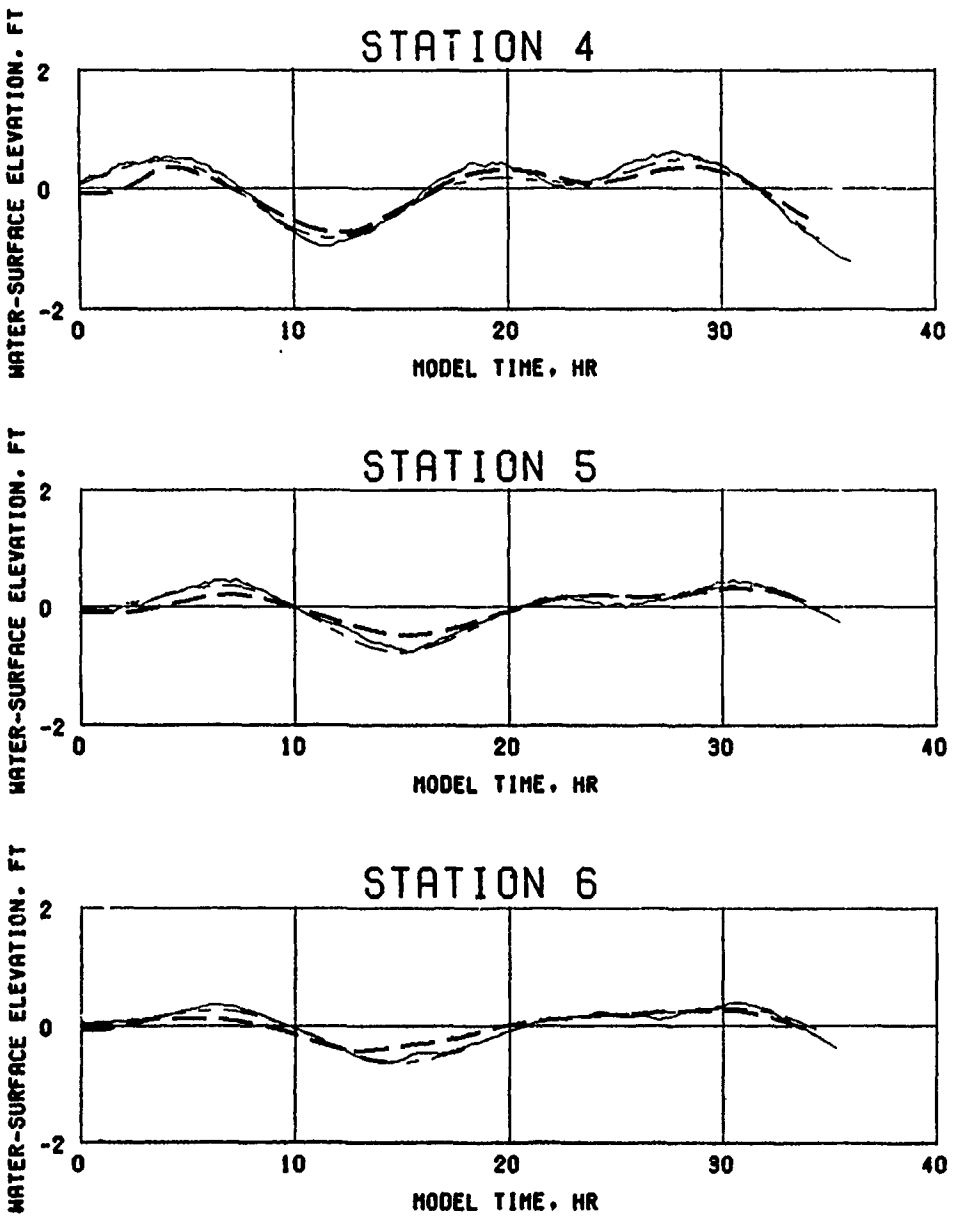

VERIFICATION OF TIDAL HEIGHTS

MESH 2
Q = 50,000 CFS
MEAN TIDE
STATIONS 4-6

PLATE 16

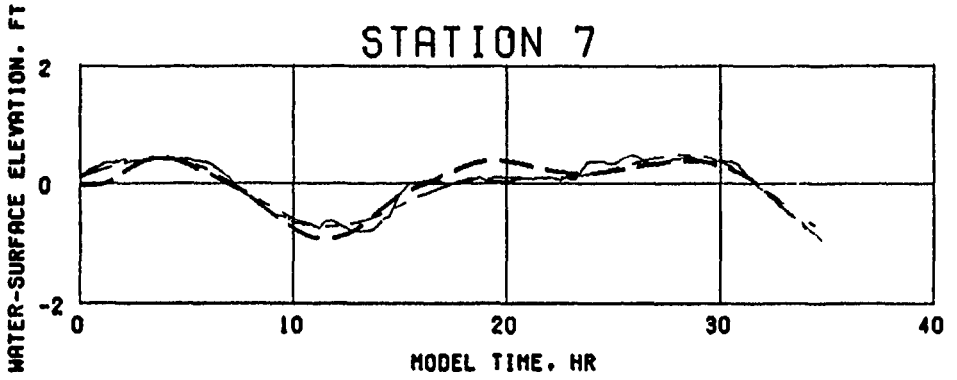

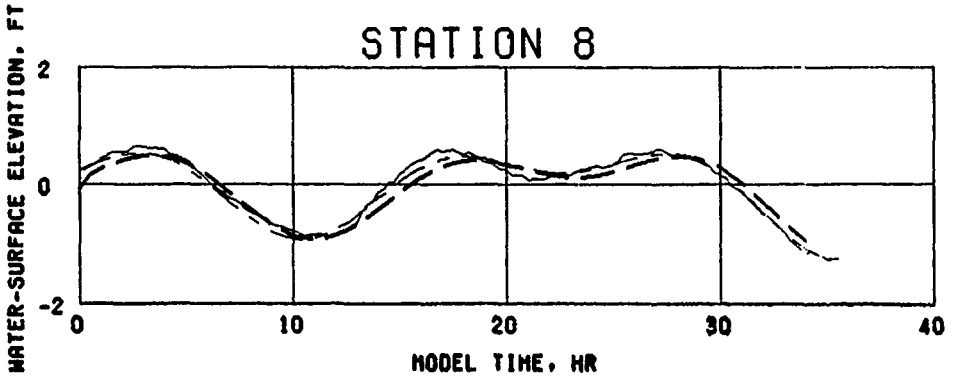

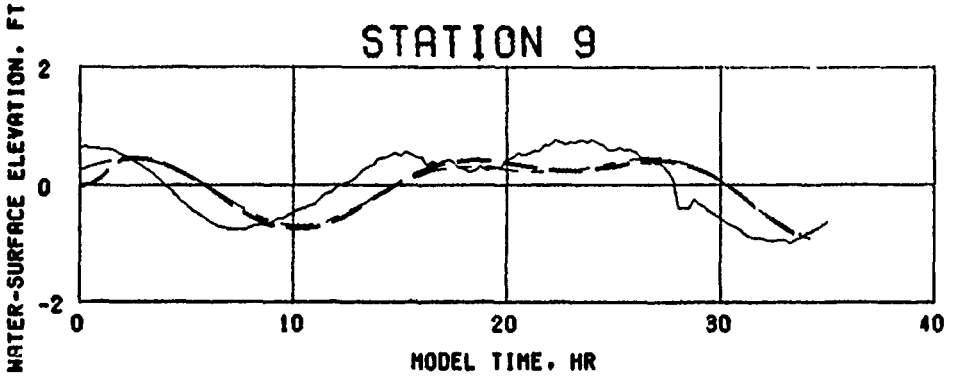

LEGEND

— — MODEL

——— PROTOTYPE

— - — SYNTHESIZED

VERIFICATION OF TIDAL HEIGHTS

MESH 2
Q = 50,000 CFS
MEAN TIDE
STATIONS 7-9

PLATE 17

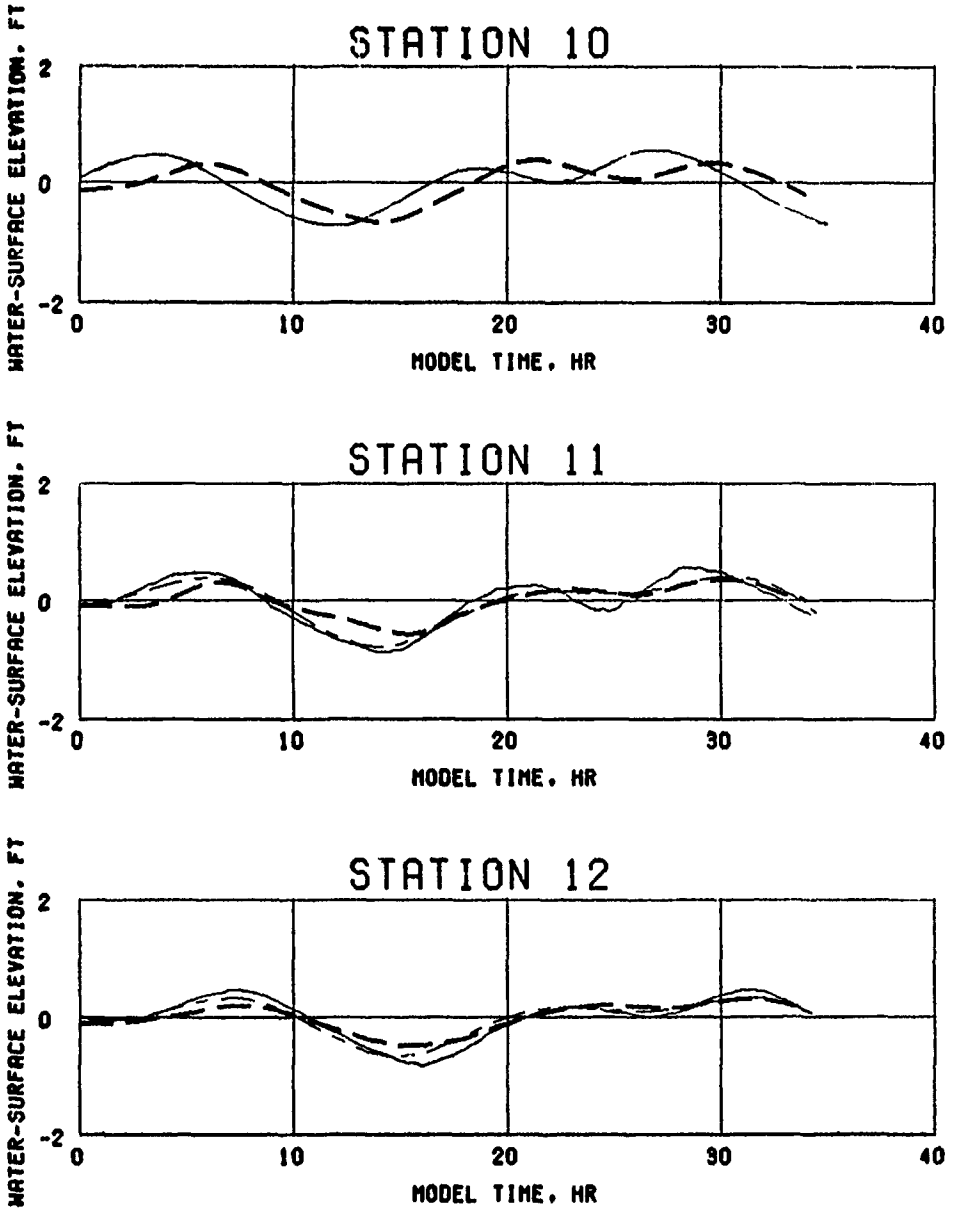

VERIFICATION OF TIDAL HEIGHTS

MESH 2
Q = 50,000 CFS
MEAN TIDE
STATIONS 10-12

PLATE 18

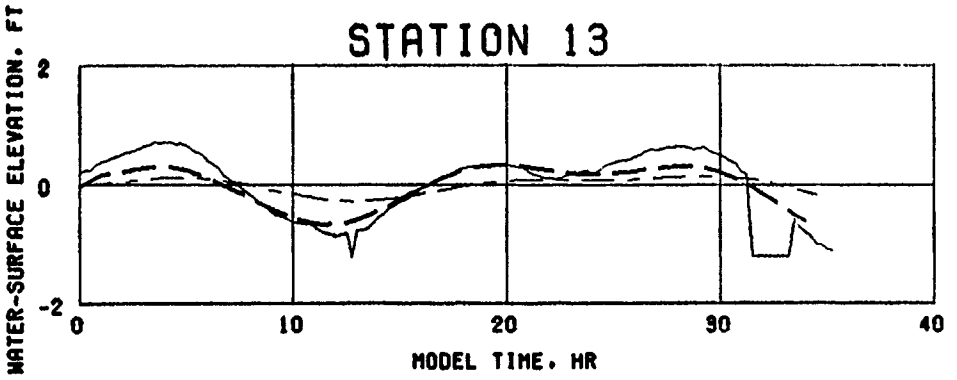

LEGEND

— — MODEL

——— PROTOTYPE

— - — SYNTHESIZED

VERIFICATION OF TIDAL HEIGHTS

MESH 2
Q = 50,000 CFS
MEAN TIDE
STATION 13

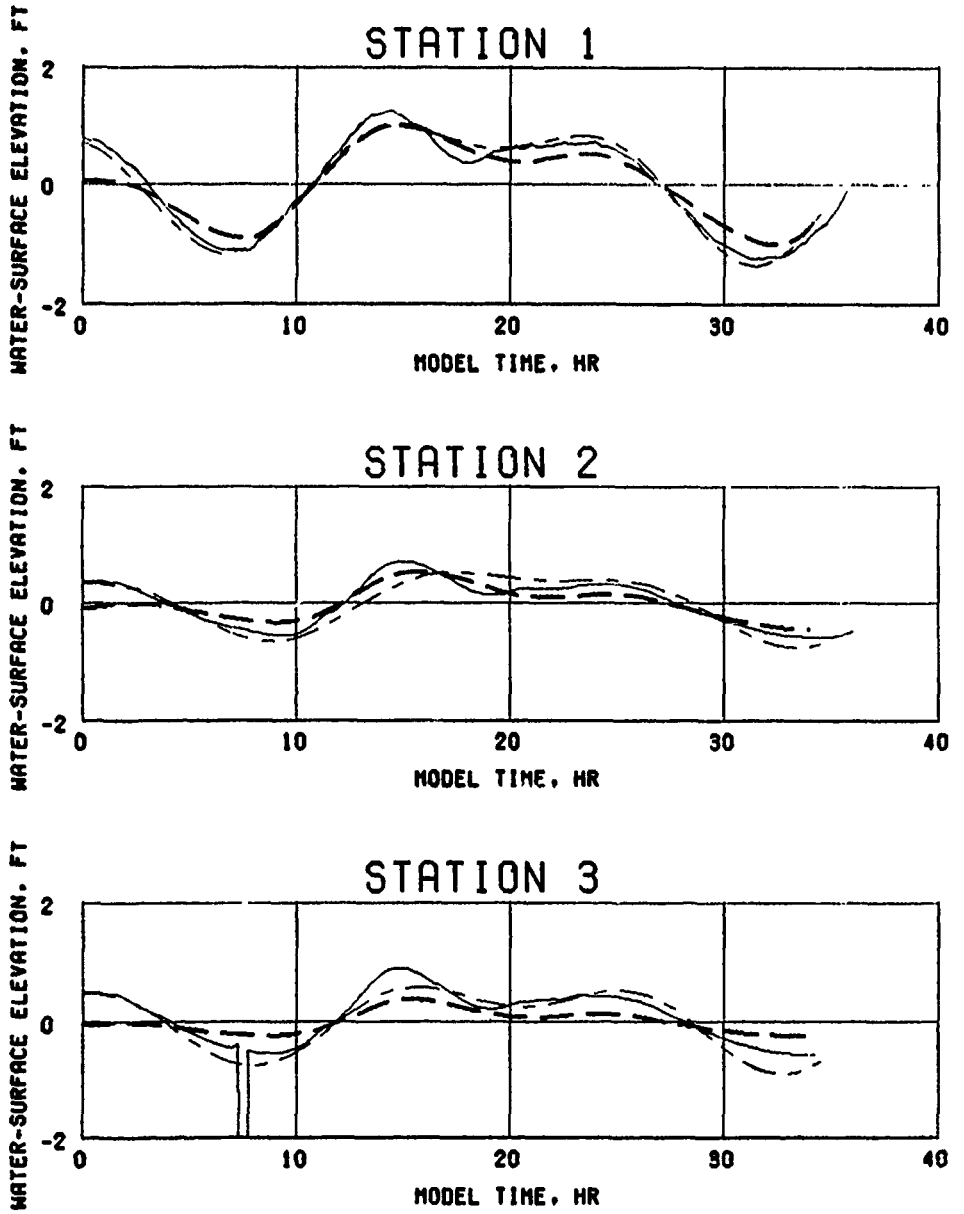

VERIFICATION OF
TIDAL HEIGHTS
MESH 2
Q = 320,000 CFS
SPRING TIDE
STATIONS 1-3

PLATE 20

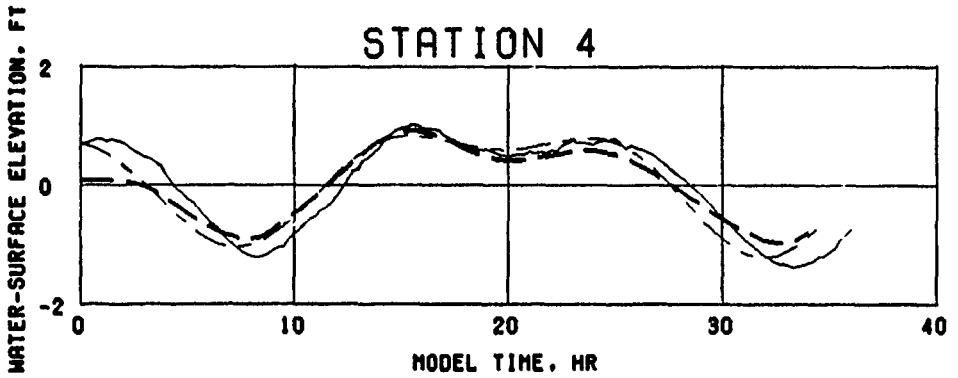

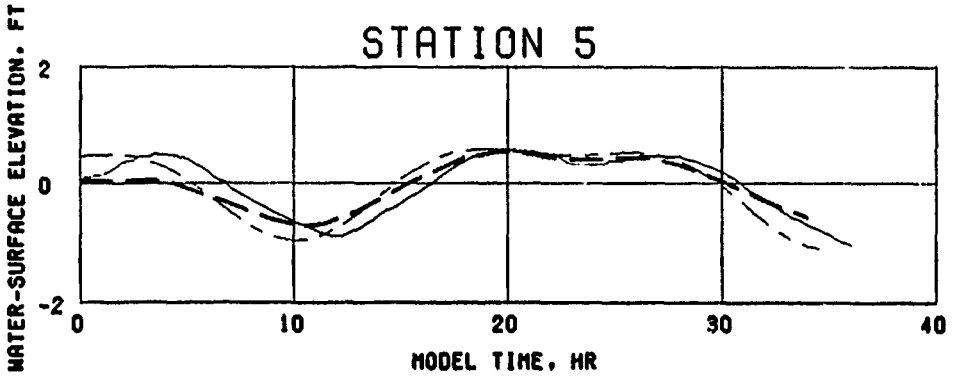

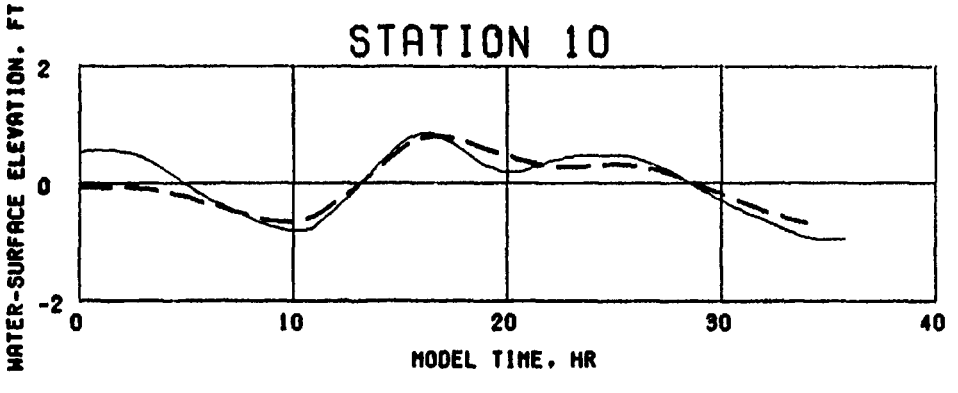

LEGEND

— — MODEL

——— PROTOTYPE

— — — SYNTHESIZED

VERIFICATION OF TIDAL HEIGHTS

MESH 2
Q = 320,000 CFS
SPRING TIDE
STATIONS 4, 5, AND 10

PLATE 21

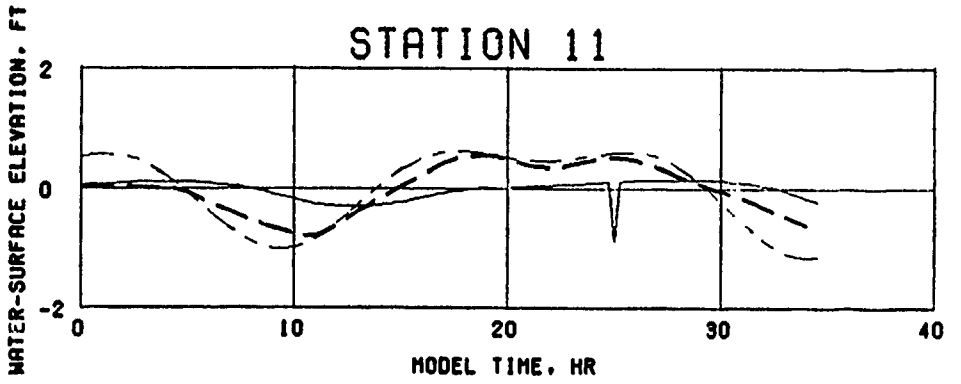

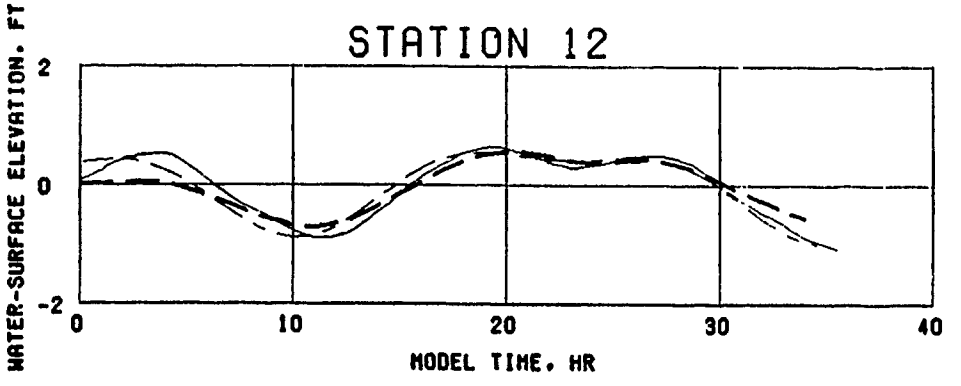

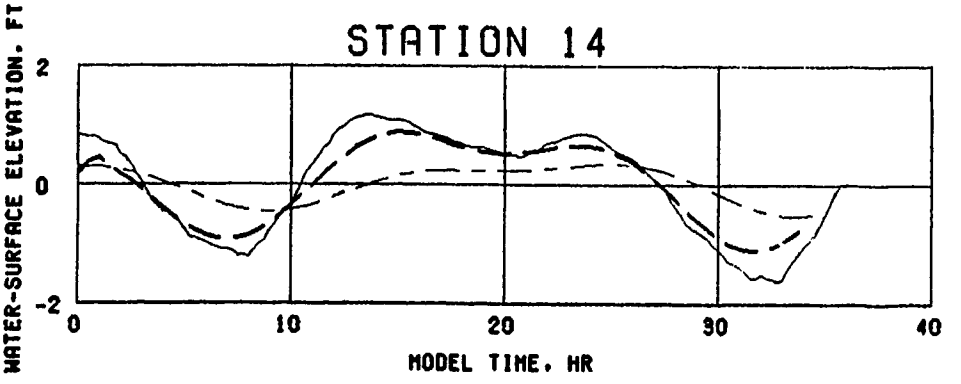

LEGEND

— — MODEL

——— PROTOTYPE

— — — SYNTHESIZED

VERIFICATION OF TIDAL HEIGHTS

MESH 2
Q = 320,000 CFS
SPRING TIDE
STATIONS 11, 12, AND 14

PLATE 22

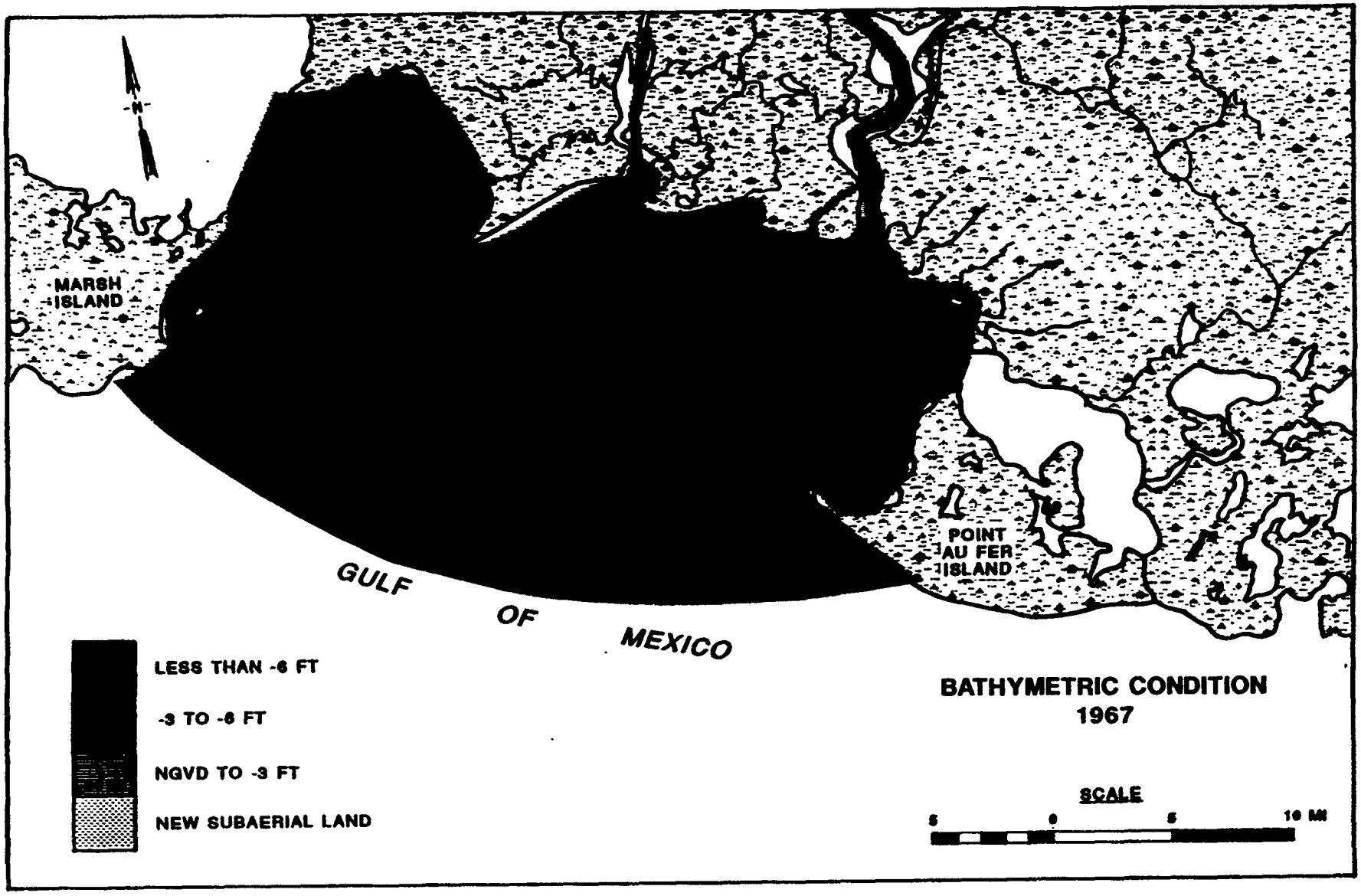
MARSH ISLAND
POINT AU FER ISLAND
GULF OF MEXICO
LESS THAN -6 FT
-3 TO -6 FT
NGVD TO -3 FT
NEW SUBAERIAL LAND
BATHYMETRIC CONDITION
1967
SCALE
5 0 5 10 MI

PLATE 23

PLATE 24

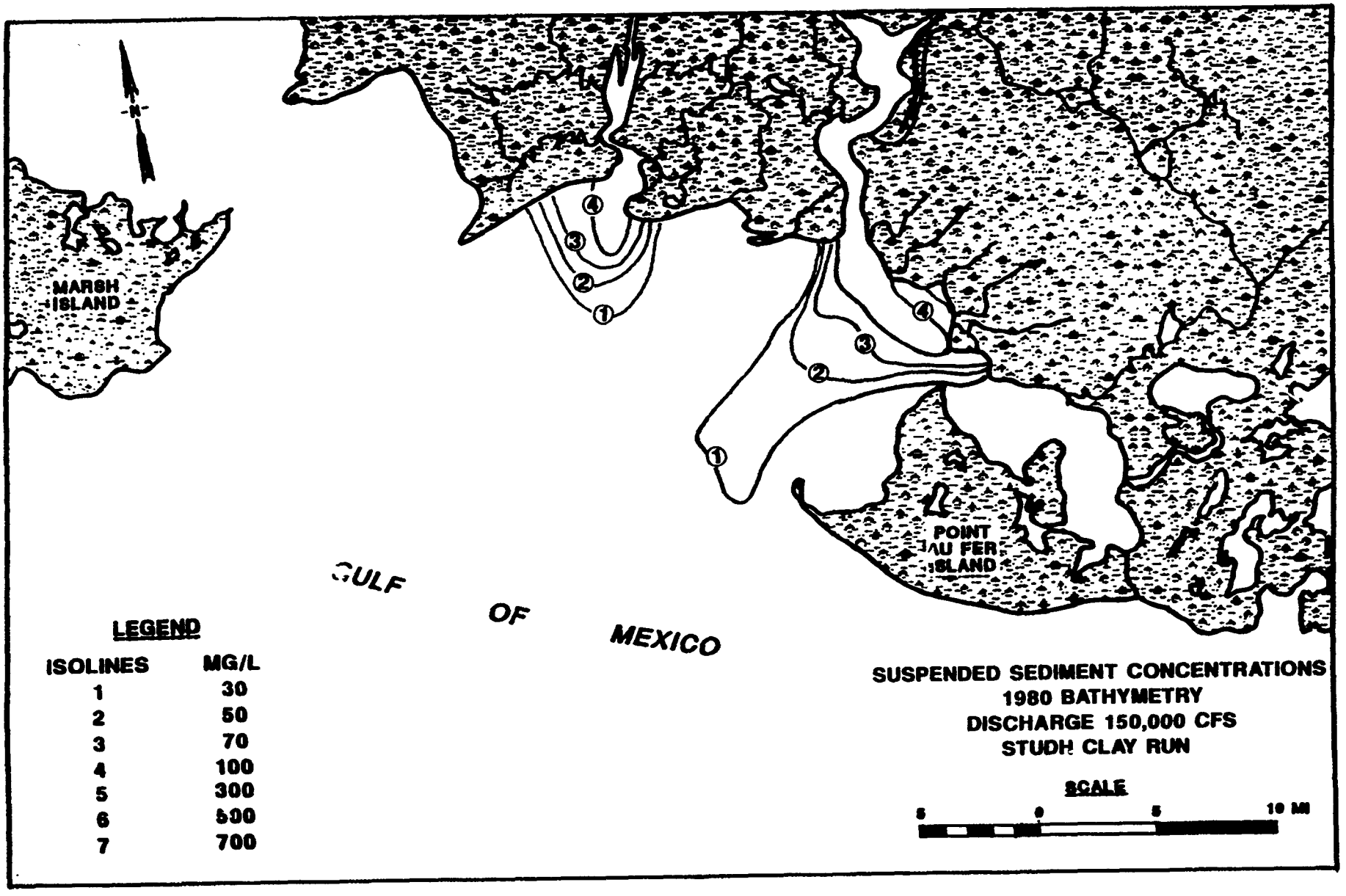
MARSH ISLAND
POINT AU FER ISLAND
GULF OF MEXICO
LEGEND
ISOLINES MG/L
1 30
2 50
3 70
4 100
5 300
6 500
7 700
SUSPENDED SEDIMENT CONCENTRATIONS
1980 BATHYMETRY
DISCHARGE 150,000 CFS
STUDH CLAY RUN
SCALE
5 0 5 10 MI

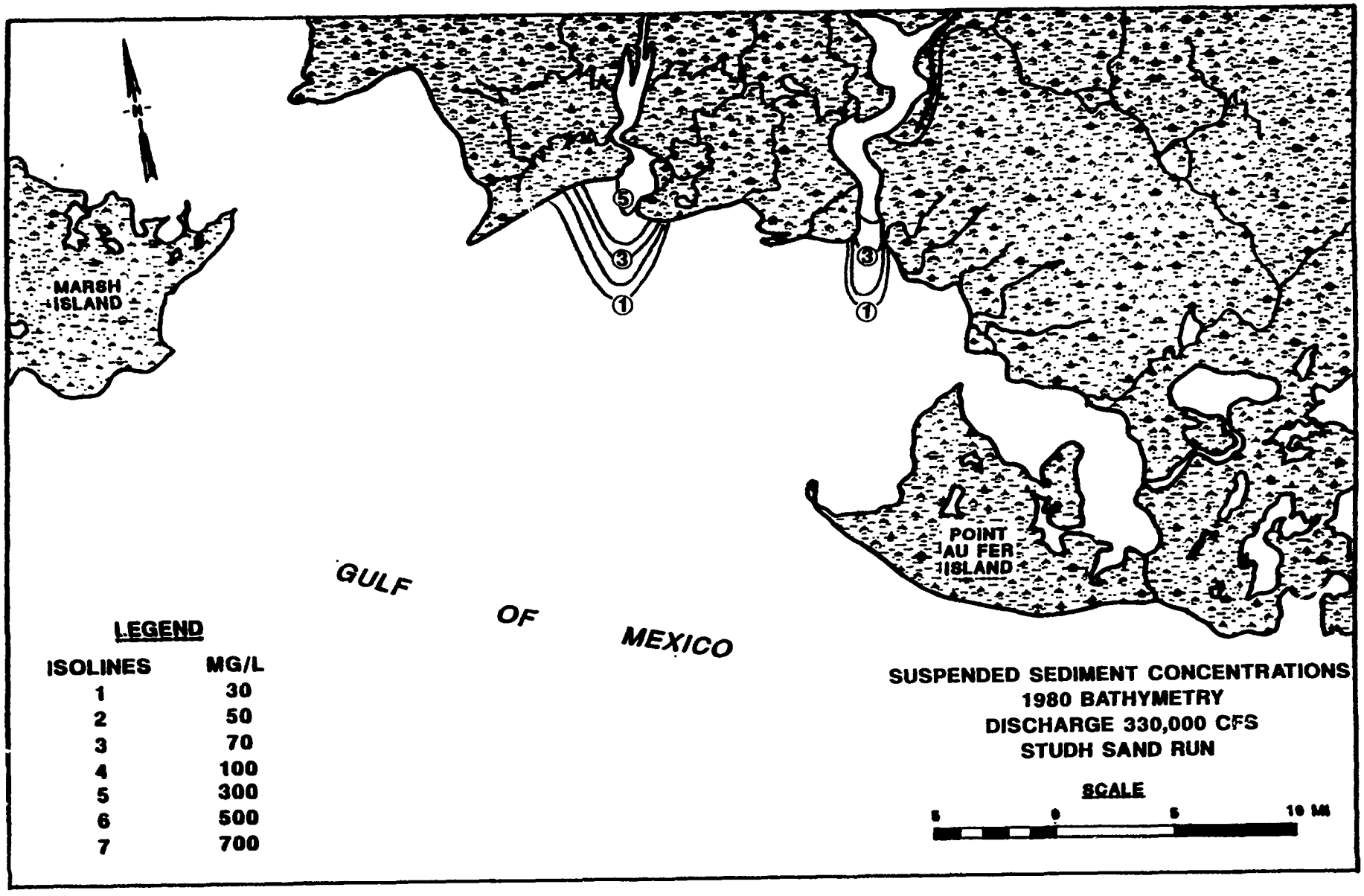

LEGEND

ISOLINES	MG/L
1	30
2	50
3	70
4	100
5	300
6	500
7	700

SUSPENDED SEDIMENT CONCENTRATIONS
1980 BATHYMETRY
DISCHARGE 330,000 CFS
STUDH SAND RUN

SCALE

5 0 5 10 MI

PLATE 25

PLATE 26

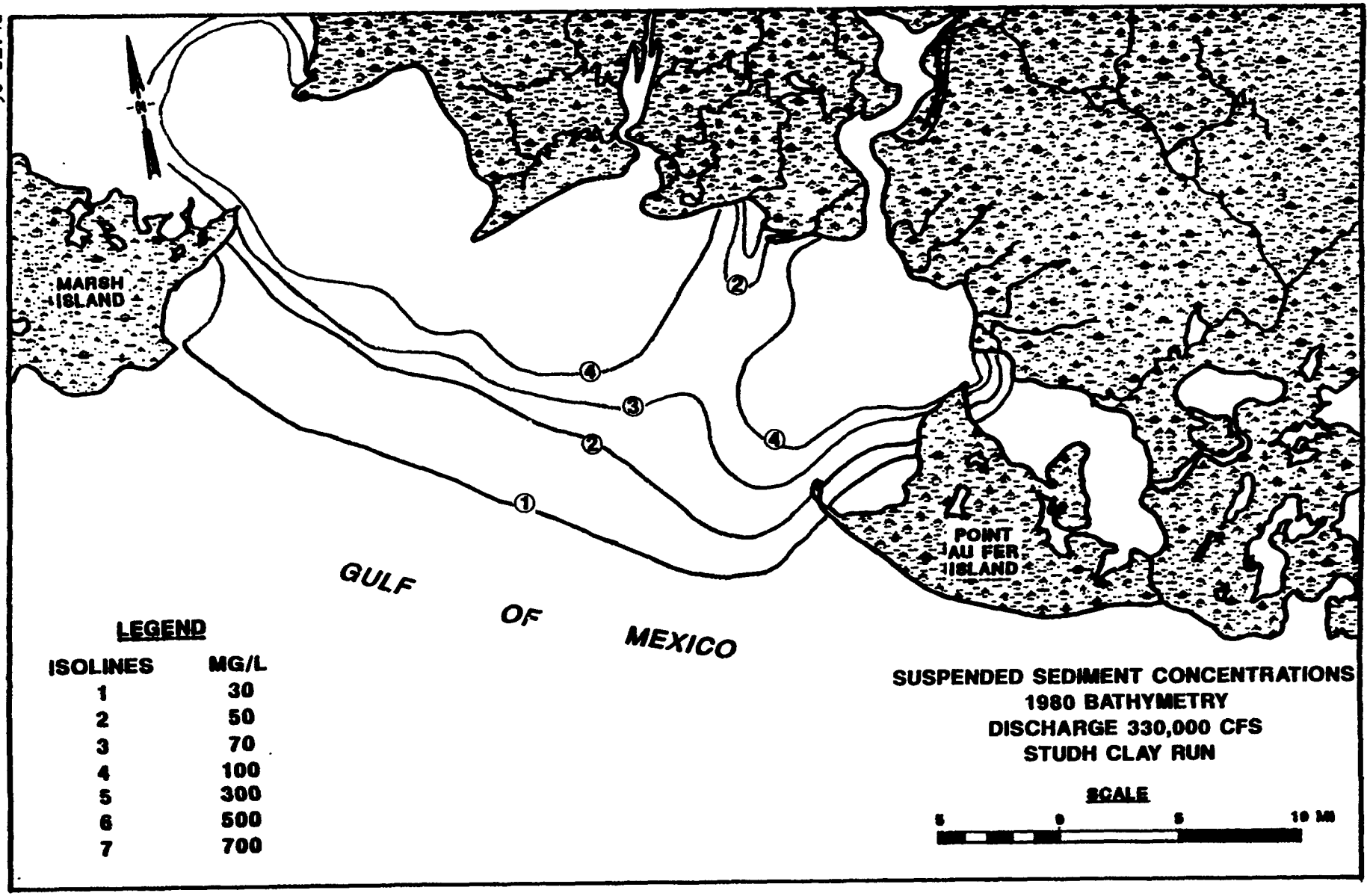
MARSH ISLAND
POINT AU FER ISLAND
GULF OF MEXICO
LEGEND
ISOLINES MG/L
1 30
2 50
3 70
4 100
5 300
6 500
7 700
SUSPENDED SEDIMENT CONCENTRATIONS
1980 BATHYMETRY
DISCHARGE 330,000 CFS
STUDH CLAY RUN
SCALE
5 0 5 10 MI

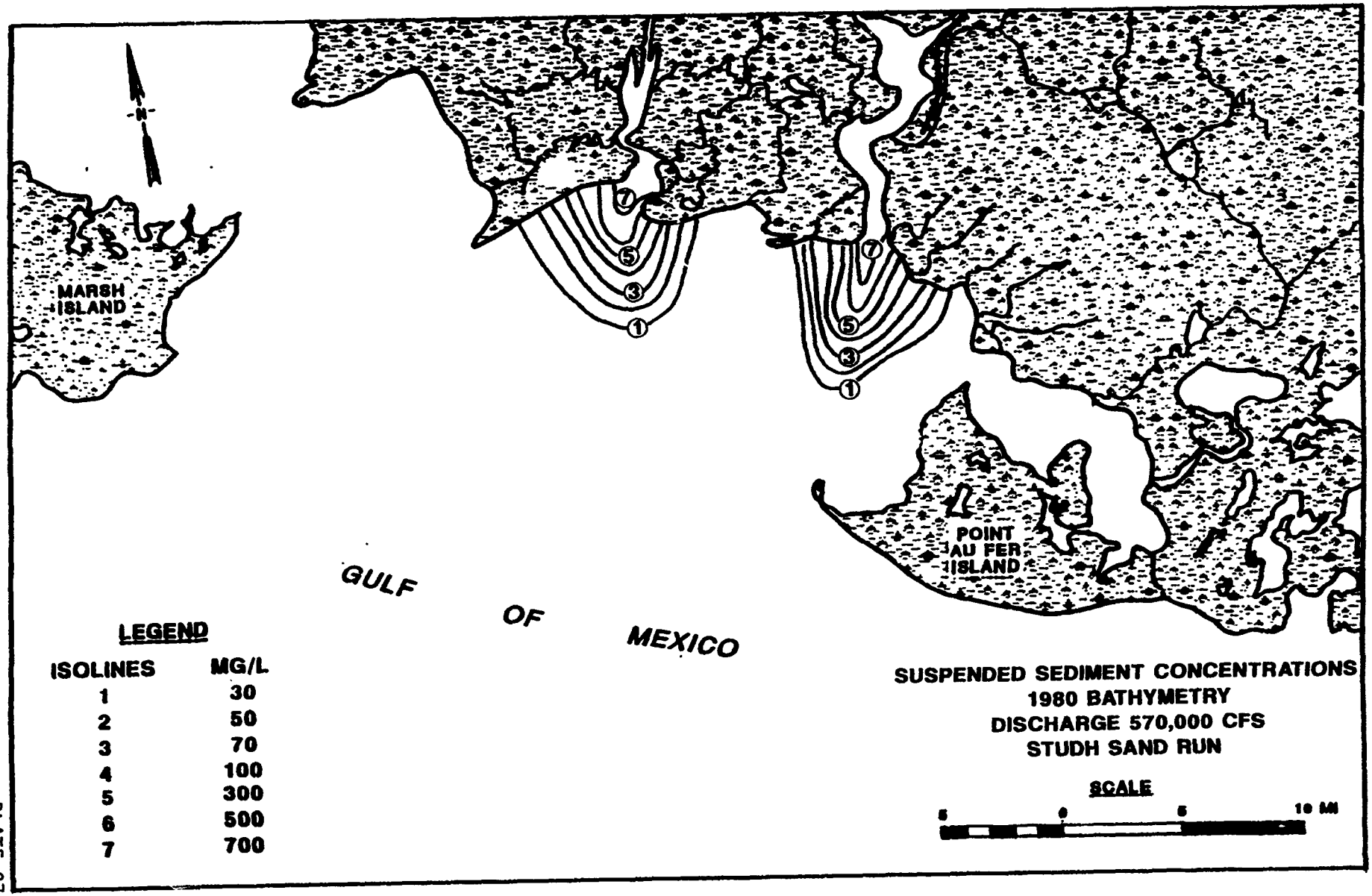
N
MARSH ISLAND
POINT AU FER ISLAND
GULF OF MEXICO
LEGEND
ISOLINES MG/L
1 30
2 50
3 70
4 100
5 300
6 500
7 700
SUSPENDED SEDIMENT CONCENTRATIONS
1980 BATHYMETRY
DISCHARGE 570,000 CFS
STUDH SAND RUN
SCALE
5 0 5 10 MI

PLATE 27

PLATE 28

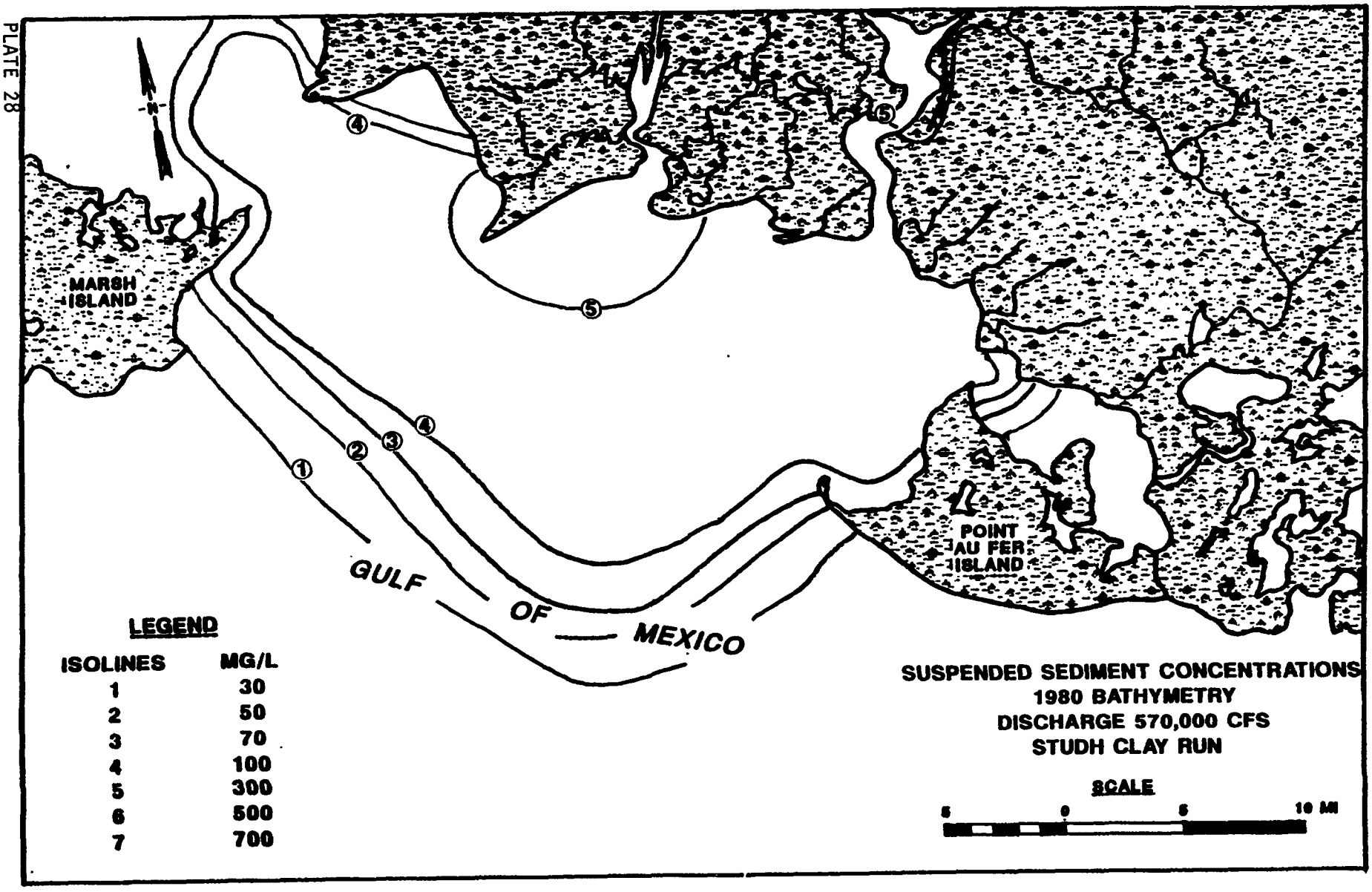
MARSH ISLAND
POINT AU FER ISLAND
GULF OF MEXICO
1
2
3
4
5
LEGEND
ISOLINES MG/L
1 30
2 50
3 70
4 100
5 300
6 500
7 700
SUSPENDED SEDIMENT CONCENTRATIONS
1980 BATHYMETRY
DISCHARGE 570,000 CFS
STUDH CLAY RUN
SCALE
5 0 5 10 MI

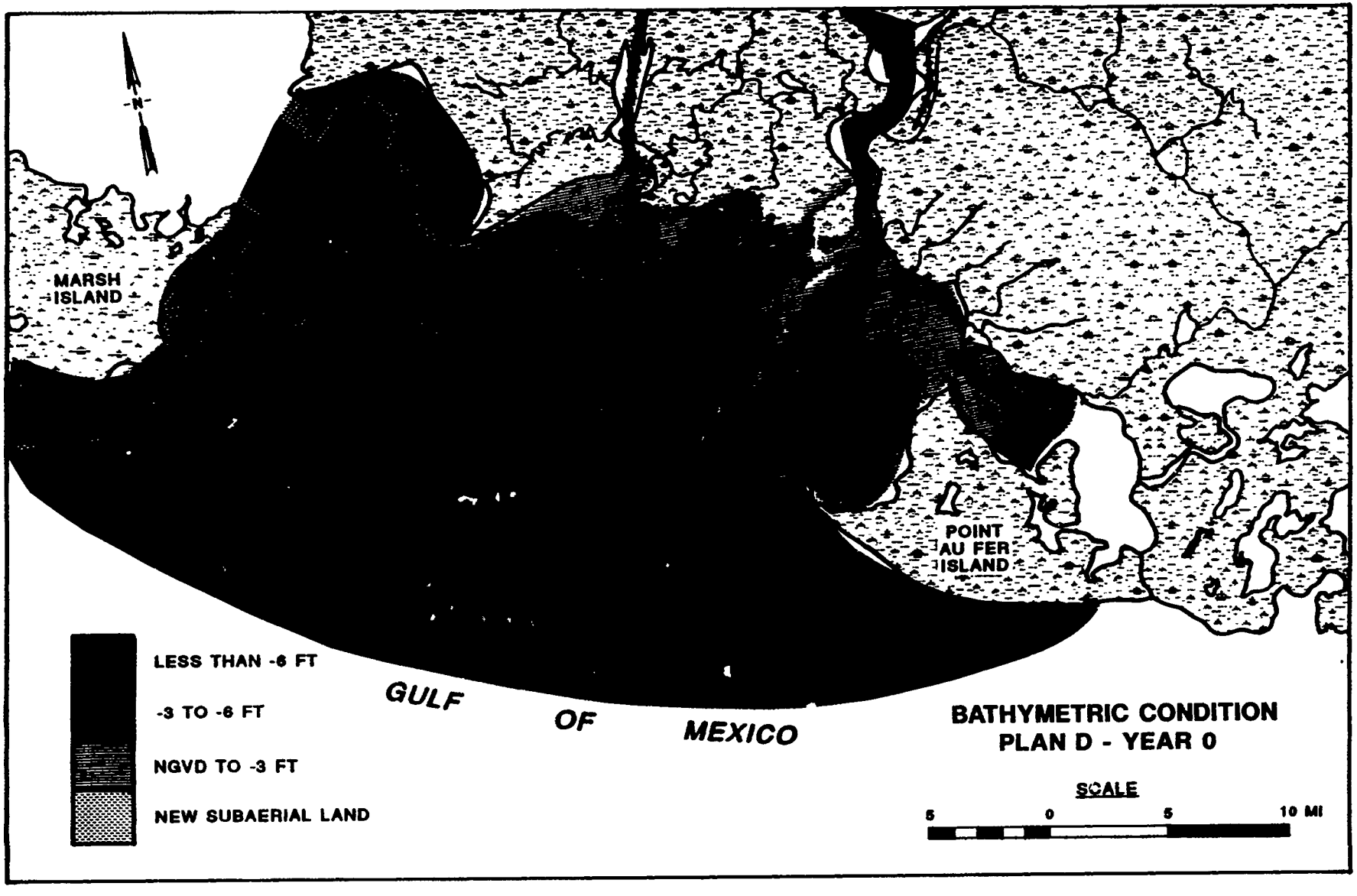
N
MARSH ISLAND
POINT AU FER ISLAND
GULF OF MEXICO
LESS THAN -6 FT
-3 TO -6 FT
NGVD TO -3 FT
NEW SUBAERIAL LAND
BATHYMETRIC CONDITION
PLAN D - YEAR 0
SCALE
5 0 5 10 MI

PLATE 29

PLATE 30

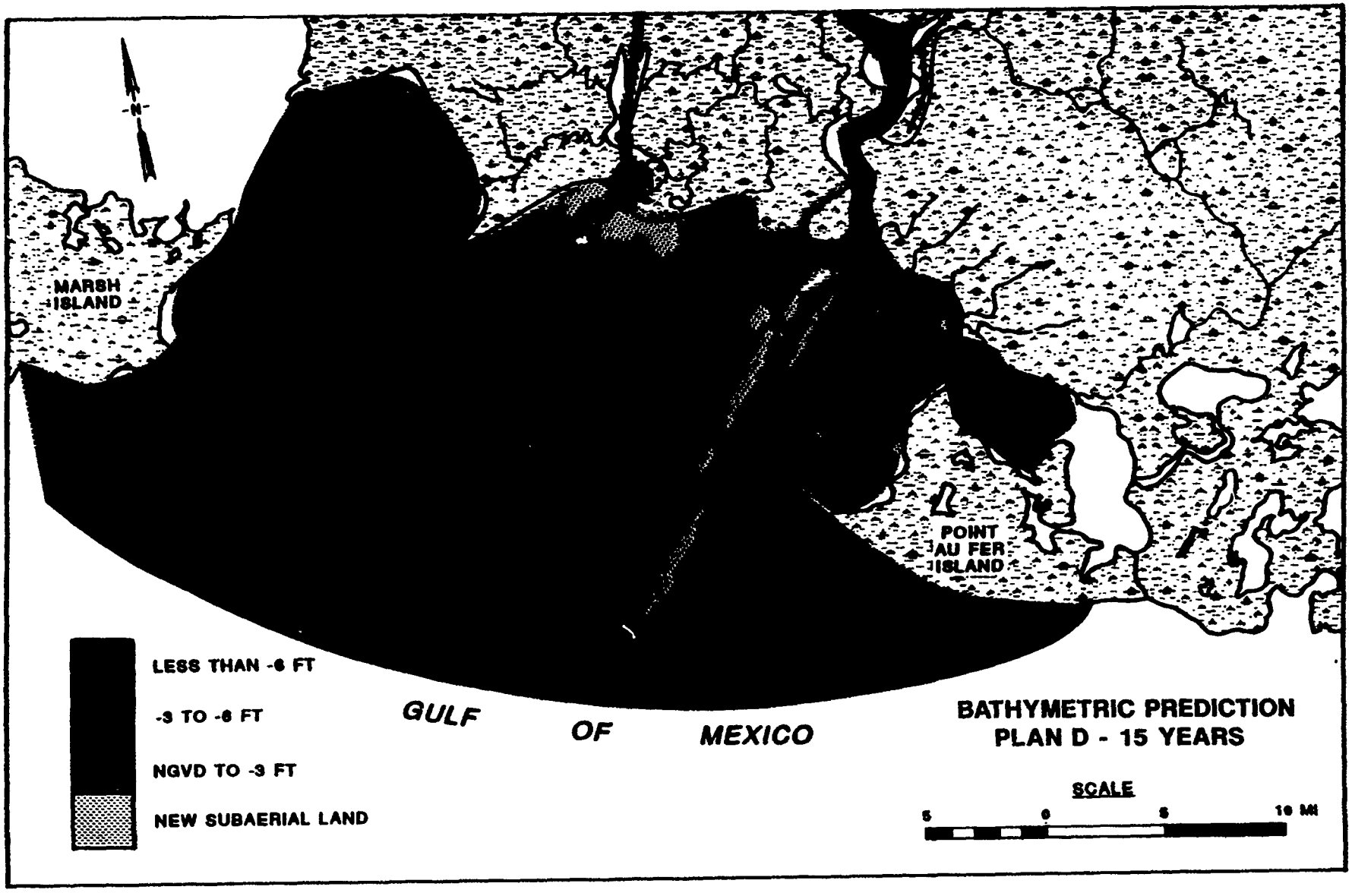
MARSH ISLAND
POINT AU FER ISLAND
LESS THAN -6 FT
-3 TO -6 FT
NGVD TO -3 FT
NEW SUBAERIAL LAND
GULF OF MEXICO
BATHYMETRIC PREDICTION
PLAN D - 15 YEARS
SCALE
5 0 5 10 MI

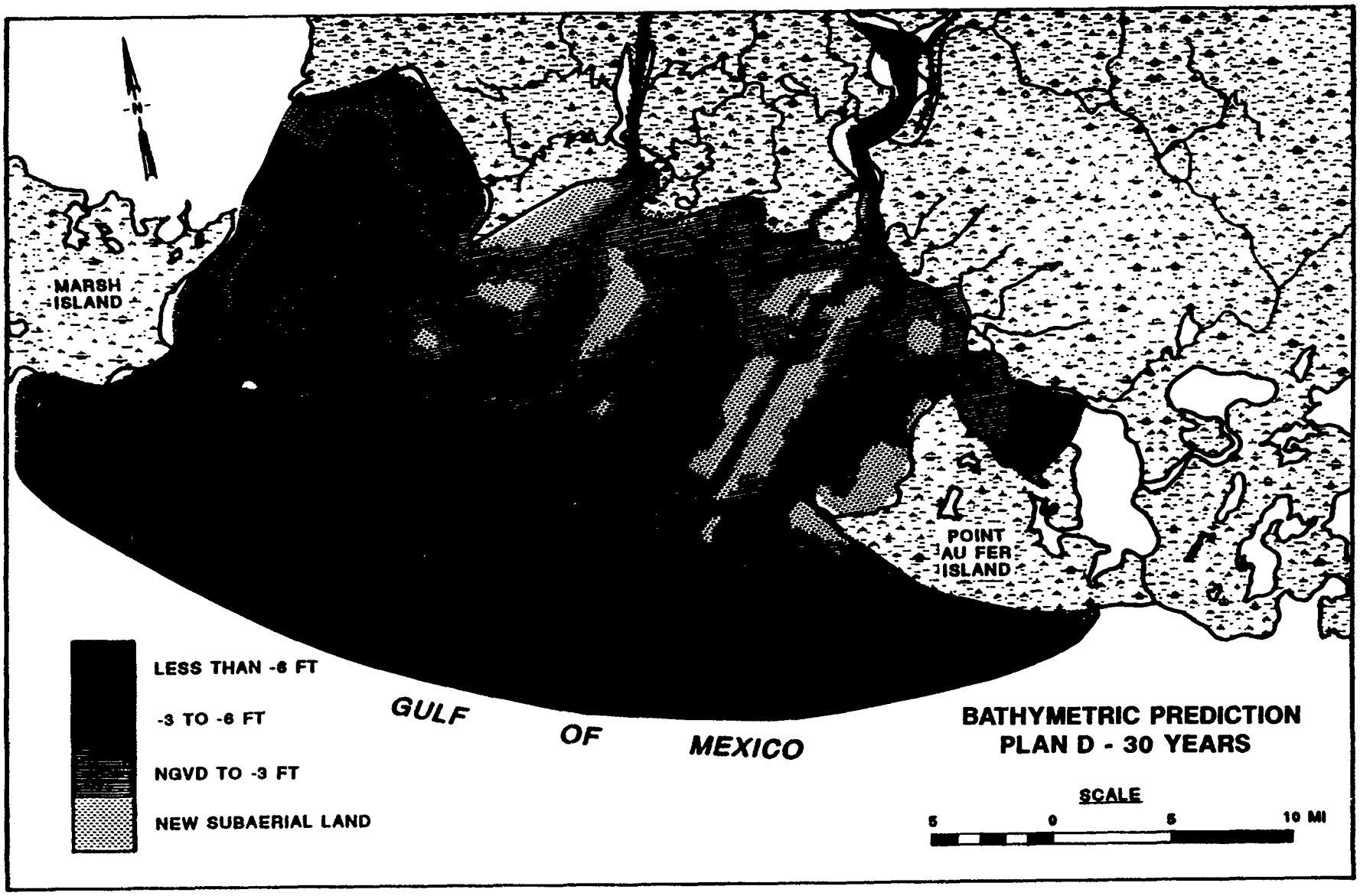
N
MARSH ISLAND
POINT AU FER ISLAND
GULF OF MEXICO
LESS THAN -6 FT
-3 TO -6 FT
NGVD TO -3 FT
NEW SUBAERIAL LAND
BATHYMETRIC PREDICTION
PLAN D - 30 YEARS
SCALE
5 0 5 10 MI

PLATE 31

PLATE 32

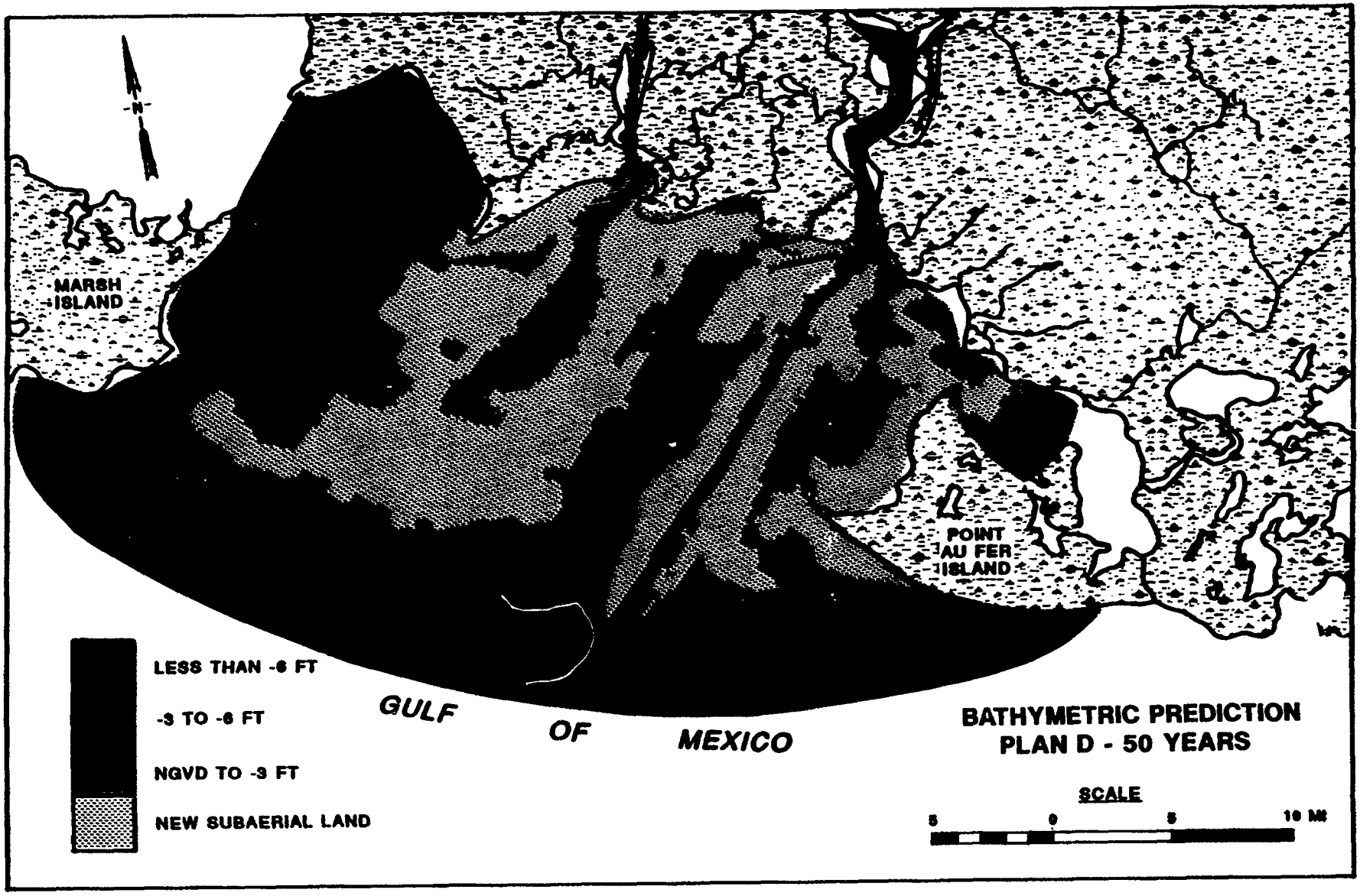
N
MARSH ISLAND
POINT AU FER ISLAND
GULF OF MEXICO
LESS THAN -6 FT
-3 TO -6 FT
NGVD TO -3 FT
NEW SUBAERIAL LAND
BATHYMETRIC PREDICTION
PLAN D - 50 YEARS
SCALE
5 0 5 10 MI

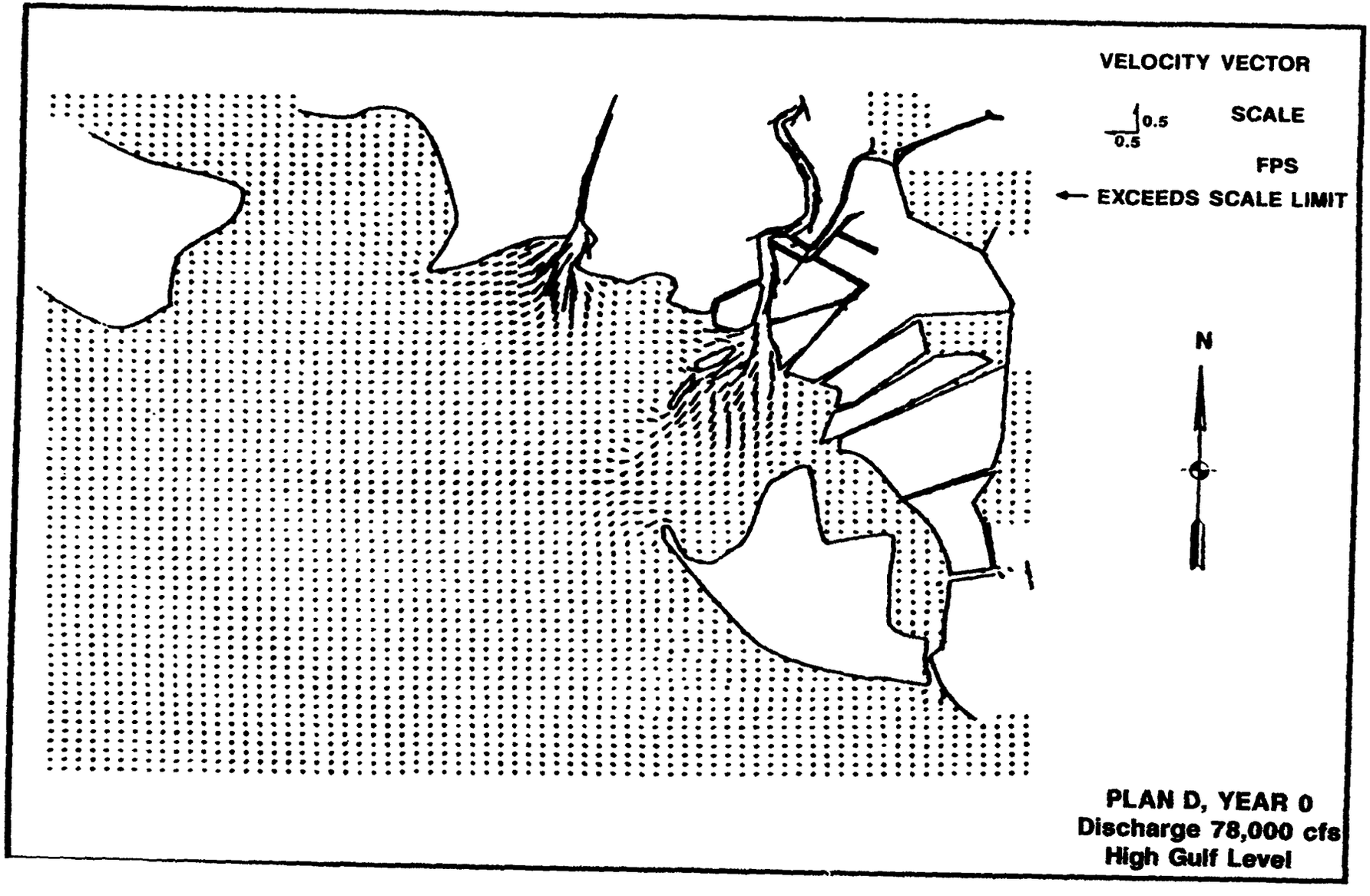
VELOCITY VECTOR
0.5
0.5
SCALE
FPS
EXCEEDS SCALE LIMIT
N
PLAN D, YEAR 0
Discharge 78,000 cfs
High Gulf Level

PLATE 33

PLATE 34

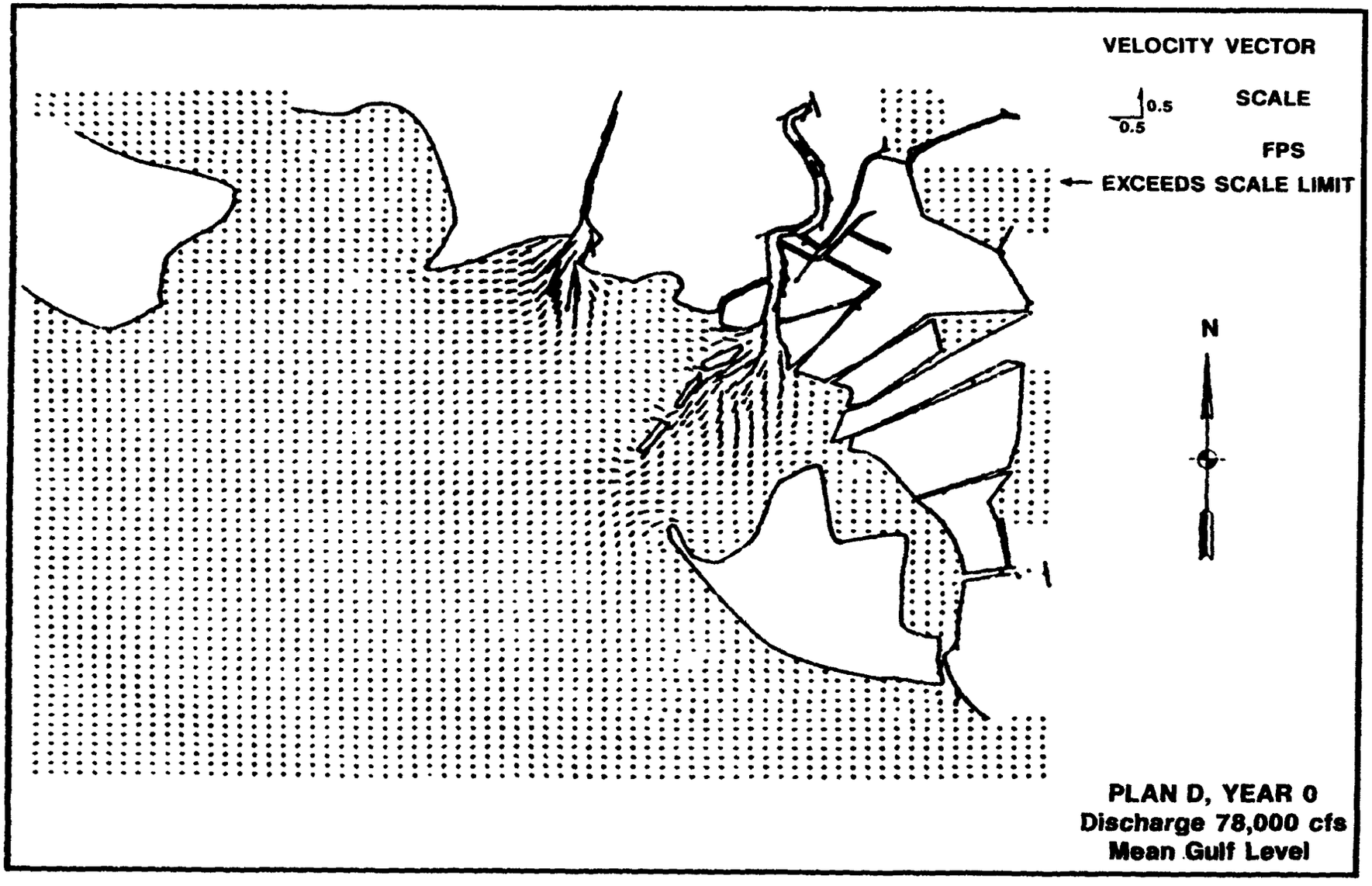
VELOCITY VECTOR
0.5
0.5
SCALE
FPS
EXCEEDS SCALE LIMIT
N
PLAN D, YEAR 0
Discharge 78,000 cfs
Mean Gulf Level

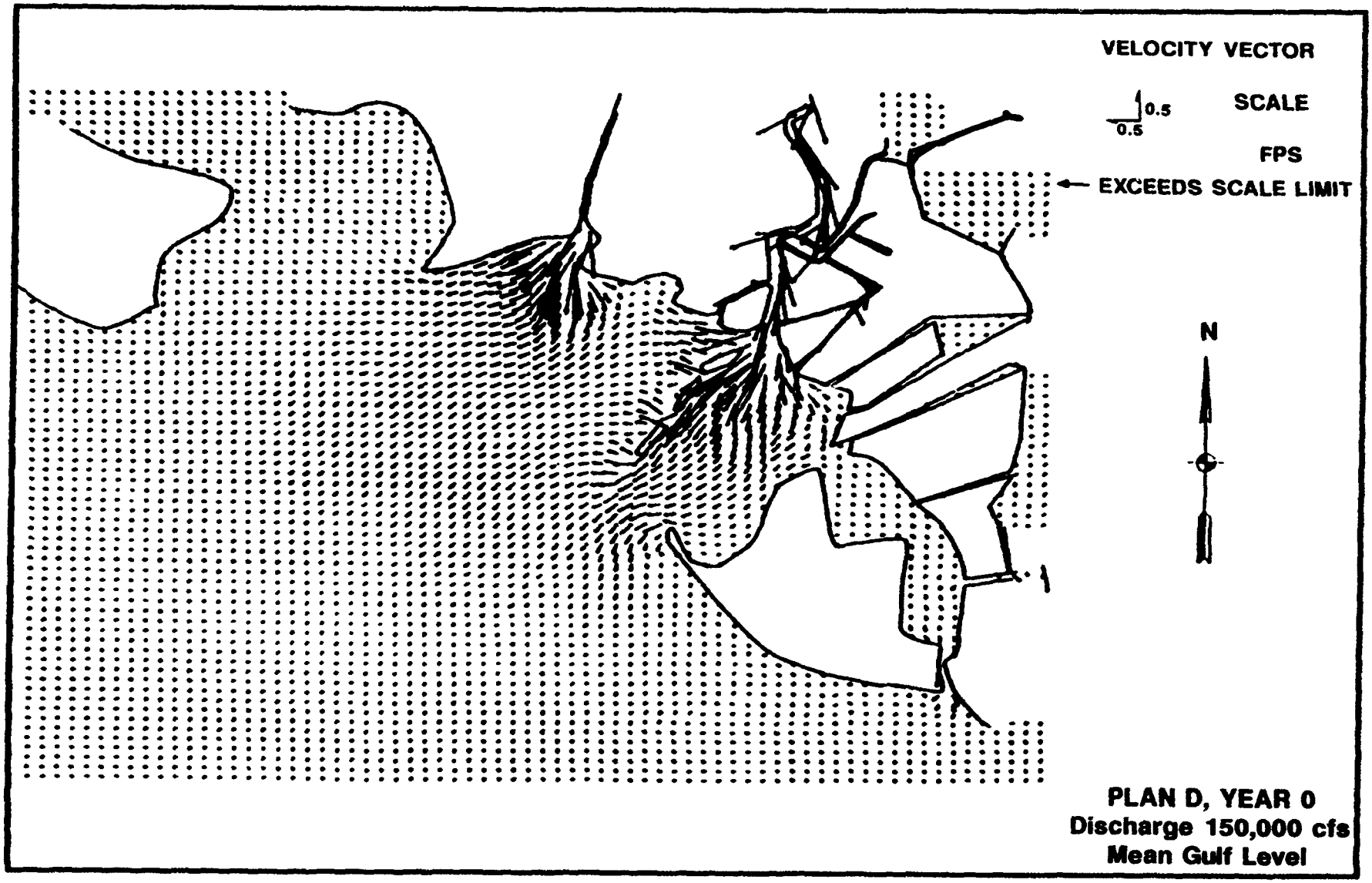
VELOCITY VECTOR
0.5
0.5
SCALE
FPS
EXCEEDS SCALE LIMIT
N
PLAN D, YEAR 0
Discharge 150,000 cfs
Mean Gulf Level

PLATE 35

PLATE 36

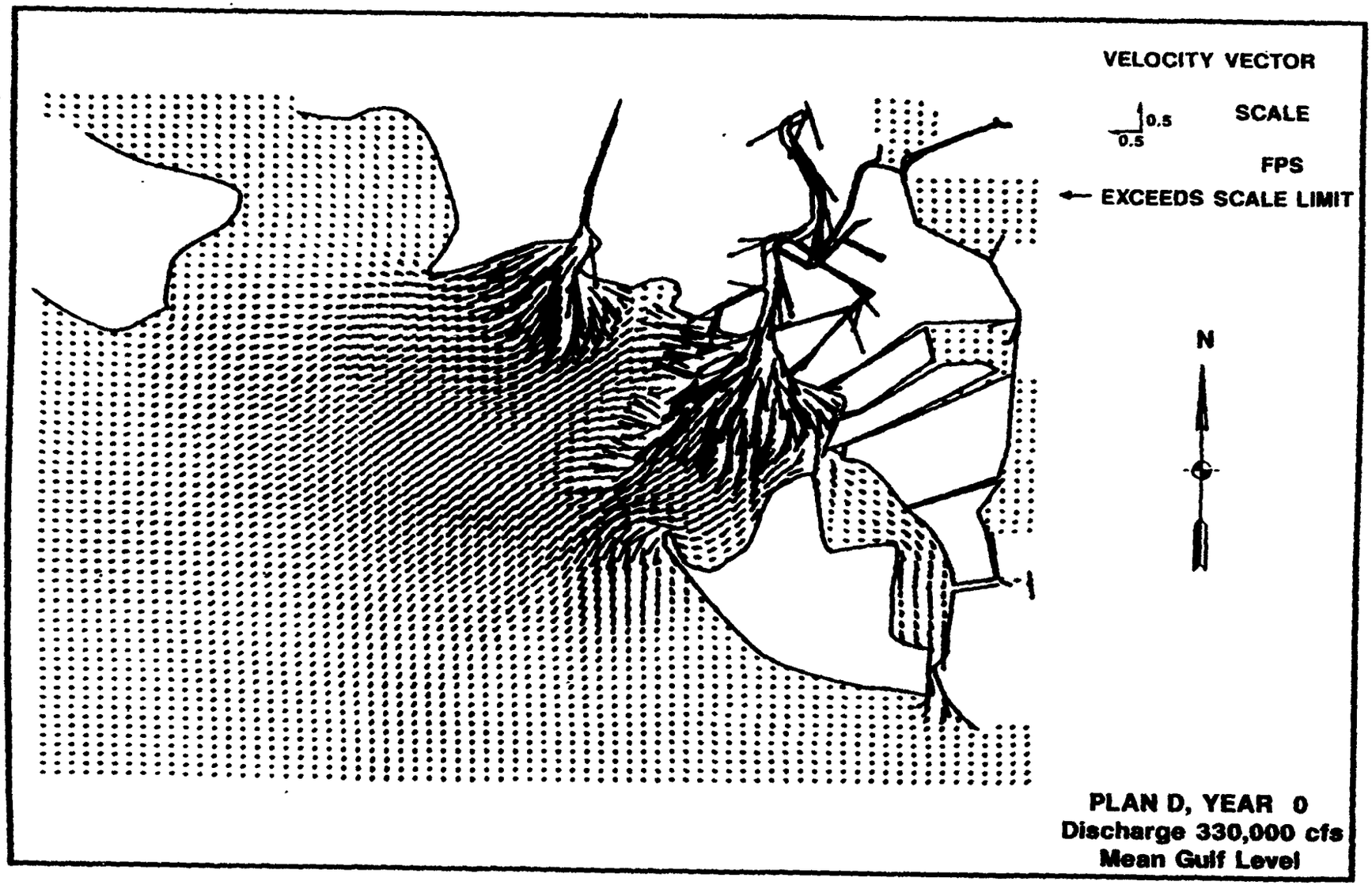
VELOCITY VECTOR
0.5
0.5
SCALE
FPS
EXCEEDS SCALE LIMIT
N
PLAN D, YEAR 0
Discharge 330,000 cfs
Mean Gulf Level

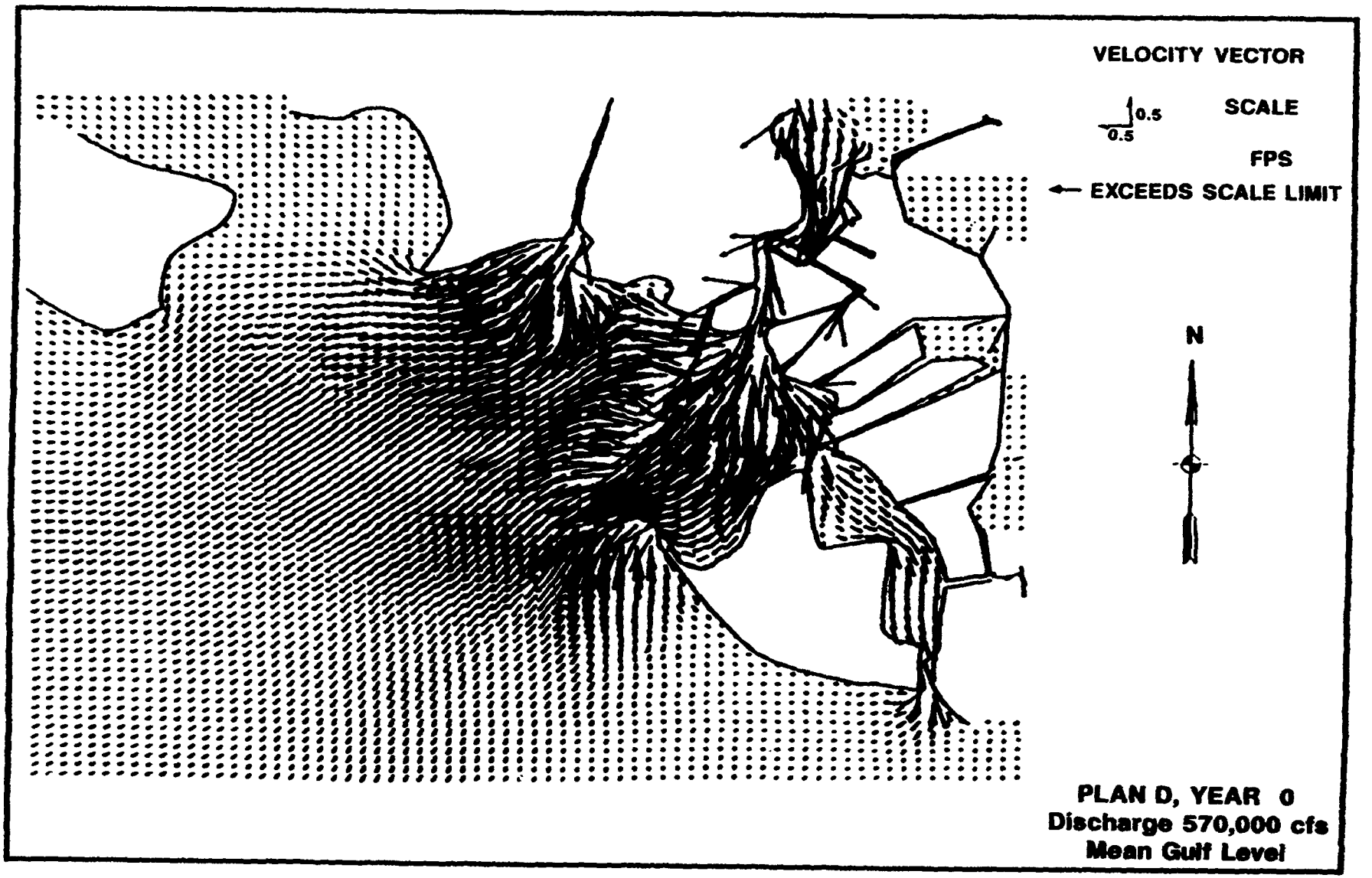
VELOCITY VECTOR
0.5
0.5
SCALE
FPS
EXCEEDS SCALE LIMIT
N
PLAN D, YEAR 0
Discharge 570,000 cfs
Mean Gulf Level

PLATE 37

PLATE 38

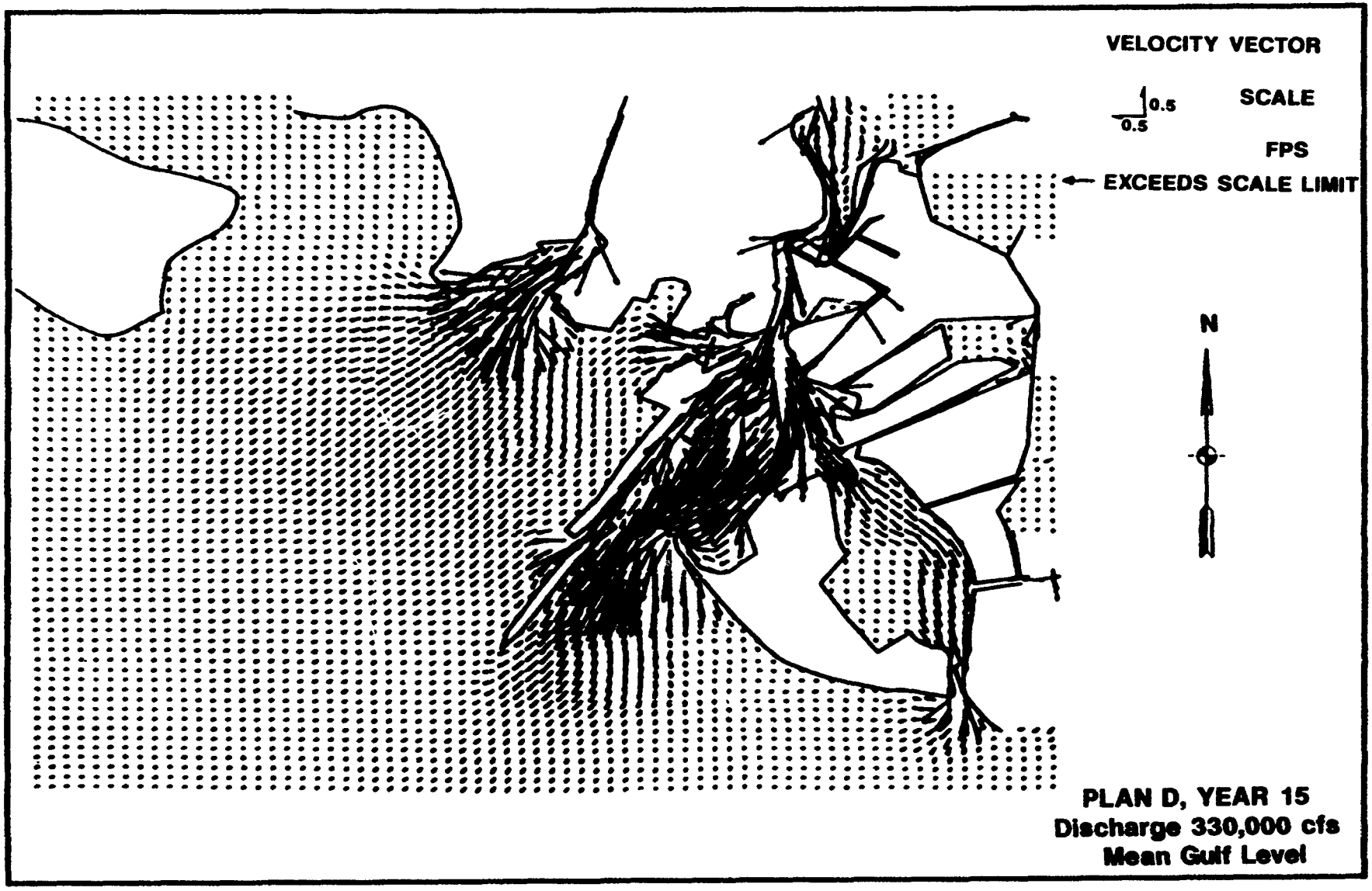
VELOCITY VECTOR
0.5
0.5
SCALE
FPS
EXCEEDS SCALE LIMIT
N
PLAN D, YEAR 15
Discharge 330,000 cfs
Mean Gulf Level

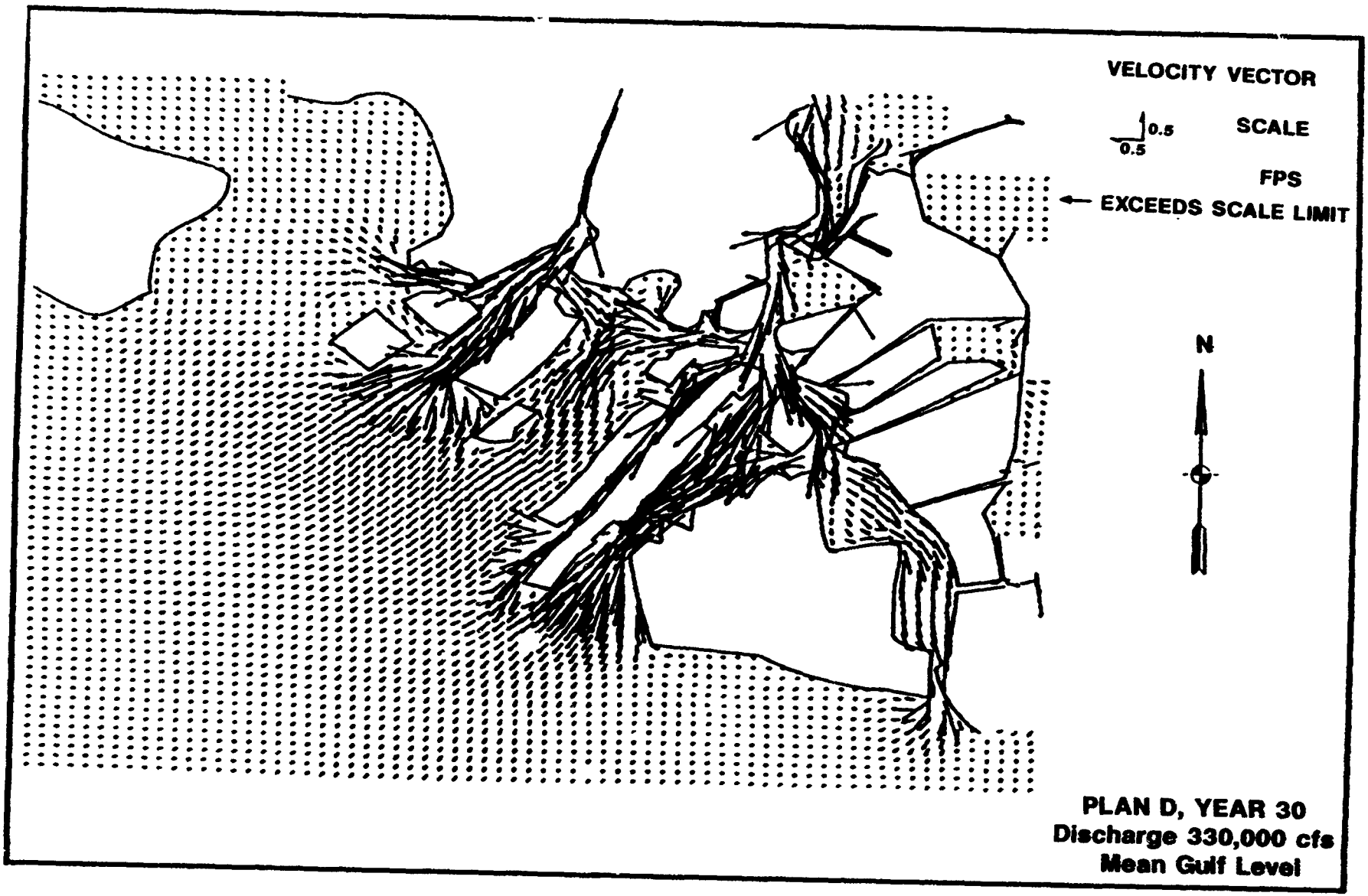
VELOCITY VECTOR
0.5
0.5
SCALE
FPS
EXCEEDS SCALE LIMIT
N
PLAN D, YEAR 30
Discharge 330,000 cfs
Mean Gulf Level

PLATE 39

PLATE 40

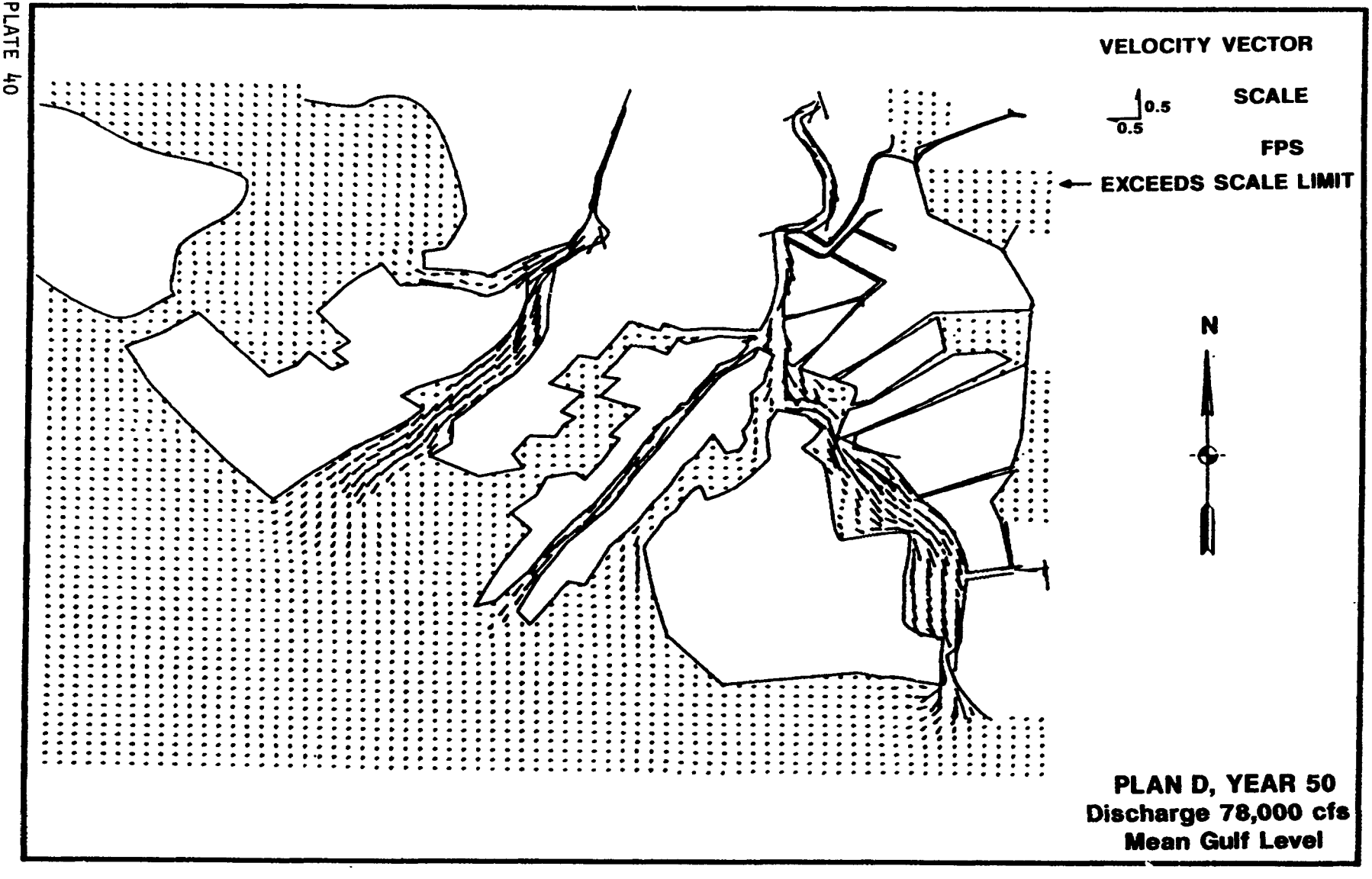
VELOCITY VECTOR
SCALE
0.5
0.5
FPS
EXCEEDS SCALE LIMIT
N
PLAN D, YEAR 50
Discharge 78,000 cfs
Mean Gulf Level

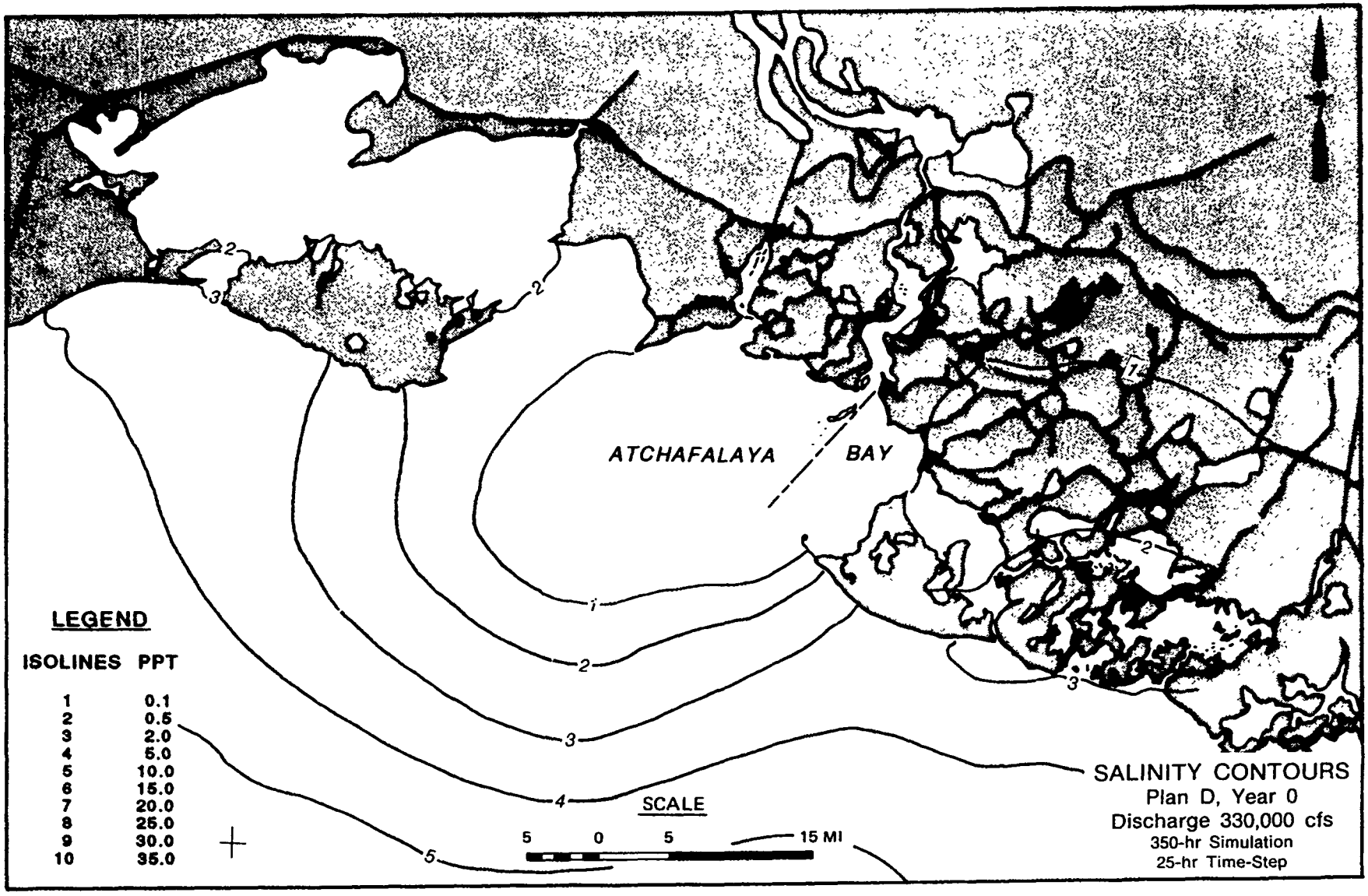
ATCHAFALAYA BAY
LEGEND
ISOLINES PPT
1 0.1
2 0.5
3 2.0
4 5.0
5 10.0
6 15.0
7 20.0
8 25.0
9 30.0
10 35.0
SCALE
5 0 5 15 MI
SALINITY CONTOURS
Plan D, Year 0
Discharge 330,000 cfs
350-hr Simulation
25-hr Time-Step

PLATE 41

PLATE 42

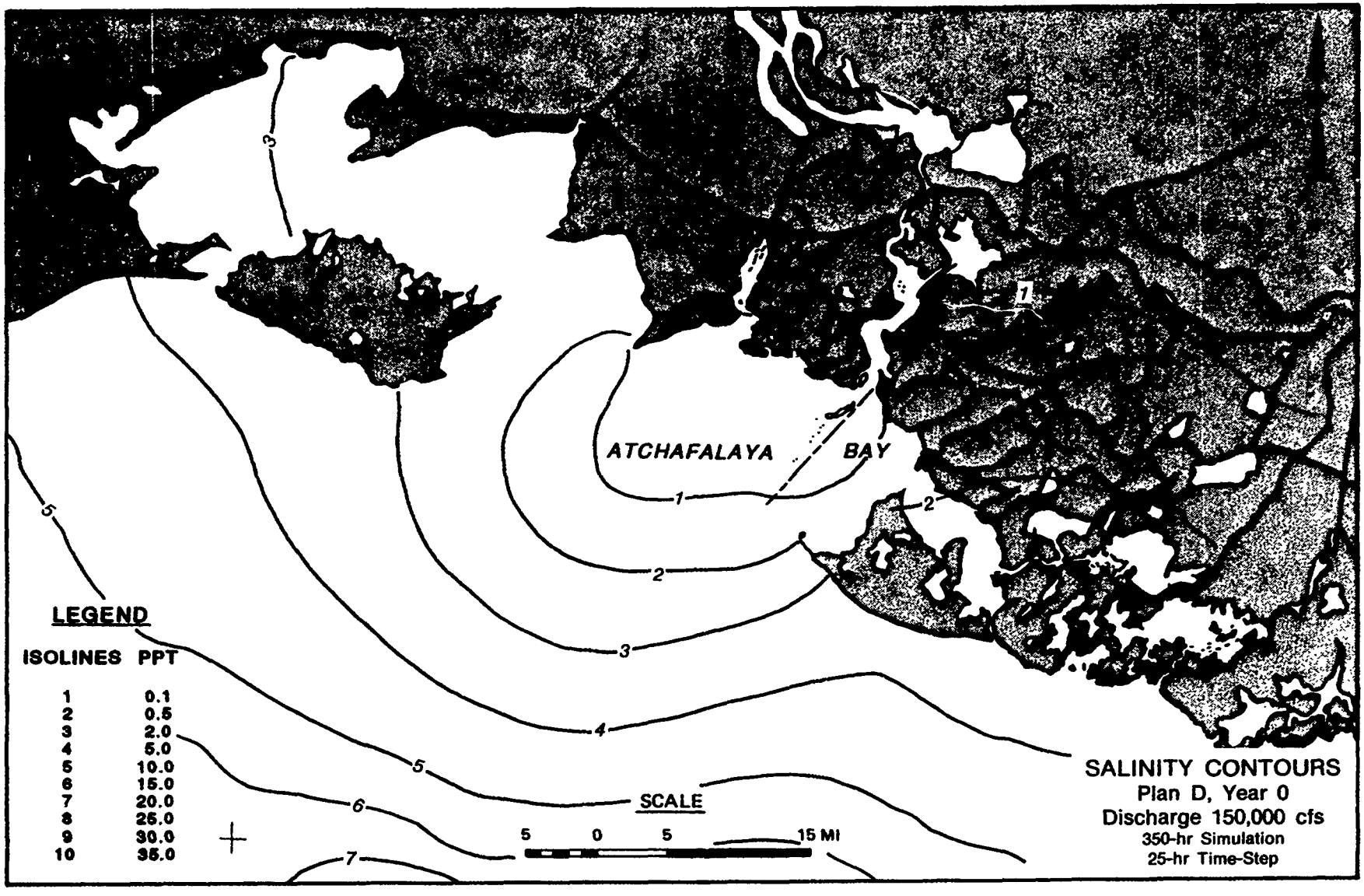
ATCHAFALAYA BAY
1
2
3
4
5
6
7
LEGEND
ISOLINES PPT
1 0.1
2 0.5
3 2.0
4 5.0
5 10.0
6 15.0
7 20.0
8 25.0
9 30.0
10 35.0
SCALE
5 0 5 15 MI
SALINITY CONTOURS
Plan D, Year 0
Discharge 150,000 cfs
350-hr Simulation
25-hr Time-Step

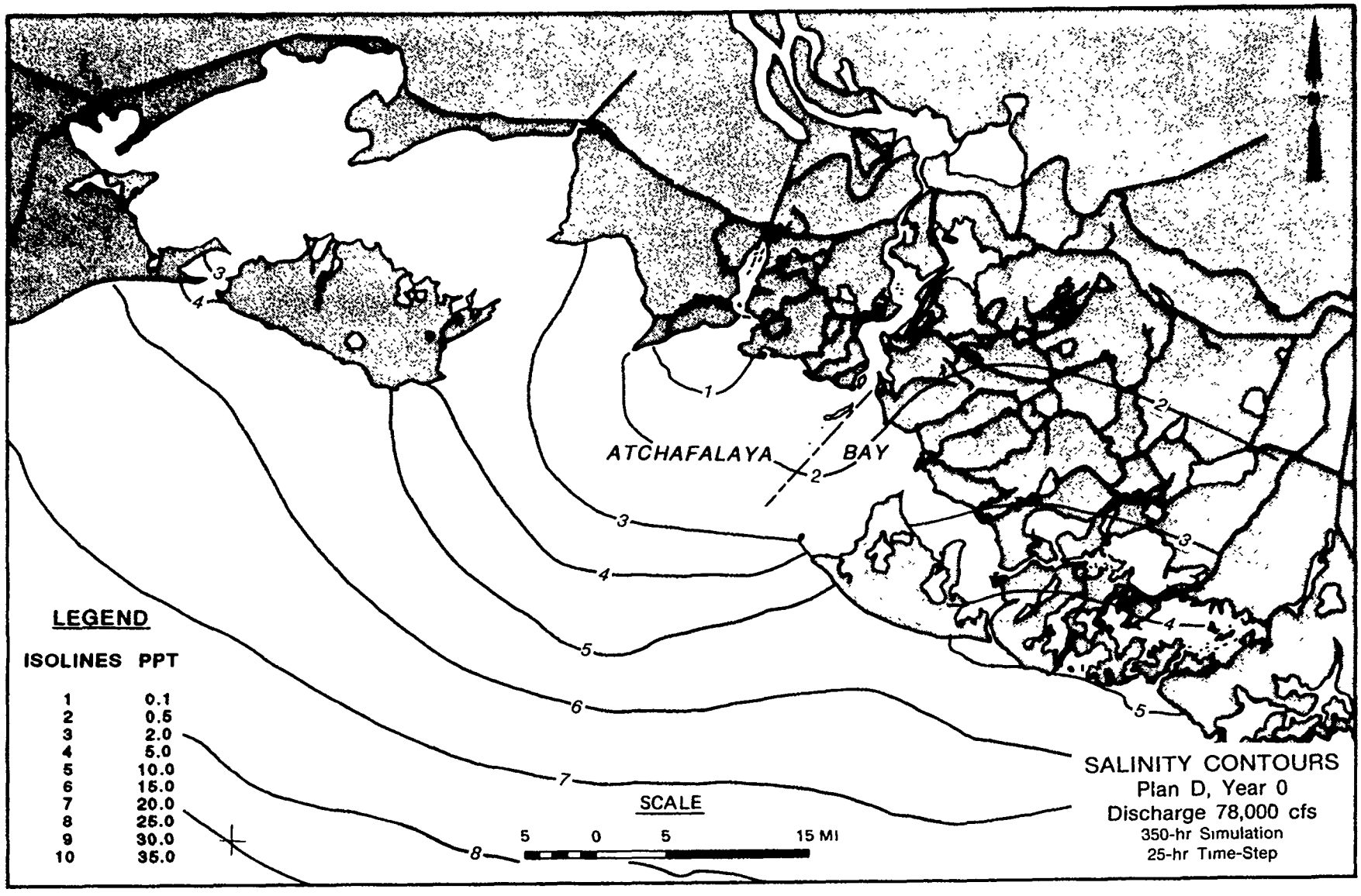
ATCHAFALAYA
BAY
LEGEND
ISOLINES PPT
1 0.1
2 0.5
3 2.0
4 5.0
5 10.0
6 15.0
7 20.0
8 25.0
9 30.0
10 35.0
SCALE
5 0 5 15 MI
SALINITY CONTOURS
Plan D, Year 0
Discharge 78,000 cfs
350-hr Simulation
25-hr Time-Step

PLATE 43

PLATE 44

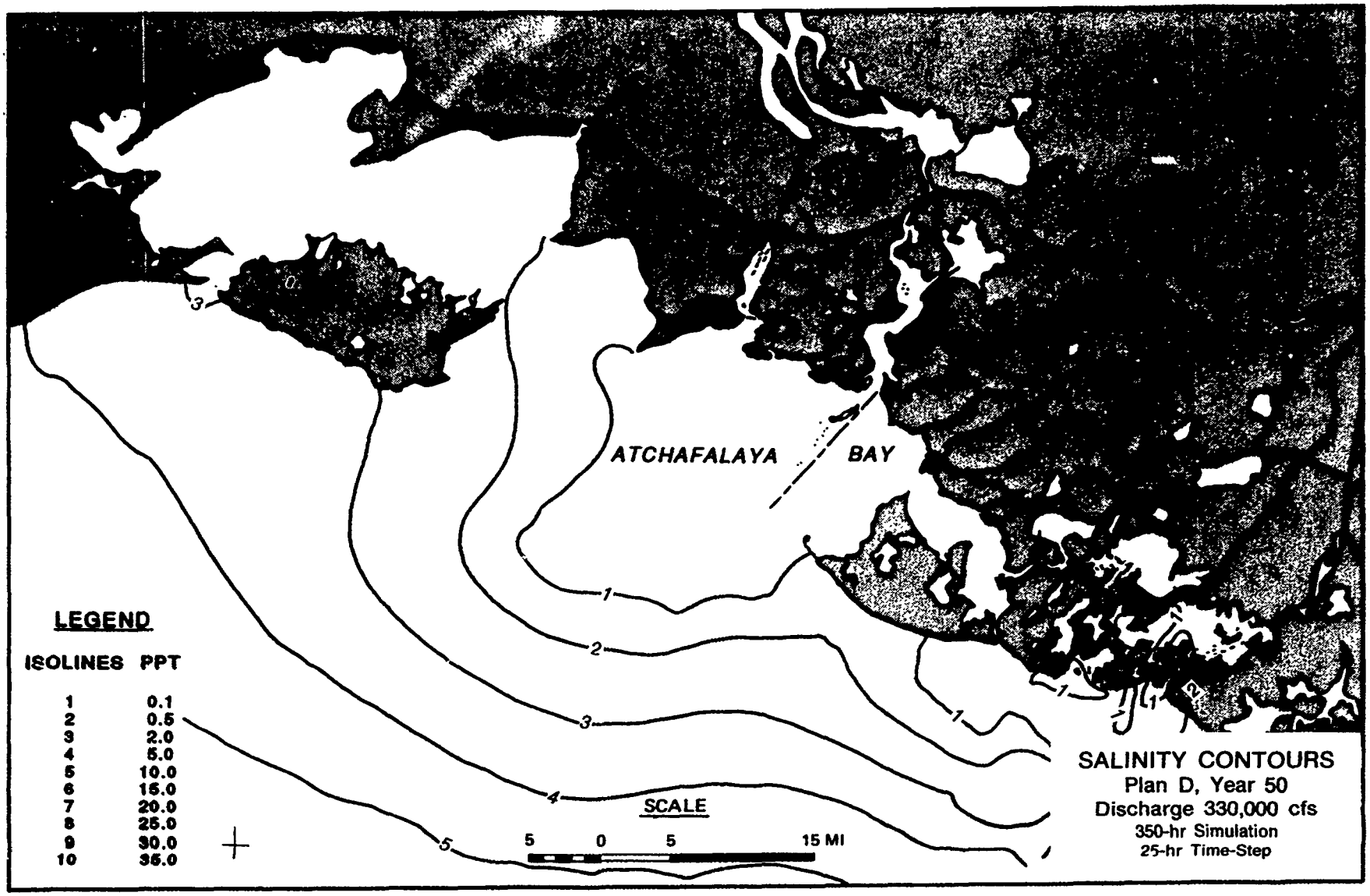
ATCHAFALAYA BAY
LEGEND
ISOLINES PPT
1 0.1
2 0.5
3 2.0
4 5.0
5 10.0
6 15.0
7 20.0
8 25.0
9 30.0
10 35.0
SCALE
5 0 5 15 MI
SALINITY CONTOURS
Plan D, Year 50
Discharge 330,000 cfs
350-hr Simulation
25-hr Time-Step

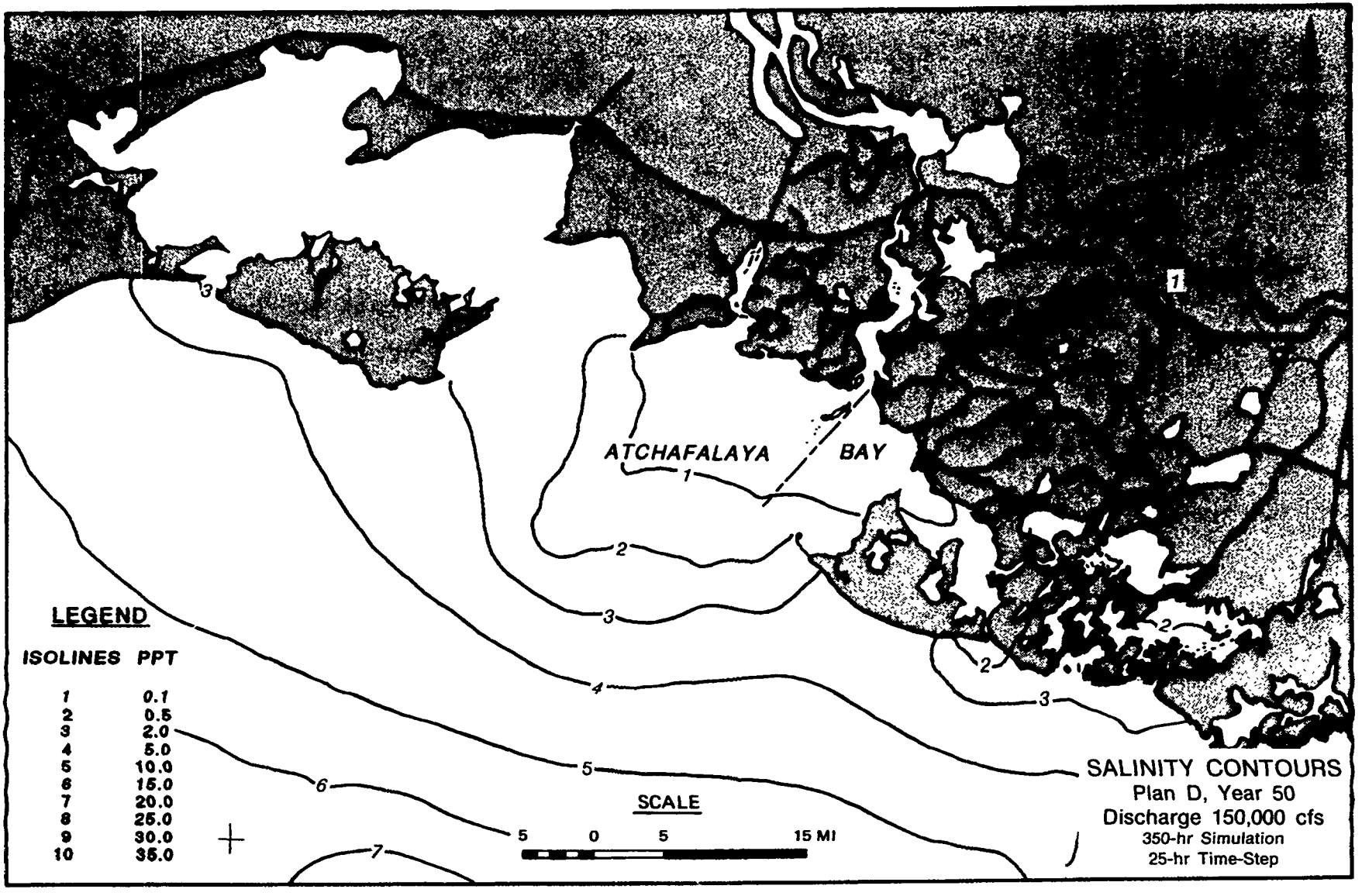
ATCHAFALAYA BAY
LEGEND
ISOLINES PPT
1 0.1
2 0.5
3 2.0
4 5.0
5 10.0
6 15.0
7 20.0
8 25.0
9 30.0
10 35.0
SCALE
5 0 5 15 MI
SALINITY CONTOURS
Plan D, Year 50
Discharge 150,000 cfs
350-hr Simulation
25-hr Time-Step

PLATE 45

PLATE 46

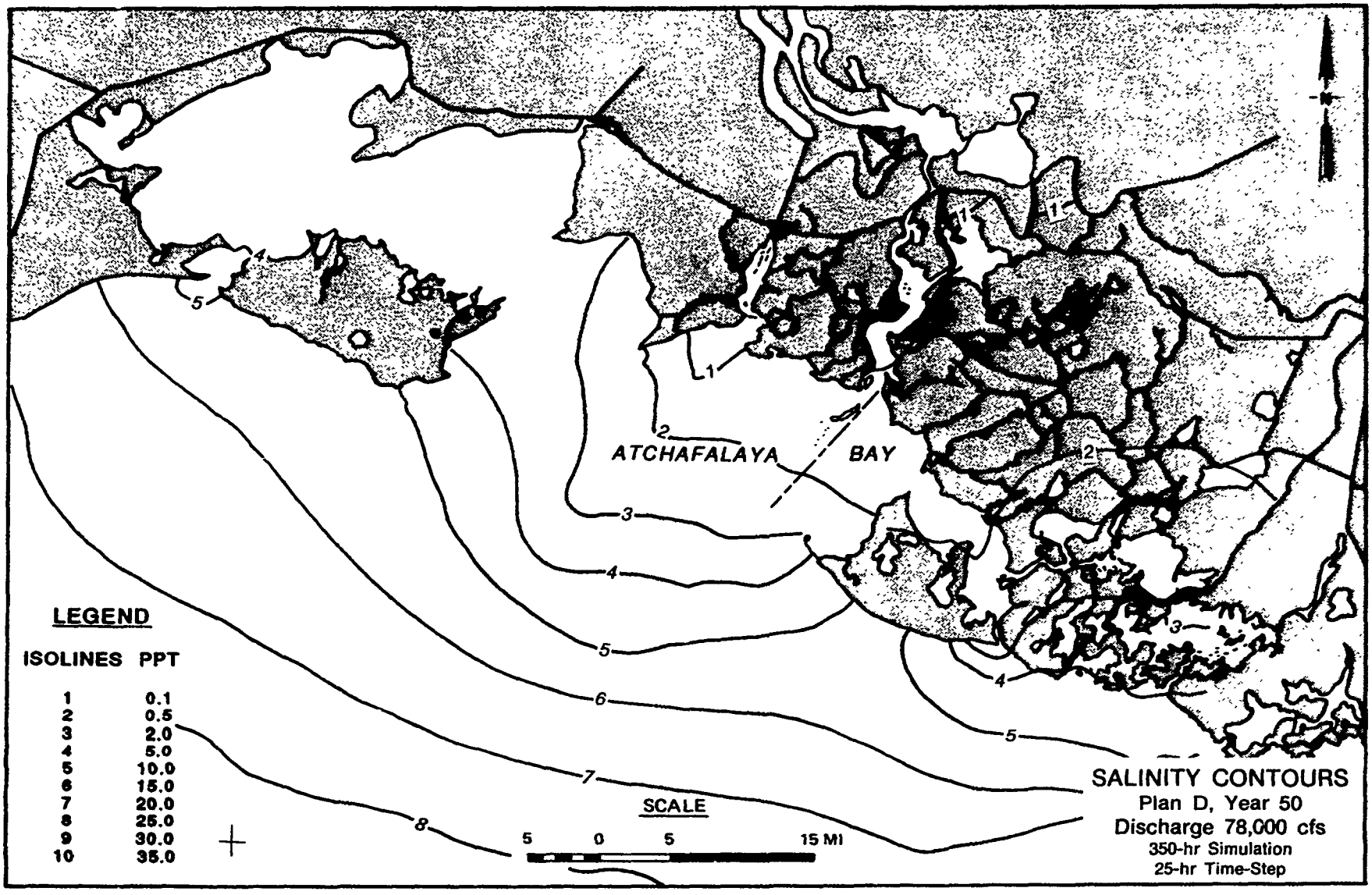
ATCHAFALAYA BAY
LEGEND
ISOLINES PPT
1 0.1
2 0.5
3 2.0
4 5.0
5 10.0
6 15.0
7 20.0
8 25.0
9 30.0
10 35.0
SCALE
5 0 5 15 MI
SALINITY CONTOURS
Plan D, Year 50
Discharge 78,000 cfs
350-hr Simulation
25-hr Time-Step

APPENDIX A: SUBSIDENCE ESTIMATES FOR ATCHAFALAYA BAY AND VICINITY

PART I: INTRODUCTION

Background

1. The entire Louisiana coast is experiencing land loss caused by the processes of land mass sinking relative to the mean Gulf water level and erosion. Prediction of long-term delta evolution for Atchafalaya Bay and vicinity necessitated estimating the long-term relationship between the mean water level and the surface of the delta. This process is generally referred to as apparent subsidence and is a complex combination of a number of factors. This appendix will discuss these factors, define what can be estimated, and present estimates of the subsidence for Atchafalaya Bay and vicinity over the next 50 years to be utilized in the long-term delta evolution projections for the bay.

Definitions

2. Apparent subsidence is defined as the lowering of the land relative to the mean sea level. A counter definition could be apparent sea level rise. There is a potential for some confusion of terms when discussing subsidence, because some geologists reserve the term subsidence for a particular process. This appendix will be discussing apparent subsidence, which is the summation of all of the separate effects. Hereafter, the term subsidence will mean apparent subsidence.

3. The following factors contribute in varying degrees to subsidence in the Atchafalaya Bay and vicinity:

- a. Actual sea level rise (global definition).
- b. Basement sinking caused by sediment load and/or subcrustal flow.
- c. Consolidation of sediments of the Gulf Coast geosyncline.
  - (1) Pleistocene and pre-Pleistocene sediments.
  - (2) Recent sediments.
- d. Local consolidation.
  - (1) Caused by the weight of minor landforms.
  - (2) Caused by the weight of man-made structures.
  - (3) Caused by the withdrawal of oil, gas, and water from coastal substrata.
- e. Tectonic activity (faulting and slumping).

If apparent total subsidence is designated as S (Kolb and Van Lopik 1978),

S has been defined by the equation

$$S = A + B + C_1 + C_2 + D_1 + D_2 + D_3 + E$$

Note that E may be positive or negative, but that generally the remaining terms will be positive if a positive value of subsidence indicates land loss. In this appendix, apparent subsidence will be referred to as S , while actual subsidence in the geologic definition would be S - A .

Actual sea level rise (A)

4. Actual global sea level rise is the result of glacial-eustatic effects. It refers to a rise in sea level referenced to a stable coastline. Gutenburg (1941) determined that the magnitude of this factor is 0.10 cm/year. His results are based on the records of 69 tide gages distributed around the world. Shlemon (1972) quotes a figure of 0.17 cm/year for actual sea level rise in the Atchafalaya Bay.

Basement sinking caused by sediment load and/or subcrustal flow (B)

5. As shown in Figure A1, a thickness of about 40,000 ft of shallow-water sediments has been deposited along the Louisiana coast since the beginning of the Tertiary Period (approximately 60 million years ago). This great mass of material was deposited here both as a result and a cause of regional downwarp, which has been occurring at an average rate of 0.02 cm/year (Kolb and Van Lopik 1958). Regional downwarp is caused by the ever-increasing depositional load and/or by the process of subcrustal flow creating a gradual subsiding trough. The hinge line of the downwarp occurs where the Recent sediments butt up against the Pleistocene Prairie Terrace. This is shown in Figure A1 as being located near Houma, LA. Fisk and McFarlan (1955) said the hinge line was near Franklin, LA, about 40 miles northwest of Houma. Kolb (1982)* said the hinge line probably bows upward along a line between these two locations.

Consolidation of sediments of the Gulf Coast Geosyncline (C)

6. Pleistocene and Pre-Pleistocene sediments (C_1). Consolidation

---

* Kolb, C. R. 1982. Written comments in 1982 Atchafalaya Review Meeting.

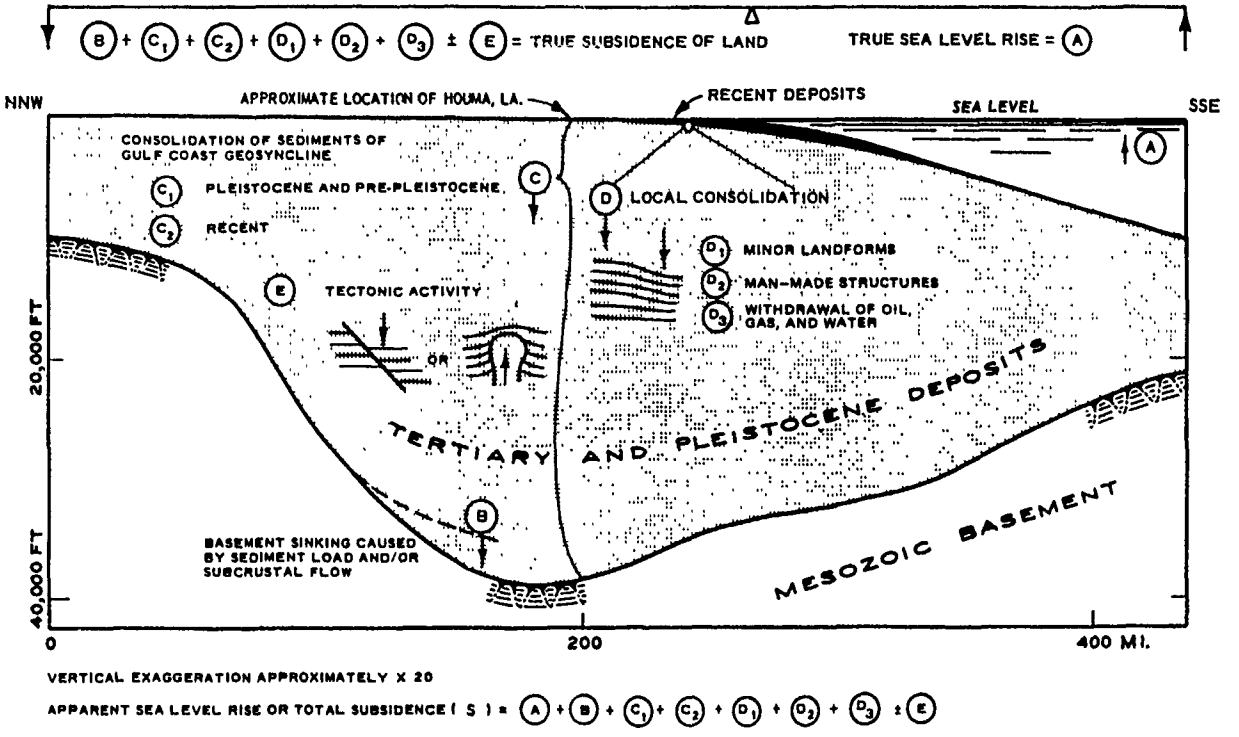

Figure A1. Generalized cross section of Gulf Coast geosyncline depicting components of apparent sea level rise (Kolb and Van Lopik 1958)

refers to the adjustment of a soil in response to increased load and involves the squeezing of water from the pores and decreasing the void ratio. This factor accounts for a significant percentage of subsidence in coastal Louisiana. The most rapid consolidation of the thick wedge of Pleistocene sediments is believed to have occurred during the Pleistocene time when sea level dropped approximately 400 ft. The sediments forming new land areas were dewatered, resulting in an above-average consolidation rate. A second cause for subsidence of the Pleistocene surface is the weight of Recent materials deposited on this surface subsequent to sea level rise. Studies by Fisk and McFarlan (1955) show the Pleistocene surface to be bowed downward in a huge east-west trending, scoop-shaped depression extending from Vermilion Parish to the Mississippi-Alabama line, and southward along a line trending northeast--southwest through Donaldsonville, LA. The estimated magnitude of this downwarping in the area ranges from 0 at Donaldsonville to 75 ft at the Atchafalaya Bay shoreline to in excess of 200 ft in Fourleague Bay (Figure A2). Assuming that this downwarping has occurred during the last 25,000 years since the last major lowering of sea level, the rate of consolidation varies from 0 near the hinge line to 0.003 ft/year (0.09 cm/year) at the coastline and in excess of 0.008 ft/year (0.24 cm/year) in Fourleague Bay.

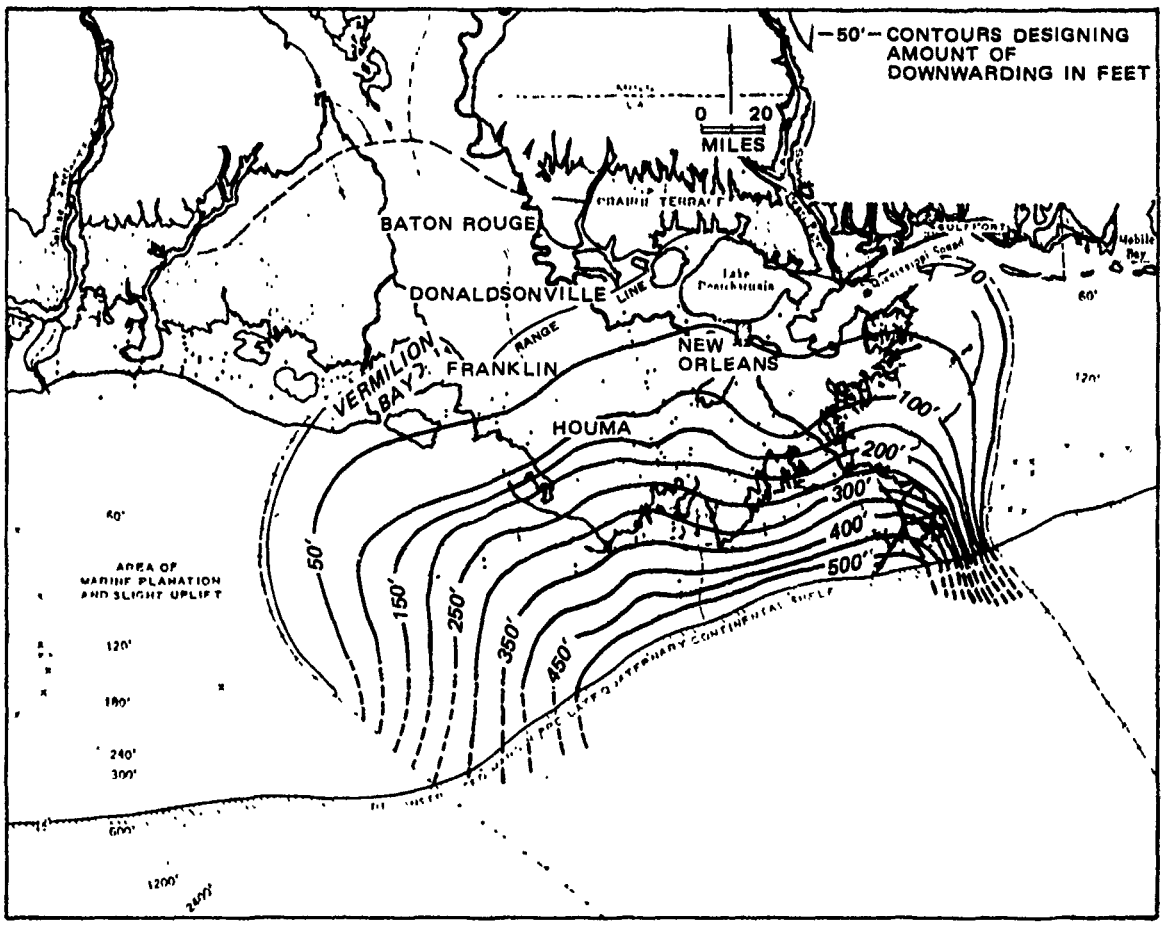

Figure A2. Amount of downwarping of the Prairie continental margin in area of late Quaternary Mississippi deltaic deposition (Fisk and McFarlan, 1955) (originally published by Geological Society of America)

7. Recent sediments (C_2). Subsidence of Recent sediments due to consolidation is most pronounced in areas of active deposition on a geological time scale. The rate of consolidation depends on the type of sediment being consolidated. According to Kolb and Van Lopik (1958), the rate of sedimentation in prodelta clays is such that consolidation occurs almost immediately, while the rate of sedimentation of intradelta and interdistributary materials is so rapid that 3,000 years may be required before they are normally consolidated. In any case, once Recent sediments become normally consolidated, any further consolidation can more logically be attributed to factors B, C_1, and E.

Local consolidation (D)

8. Caused by the weight of minor landforms (D_1). Local consolidation

is similar to the phenomena associated with consolidation of the Recent sediments (C_2). Where local consolidation occurs, the surface is depressed by amounts significantly in excess of that affecting the Recent deposits as a whole. There is also a tendency for natural landforms and man-made structures to "drag down" the adjacent areas. In these instances, downwarping occurs not only beneath the features but to considerable distances along their flanks.

9. Caused by the weight of man-made structures (D_2). It is impossible to accurately predict the amount of subsidence due to consolidation that will occur beneath a given structure. Structures built upon a marsh often subside by half their height almost immediately and then continue a slow subsidence for years. This factor could significantly affect rates at Morgan City, LA.

10. Caused by the withdrawal of oil, gas, and water from coastal substrata (D_3). The effects of withdrawal of oil, gas and water from coastal substrata may also prove to be significant. It may stimulate or accelerate the rate of subsidence due to consolidation. Theses effects have not been quantified, however, and will be represented in the analysis of more recent water level changes.

Tectonic activity (E)

11. Most faults in the Gulf Coast are down-dropped gulfward. As a result, any movement in the underlying strata accentuates the apparent sea level rise. The detailed information concerning the location and movement along faults which would allow an estimate of the magnitude of this factor are not available. Most movement probably occurs in episodic events, making it difficult to establish an average rate of movement.

12. There are two phenomena which can cause upward movement, thus negating the effects of subsidence. The study area is underlain by salt domes, many of which have intruded to within a few hundred feet of the surface. Rates of uplift vary greatly. Mud lumps and mud waves formed by the displacement of bay bottom clays might also create a local rise in land surface, but once again it is impossible to establish an average rate of uplift.

Summary of subsidence factors

13. In summary, the factors for which various investigators have been able to establish average subsidence rates are actual sea level rise (A), basement sinking (B), and consolidation of Pleistocene and pre-Pleistocene sediments (C_1). The estimated rate of subsidence resulting from these factors

is 0.28 cm/year inland and 0.31 cm/year near the Gulf. As will be shown in the following paragraphs, most investigators have estimated subsidence in the Atchafalaya Bay area three to four times larger than this. It can be concluded that the difference results from factors C_2, L_1, D_2, D_3, and E.

Literature Review

14. Most of the information presented in the preceding paragraphs was from Kolb and Van Lopik (1958). There have been numerous other studies performed related to subsidence along the Gulf Coast and/or the Atchafalaya River basin.

15. Morgan (1967) analyzed 140 detailed continuous shallow cores from the Mississippi Delta and calculated subsidence rates which varied over a 100-square-mile area from 1.52 to 3.96 cm/year. He concluded that such rapid rates resulted from the initial high water saturation of deltaic sediments. In addition, there is a lateral displacement by plastic flow in underlying fine-grained sediments which contributes to locally high subsidence rates.

16. Hicks (1968) analyzed the tide records at 41 locations around the world for the period 1940 to 1966 to determine the rate of change in apparent mean sea level rise. These data include the effects of both actual sea level rise and actual subsidence. This was computed as the slope of a least squares regression curve through the data. Along the Gulf Coast, the change ranged from 0.06 cm/year at Pensacola, FL, to 0.92 cm/year at Eugene Island, LA. An updated report in 1974 indicated that the subsidence rate at Eugene Island was still 0.92 cm/year. The data used in the updated study covered the period 1940-1970. A subsidence rate of 1.3 cm/year is obtained by computing the slope of a straight line connecting the end points of the curve in Figure A3. This is the rate estimated by Shlemon (1972).

17. Swanson and Thurlow (1973) determined actual subsidence rates along the Louisiana and Texas coasts by comparing tide records at 14 locations with the long-term tide record at Pensacola, FL, which was assumed to be stable. The records were analyzed in two parts: pre-1959 and post-1959. At those stations for which pre-1959 records were available, actual subsidence rates were found to be significantly greater during the post-1959 period. At Eugene Island, the actual subsidence rate from 1948 to 1959 was found to be 0.83 cm/year and from 1959 to 1970 the rate was 1.12 cm/year, or 0.975 cm/year

for 1948-1970. The recent trend is 15 percent greater than the long-term average. Since their analysis filtered out the effects of actual sea level rise, a value of 0.17 cm/year must be added to their results to obtain the total subsidence rates. Thus, their results indicate that the apparent subsidence rate at Eugene Island has increased from 1.00 cm/year prior to 1959 to 1.29 cm/year since 1959.

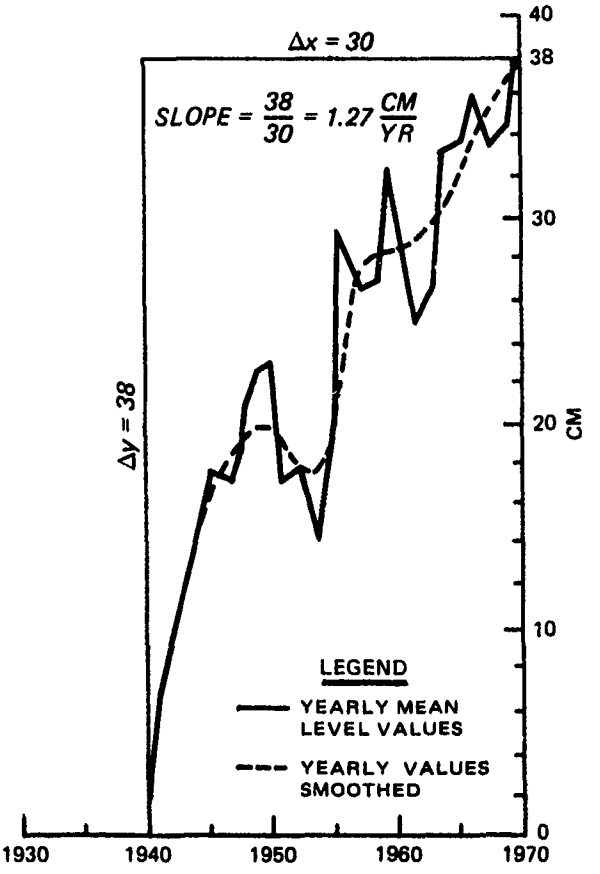

Figure A3. Relative change in sea level, 1940-1970, as interpreted from tide-gage data at Eugene Island, Louisiana (after Hicks 1972) (Shlemon 1972)(originally published by Geological Society of America)

18. Holdahl and Morrison (1974) have reported on the results of regional investigations of vertical crustal movements using precise relevelings and marigraph data. Their results have filtered out the contribution of actual sea level rise. The surface elevation changes measured in the Gulf Coast region were plotted as a contour map (Figure A4). They estimated an actual subsidence rate of 0.50 cm/year near the coastline to about 0.30 cm/year near Morgan City. This corresponds well to the regional subsidence rate quoted by Kolb and Van Lopik (1958).

19. Baumann and Adams (1981) correlated the water stages at Amelia, LA (east-southeast of Morgan City, Figure A5), with the Atchafalaya River discharge for the period 1955 to 1980. They plotted the residuals versus time in order to detect any temporal trend. The results indicated that water stages at Amelia have been rising at a rate of 0.85 cm/year independent of river discharge.

20. Conner and Day (1986) report apparent subsidence rates varying from 0.85 cm/year to 1.3 cm/year for coastal Louisiana, and a rate of 1.45 cm/year for the Lake Verret area which is about 10 miles north of Morgan City.

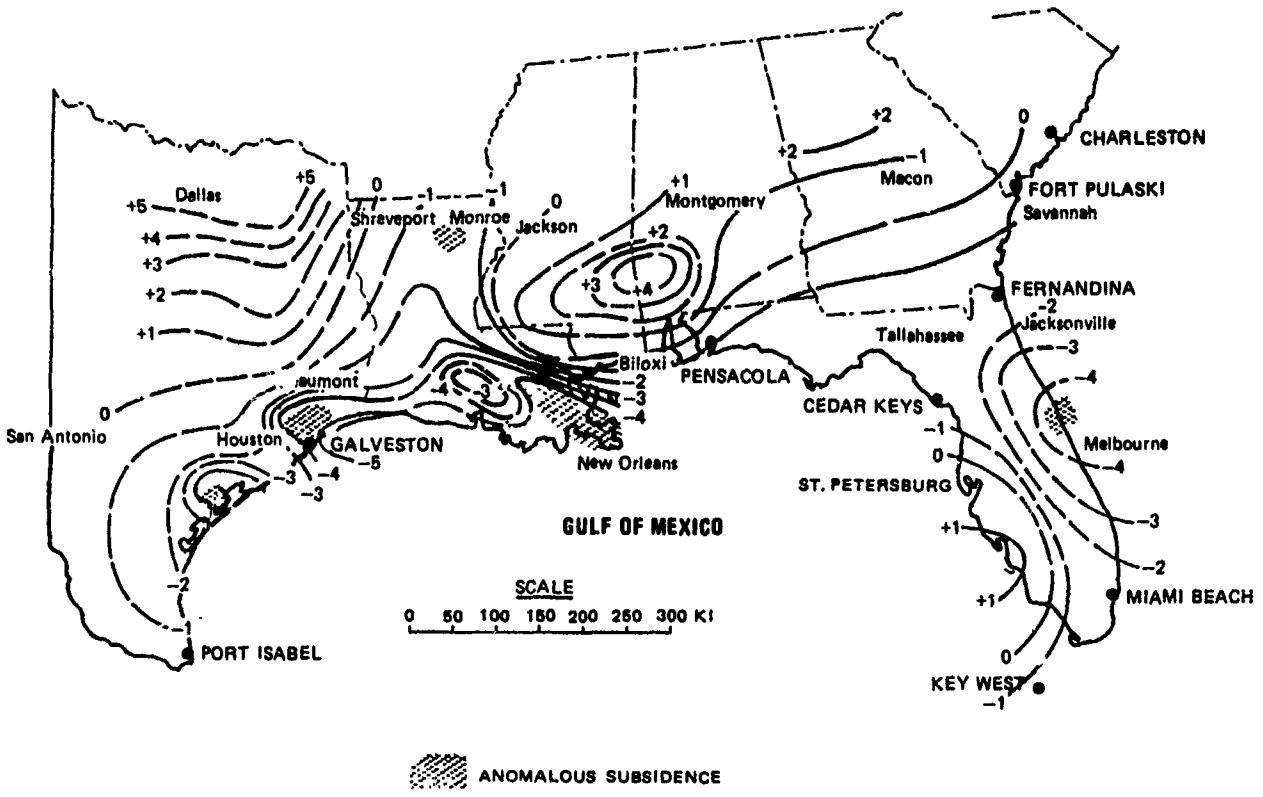

Figure A4. Preliminary rates of elevation change (Units for contour levels are mm/year)(Holdahl and Morrison, 1974)(courtesy of Elsevier Science Publishers)

21. The studies of Kolb and Van Lopik (1958) and Holdahl and Morrison (1974) indicated that the regional subsidence rate due to downwarping and consolidation of the Pleistocene and pre-Pleistocene sediments in the Atchafalaya basin is about 0.30 cm/year. Baumann and Adams (1981) estimated a rate of 0.85 cm/year at Amelia, southeast of Morgan City. In the coastal zone and in the bay, estimates of the subsidence rates range from 0.92 (Hicks and Crosby 1974) to 1.29 cm/year. The analysis of Swanson and Thurlow (1973), designed to filter out actual sea level rise from the tide records so as to estimate the actual subsidence, showed that the recent actual subsidence was 15 percent greater than the long-term long-term average. These studies by Hicks (1968, 1972) simply averaged the observed changes in apparent mean sea level. An independent estimate of actual sea level rise based on glacial melting may then be used to determine the magnitude of actual subsidence. This approach seems more straightforward and less susceptible to error. The regression was performed on the period of record, however, and gives no indication of trends. It was noted in a study by Shlemon (1972) that subsidence

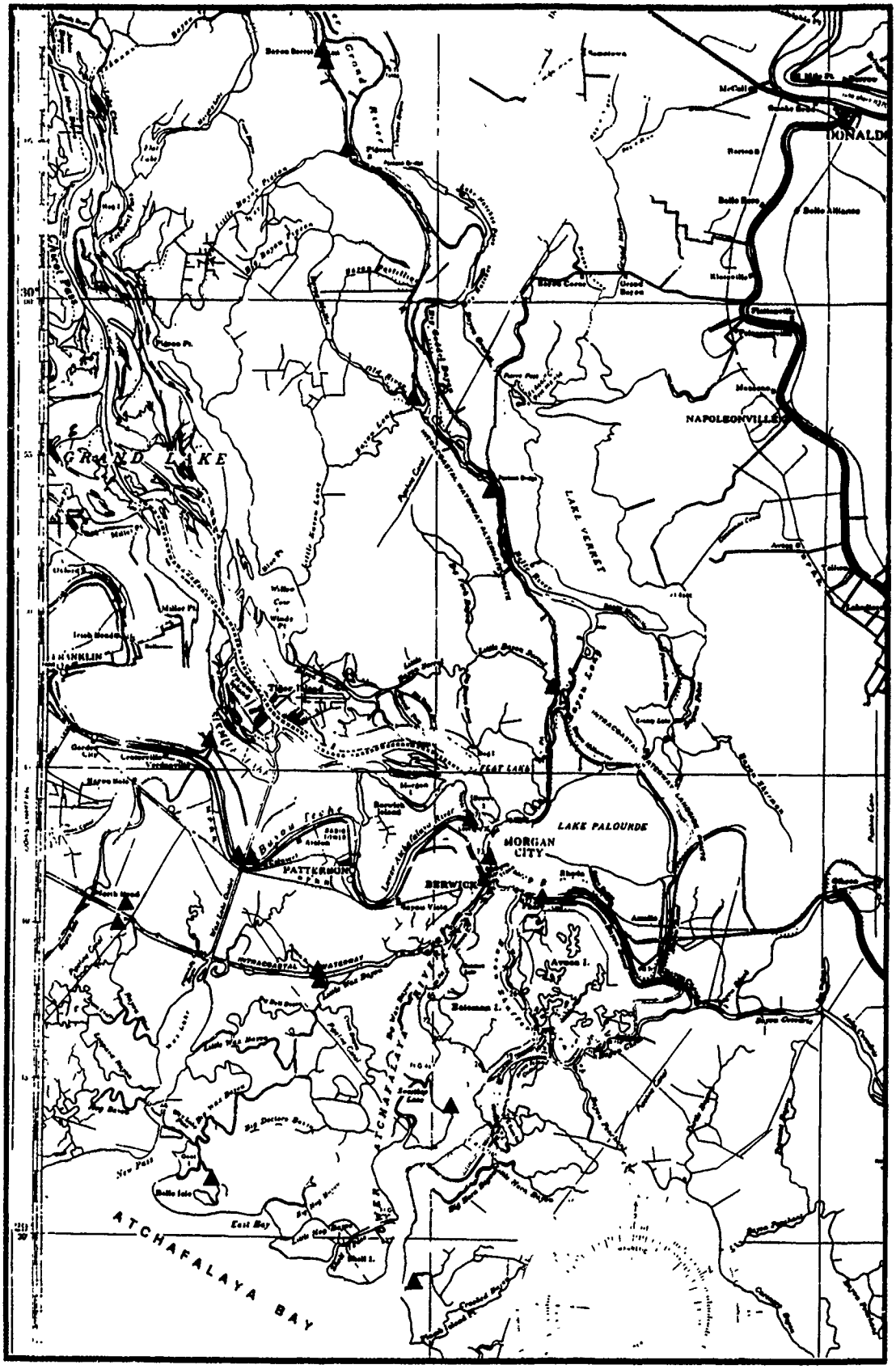

Figure A5. Location of stage data stations

in this area is likely to increase as the subaerial phase of delta develops and sands prograde over the subdelta. In this same study, he computes a subsidence rate of 1.3 cm/year by connecting the end points of Hick's data. It is felt that this interpretation of the data is too restrictive and gives too high an estimate. However, a rate somewhat larger than 0.92 cm/year may be advisable in predictions of delta growth.

22. To incorporate the findings of previous investigators into a best estimate of the subsidence rate in Atchafalaya Bay, start with the rate estimated by Hicks and Crosby (1974), 0.92 cm/year. The temporal trend noted by Swanson and Thurlow (1973) should be considered. Since their results filtered out the actual sea level rise, this rate must be substracted before applying the 15 percent increase indicated by their study. Thus (0.92 - 0.17) 1.15 = 0.86 cm/year, and adding back the actual rate of sea level rise gives an estimated subsidence rate for the bay of 1.03 cm/year. The best estimate for Morgan City appears to be 0.30 cm/year based on the results of Kolb and Van Lopik (1958) and Holdahl and Morrison (1974).

23. Penland et al. (1989) reported the results of an extensive analysis of tidal records during the period 1942-1982 for all of southern Louisiana and summarized the subsidence by coastal regions (Figure A6). The region including Atchafalaya Bay averaged a subsidence rate of 1.62 cm/year. Of particular interest is the variation in the subsidence rates over coastline. The Atchafalaya Bay area experienced the largest subsidence with reduced values in either direction. This suggests that there is an underlying spatial variation to the data that should be incorporated into the subsidence values to be used in the numerical model to predict the delta evolution.

Technical Approach

24. The prediction of delta evolution in Atchafalaya Bay must factor the subsidence effect into the growth projections. However, the only parameter in the subsidence equation that will ultimately have a bearing on the evolution will be the total combined apparent subsidence. Knowing the particular contributions will not be of any great value, therefore, for the needs of this study the technical approach which will yield the greatest return will be the analysis of historical tidal records. These records are relatively abundant and provided the spatial data to define the variability suggested previously.

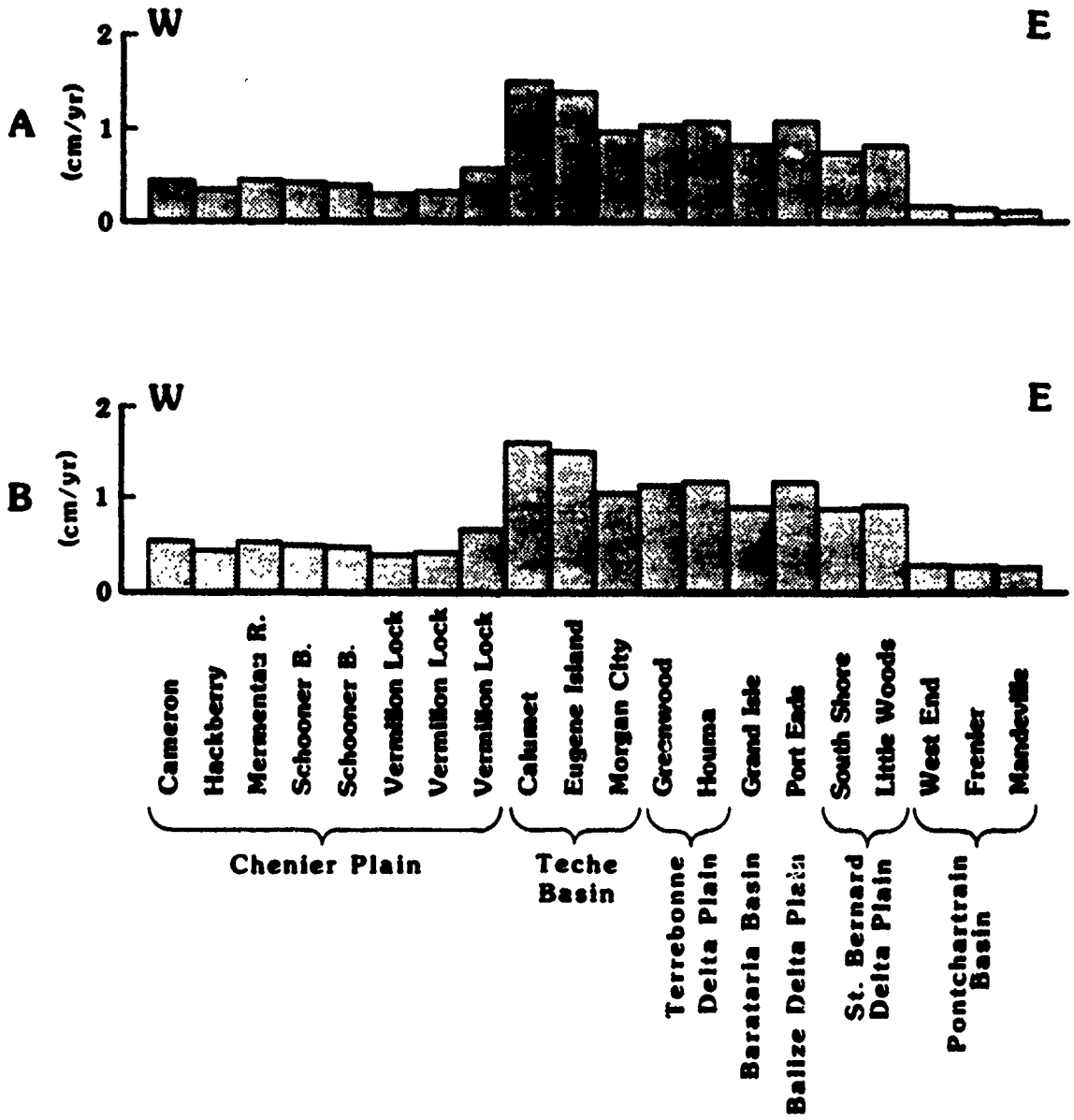

Figure A6. Subsidence in Louisiana, based on USACE tide gage data and using (A) the Gulf of Mexico relative sea level correction factor and (B) the eustatic correction factor from Penland et al. 1989 (© 1989 by the Louisiana Geological Survey)

25. The method to be used for estimating the apparent subsidence rates for the area is statistical analysis of long-term water-surface elevation records to define the trends in the mean water level. This analysis requires data stations which are established on stable foundations and are monitored for prolonged periods.

26. The statistical method used for the trend estimates was multiple regression analysis. The analysis was performed in two phases: a single-station analysis and then a combined regression of all stations. The single-station analysis provided a means of defining the importance of the river discharge and the temporal variation in subsidence. The multiple- station analysis was used to define the spatial variation in subsidence for use in the numerical model.

27. All statistical analyses were performed using the SPSS (Nie et al. 1975) statistical package on the Control Data Corporation's CYBER 865 computer available under contract to the Corps of Engineers.

Field Data Stations

28. The field data stations for long-term tidal data to support the statistical analysis are shown in Figure A5. The stage and discharge data at the 22 stations were provided to the US Army Engineer Waterways Experiment Station by the US Army Engineer District, New Orleans, on magnetic tape. The record lengths varied, but most covered the period of 1963 to 1980. There were record gaps and 4 of the 22 stations had such limited data that they could not be included in the analysis. Simmesport, LA, gage discharge data were available for the period 1963-1980, in the form of mean daily discharges.

29. Data records with gaps were not filtered for use in the regression analyses using daily discharge values, but the yearly averaging may have induced some error into the analysis for records with significant data gaps.

30. Some of the tidal data stations experienced noticeable subsidence during the period of record, and subsequently, periodic datum corrections were made at these stations. These datum corrections were added back into the data so that the subsidence estimates would not be erroneously biased low. These datum corrections were clearly evident in the time-series plots of the data.

Single Station Analysis

31. The analysis of subsidence at a single station based on long-term tidal data has proven to be the standard approach (Hicks 1968; Swanson and Thurlow 1973; Baumann and Adams 1981). This is the approach taken as an initial evaluation for the study area. This analysis, however, was performed as a series of regressions to evaluate the relative performance of a number of forms of prediction equations. An initial approach was undertaken that handled the analysis in two phases. The first phase was a regression of stage with riverflows. The second phase was a regression of the residuals from the first-phase regression with time. This approach was abandoned in order to avoid accidental correlations between river discharge and time. The remaining analyses were performed handling both flow and time in the same regression.

32. The regression analysis was performed on 18 gaging stations with eight separate regression equation forms tried. These eight equations were:

$$\text{Stage} = A * (\text{Flow})_{\text{Annual}} + B * (\text{Time}) + C \tag{A1}$$

$$\text{Stage} = A * (\text{Flow})^{p}_{\text{Annual}} + B * (\text{Time}) + C \tag{A2}$$

where p is obtained from a regression of

$$\ln (\text{Stage}) = p * \ln (\text{Flow}) + D$$

Equation A3 is the same as Equation A1 except using daily flows, and Equation A4 is the same as Equation A2 except using daily flows.

$$\text{Stage} = A * (\text{Flow})_{\text{Daily}} + B * (\text{Time}) + C * (\text{Flow})^{2}_{\text{Daily}} + D \tag{A5}$$

$$\text{Stage} = A * (\text{Flow})_{\text{Daily}} + B * (\text{Time}) + C * (\text{Flow})^{2} + D \tag{A6}$$

$$\text{Stage} = A * (\text{Time}) + B * (\text{Time})^{2} + C \tag{A7}$$

where time is measured in years 1 to 18 beginning in 1963. Equation A8 is the same as Equation A7 except time is measured in days 1 through 6575. A , B ,

C , D , and p are regression constants. The subsidence rates will then be the time derivative of these equations. For Equations A1 through A4 the subsidence will be the coefficient B , while for Equations A5 and A6 the subsidence will be B + 2 * C * (Time) . For Equation A7 and A8 it will be A + 2 * B * (Time) .

33. The results of the single station regressions are summarized in Table A1. An example of the regression analysis at Morgan City for annual stages and discharges is shown in Figure A7. The correlation coefficient R^2 for the method in equation A1 was 0.97 with a subsidence rate s of

Table A1

Summary of Computed Subsidence Rates

Name	Station	Average Subsidence Rate cm/year, 1963-1980	Correlation Coefficient* R^2
6 Mile Lake	3645	1.1 - 1.2	0.89 - 0.93
Calumet	3720	1.0 - 2.2	0.88 - 0.98
Berwick Lake	3750	1.5 - 1.6	0.84 - 0.86
Morgan City	3780	0.5 - 1.6	0.88 - 0.98
Sweetbay Lake	3820	1.6 - 1.7	0.94 - 0.95
Deer Island	3850	2.0 - 2.1	0.60 - 0.62
Big Bayou Pigeon	49635	0.5 - 0.6	0.99
Old River	49645	0.4 - 0.5	0.99
Pierre Pass	49690	0.7 - 1.7	0.89 - 0.97
Little Bayou Sorrell	49725	0.4 - 2.6	0.90 - 0.99
Lower Grand	52560	0.2 - 0.3	0.72 - 0.75
Bayou Tech (west)	64650	1.2	0.93 - 0.94
Bayou Tech (east)	64700	1.8 - 1.9	0.86 - 0.88
Bayou Boeuf (east)	76360	0.5 - 0.6	0.92 - 0.93
Bayou Boeuf (west)	76400	0.4 - 1.5	0.88 - 0.98
Wax Lake (west)	76440	1.0 - 1.1	0.98 - 0.99
Intracoastal Waterway Wax Lake (west)	76560	1.2 - 1.4	0.97
Eugene Island	88600	1.2 - 1.5	0.80 - 0.87

* Results with $R^2 < 0.6$ are not presented.

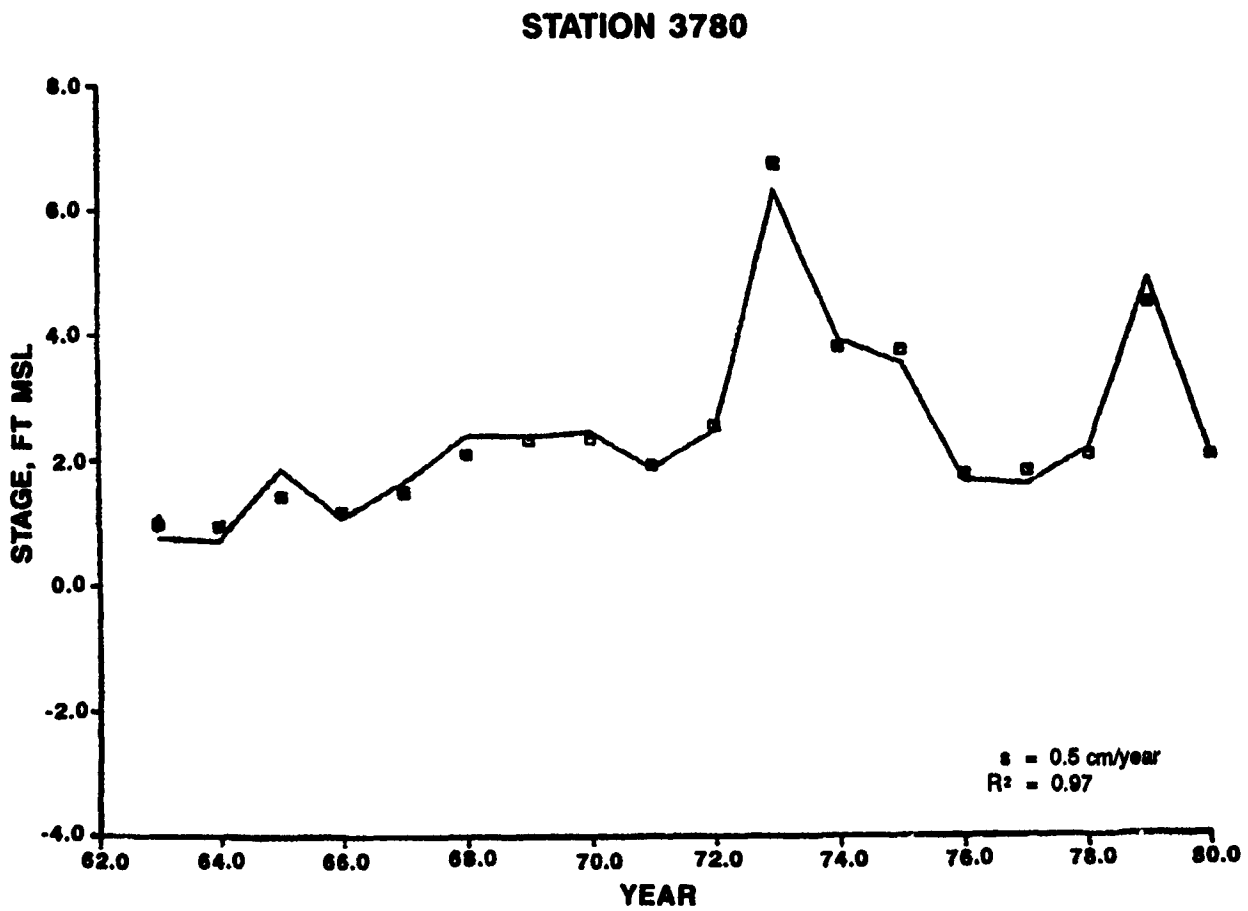

Figure A7. Regression calculated using Equation A1

0.5 cm/year. The same location with the regression method in Equation A4 using daily flows is shown in Figure A8. For this regression the subsidence rate was increased to 1.2 cm/year, but the correlation coefficient was reduced to 0.80. The subsidence value of 0.5 cm/year using the annual values agrees well with the previous estimates of Holdahl and Morrison (1974).

34. This pattern was fairly consistent with the best regression coefficients being found when the annual values were used. However, there is other previous work to suggest either of these values. Ramsey and Moslow (1987) supports the larger subsidence rates for the study area, which were derived from a similar regression analysis. These results show the possible highly localized subsidence observations in the vicinity of structure locations. This is particularly true in the vicinity of Morgan City. This variation in the computed subsidence rates suggests further analysis was necessary.

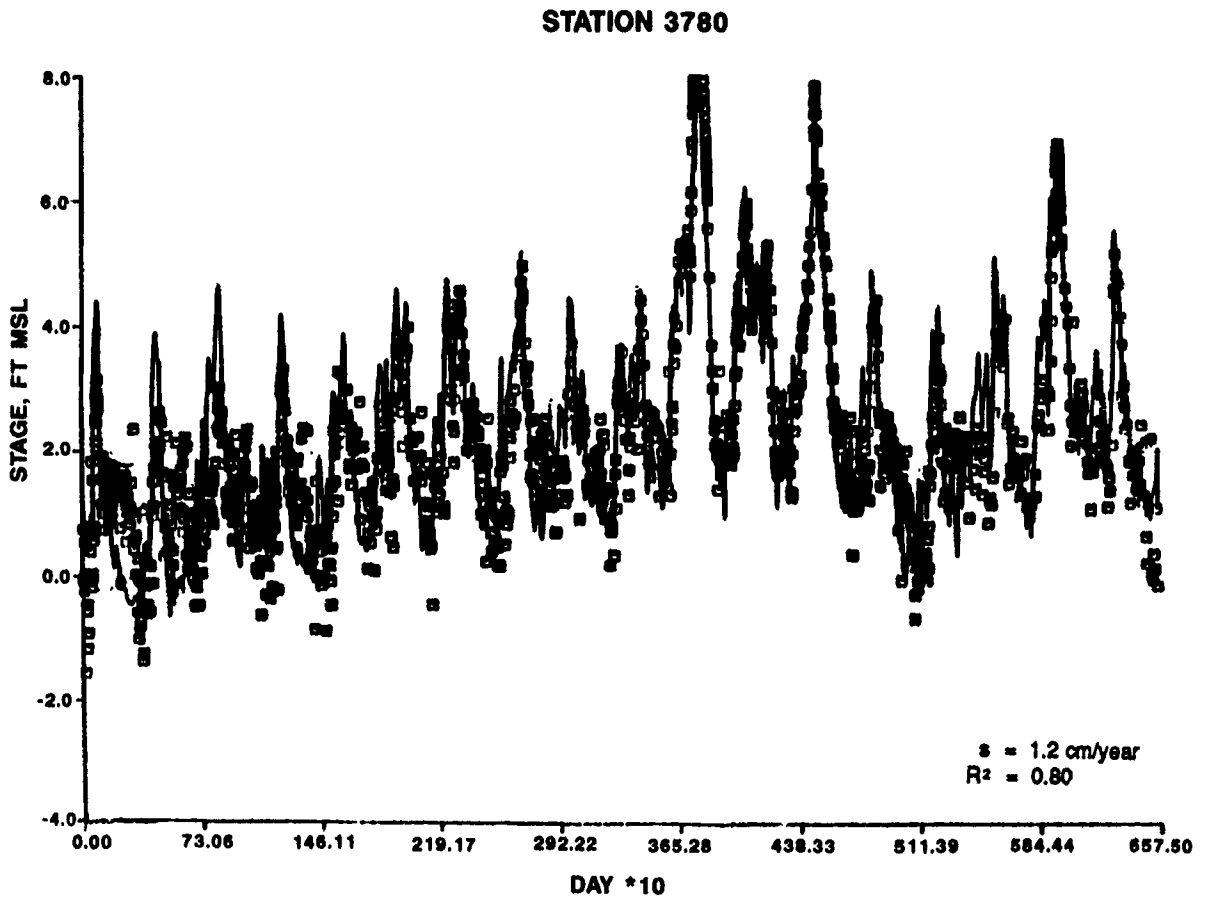

Figure A8. Regression calculated using Equation A4

Multiple Station Analysis

35. The multiple station analysis was needed to provide a spatial distribution of subsidence rates for use in the numerical model prediction of delta growth. This analysis was performed as a multiple regression analysis taking into account the locations of the stations and used an assumed form of the spatial distribution function. This analysis was performed on the full data set for every station in a single regression. Some consideration was given to performing the spatial analysis on the results from the single station regression; however, it was felt that by combining all of the data, the spatial correlations of the discharge effects will be better accounted for in the full regression. The combined regression was performed on a composite data base which had a total of 18,945 data cases.

Regression Analysis

36. The combined spatial temporal regression analysis was performed in a manner designed to avoid the possibility of sensitive oscillations in the regression equation. The form of the equation for the water surface is

$$z = A\,Q^{B} \exp\{S(x,y,Q)\}\{1 - \exp[-k(t - t_0)]\}^{p} \qquad (A9)$$

where

$S(x,y,Q)$ = a spatial distribution dependence function that is dependent the location of the station and the river discharge

Q = discharge

k = time decay constant

t = time

The form of this function is

$$S(x,y,Q) = Cx^2 + Dx + Ey^2 + Fy + Gxy + IQ + JQx + KQy + LQx^2 + MQy^2 + NQxy \qquad (A10)$$

The coefficients (C, D, E, F, G, I, J, K, L, M and N) in this function were determined from the regression analysis. The data values for x, y and Q are part of the data base for the regression. The station locations (x,y) were defined in state grid coordinates expressed in thousands of feet and the river discharge Q at Simmesport was defined in millions of cubic feet per second.

37. The time term in Equation A9 was derived from the asymptotic consolidation of a deposited sediment layer with some initial density toward a maximum density after an infinite time. The decrement from a value of one reflects the fact that the tide gage is sinking with the sediment sublayer and the apparent water level is rising with time.

38. The actual multiple linear regression was performed on the log transform of Equation A9. In order to perform the log transform the time term had to be defined as a separate variable in the regression. This then means that the variables k and t_0 cannot be regressed. Therefore, the procedure used in this study was to iteratively adjust the values of k and t_0 to

optimize the overall regression coefficient R^2 . The exponent p on the time term should in theory be 1.0; however, in doing the regression on the log transform there is no way to force it to that value. The regression will deliver the exponent that provides the best fit to the data.

39. Once the coefficients of Equations A9 and A10 were known, the subsidence rate was determined as the time derivative of Equation A10:

$$\frac{dz}{dt} = A\,Q^B \exp\left[S(x,y,Q)\right] p\{1 - \exp\left[-k(t - t_0)\right]\}^{p-1} k \exp\left[-k(t - t_0)\right] \quad \text{(A11)}$$

If the anticipated value of the exponent p on the time dependence term is one, then the subsidence rate will be

$$\frac{dz}{dt} = A\,Q^B \exp\left[S(x,y,Q)\right] k \exp\left[-k(t - t_0)\right] \quad \text{(A12)}$$

40. By using the assumed Equation A9 form, the distribution in space can be either uniform, Gaussian "bell shaped," or bowl-shaped depending on the coefficients on the terms of $S(x,y,Q)$. This assumption will be confirmed if it is a Gaussian distribution as was suggested in Figure A6, and by the general fact that the largest regional subsidence rates are occurring in the study area.

Results of the Regression

41. The iteration on the time dependence term for the regression analysis showed that the influence that the time term coefficients had on the overall correlation coefficient was not dramatic. However, the dependence of the time decay origin t_0 to provide the maximum R^2 value for a fixed time decay constant k is shown in Figure A9. For a small assumed value of k (below 10^{-6}) the t_0 value remains almost constant at about −30,000 days (−82 years). However, the change in the R^2 value is not very significant over all values of these coefficients tested. Figure A10 presents the variation of R^2 with the time decay constant k . The maximum R^2 of 0.693 occurs for a k of 0.0003; however, for all combinations tested the R^2 was

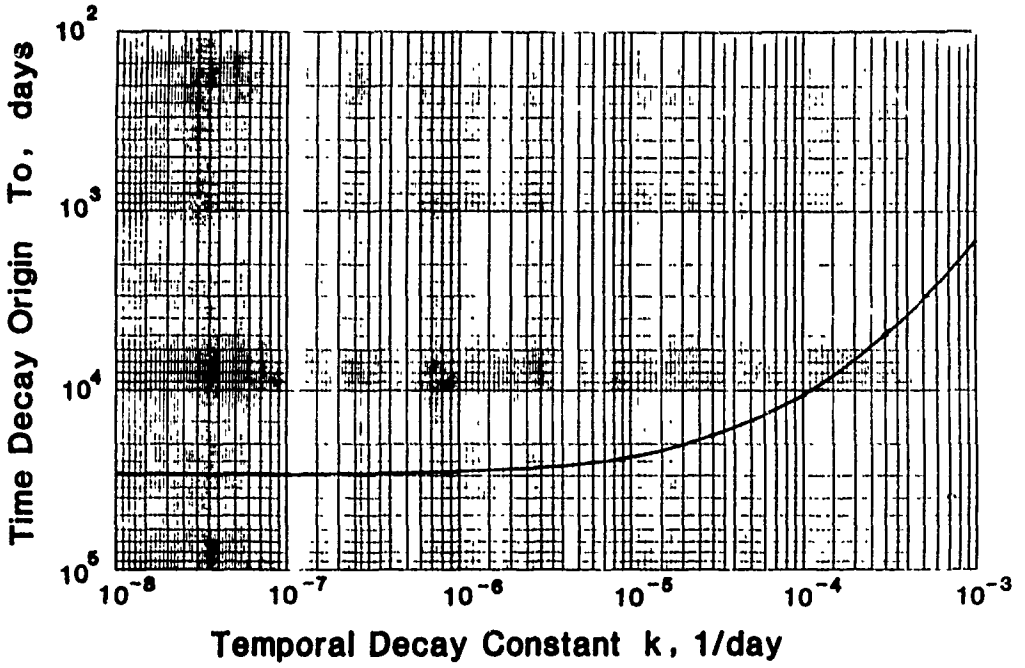

Figure A9. Relationship between k and T_o

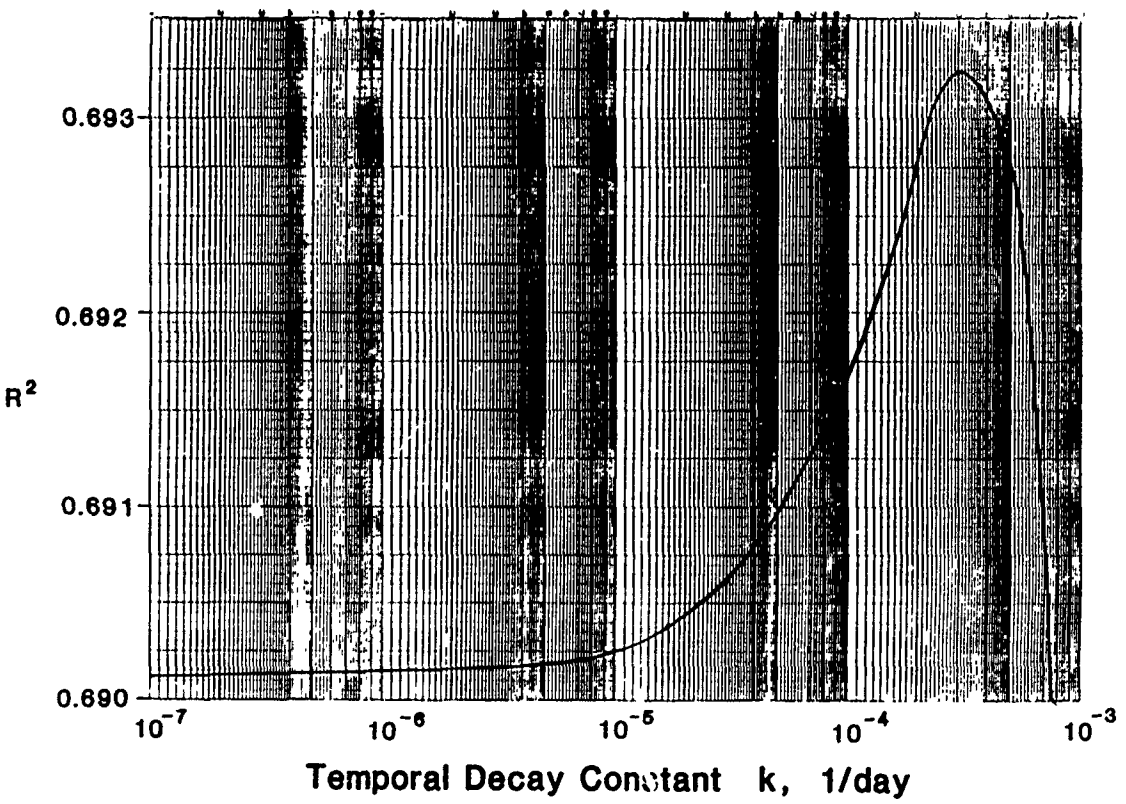

Figure A10. Temporal decay constant, k (1/day)

above 0.690. These data indicate that there is little gained from the time term in the regression and that the subsidence rates tend to be fairly constant over the period of record. As a general rule the smaller the value of k, the more constant the subsidence rates will be over the period of analysis.

42. The spatial and temporal variation in subsidence rates are illustrated in Figures A11 through A13, which show the predicted subsidence rates for 1962, 1980 and 2030, based on the regression equation for $k = 10^{-5}$/day and $t_0 = -25{,}000$ days. The contours are in cm/year and show a slight reduction in the subsidence rate with time. The estimated subsidence rate near Eugene Island changed from about 1.5 cm/year in 1962 to 1.4 cm/year in 1980 and would decrease to about 1.2 cm/year in 2030. The Gaussian distribution results in elliptical contours of subsidence rate with the major axis oriented toward the south-southeast. The maximum subsidence for the regression occurs somewhere in the vicinity of Morgan City.

43. The predicted increase in actual sea level rise may not be fully represented in the historical tidal data, and therefore the projected reduction in subsidence rates may not be realistic. Also, because of the lack of sensitivity of the regression to the time dependence term, it was felt that a more conservative prediction of subsidence would be a more constant rate over the delta projection period. This is achieved by choosing the time dependence coefficients as $k = 10^{-8}$/day and $t_0 = -28{,}500$ days. This results in a subsidence distribution as shown in Figure A14. This distribution is close to the 1980 pattern but is essentially constant over the entire extrapolation period. This is the subsidence rate that was used in the delta evolution predictions.

44. The regression analysis yielded a value of 1.02 for the exponent p on the temporal term, which was close to 1.0 as expected. A computer subroutine written in FORTRAN 77 is provided as Figure A15. The subroutine computes the subsidence rates used in the numerical model. The equation coefficients are included in that program. Potential users are cautioned to use a computer with a high level of accuracy (greater than 32 bits per word) because of the sensitivity of the regression equation to precision.

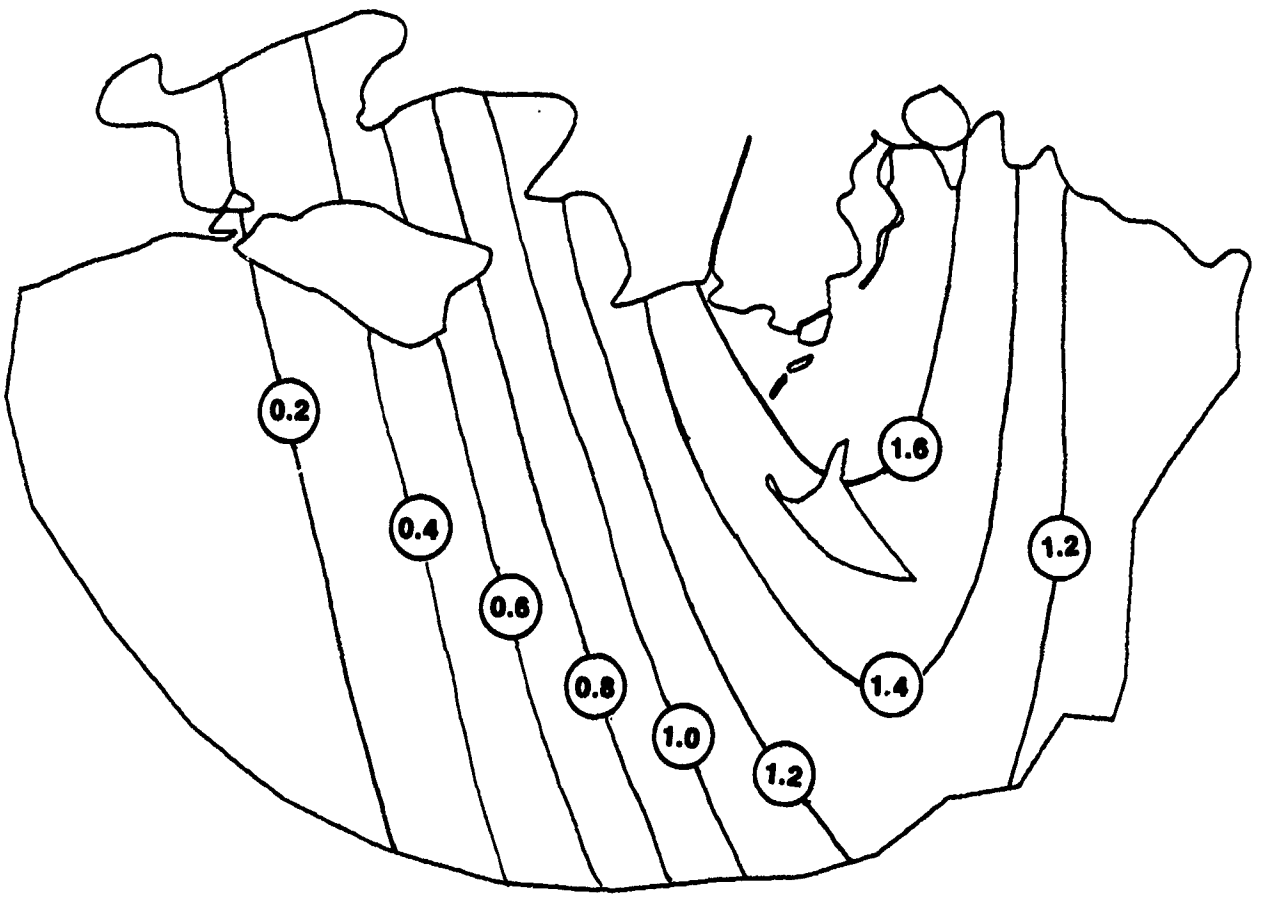

Apparent Subsidence (cm/yr)

For k=10^{-5} and To=25,000 days

1962 Subsidence Rates

Figure A11. Apparent subsidence rates for 1962

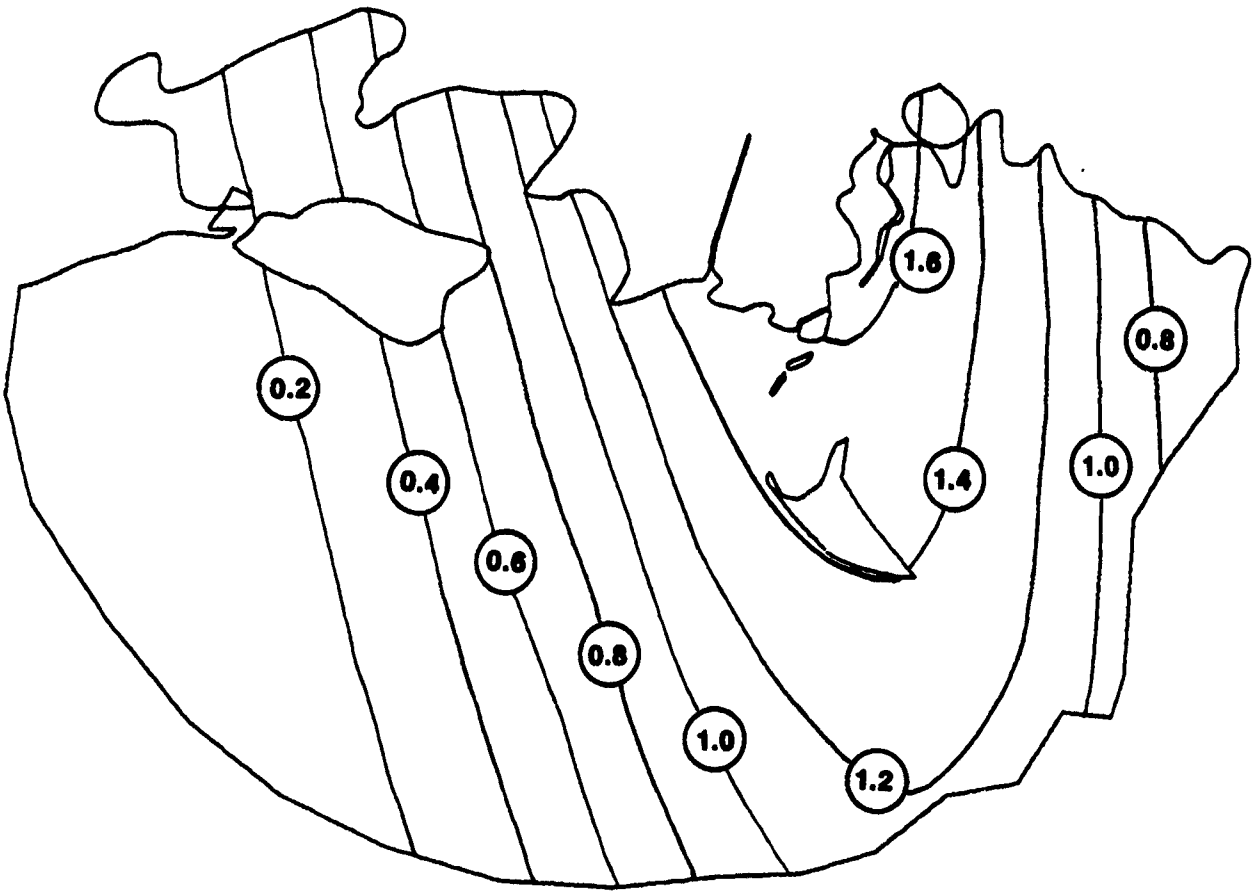

Apparent Subsidence (cm/yr)

For k=10^{-5} and To=25,000 days

1980 Subsidence Rates

Figure A12. Apparent subsidence rates for 1980

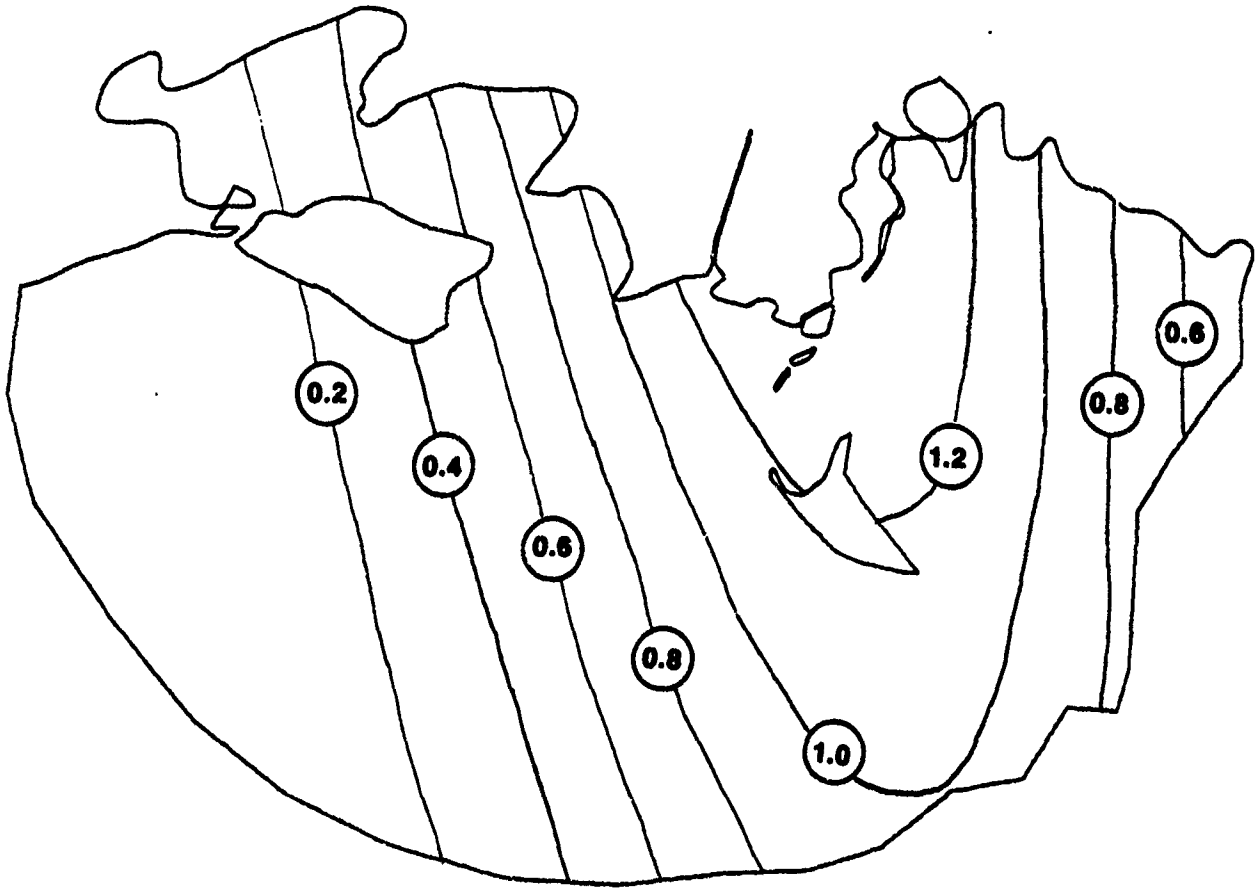

Apparent Subsidence (cm/yr)

For k=10^{-5} and To=25,000 days

2030 Subsidence Rates

Figure A13. Apparent subsidence rates for 2030

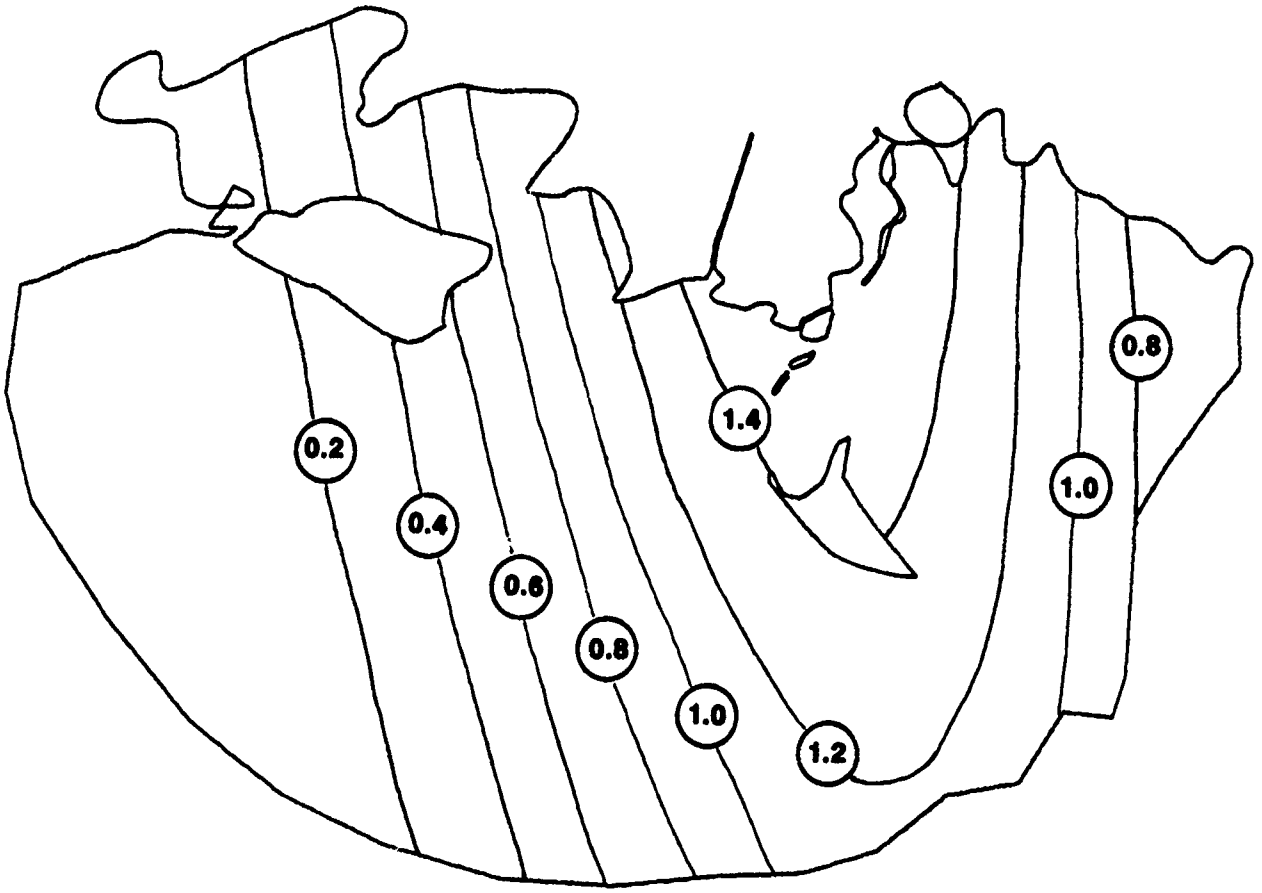

Apparent Subsidence (cm/year)

For k= 10^{-8} and To=28,500 days

For 1962 to 2030

Figure A14. Apparent subsidence rates for 1962-2030

45. The following subroutine variables are required:

a. CORD: array of Louisiana state grid (southern) coordinates in feet

b. NP: total number of nodes of interest

c. DUR: duration of period over which subsidence is to be estimated in days

The subsidence, in feet, is computed and returned in the variable array SUBS.

```
      SUBROUTINE SUBSIDE (DUR)
C
C     ROUTINE COMPUTES ATCHAFALAYA/TERREBONNE MARSHES SUBSIDENCE
C
      PARAMETER (MAXN=5500,MAXE=2000,MAXEVE=10)
      COMMON CORD(MAXN,2),SUBS(MAXN), NP
C
      T  = 25000.
      A  = EXP(-164.8506)
      C  = -0.00003972696
      D  =  0.16632871
      E  = -0.0000021152125
      F  =  0.039687267
      G  = -0.000018513637
      XI =  5.8174781
      XK = -0.031870479
      XL = -0.0000015753089
      XM = -0.0000029699728
      XN =  0.000017281952
      Q  =  0.3
      B  = -0.010518792
C
      DO 200 I = 1,NP
C        CONVERT LOUISIANA STATE GRID COORDINATES TO 1000'S OF FEET
         X = CORD(I,1) / 1000.
         Y = CORD(I,2) / 1000.
C        CALCULATE SUBSIDENCE IN METERS FOR THIS NODE...
         TEMP = C*X*X+D*X+E*Y*Y+F*Y+G*X*Y
         TEMP = TEMP+XI*Q+XK*Q*Y+XL*Q*X*X+XM*Q*Y*Y+XN*Q*X*Y
         SUBS(I) = A * EXP(TEMP) * EXP(-.00000001*(T+28500))/100000000.
         SUBS(I) = SUBS(I) * Q**B
         SUBS(I) = SUBS(I) * DUR
  200 CONTINUE
C
C     FIND MAX AND MIN SUBSIDENCE
C
      SMIN = 1.0E+20
      SMAX = -1.0E+20
      DO 400 I = 1,NP
         IF(SUBS(I) .LT. SMIN) THEN
            SMIN = SUBS(I)
            ISMIN = I
         ENDIF
        IF(SUBS(I) .LT. SMAX) THEN
           SMAX = SUBS(I)
           ISMAX = I
       ENDIF
  400 CONTINUE
      WRITE(6,600) SMIN,ISMIN,SMAX,ISMAX
  600 FORMAT(//10X,'*** ATCHAFALAYA SUBSIDENCE ***',
     * /10X,'MINIMUM ',F10.3,' METERS AT NODE',I5,
     * /10X,'MAXIMUM ',F10.3,' METERS AT NODE',I5,/)
C
      RETURN
      END
```

Figure A15. Subroutine to compute subsidence

REFERENCES

Baumann, R. H., and Adams, R. D. 1981. "The Creation and Restoration of Wetlands by Natural Processes in the Lower Atchafalaya River System: Possible Conflicts with Navigation and Flood Control Objectives," Center for Wetlands Research, Louisiana State University, Baton Rouge, LA.

Conner, W. H., and Day, John W., Jr., eds. 1986 (Apr). "Factors Affecting the Growth and Vigor of Commercial Wetland Forests Subject to Increased Flooding in the Lake Verret, Louisiana Watershed," Atchafalaya Newsletter, Issue 3, Center for Wetland Resources, Sea Grant, Louisiana State University, Baton Rouge, LA.

Fisk, H. N., and McFarlan, E. 1955. "Late Quaternary Deltaic Deposits of the Mississippi River," Crust of the Earth, Special Paper No. 62, Geological Society of America, pp 279-302.

Gutenburg, B. 1941. "Changes in Sea Level, Postglacial Uplift, and Mobility of the Earth's Interior," Bulletin, Geological Society of America, Vol 52, pp 721-772.

Hicks, S. D. 1968. "Long Period Variations in Secular Sea Level Trends," Shore and Beach, pp 32-36.

_____. 1972. "On the Classification and Trends of Long Period Sea Level Series," Shore and Beach, pp 32-36.

Hicks, S. D., and Crosby, J. E. 1974. "Trends and Variability of Yearly Mean Sea Level," Technical Memorandum NOS13, National Oceanic and Atmospheric Administration, National Ocean Survey, Rockville, MD.

Holdahl, S. R., and Morrison, N. L. 1974. "Regional Investigations of Vertical Crustal Movements in the U. S. Using Precise Relevelings and Mareograph Data," Tectonophysics, Vol 23, No. 4, pp 373-380.

Kolb, C. R., and Van Lopik, J. R. 1958 (Jul). "Geology of the Mississippi River Deltaic Plain, Southeastern Louisiana," Technical Report No. 3-483, US Army Engineer Waterways Experiment Station, Vicksburg, MS.

Morgan, J. P. 1967. "Emphemeral Estuaries of the Deltaic Environment," Estuaries, G. H. Lauff and W. K. Kellogg, eds., American Association for the Advancement of Science, Washington, DC, pp 115-120.

Nie, N. H., Hull, C. H., Jenkins, J. G., Steinbrenner, K., and Bent, D. H. 1975. SPSS; Statistical Package for the Social Sciences, Second Edition, McGraw-Hill, New York.

Penland, Shea, Ramsey, Karen E., McBride, Randolph A., Moslow, Thomas F., Westphal, Karen A. 1989. "Relative Sea Level Rise and Subsidence in Louisiana and the Gulf of Mexico," Coastal Geology Technical Report No. 3, Louisiana Geological Survey, Baton Rouge, LA.

Ramsey, Karen E., and Moslow, Thomas F. 1987. "A Numerical Analysis of Subsidence and Sea Level Rise in Louisiana," Coastal Sediments '87, American Society of Civil Engineers, New Orleans, LA, 12-14 May 1987, pp 1673-1688.

Shlemon, R. J. 1972. "Atchafalaya Bay, Louisiana: Regional Subsidence and Contemporary Delta Formation," Transactions, Gulf Coast Association of Geological Societies, Vol XXIII, pp 22-26.

Swanson, R. L., and Thurlow, C. I. 1973. "Recent Subsidence Rates Along the Texas and Louisiana Coasts and Determined from Tide Measurements," Journal of Geophysical Research, Vol 78, No. 15, pp 2665-2671.

APPENDIX B: NOTATION

2D	Two-dimensional
FD	Finite difference
FE	Finite element
GIWW	Gulf Intracoastal Waterway
JOBSTREAM	Model to model boundary condition transfer program
LAR	Lower Atchafalaya River
LP	Lake Palourde
MBM	Mississippi Basin Physical Model
MCM	Mississippi Channel Model
MESH	FE computational network
MUXTRAP	Multiple-event extrapolation
NASA	National Aeronautics and Space Administration
NOS	National Ocean Survey
RMA-2	2D hydrodynamic FE numerical model
RMA-4	2D FE water quality transport model
SEDDIST	Sedimentation distribution program
STUDH	2D sediment transport FE numerical model
TABS-2	2D numerical modeling system developed at WES
WES	US Army Engineer Waterways Experiment Station
WLO	Wax Lake Outlet